The DNA Binding Activity of the Potato NBLRR protein Rx1

DIXON, CHRISTOPHER,HUGH

The DNA Binding Activity of The Potato NBLRR Protein Rx1

Author: Christopher Dixon

Supervisor: Dr Martin Cann

PhD Thesis

Department of Biosciences

2016

Contents

List of Figures

List of Tables

Abstract

Plant NBLRR proteins are immune receptors named for their characteristic domains. Their mode of action is currently undetermined. The potato NBLRR protein Rx1 has been shown to possess a DNA binding activity *in vitro*. This thesis presents evidence that Rx1 binds DNA in response to its cognate elicitor CP106 in fixed *N. benthamiana* leaf material using a novel FRET-FLIM assay. The Rx1 CC and NBARC domains were both shown to possess this DNA binding activity. A nucleocytoplasmic distribution of Rx1 was shown to be required for DNA binding. Potential regulators of Rx1 DNA binding activity were identified using a yeast 2-hybrid screen against the CC domain of Rx1 and their effects on Rx1 DNA binding and Rx1 mediated immunity characterised. The transcription factor *Nb*GLK1 was identified and characterised as a promoter of Rx1 DNA binding using FRET-FLIM and a promotor of Rx1 mediated extreme resistance to PVX. However, *Nb*GLK1 was not found to affect Rx1 mediated HR. The protein *Nb*MLHP was also identified in the yeast 2-hybrid screen. This protein was not found to impact Rx1 DNA binding in FRET-FLIM assays. It was, however, identified as a suppressor of Rx1 mediated extreme resistance to PVX (but not HR), and Rx1 did inhibit *Nb*MLHP DNA binding.

Acknowledgements

I would like to thank my supervisor Martin Cann for all his time, help and guidance in designing and troubleshooting experiments. Phil Townsend and Stepan Fenyk for showing me how to work in a molecular biology lab and for always being willing to provide insight and assistance when things inevitably went wrong. Lars-Olof Pålsson for providing me with, and showing me how to use his FRET-FLIM imaging equipment, and Robert Pal for helping to fix it when it broke. Aska Goverse, Eric Slootweg, Rikus Pomp, Octavina Sukarta and everyone who assisted me during my visit to the University of Wageningen for being such open and helpful collaborators. I'd like to thank the BBSRC for funding my project and everyone in lab 234 and office 231 for making my PhD as good a memory as they did.

Declaration

List of Abbreviations

3-AT	3-Amino-1,2,4-triazole
AAA+	ATPases associated with diverse cellular activities
ADP	Adenosine diphosphate
ANOVA	Analysis of variance
APS	Ammonium persulfate
ATP	Adenosine triphosphate
AVR	Avirulence
BED Zinc finger	BEAF, DREF (*Drosophila* BED Zinc finger containing proteins)
BRX	BREVIS RADIX
$CaCl_2$	Calcium chloride
CC	Coiled coil
cDNA	Complimentary DNA
CHD1	Chromodomain helicase DNA binding domain protein 1
CP	Coat protein
DNA	Deoxyribonucleic acid
dNTP	Deoxynucleotide triphosphate
dsDNA	Double stranded DNA
DTT	Dithiotherital
ECL	Enhanced chemiluminescence
EDTA	Ethylenediaminetetraacetic acid
ETI	Effector triggered immunity
FRET-FLIM	Fluorescence resonance energy transfer- fluorescence lifetime imaging
GFP	Green fluorescent protein
GLK1	Golden like transcription factor 1
HA	Hemagglutinin
HCl	Hydrochloric acid
HMA	Heavy metal associated
HNL	Hyydrolase, NBARC, LRR
HR	Hypersensitive response
HRP	Horseradish peroxidase
HSP	Heat shock protein
LB	Luria broth
LRR	Leucine Rich Repeat
MES	2-N-morpholinoethanesulfonic acid
$MgCl_2$	Magnesium chloride
MLHP	Micronucleur histone linker protein
Myb	Myeloblastosis
NaCl	Sodium chloride
NaOH	Sodium Hydroxide

NBARC	Nucleotide binding, Apaf 1, certain R proteins, CED 4
NES	Nucleur export sequence
NLS	Nucleur localisation sequence
NMR	Nucleur magnetic resonance
NOD	Nucleotide binding and oligomerisation domain
OD_{600}	Optical density at 600 nm
P-loop	Phosphate binding loop
PAMP	Pathogen associated molecular pattern
PRBS	Predicted biological score
PBS	Phosphate buffered saline
PBST	Phosphate buffered saline tween20
PCR	Polymerase chain reaction
PK	Protein kinase
PTI	Pamp triggered immunity
PVPP	Polyvinylpolypyrrolidone
PVX	Potato virus X
R Protein	Resistance Protein
RNA	Ribonucleic Acid
RNBS	Resistance nucleotide binding site
Rx1	Resistance to potato virus X 1
SANT	Swi3, Ada2, N-Cor, and TFIIIB
SAR	Systemic acquired resistance
SAXS	Small angle X-ray scattering
SD	*Solanaceous* domain
SDS	Sodium dodecyl sulfate
SDS-PAGE	Sodium dodecyl sulfate poly-acrylamide gel electrophoresis
SID	Selective interacting domain
SOC	Super optimal broth with catabolite repression
ssDNA	Single stranded DNA
STAND	Signal Transduction ATPase with Numerous Domains
TAE	Tris, acetate, EDTA
TBS	Tris buffered saline
TBST	Tris buffered saline tween20
TCSPC	Time correlated single photon counting
TEMED	Tetramethylethylenediamine
TIR	Toll/ interleukin 1 like receptor
Tris	Trisaminomethane
WRKY	Transcription factor recognising WRKYGQK motif.
YEB	Yeast extract broth

1. Introduction

1.1 Overview

This thesis provides evidence that the plant NBLRR protein Rx1 binds genomic DNA to initiate pathogen defence signalling. This chapter aims to provide a review of the relative literature required to better understand and contextualise these results. A general overview of plant immune signalling will be provided with a focus on plant NBLRR proteins. This will include a review of what is known of plant NBLRR structure, function and regulation, and how these are combined to form a model of plant NBLRR pathogen defence signalling.

1.2 Rx1

This thesis describes work into the potato NBLRR protein Rx1. The *Rx1* gene encoding this protein was first identified in a study of potato strains resistant to potato virus X (PVX) and were characterised as giving resistance. Two unrelated genes, both providing resistance were identified at the same locus, and were named *Rx1* and *Rx2* respectively (Resistance to potato virus X 1 and 2) (Cockerham et al., 1970)

Rx1 has been of particular scientific interest due to an unusual defence response it induces, known as extreme resistance. This is characterised by a reduced accumulation of PVX virus particles in the infected site immediately after infection. (Kohm et al., 1993) However, Rx1 has also been characterised as causing a separate HR in infected tissue. (Bendahmane et al., 1999). Further study identified the PVX

viral coat protein as the cognate elicitor of Rx1 mediated immunity. (Bendahmane et al., 1995).

Rx1 is a plant NBLRR protein that possess the archetypal three domain structure, with an N-terminal CC domain (see Section 1.4), making it a good model protein for NBLRR structure and function.

1.3 Plant Pathogen Sensing

Plants possess an immune system similar to the animal innate immune system. The first line of plant defence signalling consists of pathogen associated molecular pattern receptors, or PAMP receptors. These are protein receptors located on the exterior of the plant cell that sense molecules that are essential to the pathogen's survival, and hence cannot be evolutionarily discarded to avoid detection e.g. bacterial flagellins (Jones et al., 2006). PAMP receptors initiate a signalling cascade that results in a defence response by the plant known as PAMP triggered immunity, or PTI. To combat plant PAMP receptors, pathogens have evolved effector proteins. Pathogen effector proteins are secreted by the pathogen and translocate themselves into the plant cell. Here they act to inhibit the defence signalling initiated by the PAMP receptor, enabling the pathogen to infect the plant host. Pathogens have also evolved small RNAs (sRNAs) that can translocate into the host and perform a similar role (Weiberg et al., 2013).

Plants have in turn evolved a means to combat effector proteins. Plant R proteins sense the effector proteins or sRNAs within the plant cell and initiate a stronger defence response known as effector triggered immunity, or ETI (Figure 1).

Plants trigger an array of different actions in response to pathogens, and many of these are observed both in ETI and PTI: The production of reactive oxygen species (ROS), cell wall thickening, the translation of pathogenesis related (PR) proteins with anti-pathogen effects, and an increased production of secondary metabolites are all commonly observed in both PTI and ETI (Yang et al., 1997). Conversely, some immune responses are specific to the type of pathogen infecting the plant rather than ETI or PTI, such as the translation of antifungal peptides in response to some fungal infections (Yang et al., 1997). However, one characteristic effect of the stronger ETI defence response triggered by R proteins that is not observed in PTI is the controlled death of the infected cell and the surrounding tissue, known as the hypersensitive response (HR) (Morel et al., 1997).

By far the most common class of R proteins are NBLRR proteins (Jones et al., 2006). These are named after two of their characteristic domains; the nucleotide binding (NB) and leucine rich repeat (LRR) domains. The exact mechanism through which R proteins initiate defence signalling is currently unknown.

A.

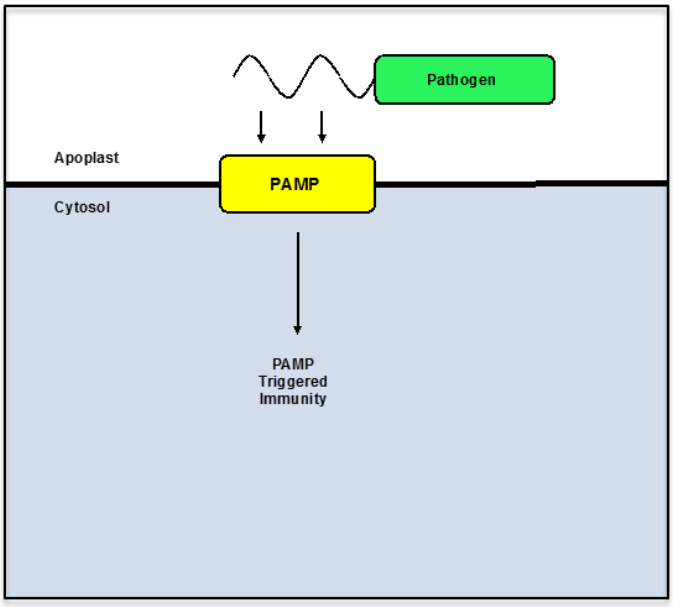
Pathogen
Apoplast
PAMP
Cytosol
PAMP
Triggered
Immunity

B.

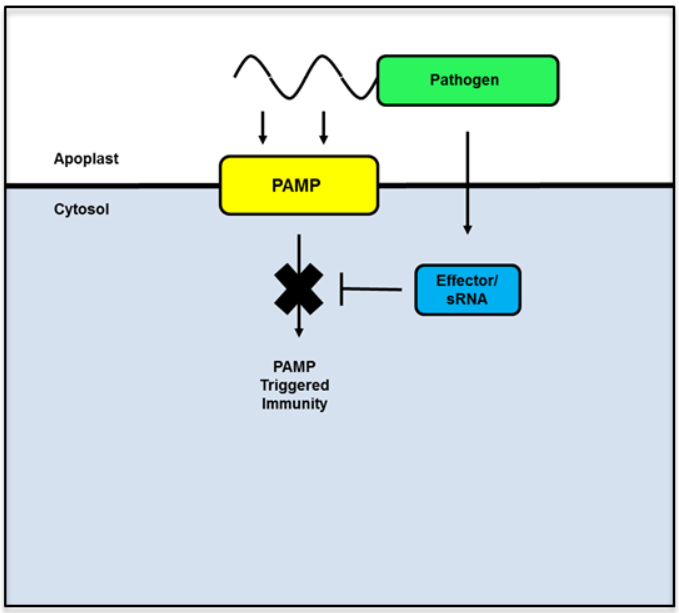
Pathogen
Apoplast
PAMP
Cytosol
Effector/
sRNA
PAMP
Triggered
Immunity

C.

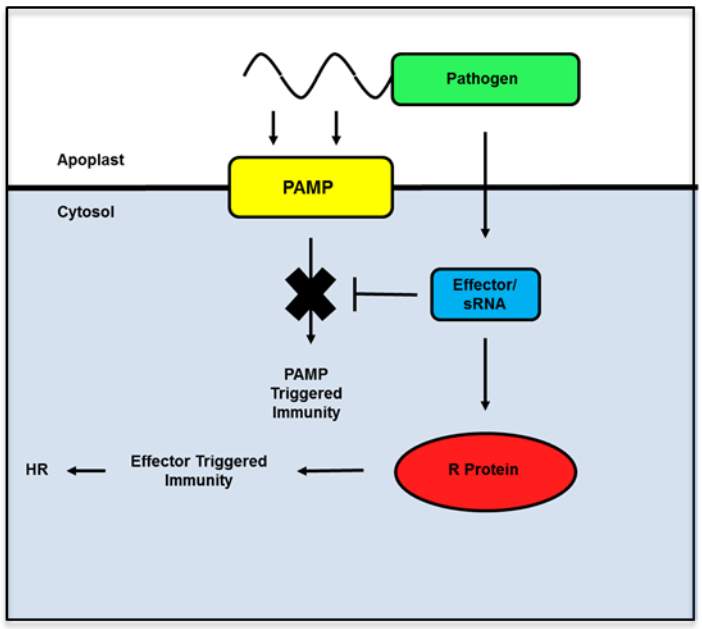

Figure 1. A schematic model of plant immune signalling. A. Plant PAMP receptors detect essential pathogen molecules to trigger an immune response. B. Pathogens evolve effector proteins which translocate into the plant cell and inhibit PAMP triggered immunity. C. Plants evolve R proteins to detect pathogen effector molecules and initiate an enhanced immune response including HR. Adapted from Jones et al., 2006.

1.4 STAND ATPases

NBLRR proteins belong to a family of signalling proteins known as STAND proteins (signal transduction ATPases with numerous domains) (Danot et al., 2009). STAND proteins are large multidomain signalling proteins possessing a sensor domain, a core conserved nucleotide binding and oligomerisation domain (NOD domain), and an effector domain that initiates signal transduction. They are believed to function as an ATPase switch, with nucleotide hydrolysis or exchange in the NOD domain resulting

in a conformational shift in the protein. This conformational shift is associated with an activation of the protein's signalling activity.

STAND proteins are hypothesised to have evolved from AAA+ ATPases, a large, diverse family of signalling ATPases. The proteins within the AAA+ family displaying the highest similarity to STAND proteins are the DNA binding transcriptional regulators Cdc6 and Orc1 (Danot et al., 2009). The characteristic NOD domain of STAND proteins is adapted from the core AAA+ domain, a *p*-loop nucleotide-binding domain with a role in oligomerisation also known to have a DNA binding activity in Cdc6 and Orc1 (Capaldi et al., 2004, Feng et al., 2002).

Various STAND proteins are known to adopt a large array of different oligomeric structures to carry out their roles, with oligomerisation mediated by the NOD domain. For example, the *E. coli* transcriptional activator MalT has been shown to form oligomeric curves using cryo-EM (Larquet et al., 2004). The crystal structures of the apoptosis regulators Apaf-1 and CED-4 are both octameric hutches (Zhou et al., 2015, Yan et al., 2007). The animal innate immune receptor STAND proteins NAIP2 and NLRC4 have been shown to initiate apoptosis by forming a ring-like structure using cryo-EM (Zhang et al., 2015).

Plant NBLRR proteins belong to a subfamily of STAND ATPases with two other proteins, the aforementioned Apaf-1 and CED-4 (Danot et al., 2009). These are both apoptosis initiating proteins known from humans and *C. elegans* respectively (Zhou et al., 2015, Yan et al., 2007). NBLRR proteins typically follow the STAND protein three-domain structure. They possess either an N-terminal coiled coil (CC) or

Toll/interleukin-1 receptor-like (TIR) domain, hypothesised to be the effector domain that initiates signal transduction. A middle NBARC domain, shared with Apaf-1 and CED-4 that functions as the NOD domain. Finally, a C-terminal leucine rich repeat (LRR) domain is proposed to act as the sensor domain. Genome analysis of multiple model organisms has revealed that all four of these domains evolved individually before prokaryotes split from eukaryotes, but the fusion of these domains together is only found in land plants (Yue et al., 2012). Both CC and TIR NBLRR proteins are found in bryophytes, which diverged from other land plants approximately 450 million years ago (Xue et al., 2012). Both are also present in dicots, but TIR containing NBLRR proteins are not present in monocots, having been lost at some point in the clades evolutionary history (Meyers et al., 1999).

1.5 Plant NB-LRR protein domains

This section will give an overview of what is known of the structure and function of the different constituent domains common to plant NBLRR proteins (summarised in Table 1).

Table 1. A schematic summary of different NBLRR protein domain architectures with examples. Including archetypal NBLRR proteins (with the sites of common motifs within the domains annotated), truncated NBLRR proteins, NBLRR proteins with novel domain fusions, and paired executor-sensor NBLRR proteins with integrated decoys. Adapted from Sukarta et al., 2016.

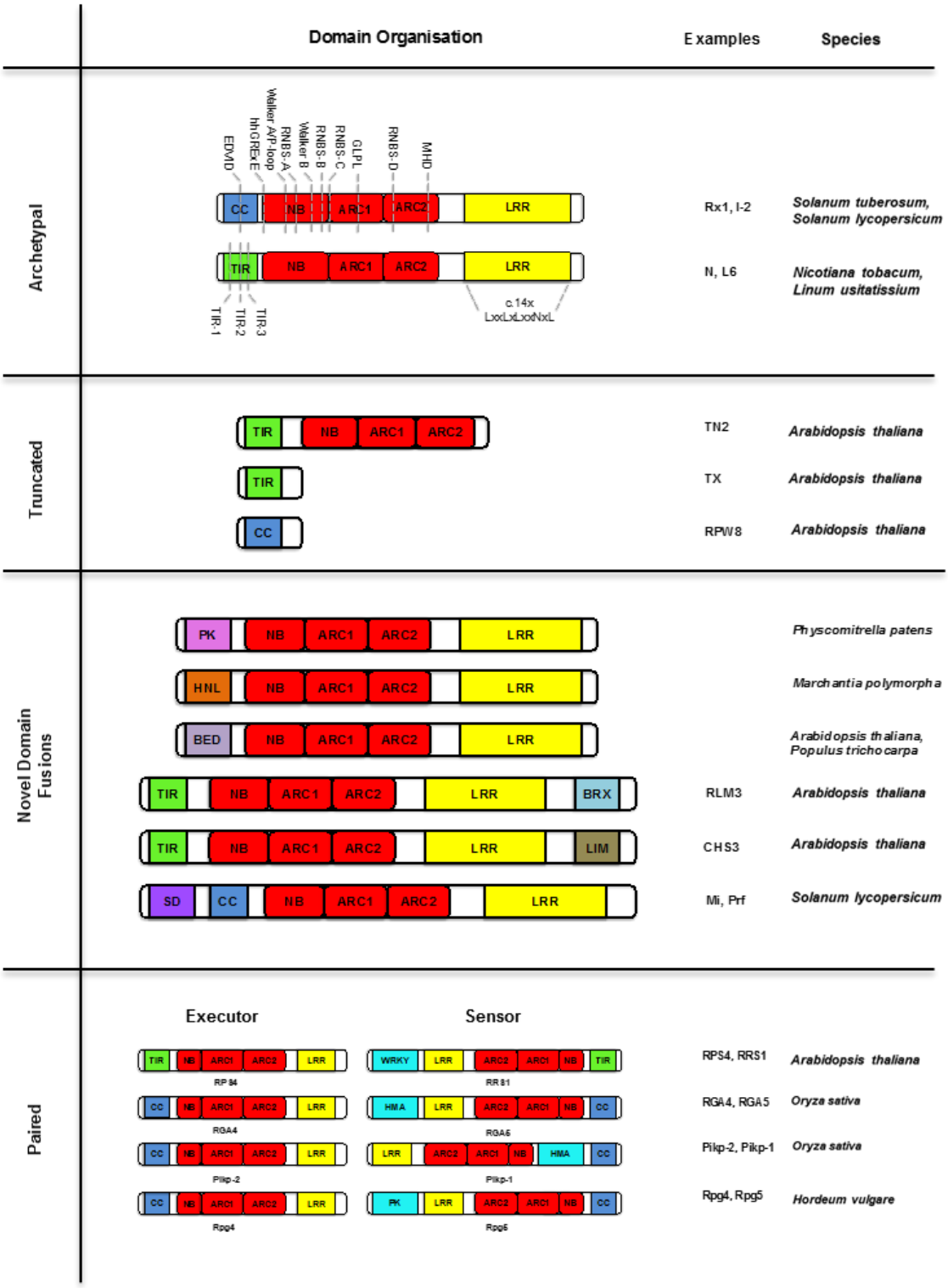
Domain Organisation
Examples
Species
Archetypal
EDVID
hhGREx-E
Walker A/P-loop
RNBS-A
Walker B
RNBS-B
RNBS-C
GLPL
RNBS-D
MHD
CC
NB
ARC1
ARC2
LRR
TIR
TIR-1
TIR-2
TIR-3
c.14x
LxxLxLxxNxL
Rx1, I-2
Solanum tuberosum, Solanum lycopersicum
N, L6
Nicotiana tobacum, Linum usitatissium
Truncated
TN2
Arabidopsis thaliana
TX
Arabidopsis thaliana
RPW8
Arabidopsis thaliana
Novel Domain Fusions
PK
HNL
BED
BRX
LIM
SD
Physcomitrella patens
Marchantia polymorpha
Arabidopsis thaliana, Populus trichocarpa
RLM3
Arabidopsis thaliana
CHS3
Arabidopsis thaliana
Mi, Prf
Solanum lycopersicum
Paired
Executor
Sensor
WRKY
HMA
RPS4
RRS1
RGA4
RGA5
Pikp-2
Pikp-1
Rpg4
Rpg5
RPS4, RRS1
Arabidopsis thaliana
RGA4, RGA5
Oryza sativa
Pikp-2, Pikp-1
Oryza sativa
Rpg4, Rpg5
Hordeum vulgare

1.5.1 The CC domain

CC domains were first predicted in 1953 as an energetically stable means of grouping alpha helices together by wrapping two or three helices around each other (Crick, 1953). These domains are commonly known to be involved in protein-protein interactions involving helices from different proteins intertwining together (Kohn et al., 1997). In NBLRR proteins, CC domains are thought to act as the effector domain. Indeed, they are known to be the sufficient for HR in some NBLRR proteins, such as MLA10 (Maekawa et al., 2011) and Rp1 (Wang et al., 2015) but there are exceptions to this (see section 1.5.3).

High sequence similarity is not observed throughout most regions of NBLRR CC domains (Sukarta et al., 2016). The exception to this is the conserved EDVID motif (consensus sequence WLxxVRELAYDA**EDV**L**D**x) that is observed in most NBLRR CC domains (Mazourek et al 2009) and is known to have a role in interdomain interactions (Rairdan et al., 2008) (see section 1.9). The EDVID motif is not universal though, and is missing within a highly conserved, smaller sub-clade of CC-NBLRR proteins (Collier et al., 2011).

The structures of three NBLRR protein CC domains belonging to the EDVID clade have been solved. The Rx1 CC domain was crystallised and solved in a complex with the WPP domain of the protein RanGap2, a known interactor. The structure revealed a group of four bundled α-helicies (Hao et al., 2013, Figure 2). Meanwhile, the structure of the MLA10 CC domain was determined via X-ray crystallography to be a homodimer of a two intertwined helix-loop-helix motifs (Maekawa et al., 2011) (Figure 2). The difference between these two structures would suggest either a

variance in CC structures between different NBLRR proteins, or a conformational change upon interaction with another protein such as RanGap2 in Rx1.

Recently, the structure of the Sr33 CC domain from barley has been solved using NMR spectroscopy. It adopts a conformation of 4 bundled α-helices, similar to Rx1, suggesting this structure is not merely a result of RanGap2 binding (Casey et al., 2016). SAXS experiments on Rx1 CC in solution suggested it also takes this conformation in the absence of RanGap2, and similar studies of MLA10 CC suggest that in solution it may also take a more compact monomeric structure (Casey et al., 2016). The dimeric MLA10 form may only be associated with the activated NBLLR protein initiating signalling.

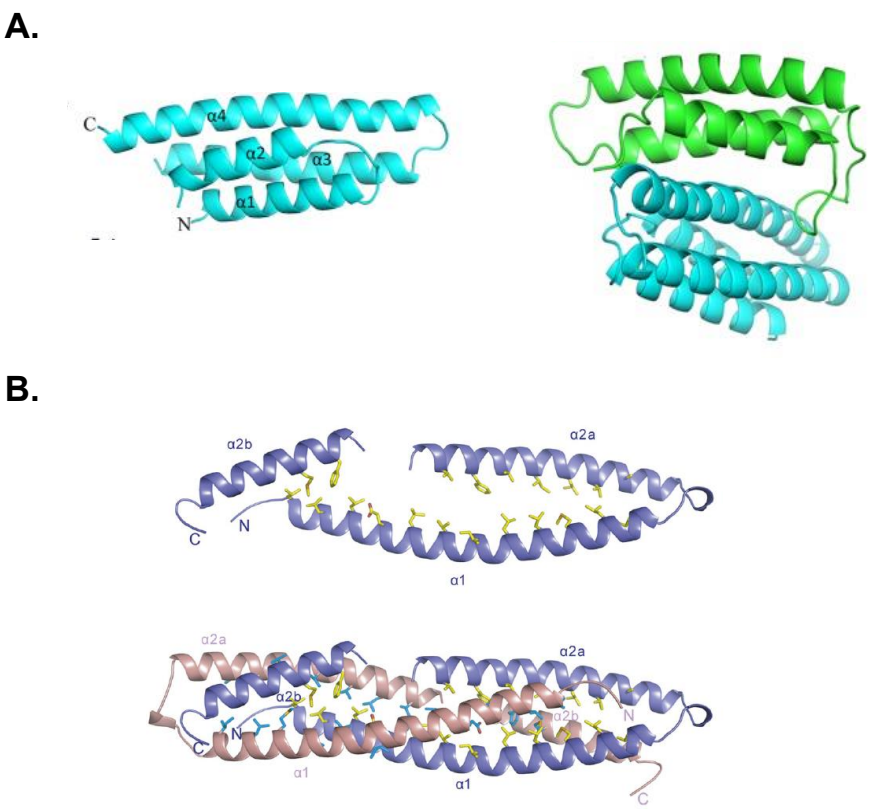

Figure 2. Structures of NBLRR CC domains A. Rx1 CC crystallised as a 4 α-helix bundle (in cyan) both with and without the RanGAP2 WPP domain (green). Adapted from Hao et al., 2013 B. The MLA10 CC domain crystal structure in a helix-loop helix conformation shown both as a monomer (in purple) and as the homodimer (purple and pink) Adapted from Maekawa et al., 2011 C. NMR structure of Sr33 CC domain as a 4 α-helix bundle (in blue) adapted from Casey et al., 2016.

1.5.2 The TIR domain

TIR domains are involved in protein-protein interactions, often mediated through interactions with other TIR domains (Ve et al., 2015). They are known to be sufficient to initiate HR by themselves in the NBLRR proteins L6 and RPS4 (Bernoux et al., 2011, Williams et al., 2014), suggesting that in these proteins the TIR domain may function as the effector domain of the protein, similar to the CC domain.

The structures of TIR domains from several NBLRR proteins are known. The first plant TIR structure to be solved was from a truncated NBLRR protein (see Section 1.5.5) containing only a TIR domain, AtTIR from *Arabidopsis.* The crystal structure revealed a globular, flavodoxin-like structure of five stranded parallel β-sheets surrounded by five α-helices. This is similar to known bacterial and mammalian TIR domain structures (Figure 3). However, an extension to the D α-helix to form an αD3-helix not seen in mammalian or bacterial TIR domains was also revealed. This was shown to be the site of many loss of function mutations from TIR domains, suggesting this extra loop is immunologically relevant (Chan et al., 2010). The flax NBLRR protein L6 has also been solved via X-ray crystallography (Figure 3) and shows a similar structure. This protein crystallised as a homodimer, with dimerization shown to be essential for the initiation of HR (Bernoux et al., 2011). This requirement for TIR domain self-interaction has also been demonstrated to be a requirement for the oligomerisation of the NBLRR protein N from tobacco (Mestre et al., 2002). The crystal structure of the paired NBLRR proteins (see section 1.5.4) RPS4 and RRS1 TIR domains has been solved as a heterodimer. It reveals both TIR domains possessing a similar structure to AtTIR and L6, although RRS1 does not possess the αD3-helix extension (Williams et al., 2014). Heterodimerisation of RPS4 and RRS1 was shown

to require each protein's TIR domains, and to be necessary for the initiation of HR (Williams et al., 2014).

Genomic analysis of TIR-NBLRR domains found three common conserved motifs; TIR-1, 2, and 3 (Meyers et al., 2003). These correspond to regions spanning the transition across from β-sheets to α-helices in the TIR structures; TIR-1 from βA to αA1, TIR-2 from βC to αC, and TIR-3 from βD to αD1 (Chan et al., 2010)

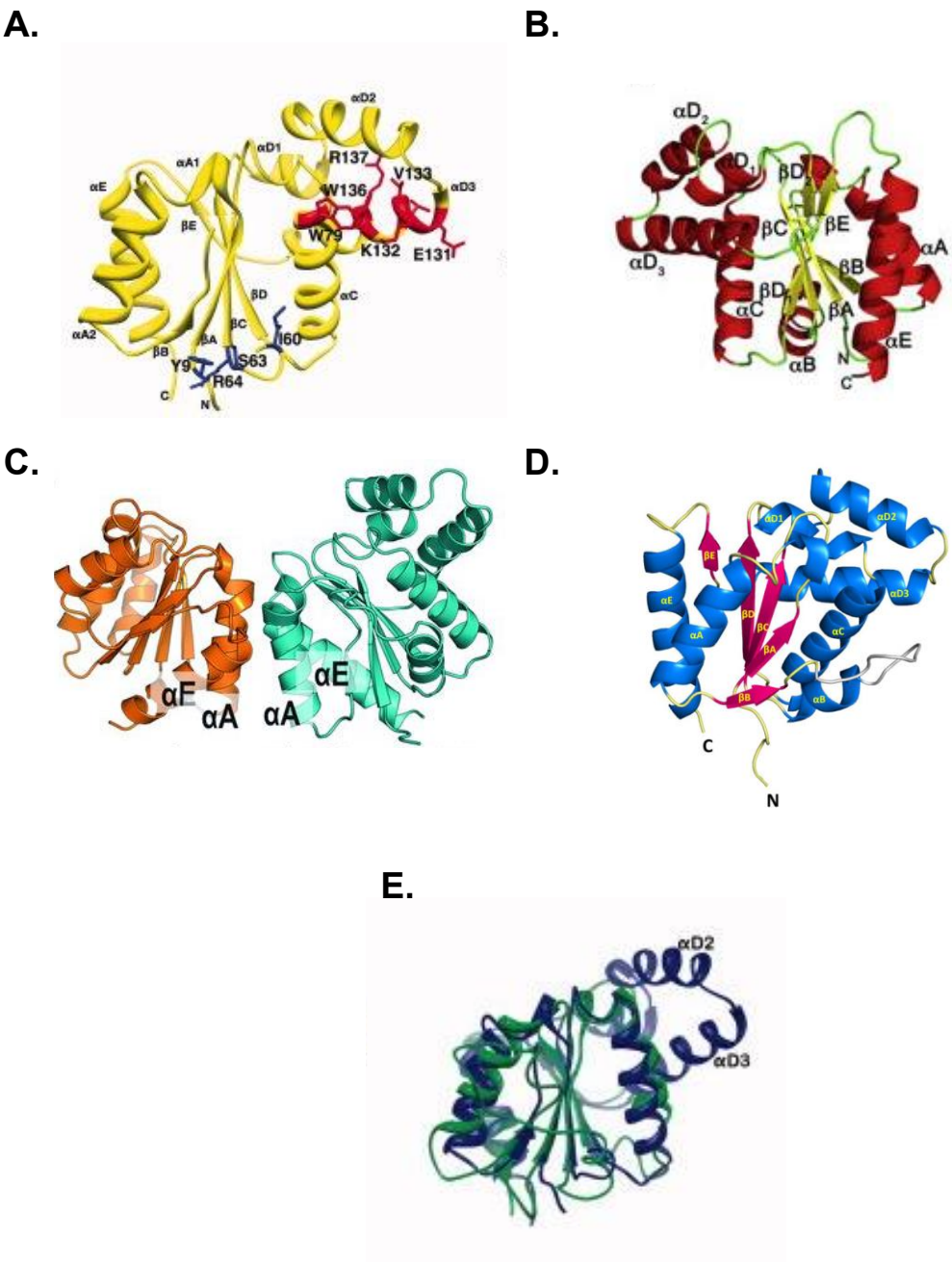

Figure 3. Crystal structures of plant NBLRR TIR domains, all displaying a 5-stranded parallel beta sheet surrounded by five α-helices. A. AtTIR (yellow) with the extra D3 helix highlighted in red. Adapted from Chan et al., 2010 B. The L6 TIR domain. Adapted from Bernoux et al., 2011 C. TIR domains from RPS4 (orange) and RRS1 (cyan) together as a heterodimer. Adapted from Williams et al., 2014. E. AtTIR (blue) superimposed on the human TIR domain structure MyDD8 (green) showing the insertion of the extra helical region. Adapted from Chan et al., 2010.

1.5.3 The NBARC domain

The central NBARC domain can be broken down into 3 sub-domains. NB, ARC-1 and ARC-2. The NB domain is named after its nucleotide binding role and the two ARC domains are named for the group of proteins that share this subdomain; Apaf-1, R proteins, and CED-4 (Takken et al., 2012). The NBARC domain is hypothesised to possess a nucleotide hydrolysis activity. This nucleotide hydrolysis activity is thought to result in a conformational shift that activates the protein, switching it between an 'on' and 'off' state to enable signalling (Takken et al., 2012). In the potato NBLRR Rx1 the NB subdomain is sufficient to induce HR (Rairden et al., 2008), suggesting that in some cases this domain may also have an independent signalling effector activity. There are currently no solved crystal structures of NBLRR NBARC domains. The aforementioned Apaf-1 and CED-4 structures have both been solved using X-ray crystallography (Zhou et al., 2015, Yan et al., 2007). These both show a hutch-like structure consisting of a tetramer of homodimers.

Homology models of NBLRR NBARC domain structure have been generated based on Apaf-1, CED-4 and other STAND proteins (Figure 4.). The NB domain is predicted to consist of a five-stranded parallel β-sheet surrounded by seven α-helices. ARC1 is predicted to form a bundle of four α-helices, and ARC-2 a winged helix fold. Several motifs common to AAA+ ATPases are predicted within the NBARC domain of NBLRR proteins, and have been found to be conserved across multiple NBLRR proteins. These include the hhGRExE, walker A/*p*-loop, MHD, Walker B, GLPL, and RNBSA to D motifs (Meyers et al., 2003). The consensus sequences and any known functional roles of these motifs in ATP hydrolysis are summarised in Table 2.

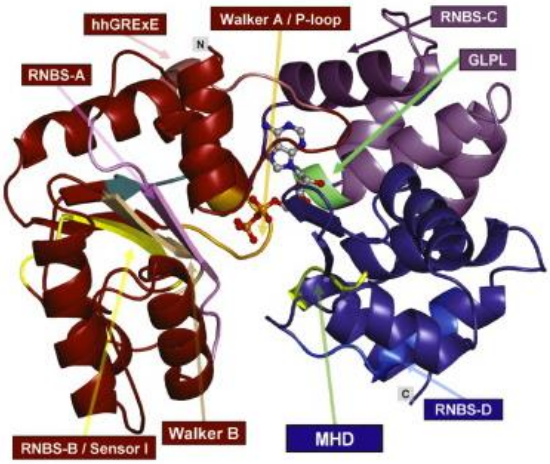

Figure 4. A homology model of the NBARC domain of I-2 bound to ADP modelled on Apaf-1. The NB, ARC1 and ARC2 subdomains are coloured red, purple and blue respectively. Conserved motifs are marked. Adapted from Lukasik et al., 2009.

Table 2. Conserved protein motifs found in plant NBLRR protein NBARC domains, their subdomain location, consensus sequence and any putative ATP hydrolysis function. x denotes any amino acid residue, h a hydrophobic residue, o an alcoholic residue. Adapted from Takken et al., 2006 and Meyers et al., 2003.

Motif	**Subdomain Location**	**Consensus Sequence**	**Putative Function**
hhGRExE	NB	hhGRExE	R forms H-bond with adenine base via a water molecule
P-loop/ Walker A	NB	GxxxxGKS/T	K Binds α and β Phosphates, S/T coordinates Mg^{2+} ion
RNBS-A	NB	FDLxAWVCVS QxF	S forms ATP binding biding pocket
Walker B	NB	hhhhDD/E	D coordinates second Mg^{2+} ion via a water molecule, D/E is an acid catalyst for ATP hydrolysis
RNBS-B	NB	hhhhToR	R senses γ-phosphate and relays the information to other parts of the protein
RNBS-C	ARC1	YEVxxLSEDEA WELFCKxAF	Unknown, not predicted to form binding pocket
GLPL	ARC1	GxP	G and P form ATP binding biding pocket
RNBS-D	ARC2	FLxxAxF	Unknown, not predicted to form binding pocket
MHD	ARC2	hxhHD	H interacts with β-phosphate

The ATPase activity of plant NBLRR NBARC domains have been demonstrated *in vitro* using recombinant CCNBARC domain from the tomato NBLRR protein I-2 (Tameling et al. 2002). Mutation to residues in the RNBS-A and Walker B motifs that prevent nucleotide hydrolysis have been shown to result in autoactivation of immune signalling in I-2, whereas mutations to the *p*-loop of this protein that prevent nucleotide binding result in immunologically inactive protein (Tameling et al., 2006). This suggests that I-2 is bound to ATP in an active state and ADP in an inactive state. Recombinant Mi-1 from tomato has similarly been shown to have an ATPase activity (Tameling et al., 2002). M from flax giving resistance to rust disease has also been shown to co-purify with ADP in an inactive state, and autoactive M to co-purify with ATP. This suggests that the ADP 'off' state and ATP 'on' state model may be conserved across multiple NBLRR proteins (Williams et al., 2011).

However, this mode of action is not universal. The R protein N from tobacco co-purifies with ADP in the active state and ATP in the inactive state (Ueda et al., 2006), in a reversal of what is seen in I-2 and M. Recombinant NB domain of the rice NBLRR protein R1, as well as NBARC PSiP from corn and RPM1 from *A. thaliana* have been shown to not possess a simple ATPase activity. Instead, they cleave ATP down to its nucleoside via a sequential removal of all three phosphates (Fenyk et al 2012). These cases of differing nucleotide hydrolysis activities and differing effects of nucleotide hydrolysis on NBLRR protein function suggest that one simple 'ATPase switch' model is not conserved across all NBLRR proteins. Instead, it appears that different NBLRR proteins have evolved to adapt NBARC domain nucleotide hydrolysis activity to different ends.

Some studies have also suggested that the NBARC domain may have a role in effecting signal transduction in addition to its role as a conformational switch. Homology modelling of Rx1 NBARC domain showed a high a degree of similarity to the DNA binding AAA+ ATPases CDC-6 and Orc1, leading to the hypothesis that this NBLRR protein may also bind DNA (Fenyk et al., 2015). Recombinant Rx1 CCNBARC refolded from *E. coli* was shown to bind DNA, distort DNA in response to ATP and induce DNA melting *in vitro* using EMSA and FRET-FLIM. DNA binding was confirmed not to be an artefact of refolding using *in vitro* EMSA assays on full length Rx1 expressed in and purified from *N. benthamiana* leaves (Fenyk et al. 2015). Rx1 has a preference for binding ssDNA over dsDNA. Mutation of the *p*-loop was not found to affect DNA binding in Rx1, but did prevent DNA deformation in response to ATP (Fenyk et al., 2015), suggesting nucleotide hydrolysis may be involved in this.

Recombinant I-2 NBARC domain has also been found to have a DNA binding activity (Fenyk et al., 2016), suggesting DNA binding may be a conserved activity across multiple NBLRR proteins. However there were differences in the DNA binding properties of I-2 compared to those of Rx1. I-2 showed a preference for double stranded DNA over single stranded, the reverse of Rx1's affinity. It was found to bend DNA to lesser angle than Rx1. I-2 also had a stronger affinity for DNA in the presence of ATP and with a non-hydolysable ATP analogue than with ADP. DNA binding was shown stimulate I-2 ATPase activity (Fenyk et al., 2016). These results suggest that I-2 may bind DNA in an activated ATP bound state to initiate ETI. DNA binding studies have currently only been performed in an *in vitro* system, leaving the biological relevance of this DNA binding activity in the plant cell currently undetermined.

1.5.4 The LRR domain

LRR domains are common to many proteins and are known to be involved in protein-protein interactions (Kobe et al., 2001). They contain a characteristic LxxLxLxxNxL pattern of leucine and other hydrophobic residues interspersed with hydrophilic residues repeated multiple times (Padmanabhan et al., 2009). In NBLRR proteins the C–terminal LRR domain is believed to be the sensor domain that mediates pathogen detection. This region displays high variability in the sequence and length of these repeats across different NBLRR proteins, which may be the result of a high evolutionary pressure to detect different effector proteins (Padmanabhan et al., 2009).

No LRR structures have been solved for NBLRR proteins. However, many LRR structures have been solved for other proteins. Homology modelling of the Lr10 LRR domain based on these other LRR structures reveals an elongated horseshoe-like structure giving a large surface area for interaction with other proteins. This was predicted to possess a positively charged N-terminal and a hydrophobic C-terminal region (Sela et al., 2012). It is hypothesised that an association between the LRR domain and a pathogen effector, perhaps through an intermediary protein, results in a conformational shift in the LRR domain that leads to activation of the NBLRR protein and the initiation of defence signalling (Padmanabhan et al., 2009). Mutation of putative surface hydrophobic residues in NBLRR proteins such as LR10 (Sela et al., 2012) and L6, L7 and L8 (Dodds et al., 2006) is known to reduce the specificity of disease resistance, supporting this hypothesis.

1.5.5 Domain Variations

There are many instances known of variations on this archetypal three domain structure; cases of NBLRR proteins with extra domains, different domains and missing domains have all been described (Table 1). Alternative N-terminal domains can be seen in bryophytes (mosses and liverworts), which branched off from other plant lineages approximately 450 million years ago. A survey of the genome of the moss *Physcomitrella patens* found a class of NBLRR proteins where the N-terminal CC/TIR domain is replaced with a protein kinase (PK) domain (Xue et al., 2012). A similar survey of the liverwort *Marchantia polymorpha* found a class of NBLRR proteins where the N-terminal CC/TIR domain is replaced with a domain homologous to α/β-hydrolase known as an HNL domain (Xue et al., 2012). Different N-terminal domains in poplar and *Arabidopsis* are also known. A genome wide analysis of these species identified NBLRR proteins containing a BED Zinc-ring finger DNA binding domain in lieu of the CC/TIR domain (Kohler el al., 2008).

Additional domains are also seen in multiple instances. A subclass of NBLRR proteins in *Solanaceous* plants contain an N-terminal leucine zipper domain (known as a *Solanaceous* domain, abbreviated to SD), known to be involved in DNA binding, in addition to their CC domain (Milligan et al., 1998). Examples of these include the tomato NBLRR proteins Prf and Mi. An Additional LIM domain is incorporated into the C-terminus of CSH3, an *Arabidopsis* NBLRR protein (Yang et al., 2012). CSH3 is known to have a role in freezing resistance (Yang et al., 2012), but LIM domain mutation results in immunological autoactivity, suggesting these domains can also have an immune function (Bi et al., 2011). RLM3 from *Arabidopsis* has an extra

BREVIS RADIX (BRX) domain incorporated at its C-terminus and provides immunity to a broad range of necrotrophic fungal infections (Staal et al., 2008).

Some NBLRR proteins are known to act in pairs, often where one protein takes on a role as the sensor of the effector and another acts as the executor of defence signalling after interacting with the first (Sukarta et al., 2016). It is common in these proteins to see extra domains incorporated into the sensor NBLRR protein (Table 1). These are thought to be domains that mimic the targets of effector proteins. The effector proteins will bind these domains integrated into the NBLRR sensor, resulting in a conformational shift that initiates defence signalling. This is known as the integrated decoy hypothesis (van der Hoorn et al., 2008).

An example of this can be seen in the sensing of PopP2 by RRS1. The bacterial effector protein PopP2 interferes with WRKY transcription factors that play a role in PAMP-mediated immunity through a lysine acetylase activity (Sarris et al., 2015). The *Arabidopsis* NBLRR protein RRS1 (paired with RPS4) has a WRKY domain incorporated into its N-terminus. PopP2 binds this domain, which will results in RRS1 initiating defence signalling (Césari et al., 2014).

Similarly, HMA (heavy metal associated) domains are also hypothesised to be used by some NBLRR proteins as integrated decoys. HMA proteins are the target of AVR-Pik effector proteins (Maqbool et al., 2015). For instance, RGA4 (paired with RGA5) has a C-terminal HMA domain used to detect the effector proteins AVR-Pia and AVR1-CO39 (Césari et al., 2013). Pikp1 (paired with Pikp-2) has an HMA domain between

the CC and NBARC domains. This is used to sense the effector protein AVR-PikD (Maqbool et al., 2015).

The barley NBLRR protein RPG5 has been shown to act as pair with RPG4 to provide resistance against wheat stem rust (Brueggeman et al., 2008). RPG5 possesses a serine/threonine protein kinase-like domain integrated at its C-terminus that is known to be required for the protein to function (Brueggeman et al., 2008). This kinase domain displays homology to the surface localised receptor kinase protein Pto, a known effector target that is guarded by the NBLRR protein Prf (Brueggeman et al., 2008). It is hence hypothesised that this domain is another integrated decoy used to sense these effectors.

Examples of truncated versions of the archetypal three domain NBLRR protein are also known (Table 1). RPW8 consists solely of a CC domain, with no NBARC or LRR but is still known to confer resistance to powdery mildew in *Arabidopsis* (Xiao et al., 2001).

Many plant TIR containing proteins without LRR domains (known as TNS proteins), or without both an NBARC and an LRR domain (known as TX proteins) have also been shown to have immunological functions (Nandety et al., 2013). TN2 is a TNS protein that has been shown to be required to activate defence responses using exocytosis compromised *Arabidopsis* mutants (Zhao et al., 2015).

1.6 Subcellular Localisation of NBLRR Proteins.

Many NBLRR proteins possess a nucleocytoplasmic distribution within the cell. Examples of this include Rx1, RPS4 and MLA10 (Slootweg et al., 2010, Wirthmueller et al., 2008, Shen et al., 2008). This distribution is known to be required for immunity. A purely nuclear or cytoplasmic distribution can result in a lack of HR (Slootweg et al., 2010).

The way this distribution is maintained varies for different NBLRR proteins. Some NBLRR proteins are known to possess signal peptides that aid in their subcellular localisation. For example, RPS4 possesses an NLS signal peptide that allows trafficking of the protein to the nucleus (Wirthmueller et al., 2008). Meanwhile, the localisation of Rx1 is thought to depend more on its constituent domains. Deletion of the CC domain results in cytoplasmic distribution while deletion of the LRR results in a nuclear distribution. Mutation of the *p*-loop region also results in a cytoplasmic rather than a nucleocytoplasmic distribution. However, this effect is only seen in full-length constructs; truncated NBARC *p*-loop mutant constructs maintain a normal distribution (Slootweg et al., 2010). This nucleocytoplasmic distribution is also known to be dependent on multiple interacting proteins (see section 1.7.3 for details).

Some NBLRR proteins, however, are known to deviate from this typical nucleocytoplasmic distribution. This is common in paired NBLRR sensor proteins, which are often localised to the site of action of their cognate effector proteins. Their paired executors, meanwhile, tend to maintain a nucleocytoplasmic distribution to effect ETI signalling. An example of this is RRS1-R, which is localised to the nucleus (Deslandes et al., 2003) where it senses the effector PopP2 that targets transcription

factors (Césari et al., 2014)(section 1.5.5). Its signalling executor pair RPS4, meanwhile, has a nucleocytoplasmic localisation (Wirthmueller et al., 2008).
Similarly, the paired receptor sensor Rpg5 is known to be localised to the plant cell membrane to aid the sensing of effectors that target PTI signalling kinases there (Brueggeman et al., 2008).

A nuclear localisation of NBLRR proteins has been associated with generic defence signalling, whereas a cytoplasmic localisation is thought to be involved in initiating HR (Heidrich et al., 2011).

1.7 NB-LRR Protein interactors

This section aims to review the various inter-protein interactions known to play a role in NBLRR protein function.

1.7.1 Effector, Guardee and Decoy Interactors

Some R proteins have been shown to interact directly with their bacterial effector p roteins to initiate signalling (Figure 5). For example, Pi-ta binds AVR-pita (Jia et al., 2000) and L5, L6 and L7 in flax all physically interact with AVR-L5,6 and 7 in a yeast 2-hybrid assay. Like for like changes in surface hydrophobic residues of the LRR and L5-6 regions can lead to changes in effector allele resistance (Dodds et al., 2006) suggesting it is the LRR domain mediating this direct binding.

However, these cases are in the minority. Most NBLRR proteins require some sort of intermediary plant protein to bind to that in turn binds the effector. These can be the

targets of effector proteins that an R protein will bind to and utilise to sense the effector (Figure 5). These are known as guardee proteins as they are 'guarded' by the R protein. An example of this is RPS5, which binds its guardee PBS1 and detects conformation change in it caused by AVRPphb cleaving its activation loop (Qi et al., 2012). Often the N-terminus of the R protein is used to interact with the guard. The LRR then detects specific change in the guard protein conformation caused by effector. RPS5 detects PPBS1 via its CC domain, and activation loop cleavage is detected by the LRR (Qi et al., 2012).

Another example of guardee mediated sensing is seen in the tobacco NBLRR protein N. N is known to sense the viral effector p50 in an interaction mediated by the guardee NRIP1, a functional rhodanese sulfurtransferase. NRIP1 is required for N mediated immunity and has been shown to interact both with N (through its N-terminal TIR domain) and with p50 via co-immunoprecipitation (Caplan et al., 2008).

Proteins that mimic targets of effectors but are not themselves functional PTI signalling molecules are also known to be used as intermediary interactors between NBLRR proteins and pathogen effectors, and are known as decoys (Figure 5, see section 1.5.5 for a description of decoy domains integrated into NBLRR protein structure resulting in direct binding of the effector). An example of a decoy is ZED1. ZED1 is acetylated by the *Pseudomonas* effector protein HopZ1A, which targets receptor like cytoplasmic kinases that trigger PTI (Lewis et al., 2013). The NBLRR protein ZAR1 interacts with ZED1 to detect HopZ1A. However, ZED1 has no kinase activity itself, which suggests that it is a non-functional decoy, rather than a guard (Lewis et al., 2013).

FLS2 and BAK1 are kinases that form a PTI signalling complex after the recognition of bacterial flagellins (Xiang et al., 2008). They are targeted by the effector proteins AvrPto and AvrPtoB to inhibit PTI (Shan et al., 2008). Pto is a surface signalling kinase that also binds AvrPto and AvrPtoB and forms a complex with the NBLRR protein Prf (which has a unique N-terminal domain that mediates this reaction) but does not signal PTI (Ntoukakis et al., 2013). Instead, effector binding activates the Pto-Prf complex to initiate ETI signalling, making Pto another instance of a decoy rather than a guard (Ntoukakis et al., 2013).

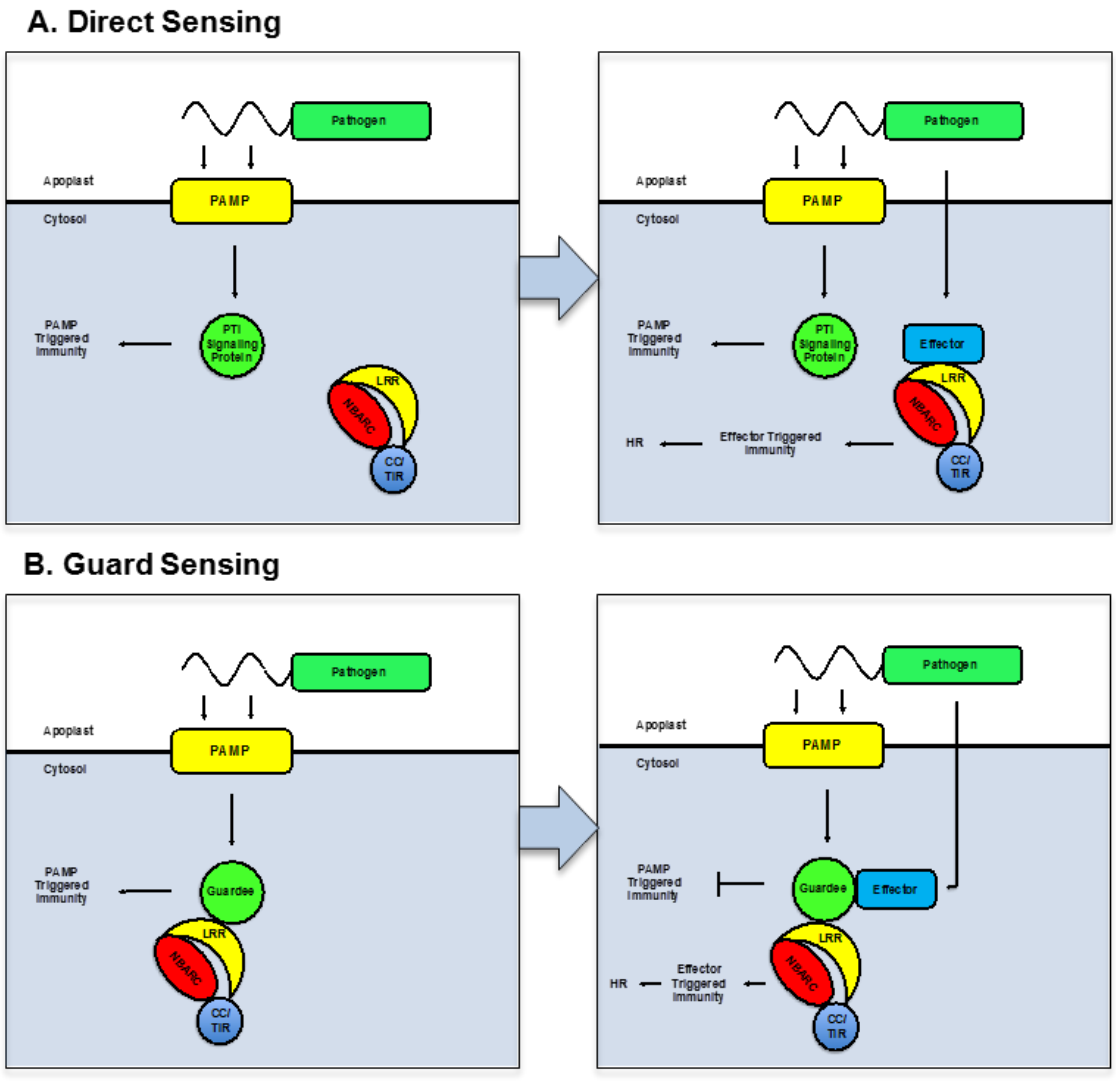

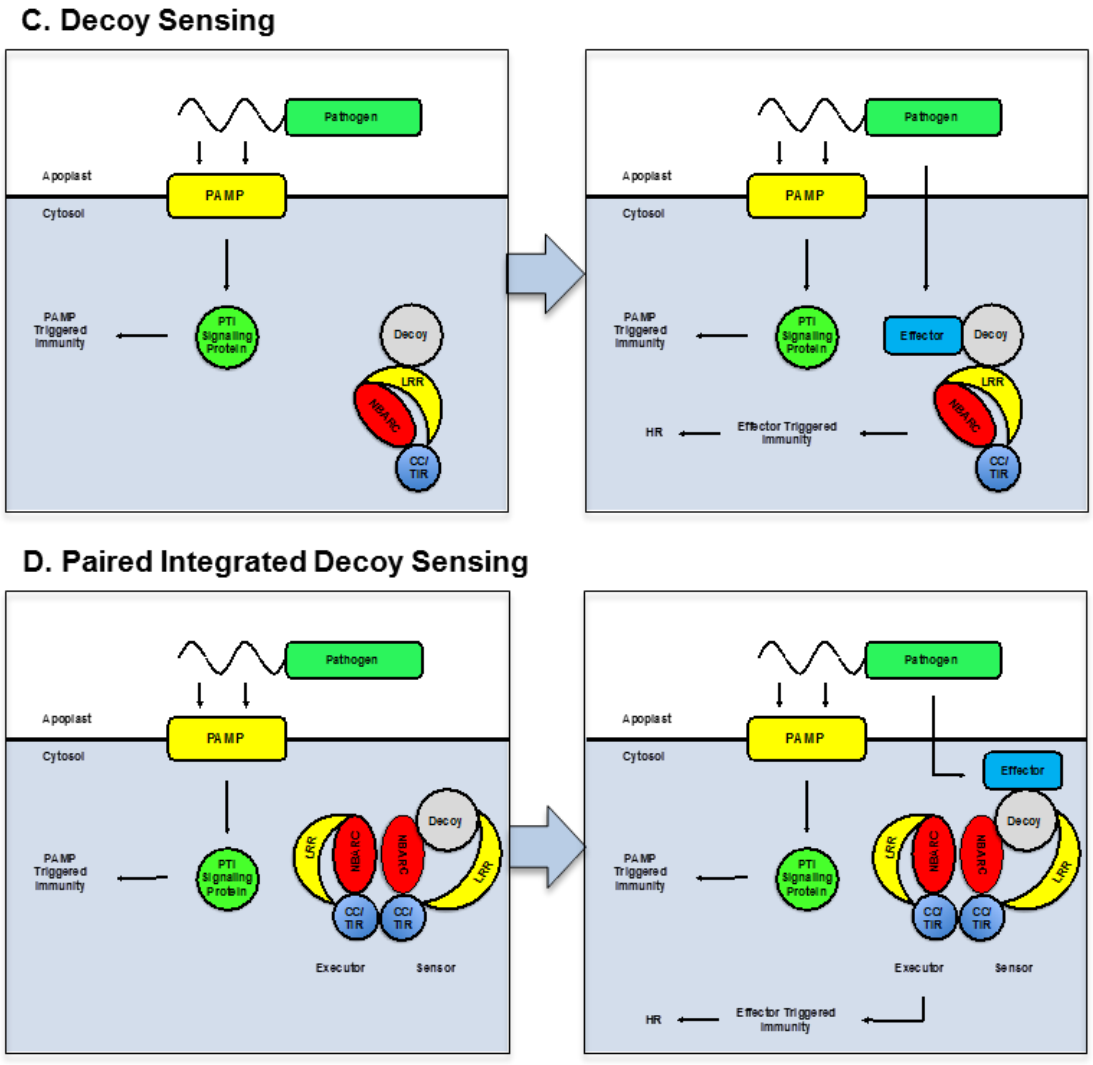

Figure 5. A schematic of different modes of NBLRR effector protein sensing. A. Direct sensing of effector proteins by the NBLRR protein. B. The NBLRR 'guards' a target of the effector protein by interacting with it, detecting the binding of the effector to the guardee. C. The NBLRR protein interacts with a decoy. The decoy is a nonfunctional imitation of the effector protein target that the effector will also bind to. The NBLRR protein then detects effector-decoy binding. D. Decoy domains can be integrated directly into the NBLRR protein structure in a paired integrated decoy NBLRR protein where one NBLRR protein senses the effector and another initiates ETI (see section 1.5.5).

1.7.2 NBLRR Folding Interactors

The strong immune activation triggered by NBLRR proteins, and the lethal consequences for the cell upon their activation, result in a strong need for regulation of NBLRR proteins. Many other proteins have been shown to interact with NBLRR protein to help provide this regulation.

Hsp90 is an ATP driven chaperone that assists protein folding. PP5 (protein phosphatase 5) complexes with Hsp90 and also aids NBLRR protein folding (Muskett et al., 2002). RAR1 also complexes with Hsp90 and enables sufficient MLA6 accumulation to provide resistance (Bieri et al., 2004) and has also been shown to aid in the folding of N (Liu et al.,2004). RSI2 is an ATP independent chaperone, separate from this complex, the silencing of which prevents I-2 accumulation (Van Ooijen et al., 2010) suggesting it also aids in NBLRR protein folding.

SGT1 (suppressor of the G2 allele of Skp1) is an HSP90 specific adaptor that helps form the Hsp90 complex (Kadota et al 2008). Rx1 has been shown to associate with SGT1. SGT1 also binds the SCF complex. SCF complexes are ubiquitin E3 ligases that target proteins for proteosomal degradation. The protein COP9 is known to interact with this promoting protein recycling. Both COP9 and the SCF complexes are also known to interact with NBLRR proteins such as N (Cheng et al., 2011, Liu et al., 2002). It is thought that SGT1 mediates NBLRR proteins between the Hsp90 complex for proper folding, and the SCF complex for degradation to prevent the build-up of harmful excess of misfolded NBLRR protein.

1.7.3 Regulators of NBLRR localisation

Regulation of NBLRR protein localisation has also been linked to interacting proteins. The aforementioned SGT1 is also required for nucleocytoplasmic distribution of Rx1 and N. Silencing of SGT1 results in a cytoplasmic accumulation of Rx1 (Slootweg et al., 2010). It is hypothesised that SGT1 ensures proper folding of NBLRR proteins before they are trafficked into the nucleus away from the cell's protein folding regulators.

The CC domain of Rx1 has been shown to interact with the protein RanGap2 (Sacco el al., 2007). The regions of the CC domain flanking a conserved EDVID motif rather than the motif itself have been found to be required for this interaction (Rairdan et al., 2008). It has been hypothesised that RanGap2 is required to help maintain the nucleocytoplasmic distribution of Rx1 that is required for protein function. The CC domain is known to favour a nuclear localisation of Rx1 and the LRR a cytoplasmic (Slootweg et al., 2010).

1.7.4 Potential DNA binding regulators

Section 1.5.3 describes a potential DNA binding activity of Rx1. Some R proteins are known to interact with transcription factors that could be regulators of an NBLRR DNA binding activity. Interaction between MLA10 and its cognate effector A10 has been shown to lead to an interaction with the transcription factors WRKY and MYB6 (Shen et al., 2008, Chang et al., 2013). WRKY acts as a suppressor of PTI and MYB6 as a promoter. The MLA10 interaction suppresses the suppressor WRKY activity and

promotes MYB6 (Chang et al., 2013). However, section 1.5.5 described the use of a WRKY domain as an integrated decoy in RRS1, and the possibility of these transcription factors being guardee proteins for MLA10 has not been excluded.

1.8 NBLRR protein oligomerisation

Section 1.5 stated that many STAND proteins are known to initiate signalling transduction through the formation of a diverse array of oligomeric structures, and it has been hypothesised that this is also the case for NBLRR proteins. Indeed, there are some known examples of NBLRR proteins oligomerising to initiate signal transduction. The Pto-Prf complex described in section 1.7.1 is known to be oligomeric, with the activation of ETI signalling caused by Pto proteins phosphorylating each other within the oligomer (Ntoukakis et al., 2013). N from tobacco is also known to oligomerise when initiating signalling transduction in the presence of the viral elicitor p50 and its guard NRIP1 (Mestre et al., 2006). Finally, RPS5 has also known to self-associate to form dimers or possibly oligomers using co-immunoprecipitation via all three of its archetypal domains (Ade at al., 2007). Many examples of dimerisation are known to be mediated by CC and TIR domains, and these have been shown to be sufficient to initiate HR (Bernoux et al., 2011, Maekawa et al., 2011, Williams et al., 2015, see Sections 1.4.1 and 1.4.2).

However, this activity like many others is not universal across all NBLRR proteins: The CC domain of Rp1 has been shown to initiate HR and self-associate, like many other NBLRR CC domains. However, mutants deficient in self-association are not deficient in HR. This implies Rp1 can initiate HR in a monomeric state, and

dimerization may not be required for the protein to function (Wang et al., 2015). Additionally, RNBS-A mutants of N, compromised in putative nucleotide hydrolysis activity, are unable to initiate ETI. They can, however, still oligomerise. Hence, oligomerisation in and of itself is not sufficient to induce ETI in this instance (Mestre et al., 2006).

1.9 Interdomain interactions

The different NBLRR domains are known to be involved in many interdomain interactions that help to regulate protein function. Co-immunoprecipitation experiments have shown the Rx1 NBARC domain to interact with Rx1 LRR when expressed in trans (Bendahmane et al., 2002), specifically between the ARC-2 subdomain and the N-terminal region of the LRR domain (Rairdan et al., 2006). Rx1 CCNBARC binds the Rx1 LRR domain in the absence but not presence of its cognate effector CP106 (Moffet et al., 2002), suggesting the interaction with the LRR is inhibiting CCBARC activation and this inhibition is released by the effector.

Mutations to the ARC-2 region responsible for this interaction, such as the D to V mutation to the MHD motif and mutations to the RNBS-D motif, result in protein autoactivity (Bendahmane et al., 2002). The ARC2 region is hence thought to mediate changes from the LRR to the NBARC domain, repressing NBARC activity in the absence of the effector and activating it in its presence.

Coevolution between interacting domains maintains this interaction. Incompatibility results in autoactive protein lethal to the plant cell and this results in a strong selection pressure for interacting domains. Changes in sequence in one domain that would

compromise the interaction are compensated for by changes in the other domain. This effect can be seen in studies examining interactions between NBARC and LRR domains of 2 different NBLRR proteins. For example RPS5 and RPS2 NBARC and LRR domains will interact but the resulting chimera is autoactive, showing that inhibition has been compromised by their divergent sequences (Qi et al., 2012). More closely related NBLRR proteins, however, such as Rx1 and Gpa2 (both from the same gene locus in tomato, and displaying high sequence similarity) will interact to form a functional autoinhibited protein (Slootweg et al., 2013).

These interactions between different NBLRR protein domains have been used as a tool to characterize the interaction. In Rx1 and Gpa2 these interactions were modelled to be between an acidic loop in the ARC2 region and the N-terminal charged region of the LRR (Slootweg et al., 2013). Stepwise truncation of RPS5 LRR domain shows the 4 N-terminal repeats responsible for the interaction (Qi et al., 2015). Mutations to the *p*-loop do not affect LRR binding (Rairdan et al., 2006), however some mutations to the Rx1 nucleotide-binding pocket have been shown to broaden the range of pathogens that activate the protein, showing again that sequence variations within the two domains changes the dynamic of this interaction (Harris et al., 2012). These studies have led to the conclusion that the LRR domain has an autoinhibiting effect on the NBARC domain, maintaining an 'off' configuration with regards to nucleotide hydrolysis. This maintains a stable resting state in the protein that prevents premature activation of the protein and cell death.

Interactions between other domains are also important for protein function. The Rpm1 CC interacts with the NBARC domain. This inhibits CC mediated HR, showing that

in certain cases the NBARC domain can also have an autoinhibitory role. Mutation of the conserved EDVID motif within the CC domain reduced the strength of this interaction and restores HR. (Wang et al., 2015). The CC domain has also been shown to interact with both the LRR and NB domains of Rx1 using co-immunoprecipitation. The EDVIV motif within the CC domain has been shown to be required for this interaction (Rairden et al., 2008). The LRR domain does not interact with the CC domain in Rpm1 (Wang et al., 2015) showing that there are differences in interdomain interactions between different NBLRR proteins.

Novel domains in NBLRR proteins can also play a role in autoinhibition. Section 1.4.5 described a class of NBLRR proteins in *Solanaceous* plants with a novel N-terminal SD domain. This SD domain (specifically an SD2 subdomain) interacts with the CC domain in Mi1.2 and inhibits its HR activity (Lukasik-Shreepaathy et al., 2012).

1.10 A model of archetypal NB-LRR function

This leads us to an archetypal model of a protein switch, moderated by a nucleotide binding/hydrolysis activity in the central NBARC domain. This activity is autoinhibited by the LRR domain in a resting state. Effector/guard/decoy binding then results in a conformational shift in the LRR domain. This weakens the interaction with the NBARC domain, which in turn ends LRR mediated inhibition of the NBARC domain nucleotide hydrolysis/exchange activity. The resulting conformational shift within the NBARC domain to an 'ON' state, associated with nucleotide hydrolysis/exchange, ends NBARC domain inhibition of the CC/TIR effector domain (Figure 6). The activated protein then initiates defence signalling by an unknown

mechanism through the TIR/CC effector domain, possibly DNA binding, to initiate ETI and HR. Every step of this is tightly regulated by a range of interacting proteins to help prevent premature activation and cell death.

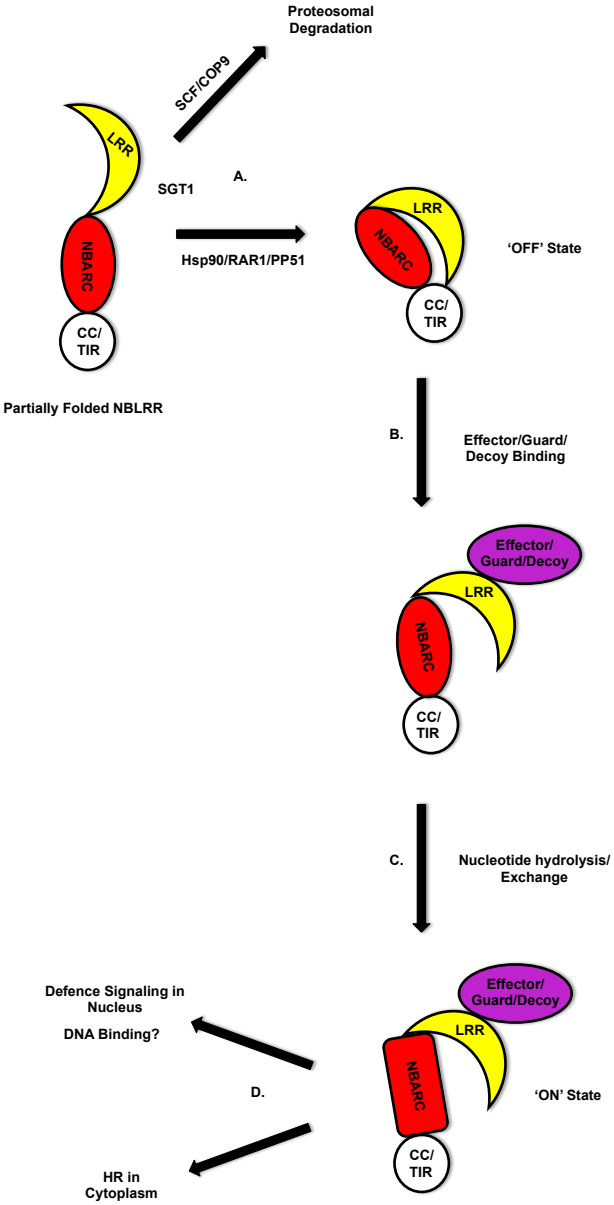

Figure 6. A simplified model of archetypal NB-LRR protein function. Adapted from Takken et al., 2010 A. SGT1 mediates between correct folding of the NBLRR protein by chaperones and proteosomal degradation of excess protein. B. The protein remains in an autoinhibited 'off' state by interdomain interaction until activation by effector/guard/decoy protein binding releases these via a conformational shift. C. Some form of nucleotide hydrolysis/exchange in the uninhibited NBARC domain induces a conformational shift to the 'ON' state. D. The activated NBLRR protein induces HR and defence signalling through an unknown mechanism, possibly DNA binding.

1.11 Conclusion

NBLRR proteins are a large family of plant immune receptors that mediate an extreme form of defence signalling. They are characterised by their three domains: an N-terminal CC or TIR domain, believed to be an effector domain; a middle NBRAC domain, thought to act as a molecular switch to toggle the protein between an active an inactive state; and finally a C-terminal LRR domain believed to be involved in pathogen sensing.

The mechanism through which NBLRR proteins initiate defence signalling is currently unknown. There is evidence that the central NBARC domain is involved in DNA binding and unwinding in the NBLRR proteins Rx1 and I-2, and this could indicate these proteins acting as transcription factors to initiate the defence response.
However, currently the immunological effect of any DNA binding activity remains unknown.

It should also be noted that there can be a high degree of variability between different NBLRR proteins in sequence, structure, subcellular localisation and biochemical

activity. What is known to be the case for one NBLRR protein cannot be generalised to all or even many others without further supporting evidence.

This thesis describes experiments with the aim of demonstrating Rx1 DNA binding activity in plant leaf material. This shall determine if the *in vitro* activity previously shown is biologically relevant, and what affect this activity has on Rx1 triggered immunity. Experiments with the aim of describing how any Rx1 DNA binding activity in plants is regulated are also described.

Aims and Objectives

Previous work had shown plant NBLRR proteins binding DNA *in vitro* (Fenyk et al., 2015). It was hypothesised that NBLRR proteins bind DNA *in planta* and that this activity plays a role in the currently unknown mechanism through which they initiate defence signalling. This thesis describes experiments with the aim of demonstrating the DNA binding activity of the potato NBLRR protein Rx1 *in planta*, determining which protein domains are responsible for DNA binding, under what biological conditions DNA binding occurs. Additionally, experiments that attempt to identify proteins that interact with Rx1 to regulate its DNA binding activity are described. Together, these experiments aim to build a model of how Rx1 specifically and NBLRR proteins in general might initiate defence signalling through DNA binding.

2. Materials and Methods

2.1 Chemical reagents and equipment

All materials purchased were from sigma unless otherwise stated.

2.2 DNA methods

2.2.1 PCR

DNA fragments were amplified using Phusion polymerase (Thermo Scientific). The PCR reaction mixture was set up as per the manufacturer's instructions. The reaction was heated to 95 °C for 2 min. It was then annealed at 58° C for 1 min, elongated at 72 °C for 30 seconds per kilobase of DNA in the fragment, and then denatured at 95 °C for 1 min. This was repeated for 30 cycles, after which the reaction was cooled to 4 °C. The product was resolved using agarose gel electrophoresis (2.2.11).

2.2.2 LR and BP gateway cloning Reactions

PCR product (10 ng) was mixed with 100 ng of target vector in a total reaction volume of 8 µl with TE reaction buffer pH 8.0. 2 µl of the appropriate Clonase enzyme mix (Invitogen) was added (Gateway® LR Clonase® II enzyme mix and Gateway® BP Clonase® II enzyme mix respectively) and the mixture incubated at 25 °C for 1 hour. 1 µl of Invitrogen proteinase K mixture (2 µg/µl proteinase K) were added and the mixture incubated at 37 °C for 10 min.

2.2.3 Miniprep of plasmid DNA

The manufacturer's instructions were used (Qiagen Miniprep kit), and the product quantified using a Nanodrop spectrophotometer (2.2.12).

2.2.4 Preparation of chemically competent *E. coli* via $CaCl_2$

LB containing the appropriate antibiotic (100 ml) was seeded with 2 ml of overnight *E. coli* culture and grown to OD_{600}= 0.5 at 37°C and 200 rpm. The culture was cooled to 4°C and centrifuged at 4000 g for 10 min at 4°C. The supernatant was discarded and the pellet resuspended in 50 ml of a solution of 20 mM $CaCl_2$, 80 mM $MgCl_2$ at 4°C. This was again centrifuged at 4000 g for 10 min at 4°C, the supernatant discarded and the pellet resuspended in 4 ml of 100 mM $CaCl_2$, 20% (v/v) glycerol. The resulting suspension of competent *E. coli* was separated into 80 µl aliquots and frozen at -80°C until further use (Sambrook et al., 1989).

2.2.5 Transformation into *E. coli*

Between 10 to 150 ng of DNA were added to 80 µl of *E. coli* cells made competent with $CaCl_2$ (2.2.4). This was incubated on ice for 20 min, then heat shocked at 42°C for 45 seconds before being returned to ice for 2 min. 1 ml of SOC media at 37°C was added and the resulting mixture incubated at 37°C for 1 hour. 100 µl of culture was spread onto an LB agar plate containing the appropriate antibiotic. The remaining culture was centrifuged at 4000 g for 5 min, the supernatant discarded, and the pellet resuspended in 100 µl of SOC media. This was spread onto another LB agar plate containing the appropriate antibiotic. Plates were incubated overnight at 37°C (Sambrook et al., 1989).

2.2.6 Colony PCR

A 25 µl reaction mixture was setup containing 17 µl of milliQ water, 2.5 µl of dNTPs (200 µM), 2.5 µl 10x Taq Bioline Red reaction buffer, 1.5 mM $MgCl_2$, 1 µl of each primer (1 ng/µl) and 0.5 µl (2.5 units) of Taq Bioline Red polymerase. A pipette tip was then touched to a colony and dipped into the reaction mixture. The mixture was then subjected to PCR with the same reaction conditions as 2.2.1.

2.2.7 Agarose gel electrophoresis

DNA solution (20 µl) was loaded onto a 1 % (v/w) agarose TAE (40mM Tris, 20mM acetic acid, and 1mM EDTA) gel containing 10 ng/ml ethidium bromide. 5µl of DNA Hyperladder 1 (Thermo-Scientific) was added to an adjacent lane to resolve fragment size. The gel was then run in TAE buffer for 20 min at 120 V. The DNA bands were then visualized under UV light.

2.2.8 DNA purification from an agarose gel

The desired band was excised from the gel and transferred to a 1.5 ml eppendorf tube. 1 ml of DNA binding buffer (6 M sodium perchlorate, 50 mM Tris-HCl pH 8.0, 10 mM EDTA) was added and the mixture incubated at 60°C for 30 min to dissolve the agarose. 8 µl of DNA binding matrix was added and the mixture incubated at 20°C for half an hour (30 min) with regular agitation. The mixture was microfuged for 1 min at 13,500 g and the supernatant discarded. The pellet was washed once with 125 µl of DNA binding buffer, and then twice with 750 µl of DNA wash buffer (20 mM Tris-HCl p.H. 7.5, 2 mM EDTA, 400 mM NaCl, 50% (v/v) ethanol). The resulting pellet was dried for 5 min at 37°C before being resuspended in 15 µl of water. This was

incubated for 10 min at 37°C before being microfuged for 1 min at 13500 g. The supernatant was removed and the pellet discarded.

2.2.9 Preparation of bacterial glycerol stocks

A 5 ml culture of bacteria containing the desired construct was grown overnight in LB media with the appropriate antibiotic in an shaking incubator at 30°C and 200 rpm. This was centrifuged at 4000 g for 5 min and the supernatant discarded. The pellet was resuspended in YEB media with 40% (v/v) glycerol and then frozen at -150°C.

2.2.10 Preparation of chemically competent *Agrobacterium tumefaciens* GV3101 via $CaCl_2$

A 5 ml culture of *A. tumefaciens* GV3101 in YEB media was grown overnight in a shaking incubator at 30°C and 200 rpm. This was added to 50 ml of YEB and the mixture incubated at 30°C and 200 rpm until $OD_{600} = 0.5$. The culture was centrifuged at 4000 g for 5 min. The supernatant was discarded and the pellet resuspended in 25 ml of 4°C 150 mM NaCl. The suspension was incubated on ice for 15 min before centrifugation for 5 min at 4000 g. The supernatant was discarded, and the pellet resuspended in 20 ml $CaCl_2$ and aliquoted into 100 µl portions. These were frozen on dry ice and then either used immediately for transformation or stored at -80 °C.

2.2.11 Transformation into *Agrobacterium tumefaciens* GV3101

A 100 µl aliquot of competent *Agrobacterium tumefaciens* GV3101 was thawed on ice and 1 µl of the appropriate construct added. The cells were frozen on dry ice, and then incubated at 37°C for 5 min. 1 ml of YEB medium was then added and the culture grown in a shaking incubator for 2-4 hours at 30°C and 200 rpm. The cultures were centrifuged at 800 g for 3 min and spread onto a YEB plate containing the appropriate antibiotic, which was incubated at 30°C for 2 days.

2.2.12 Determination of DNA Concentration Via Nanodrop Spectrophotometer

A Nanodrop spectrophotometer (Thermo-Scientific) was blanked using 2 µl of milliQ water. 2 µl of DNA solution were placed on the Nanodrop and the absorbance measured at 260 nm with 260:280 nm absorbance ratio used to assess purity.

2.2.13 Cloning of *GFP-NbMLHP* and *GFP-NbGLK1*

Template DNA was amplified via PCR (section 2.2.1)(primers 1,2 for *Nb*MHP, 3,4 for *Nb*GLK1, see Table 3), inserting *attr1* and *attr2* recombination sites. The reaction was separated via agarose gel electrophoresis (section 2.2.7) and purified (section 2.2.8). Construct DNA was inserted into a pDONR207 entry vector using a BP clonase reaction (section 2.2.2) and transformed into chemically competent DH5α *E. coli*. Colonies were tested for the presence of pDONR207 containing construct via colony PCR (see Section 2.2.6, primers 1,5 for *Nb*MHP, 3,5 for *Nb*GLK1). Construct was purified from positive colonies via miniprep (section 2.2.3). The construct was then inserted into pK7WGF2 destination vector via LR clonase reaction (section 2.2.2). This mixture was transformed into chemically competent DH5α *E. coli*. Colonies were

tested for the presence of pK7WGF2 containing construct via colony PCR (section 2.2.6) (primers 1,6 for *Nb*MHP, 3,6 for *Nb*GLK1). The completed vector was then purified via miniprep (section 2.2.3) and transformed into competent *A. tumefaciens* GV3101 for infiltration.

Table 3. Primers used in the construction of GFP-*Nb*MLHP and GFP-*Nb*GLK1

Primer No.	Description	Sequence	Sense/ Antisense
1	*Nb*MLHP Forward	GGGGACAAGTTTGTACAAAAAAGCAG GCTACATGGAAAAAGAGTACGGC	Sense
2	*Nb*MHLP Reverse	GGGGACCACTTTGTACAAGAAAGCTGG GTCACCTCCTTGACCGTTTCTTTG	Anti-sense
3	*Nb*Glk1 Forward	GGGGACAAGTTTGTACAAAAAAGCAG GCTACATGCTAACTATATCACCTTTG	Sense
4	*Nb*Glk1 Reverse	GGGGACCACTTTGTACAAGAAAGCTGG GTCATGGAGGTATTTTATTAATC	Anti-sense
5	pDONR207 Internal	TCGCGTTAACGCTAGCATGGATCTC	Sense
6	pK7WGF2 Internal	CTGCTGGAGTTCGTGACC	Sense

2.3 Plant Methods

2.3.1 Infiltration of *Nicotiana Benthamiana* via *Agrobacterium tumefaciens GV3101*

A 5 ml *Agrobacterium tumefaciens GV3101* culture in YEB media with the appropriate antibiotic (see Table 4.) was grown overnight in a shaking incubator at 30°C and 200 rpm. This mixture was centrifuged at 2,500 g for 5 min and the supernatant discarded. The pellet was washed twice in 2 ml of infiltration buffer (10 mM MES p.H. 6.5, 10 mM $MgCl_2$, 200 μM acetosyringone) before being resuspended in 2 ml of infiltration buffer and incubated for 2-3 hours at 20°C. The mixture was infiltrated into 3 week

old *N. benthamiana* leaves at an OD_{600} of 0.01-0.5, by pressing a 2 ml syringe to the underside of the leaf and exerting a counter pressure with a finger on the other side.

Table 4. Plasmid constructs used for infiltrations in the experiments described in this thesis with the vector they are contained in, the appropriate antibiotics for an overnight culture, and the source of the vector (see section 2.3.1).

Gene	Vector	Antibiotic Resistance(S)	Origin of Vector
GFP	pK7WGF2	Spectinomycin	Gift of S. Fenyk
GFP-H2B	pK7WGF2	Spectinomycin	Gift of S. Fenyk
GFP-CC	pBin35s	Kanamycin	(Slootweg et al., 2010)
GFP-CC-NBARC	pBin35s	Kanamycin	(Slootweg et al., 2010)
GFP-NBARC	pBin35s	Kanamycin	(Slootweg et al., 2010)
GFP-NBARC-LRR	pBin35s	Kanamycin	(Slootweg et al., 2010)
LRR-GFP	pBin35s	Kanamycin	(Slootweg et al., 2010)
GFP-Rx1	pBin35s	Kanamycin	(Slootweg et al., 2010)
CP106	pBin35s	Kanamycin	(Slootweg et al., 2010)
CP105	pBin35s	Kanamycin	(Slootweg et al., 2010)
Pto/AvrPto	pLSU-16	Tetracycline	Gift of F. Takken
GFP-Rx1-nls	pBin35s	Kanamycin	(Slootweg et al., 2010)
GFP-Rx1-nes	pBin35s	Kanamycin	(Slootweg et al., 2010)
GFP-Rx1 D460V	pBin35s	Kanamycin	(Slootweg et al., 2010)
GFP-Rx1 CCNBARC K176R	pBin35s	Kanamycin	(Slootweg et al., 2010)
GFP-Rx1 CCNBARC S202F	pBin35s	Kanamycin	Gift of E. Slootweg
GFP-Rx1 CCNBARC D225E	pBin35s	Kanamycin	Gift of E. Slootweg
*Nb*GLK1-HA	pBin35s	Kanamycin	Gift of P. Townsend
Rx1-HA	pBin35s	Kanamycin	(Slootweg et al., 2010)
GFP-*Nb*GLK1	pK7WGF2	Spectinomycin	Section 2.2.16
PVX:GFP	pGR208	Kanamycin	(Peart et al., 2002)
p19	pBin61	Kanamycin	(Voinnet et al., 2003)
GFP-LRR-HA	pBin35s	Kanamycin	Gift of E. Slootweg
AvrRPS4-HA	pBin35s	Kanamycin	Gift of D. Baulcombe
*Nb*MLHP-HA	pBin35s	Kanamycin	Gift of P. Townsend
GFP-*Nb*MLHP	pK7WGF2	Spectinomycin	Section 2.2.16
*Nb*MLHP-HA Y335F	pBin35s	Kanamycin	Gift of P. Townsend
*Nb*MLHP-HA E385L	pBin35s	Kanamycin	Gift of P. Townsend

2.3.2 Preparation of Leaves for TCSPC

N. benthamiana leaves were infiltrated with *Agrobacterium tumefaciens* as described previously (see section 2.3.1) at the appropriate OD_{600}. The plants were grown for 3 weeks at 25°C with 16 hours of light. The leaves were infiltrated with 10 g/ml LDS-751 dye in infiltration buffer before being fixed in 4% formaldehyde (v/w) in PBS overnight at 20°C in the dark. The leaves were then quenched with 125 mM glycine in PBS for 1-2 hours at 20°C in the dark, and stored in PBS in the dark at 4°C until use.

2.3.3 TCSPC Data Collection

A section of the leaf was excised, mounted onto a microscope slide and data collected using a modified Zeiss Axiovert inverted epifluorescence microscope. The GFP fluorophore was excited with a Picoquant pulsed diode laser LDH-P-C-440 at 440nm, 70 ps pulse FWHM at 20 MHz. This was focused on the leaf using a Zeiss 100x oil immersion Ph3 lens. The emission of the sample was detected using an Id Quantique 100-50 counting module with a Carl Zeiss bp510 nm filter to block unwanted sources of fluorescence. Readings were taken for an hour each at 2 points on each leaf and data was collected from 6-11 leaves per construct. The data was re-convoluted using a Decay Analysis Tool Vs 1.2.1 for Microsoft Excel on PC. The instrument response function was pasted into the 'Inst. Resp. Raw Data' column, and the photon counts from channels 1069 to 2100 were pasted into the 'Raw measured Data' column. These were the channels that produced a decay that corresponded closest to the instrument response function. A Grindvald-Steinberg re-convolution routine was used to fit an instrument response to the lifetime decay profile. The data were fitted to a sum of exponentials using an iterative least squares reconvolution procedure with the

optical/electrical excitation profile to produce a biexponential decay containing two lifetimes. If the solver failed to return a result, the parameters of the instrument response were adjusted one at a time to produce a closer fit and the solver run again. The parameters were Amp (Amplitude) 1, Amp 2, Amp 3, Amp 4, Tau (lifetime) 1, Tau 2 Tau 3, Dback, iback and shift. If modifying the parameters failed to return a solution the channels the data was taken from were adjusted to provide a better fit with the instrument response. These steps were repeated until a suitable solution was generated to re-convolute the data. A ratio of the yield of the two main lifetimes (at 0.25-0.9 ns and 1.1-1.6 ns respectively) was calculated for each data set. If the solver generated 2 lifetimes the same to 4 decimal places, they were treated as the same lifetime and summed together before the ratio was calculated. If a longer lifetime of 2-3 ns was detected instead of a 1.1-1.6 ns lifetime, the yield of this longer lifetime was used instead. An average lifetime ratio for each leaf (the individual replicate) was then calculated from the ratio of the two points data was recorded from. An average ratio for each construct was then calculated from the average ratio of each leaf. Statistically significant variations in lifetime ratios between constructs were then determined via ANOVA. To generate an intensity reading for the measured fluorescence decays, the decays were integrated using the trapezium rule (Atkinson, K.E., 2008). treating the area between each time channel as a trapezium.

2.3.4 *Nicotiana benthamiana* Hypersensitive Response (HR) Assay

N. benthamiana leaves were infiltrated with *Agrobacterium tumefaciens* as described previously (2.3.1) at the appropriate OD_{600}. The plants were then grown for 4 days at 25°C with 16 hours of light. The leaves were harvested, visually inspected, photographed and scored 1-5 for cell death; 1 being no visual sign of any cell death

whatsoever in the infiltrated region. 5 being complete cell death throughout the infiltrated region (see Figure 7. for scale). 24 leaves were infiltrated and scored for each set of constructs and statistically significant variations in cell death scores calculated via ANOVA.

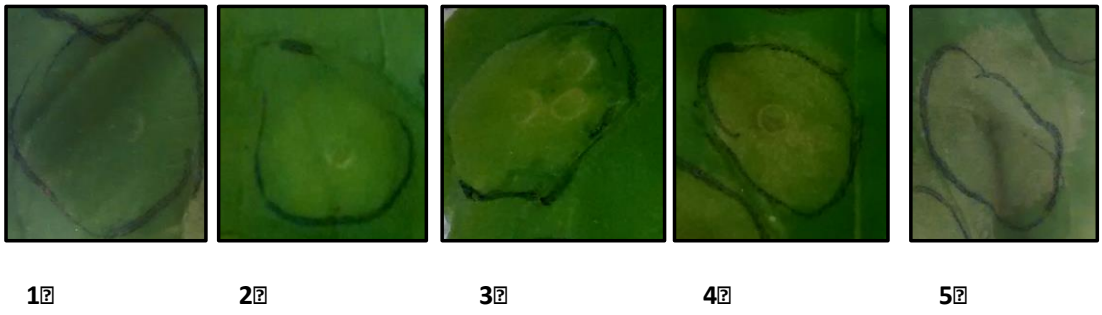

Figure 7. A scale of scored cell death in infiltrated *N. benthamiana* leaves from no visible cell death (1) to complete cell death across the entire infiltrated area (5).

2.3.5 Fluorescence Viral Replication Assay

Different regions of a single *N. benthamiana* leaf were infiltrated (see section 2.3.1) with fluorescently tagged PVX virus both mixed with and without the appropriate test constructs. Leaves were grown for 4 days and then harvested. For each infiltrated area, 3 different 10 mm leaf discs were cut out and placed in a 96 well plate. The fluorescence intensity of each leaf disc was measured using a synergy H4 plate reader, exciting at 410 nm and measuring emission at 550 nm with a 20 nm bandwidth. An average of the fluorescence intensities for the 3 leaf discs were then calculated to give a value for each infiltrated area. The fluorescence of each area was then normalised to the control area on each leaf infiltrated with only fluorescent PVX. 8-20 leaves were infiltrated and measured for each set of constructs and statistically significant variations in fluorescence intensity assessed via ANOVA.

2.4 Protein Methods

2.4.1 Sodium dodecyl sulfate poly-acrylamide gel electrophoresis (SDS-PAGE)

0.75-1.5 mm thick resolving gels were used with 10% acrylamide (v/v), 375 mM Tris-HCl pH 8.8, 0.1 % SDS (w/v), 0.1% APS (w/v), 0.01 % TEMED (v/v). Stacking gels were made with 5 % acrylamide (v/v), 130 mM Tris-HCl pH 6.8, 0.1 % SDS (w/v), 0.1% APS (w/v), 0.01 % TEMED (v/v). Samples were mixed 4:1 with SDS-PAGE loading buffer (250 mM Tris-HCl pH 6.8, 10 % (w/v) SDS, 0.5 % (w/v) bromophenol blue, 50 % (w/v) glycerol, 500 mM DTT), incubated at 95°C for 3 min and 10-20 µl loaded into each lane of the gel. 5 µl of protein ladder (SDS PAGE ruler plus, thermo scientific) was added an adjacent lane to establish protein size. The gels were then run at 160 V for 40 min in running buffer (25mM Tris-HCl pH 8.35, 192 mM glycine, 0.1 % (w/v) SDS) (Sambrook et al., 1989).

2.4.2 Western blotting

Protein was resolved via SDS-PAGE (see section 2.4.1) and then transferred to a nitrocellulose membrane overnight at 55 V in transfer buffer (25 mM Tris-HCl pH 8.35, 192 mM glycine, 20 % methanol (v/v)). The membrane was then blocked with blocking buffer (5 % (w/v) milk in phosphate buffered saline solution with 0.1 % (v/v) Tween 20 (PBST)). The membrane was washed in blocking buffer containing primary antibody at the appropriate dilution (see Table 5) for 2 hours, and then washed 3 times with PBST for 5 min each to remove any background antibody binding. If secondary antibody was required, the membrane was incubated at the appropriate dilution (see Table 5.) in blocking buffer for 45 min, and washed 3 times in PBST for 5 min to

remove background. The signal was detected using enhanced chemiluminescence (ECL) detection system (GE Healthcare) (Sambrook et al., 1989).

Table 5. Antibody dilution factors in blocking buffer for western blot staining.

Antibody	Dilution Factor in Blocking Buffer
Rabbit Anti-Myc	1 in 5000
Goat Anti-GFP	1 in 5000
Rabbit Ant HA, HRP Fused	1 in 1000
Mouse Anti-Rabbit, HRP Fused	1 in 20 000
Mouse Anti-Goat, HRP fused	1 in 20 000

2.4.3 Co-immunoprecipitation

0.1 g of infiltrated *N. benthamiana* leaves (see section 2.4.1) were ground up on dry ice in extraction buffer (50 mM Tris-Cl pH 7.5, 50 mM NaCl, 20 % glycerol (v/v), 0.1 % Tween 20 (v/v), 0.1 mM DTT, 2.5 % PVPP (w/v) 1% protease inhibitor cocktail (v/v) (Sigma)) using a pestle and mortar. The mixture was then centrifuged at 13,000 g for 10 min at 4°C. The supernatant was passed through a Sephadex G25 column and plant protease inhibitor cocktail (Sigma) added (1 % v/v). The mixture was then incubated with 60 µl rabbit anti-Ig agarose (Sigma) for 1 hour at 4°C, and centrifuged at 13,000 g for 1 min at 4°C. The pellet was discarded and the supernatant added to 60 µl of anti myc-agarose (sigma) and incubated for 2 hours at 4°C. The mixture was washed 3 times with G25 buffer (50 mM Tris-Cl pH 7.5, 50 mM NaCl, 20 % glycerol (v/v), 0.1 % Tween 20 (v/v), 0.1 mM DTT) to remove non-specifically bound material. Protein was eluted from the resin by incubating with 60 µl of elution buffer (50 mM NaOH) for half at hour at 4°C, and then microfuging at 4000 g for 4 min at 4°C. The eluent was then analysed via Western blotting (see section 2.3.2).

2.4.4 Yeast Two-Hybrid Screen

The Yeast two-hybrid screen was performed by Hybrigenics service SAS. Bait protein was cloned into a pB27 bait plasmid as a C-terminal fusion to LexA (pB27 construction is described in Formstecher et al., 2005). The initial screen was performed against a random-primed mixed tissue *Nicotiana benthamiana* cDNA library constructed into a pP6 prey plasmid (pB27 construction is described in Formstecher et al., 2005). 96 Million clones were screened giving 9-fold library coverage using a mating approach with Y187 (matα) and L40 GLl4 (mata) yeast strains. Positive clones were selected on medium lacking leucine, tryptophan, and histidine. Positive clones were picked, sequenced, and overlapping sequences combined to generate a Selective Interacting Domain (SID) that represented one interaction. Each interaction was assessed computationally for the probability of a non-specific interaction. This assessment gave each interaction a PRBS (predicted biological score) from A (lowest probability of non-specificity) to E (highest probability of non-specificity) (see Table 6). To confirm protein-protein interactions, freshly transformed yeast colonies were resuspended in 1 mL sterile deionized water, and 10 µL aliquots were spotted onto medium lacking leucine and tryptophan (−L/−W) and medium lacking leucine, tryptophan, histidine (−L/−W/−T), supplemented with 10 or 50 mM 3-Amino-1,2,4-triazole (3-AT). Growth was scored after 5 to 7 d of incubation at 28°C.

Table 6. Definition and explanation of each category of Predicted Biological Scores (PRBS) generated by computational analysis to judge the reliability of each interaction generated by the initial yeast two-hybrid screen (Formstecher et al., 2005)

Global PRBS (for Interactions represented in the Screen)		**Nb**	**%**
A	Very high confidence in the interaction	6	7.60%
B	High confidence in the interaction	2	2.50%
C	Good confidence in the interaction	3	3.80%
D	Moderate confidence in the interaction This category is the most difficult to interpret because it mixes two classes of interactions: - False-positive interactions - Interactions hardly detectable by the Y2H technique (low representation of the mRNA in the library, prey folding, prey toxicity in yeast)	68	86.10%
E	Interactions involving highly connected (or relatively highly connected) prey domains, warning of non-specific interaction. The total number of screens performed on each organism is taken into account to set this connectivity threshold: 20 interactions to different bait proteins in our entire database for Human, 10 for Mouse, Drosophila and Arabidopsis and 6 for all other organisms. They can be classified in different categories: - Prey proteins that are known to be highly connected due to their biological function - Proteins with a prey interacting domain that contains a known protein interaction motif or a biochemically promiscuous motif	0	0.00%
F	Experimentally proven technical artefacts	0	0.00%
Non Applicable			
N/A	The PRBS is a score that is automatically computed through algorithms and cannot be attributed for the following reasons: - All the fragments of the same reference CDS are antisense - The 5p sequence is missing - All the fragments of the same reference CDS are either all OOF1 or all OOF2 - All the fragments of the same reference CDS lie in the 5' or 3' UTR		

2.5 Computer Software and Statistical Analysis

Data was analysed using either Microsoft Excel or GraphPad Prism 6.0, with the former being used to calculate averages, standard errors of means and standard deviations and latter being used to produce graphical representations. All error bars shown depict the standard error of the mean. Multiplicity adjusted p-values were calculated using a Dunnett-Wilson Multiple Comparison ANOVA test in Graphpad Prism 6.0 with a 95 % confidence interval. Statistical significance was defined as $p > 0.05$.

3. FRET-FLIM DNA binding assay in fixed *Nicotiana benthamiana* leaves

3.1 Introduction

NBLRR proteins belong to the STAND *p*-loop ATPase AAA+ superfamily. Members of this superfamily, including Cdc6 and Orc-1, are known to have a DNA binding activity (Capaldi et al, 2004). The exact mechanism through which NBLRR proteins induce signal transduction is unknown. Nuclear localisation and interaction with DNA-binding proteins has been shown to be required for signal transduction in several NBLRR proteins; the wheat NBLRR protein MLA-10 has been shown to associate with WRKY and MYB6 transcription factors (Chang et al. 2013), while various NB-LRR proteins have known DNA binding domains, such as leucine zippers, incorporated into their structures (Milligan et al., 1998). It was therefore hypothesised that NB-LRR proteins induce their signal response through a DNA binding activity. This was previously demonstrated *in vitro* using recombinant Rx1 and protein purified from *N. benthamiana* leaves via electromobility gel shift assays and FRET-FLIM on fluorescently tagged oligonucleotides (Fenyk et at., 2015). However, no Rx1 DNA binding activity has been previously described *in vitro*, leaving it possible that this is an artefact of using recombinant protein. This chapter describes the development of a method to investigate protein-DNA interactions *in planta* to further support this hypothesis, ruling out the possibility of an artefact, and elucidating the biological effect of this activity.

In the experiment developed, *N. benthamiana* leaves were infiltrated to transiently express GFP tagged proteins. The DNA binding dye LDS-751 was then infiltrated as a fluorescence energy acceptor, and the leaves fixed. Protein-DNA binding activity

was then measured using FRET-FLIM. FRET-FLIM has been used previously to demonstrate protein-DNA interactions in fixed mammalian cells (Cremazy et al., 2005).

This chapter uses this procedure to present evidence that the NB-LRR protein Rx1 displays a DNA binding activity. This activity stems from the CC and NBARC domains and is activated in the presence of the PVX coat protein, CP106.

3.2 GFP and GFP- H2B fluorescence lifetime analysis

Controls were established against which Rx1 DNA binding *in planta* could be assessed. Free GFP was used as a negative control. The histone H2B is known to bind DNA (Cremazy et al., 2005), and the *Arabidopsis* ortholog of this protein was N-terminally fused to GFP and used as a positive control. Both were transiently expressed in *N. benthamiana* leaves. These were stained with the cell permeable nucleic acid binding dye LDS-751 and fixed in formaldehyde. LDS-751 has an absorption spectrum that overlaps with the emission spectrum of GFP when bound to DNA. Since energy transfer from the GFP to the LDS-751 would result in a decrease in GFP fluorescence lifetime, it was hypothesised that a decrease in GFP fluorescence lifetimes would be observed upon a protein-DNA interaction. The GFP fluorophore was excited at 410 nm and fluorescence decays recorded for both constructs using a microscope adapted for time correlated single photon counting (see Section 2.2.3).

Fluorescence decays showed a decrease in lifetime from the free GFP negative control to the DNA binding GFP-H2B fusion (Figure 8). However, the difference between

most of the resulting fluorescence lifetimes was too small to be measured using single average fluorescence lifetime. Hence, a different, more accurate method of lifetime analysis was developed.

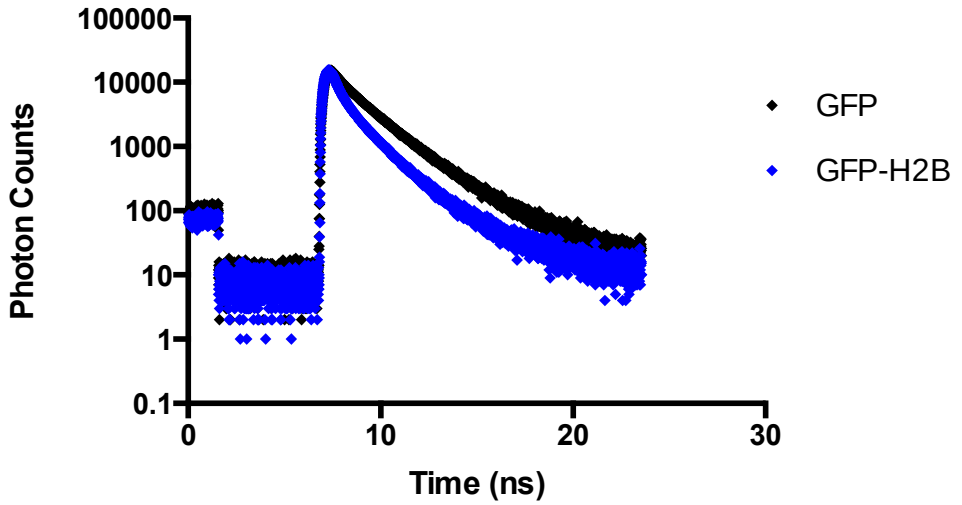

Figure 8: Fluorescence decays produced by exciting fixed *N. benthamiana* leaves infiltrated with GFP and GFP-H2B, respectively, and stained with LDS-751. Leaf samples were excited at 410 nm and fluorescence measured at 510nm . A decrease in fluorescence lifetime can be seen from the free GFP to the DNA binding GFP-H2B as the latter transfers energy to LDS-751.

The fluorescence decays were reconvoluted to determine their constituent lifetimes. For all decays, this resulted in a bi-exponential decay with one lifetime of approximately 0.4 ns and another of approximately 1.2 ns (Figure 9). A shortening of the yield of the longer lifetime towards the decay relative to the shorter was observed from the free GFP to the H2B-GFP. The longer lifetime was hypothesised to be emission of energy via fluorescence, and the shorter lifetime transfer of energy to an adjacent acceptor. Some transfer of energy to an acceptor would still be expected to occur from free GFP due to non-specific interactions with DNA, LDS-751, and any other acceptors naturally present in the plant cell. This shorter lifetime was therefore

always expected to be present in the data set. However, a specific interaction between the construct and DNA would display a far greater amount of energy transfer than any non-specific interaction, resulting in a higher yield in the shorter lifetime.

To measure the decrease in the yield of the longer lifetime, a ratio of the yield of the shorter lifetime to the longer lifetime was calculated (Figure 10.). The GFP-H2B infiltrated leaves showed a statistically significant decrease in the ratio of lifetime yields compared to the leaves infiltrated with free GFP. This demonstrates that energy transfer from the GFP construct to the LDS-751 could be measured upon the protein binding DNA.

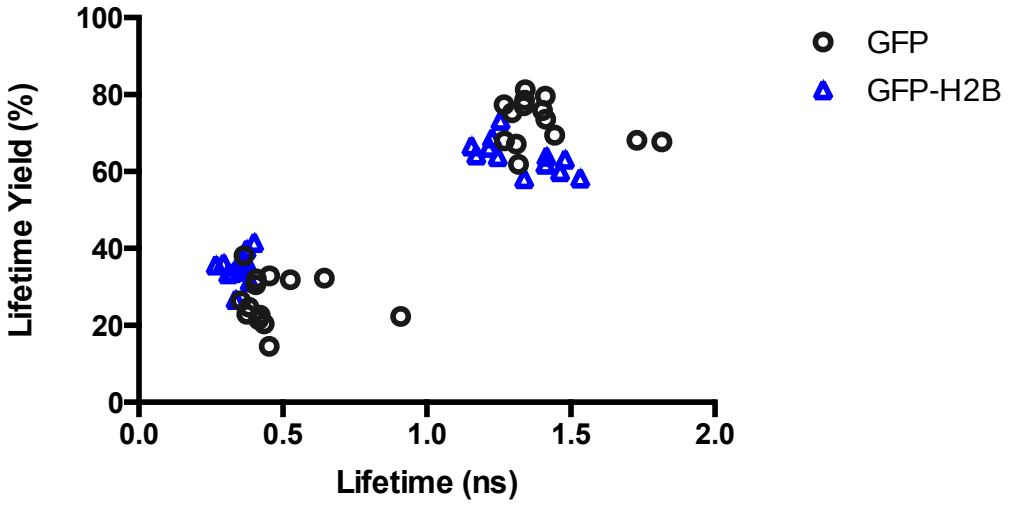

Figure 9: Plot showing the yield of fluorescence lifetimes produced by reconvoluting fluorescent decays of GFP and GFP-H2B infiltrated *N. benthamiana* leaves stained with LDS-751 and fixed with formaldehyde. Each decay contained a longer lifetime at approximately1.2 ns and a shorter at 0.5 ns.

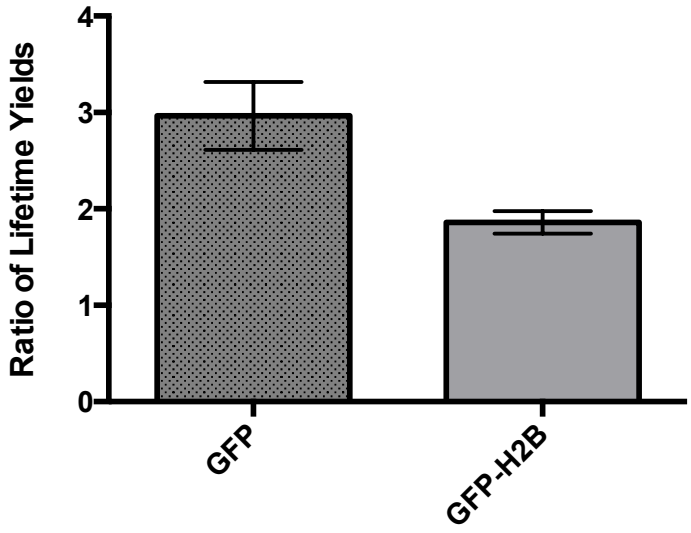

Figure 10: The average ratio of fluorescence lifetime yields (long lifetime yield/ short lifetime yield) of GFP and GFP-H2B infiltrated *N. benthamiana* leaves stained with LDS-751 and fixed with formaldehyde. n = 6-7, $p < 0.05$; Students t test

3.3 Assaying Rx1 domain DNA binding activity with FRET-FLIM

The previous section described the development of a FRET-FLIM DNA binding assay using control constructs. This section describes the application of this method to the different constituent domains of the potato NB-LRR protein Rx1 to determine if they possess a DNA binding activity. The domains were tested first before full-length Rx1 as interactions between the domains in full length protein are known to inhibit immune signalling activity in the absence of the PVX coat protein, CP106 (Slootweg et al., 2013), and it was hypothesised that this may also inhibit any DNA binding activity. Expressing domains individually rather than together allowed any DNA binding activity to be identified in the absence of any autoinihibition.

GFP tagged constructs were expressed in *N. benthamiana* leaves. The leaves were stained with LDS-751 and fixed in formaldehyde. GFP fluorescence lifetimes were

recorded and compared to the control constructs from the previous section. All Rx-1 constructs were N-terminally tagged with GFP, bar the leucine rich repeat domain (LRR), which had been previously demonstrated to only express in *N benthamiana* with a C-terminal GFP tag (Figure 11.) (Slootweg et al., 2010).

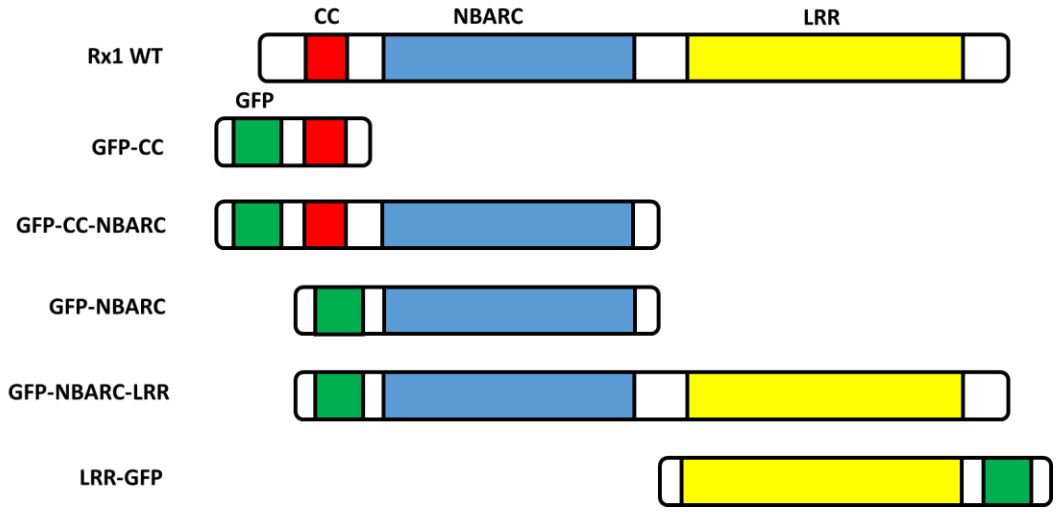

Figure 11: Schematic diagram of wild type Rx1 (top bar) and the truncated GFP tagged Rx1 constructs assayed for DNA binding, indicating the position of protein domains. Coiled coil (CC) domain shown in red, NBARC domain shown in blue, Leucine rich repeat (LRR) domain shown in yellow, and GFP tag shown in green.

A statistically significant difference was observed between free GFP fluorescence lifetimes and all combinations of GFP tagged Rx1 constructs except the LRR repeat on its own (Figure 12.). This demonstrates both the NBARC domain and the CC domain transferring a significant amount of energy to the DNA binding dye in the plant cell, indicating a close physical association with chromatin. The NBARC domain is modelled as showing structural similarity to the DNA binding ATPases Cdc6 and Orc-1 and is hypothesised to be the source of Rx1 DNA binding activity (Fenyk et al.,

2015), suggesting the association with chromatin and energy transfer was coming from this DNA binding activity. The CC domain was not anticipated to also bind DNA, but has been observed previously to interact with a high density complex inside the nucleus that could be chromatin (Slootweg et al., 2010). CC domains are commonly known to be involved in protein-protein interactions (Kohn et al., 1997). The CC domain-DNA interaction could therefore be due to a mediating protein interacting with both, perhaps in a regulatory function (see Chapters 4 and 5). The LRR domain was not hypothesised to possess a DNA binding activity. LRR domains are commonly involved with hydrophobic protein-protein interactions and are thought to be involved with the sensing of pathogen effectors in plant NB-LRR proteins (Takken et al., 2012).

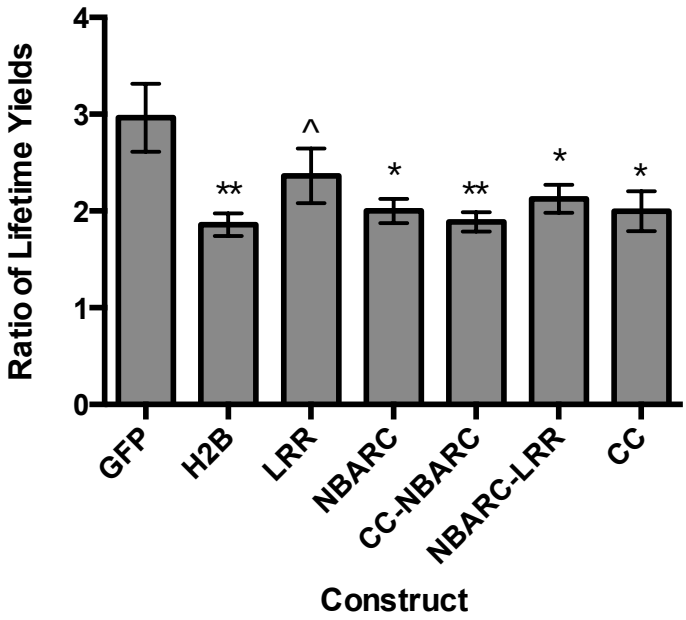

Figure 12: Graph of ratio of lifetime yields of Fixed *N. benthamiana l*eaves infiltrated with GFP tagged Rx1 domains compared with a free GFP control. $n = 6$. ^ indicates adjusted p value > 0.05, * indicates adjusted p value < 0.05, ** indicates adjusted p value < 0.01 calculated using a Dunnett-Wilson Multiple Comparison ANOVA test.

A second means of measuring any FRET occurring was also employed for the constructs of Figure 12; comparing the fluorescence intensity of the 2

fluorophores. More energy transfer would result in a higher intensity of LDS-751 fluorescence relative to GFP fluorescence. The GFP fluorophore was excited at 410 nm and fluorescent decays were recorded for both LDS-751 and GFP emission. The decays were integrated to give a measure of fluorescence intensity, and a ratio of GFP to LDS-751 fluorescence intensity was calculated. This successfully demonstrated a statistically significant difference between both control constructs (Figure 13). Furthermore, this analysis matched the results of the lifetime ratios for all but one Rx1 construct: The NBARC domain by itself showed no statistically significant difference from free GFP, whereas such a difference was observed in the lifetime analysis. This construct also displayed a higher standard deviation of ratio values with this method compared to the lifetime analysis. Variation in protein expression levels impact tests based on fluorescence intensity, but have little effect on changes in fluorescence lifetime. It was concluded that fluorescence intensity readings were less reliable than fluorescence lifetime readings due to the greater impact of protein expression level on the results. Although the influence of altered protein expression levels could be resolved by normalising to protein content through Western blotting it was decided to solely proceed with the quicker lifetime analysis method that did not require normalisation.

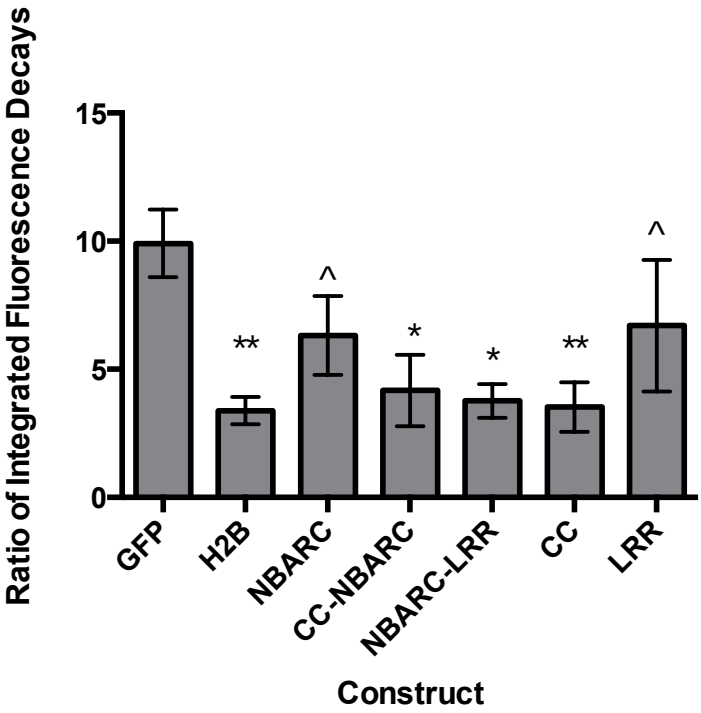

Figure 13: Graph showing the ratio of the integrated fluorescence decays of fixed *N. benthamiana* infiltrated with various GFP labelled constructs. Decays were measured for GFP and LDS-751 fluorescence, and the fluorescence decays recorded integrated to give an intensity measurement. A ratio of LDS-751 to GFP florescence intensity was then calculated to measure energy transfer to the DNA bound dye. $n = 6$. ^ indicates adjusted p value > 0.05, * indicates adjusted p value < 0.05, ** indicates adjusted p value < 0.01 calculated using a Dunnett-Wilson Multiple Comparison ANOVA test.

3.4 Rx1 binds DNA in response to CP106

With the individual domains characterised in section 3.3, this section investigates the behaviour of the full length wild type protein. Full length GFP-Rx1 was assayed both in isolation and when co-expressed with either avirulent or virulent PVX coat protein (CP106 and CP105 respectively (Bendahmane et al., 1995)). Full length Rx1 displayed no statistically significant DNA binding activity by itself, and none with virulent CP105 (Figure 14). But when co-expressed with avirulent CP106, Rx1 DNA binding was induced. This result suggests that the protein exists in an autoinhibitory state with regards to DNA binding, as it does with immune signalling (Rairdan et al., 2008). The

domains interact with each other to hold the protein in an inactive state, preventing the NBARC and CC domains binding DNA. The presence of CP016 in the plant cell then initiates a conformational shift in the protein, allowing DNA binding and potentially initiating immune signal transduction. The absence of a drop in fluorescence lifetimes upon coexpression with virulent CP105 confirms that it is CP106 induced defence signalling that is causing the drop in lifetime ratio, and the result is not merely an artefact of coat protein co-expression.

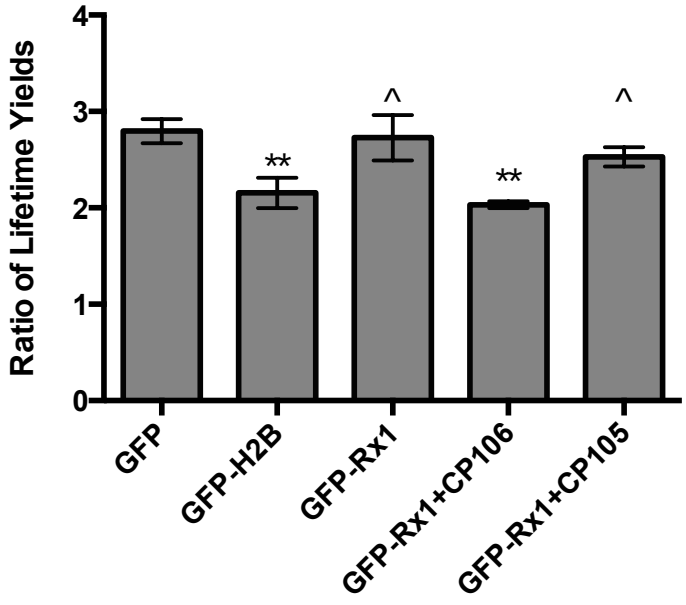

Figure 14: Average ratio of lifetime yields of fixed *N. benthamiana* leaves infiltrated with GFP tagged Rx1 with and without avirulent (CP106) and virulent (CP105) PVX viral coat protein compared to GFP-H2B and GFP infiltrated s controls. $n = 6$. ^ indicates adjusted p value > 0.05, * indicates adjusted p value < 0.05, ** indicates adjusted p value < 0.01 calculated using a Dunnett-Wilson Multiple Comparison ANOVA test.

3.5 Fluorescence lifetimes do not decrease upon non-specific defence activation

Necrosis caused by NLR protein triggered immunity can cause changes in the levels of fluorescent pigments present in *N. benthamiana* leaves such as chlorophyll (Harris et al., 2014). To ensure the changes in lifetimes being observed was not due to such changes, *N. benthamiana* leaves were infiltrated with GFP-Rx1, the tomato NB-LRR protein Pto, and the bacterial effector protein AvrPto. Pto senses AvrPto and induces defence signalling in response (Tang et al., 1996). No change in lifetimes were seen in the leaves expressing GFP-Rx1 alone or GFP-Rx1, Pto and AvrPto together relative to the GFP control expression (Figure 15), but a drop in the ratio of fluorescent lifetimes was observed when GFP-Rx1 and CP106 were co-expressed. This demonstrates that DNA binding caused a change in the ratio of lifetimes, rather than changes in fluorescence resulting from a generic immune response. It also shows that Rx1 DNA binding is only induced by its specific cognate elicitor, and not by a generic immune response.

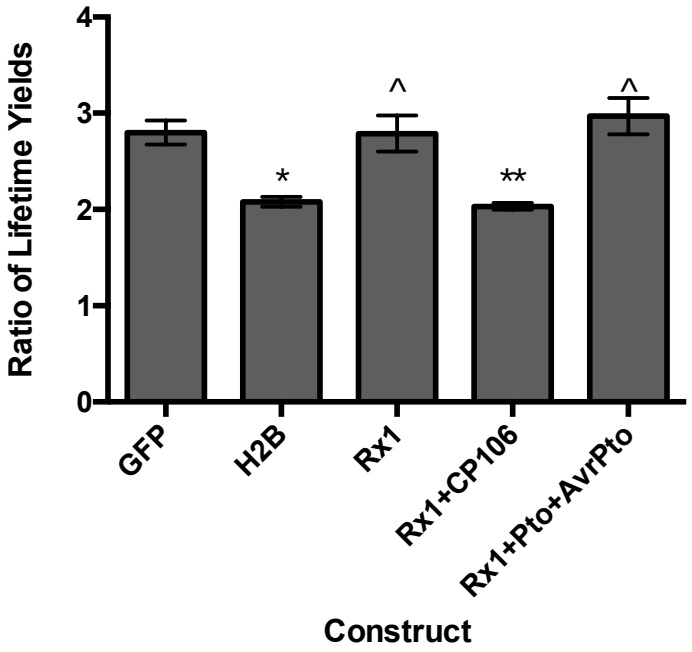

Figure 15: Average ratio of lifetime yields of fixed *N. benthamiana* leaves infiltrated with GFP tagged full length Rx1 mutants with and without CP106, GFP-Rx1with Pto and AvrPto GFP-H2B and a GFP infiltrated control. n = 4-8. ^ indicates adjusted p value > 0.05, * indicates adjusted p value < 0.05, ** indicates adjusted p value < 0.01 calculated using a Dunnett-Wilson Multiple Comparison ANOVA test.

.

3.6 Nucleocytoplasmic distribution of Rx1 is required for DNA binding

It has been previously shown that for Rx1 to induce defence signalling a nucleocytoplasmic distribution of protein is required, as Rx1 tagged with either a nuclear localisation (nls) or export (nes) signal displayed a reduced ability reduce accumulation of PVX in infected leaves (Slootweg et al., 2010). It was also shown that that Rx1 mediated sensing of CP106 occurs in the cytosol, as reduced HR was observed when Rx1 was co-infiltrated with CP106 with an nls tag (Slootweg et al., 2010). It was therefore of interest as to whether this nucleocytoplasmic distribution was also a requirement for Rx1 DNA binding, or whether nuclear localisation is sufficient, and whether CP106 induced Rx1 DNA binding also required cytoplasmic recognition of CP106. To test this GFP tagged Rx1 constructs with both nuclear localisation and nuclear export sequences were assayed with and without CP106

(Figure 16). Both these tags have been shown to localise Rx1 to the nucleus and cytoplasm respectively (Slootweg et al., 2010). GFP-Rx1-nls displayed no statistically significant DNA binding activity, demonstrating that nuclear localisation alone is insufficient to induce DNA binding (this also suggests overexpression of Rx1 in the nucleus does not result in a drop in lifetime ratio via a non-specific interaction with chromatin). The coexpression of GFP-Rx1-nls with CP106 also displayed no statistically significant DNA binding activity. This shows that Rx1 cannot elicit a nuclear DNA binding response to CP106 without first sensing it in the cytosol. The GFP-Rx1-nes displayed no statistically significant DNA binding both in the presence and absence of CP106. This demonstrates that transport of Rx1 from the cytosol to the nucleus after detection of CP106 is required. A signal cannot be sent from the cytosol itself. Hence, a nucleocytoplasmic distribution of protein is therefore required for DNA binding as it is for immune signalling.

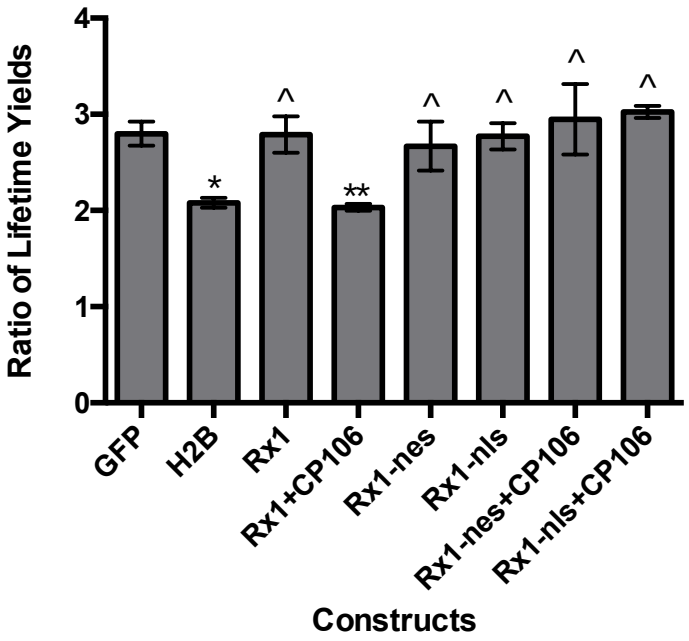

Figure 16: Average ratio of lifetime yields of fixed *N. benthamiana* leaves infiltrated with GFP tagged full length Rx1, Rx1-nes, Rx1-nls all with and without CP106, GFP-H2B and a GFP infiltrated control. n = 4-8. ^ indicates adjusted p value > 0.05, * indicates adjusted p value < 0.05, ** indicates adjusted p value < 0.01 calculated using a Dunnett-Wilson Multiple Comparison ANOVA test.

3.7 Autoactive and inactive Rx1 DNA binding mutants

It was hypothesised that mutations that affect immune signalling in Rx1 would also affect DNA binding activity. In this section different Rx1 mutants were screened for their ability to bind DNA (Figure 17). Rx1 D460V is an autoactive mutation in the MHD motif in the NBARC domain that elicits an immune response in the absence of any coat protein (Bendahmane et al., 2002) and is thought to do this by weakening the autoinhibiting effect the LRR has on the NBARC domain (Slootweg et al., 2013). K176R is a mutation in the putative *p*-loop region of the NBARC domain that inactivates any potential nucleotide binding activity and is unable to induce HR in response to CP106 (Slootweg et al., 2010, Bendahmane et al., 2002). S202F and

D225E are mutations in Rx1 designed to replicate the mutants S233F and D283E from the tomato NB-LRR protein I-2. These are mutations to the RNBS-A domain and Walker B motifs of the NBARC domain respectively, and deactivate the nucleotide hydrolysis activity of I-2 and lead to an autoactive immune response (Tameling et al., 2006). However, the effect of the S202F and D225E mutations on Rx1 immunological activity is currently unknown.

Some Rx1 mutations are known to effect distribution in the full-length protein, resulting in cytoplasmic rather than nucleocytoplasmic distribution (Slootweg et al., 2010), preventing any potential DNA binding *in vivo*. However, when expressed as a truncated protein containing only the CC and NBARC domains, these proteins revert back to a nucleocytoplasmic distribution. For this reason Rx1 K176R, S202F, and D225E were assayed in this truncated form rather than as a full-length protein. Full length Rx1 D460V is not known to display a non-cytoplasmic distribution and so was assayed as a full-length protein rather than in a truncated form.

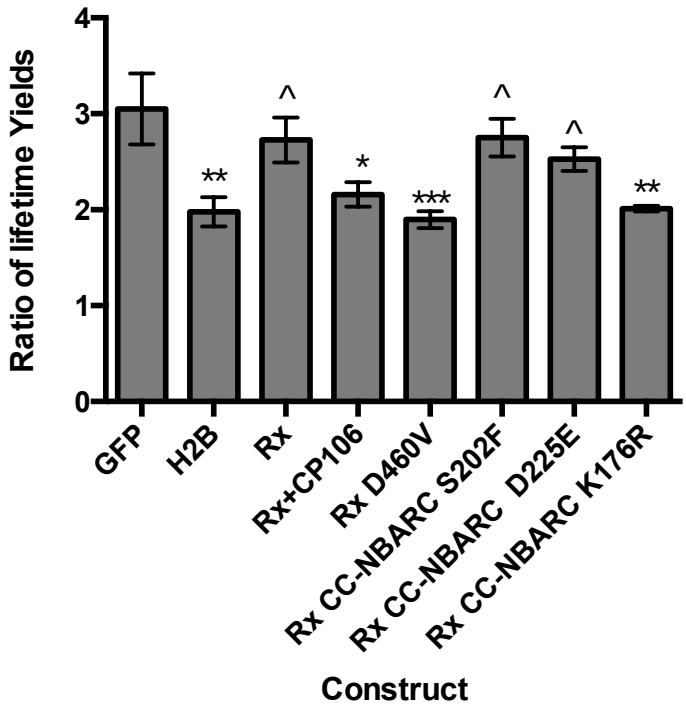

Figure 17.: Average ratio of lifetime yields of fixed *N. benthamiana* leaves infiltrated with GFP tagged full length and truncated Rx1 mutants compared to wild type Rx1 and coat protein, GFP-H2B and a GFP infiltrated control. $n = 6$. ^ indicates adjusted p value > 0.05, * indicates adjusted p value < 0.05, ** indicates adjusted p value < 0.01, *** indicates adjusted p value < 0.001 calculated using a Dunnett-Wilson Multiple Comparison ANOVA test.

The full-length autoactive Rx1 D460V behaved in the same manner as wild type Rx1 protein in the presence of CP106, binding DNA (Figure 17.). Previous work on this mutant concluded that it weakened the interactions between the NBARC and LRR domains that held the protein in an inactive resting state (Slootweg et al., 2013). The results suggest that disrupting this interaction leads to protein DNA binding, and links DNA binding to an Rx1 immune signalling. However it has also been hypothesised that this mutation disrupts nucleotide binding and the connection between the ARC subdomain and the nucleotide binding pocket. Loosening nucleotide binding is thought to allow easy nucleotide exchange. This hypothesis states that the easy exchange of ADP for activating ATP is what results in autoactivity (Tameling et al.,

2006). This nucleotide exchange could also be what activates Rx1 in regards to DNA binding, leading to the result observed.

The *p*-loop mutant K176R behaved identically to the wild type CC-NBARC truncation (Figure 17), constitutively binding DNA. However, truncated S202F and D225E both failed to bind DNA, unlike the wild type truncation. These results implied that inactivating nucleotide binding (K176R) did not affect DNA binding, but inactivating nucleotide hydrolysis (S202F, D225E) did.

Previous work performed on I-2 mutants showed that mutants unable to bind nucleotides (K207R) were not autoactive while mutants able to bind nucleotides but unable to hydrolyse them (S233F and D283E) led to protein autoactivity. Double mutants that could neither bind nor hydrolyse nucleotides were not autoactive. It was concluded that that ATP binding activated I-2, initiating defence signalling, and nucleotide hydrolysis deactivated it (Tameling et al., 2006). The results of the mutant DNA binding assay suggest that Rx1 behaves differently, with ATP hydrolysis activating DNA binding (and potentially immune signalling), rather than nucleotide binding.

It is important to note, however, that no nucleotide hydrolysis has been detected in recombinant Rx1 as it has in I-2, and that full length S202F and D225E mutants have not been observed to trigger an autoactive hypersensitive response in *Agrobacterium* infiltrated *N. benthamiana* as would be expected if these mutations were leading to autoactive DNA binding and immune signalling.

3.8 Co-infiltration of Truncated Rx1 mutants with the LRR domain

Section 3.7 included investigations into the activity of some truncated Rx1 mutants whose cytoplasmic distribution in a full-length Rx1 construct made the analysis of DNA binding intractable *in vivo*. These results do not show the effect the interaction between the NBARC domain and the LRR has on these mutations. This interaction is known to regulate the protein, inhibiting NBARC domain activity to prevent premature defence signalling activation. How this interaction affects these activity compromised mutants in a full-length protein was therefore of interest.

It has been shown that the Rx1 CC-NBARC domains will interact with the LRR domain *in planta* if the two are co-expressed (Moffet et al., 2002). It was hypothesised that if the truncated mutants were co-expressed with wild type LRR, the two domains should physically interact and behave as full length Rx1 mutant, but with a nucleocytoplasmic distribution. The DNA binding activity of the two domains co-expressed could then be assayed.

To optimise the experimental conditions for this interaction, wild type GFP-CCNBARC and LRR-GFP were infiltrated into *N. benthamiana* leaves at a range of OD_{600} values and the resulting lifetime ratios measured and compared to a full length wild type Rx1 control (Figure 18). The two domains interacting were hypothesised to behave as wild type Rx1 and not bind DNA, resulting in a similar higher lifetime ratio of approximately 2.5 (section 3.4). If the CCNBARC and LRR domains did not interact the free CC-NBARC was hypothesised to bind DNA, giving a lower lifetime ratio (section 3.3). A Dunnett-Wilson Multiple Comparison ANOVA test was used to determine similarity of the lifetime ratios to a full length Rx1 control column. The

conditions giving the highest adjusted p-values in the test were judged to have behaved most similar to wild type full length Rx1. The highest p-value of 0.5171was given when the CC-NBARC was infiltrated at OD_{600} = 0.01, and the LRR was infiltrated at OD_{600} = 0.5, indicating these conditions optimised CC-NBARC and LRR interaction.

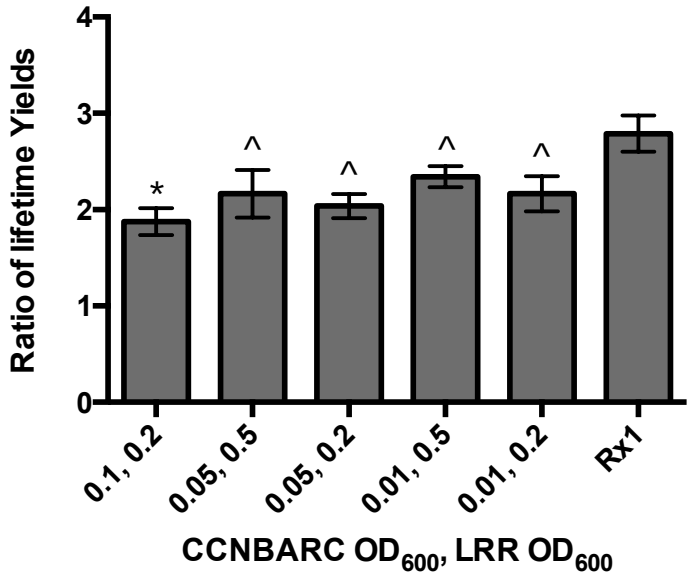

Figure 18: Average lifetime ratios of fixed *N. benthamiana* leaves co-infiltrated with GFP-CC-NBARC and LRR-GFP at a range of OD_{600} values compared to an Rx1 full-length control. The ratio lifetime yields increases as the OD_{600} of the GFP-CCNBARC decreases relative to the LRR-GFP. n = 3. ^ indicates adjusted p value > 0.05, * indicates adjusted p value < 0.05, ** indicates adjusted p value < 0.01, calculated using a Dunnett-Wilson Multiple Comparison ANOVA test.

The mutants S202F, D225E and K176R and wild type Rx1 were infiltrated with the LRR domain at the optimised OD_{600} values both with and without CP106. Fluorescence lifetime yields were then recorded. These were then compared to controls of wild type full length Rx1 with and without CP106. The results are summarised with a comparison to the lifetime ratios for truncated CCNARC constructs in Table 4.

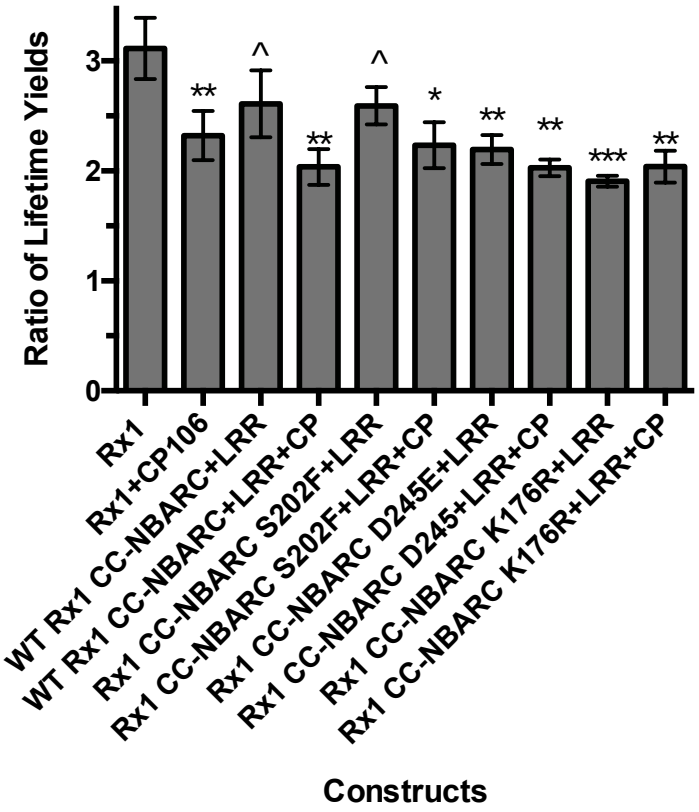

Figure 19: Average ratio of lifetime yields of fixed *N. benthamiana* leaves infiltrated with GFP tagged truncated Rx1 mutants coinfiltrated with LRR-GFP compared to wild type Rx1. Rx1 and CCNBARC domains were infiltrated at OD_{600} = 0.01, all other constructs were infiltrated at OD_{600} = 0.5. *n* = 10. ^ indicates adjusted *p* value > 0.05, * indicates adjusted *p* value < 0.05, ** indicates adjusted *p* value < 0.01, *** indicates adjusted *p* value < 0.001 calculated using a Dunnett-Wilson Multiple Comparison ANOVA test.

Table 7. FRET-FLIM analysis of DNA binding in fixed *N. benthamiana* leaf material for wild type Rx1, Rx1 K176R, Rx1 S202F, and Rx1 D225E. All proteins were assayed as truncated CCNBARC, CCNBARC + LRR, and CCNBARC + LRR + CP106. Where relevant, the motif any mutation is present in, and the putative Rx1 activity targeted by the mutation is listed.

Rx1 Construct	Mutated Motif	Mutation target	CCNBARC DNA binding	CCNBARC + LRR DNA binding	CCNBARC+ LRR+CP106 DNA binding
Wild Type	N/A	N/A	+	-	+
K176R	*P*-loop	Nucleotide Binding	+	+	+
S202F	RNBS-A	Nucleotide Hydrolysis	-	-	+
D225E	Walker B	Nucleotide Hydrolysis	-	+	+

K176R+LRR constitutively bound DNA with and without CP106 present. This represents a change from wild type Rx1 that would bind only when activated by CP106 (Figure 19). The truncated K176R previously bound DNA in the absence of LRR (Table 4). Previous work has shown *p*-loop CCNBARC mutants being capable of physically interactively with LRR domains (Moffett et al., 2002), so the mutation cannot be preventing LRR inhibition of DNA binding in the absence of CP106 by completely preventing binding. The K176R mutation could allow the LRR to bind the CCNBARC but prevents an inhibiting conformation being adopted. Whether this is due to an inability to bind nucleotides or a general destabilisation of the protein is unclear.

S202F+LRR failed to bind DNA in the absence of coat protein, but then bound in the presence of CP106, behaving identically to the wild type protein (Figure 19). This was a distinct change from the truncated S202F that did not bind DNA as the truncated wild type does (Table 4). The result suggests that the physical interaction with the LRR may be buffering a structural destabilising effect of the S202F mutant on the NBARC domain and restoring function. The previous results with the truncated protein can therefore not be concluded to be the result of the loss of any nucleotide hydrolysis activity.

D225E+LRR constitutively bound DNA both with and without CP106 (Figure 19). Previously the truncated mutant failed to display any statistically significant DNA binding activity (Table 4). This could imply that the LRR was stabilising the mutant NBARC domain as for S202F, but the interaction adopts a conformation that permits DNA binding in the absence of coat protein. Again, this could imply that the truncated

mutant failed to bind due to being structurally unstable rather than any compromised nucleotide hydrolysis activity.

The results of co-infiltrating these mutants with LRR demonstrate how little is understood of how the mutations affect Rx1 activity. The drastic changes in DNA binding behaviour in response to the LRR could indicate any previous lack of DNA binding activity was due to changes in Rx1 structural stability rather than changes in nucleotide binding and hydrolysis. There is an absence of any biochemical data on Rx1 nucleotide binding or hydrolysis, and the effect of these mutations on such an activity. This makes it impossible to reliably conclude whether changes in DNA binding upon mutation are linked to changes in nucleotide binding/hydrolysis or changes in protein folding and stability. Further *in vitro* characterisation of these mutants is required (see discussion Chapter 6).

3.9 Conclusion

This chapter demonstrates Rx1 associates with plant genomic DNA in fixed plant material using a novel FRET-FLIM assay. This association is observed in both the CC and NBARC domains, but not the LRR domain. It is thought that in the NBARC domain this association is the result of a DNA binding activity possessed by the domain that has been demonstrated previously using recombinant protein in an *in vitro* assay (Fenyk et al., 2015). In the case of the CC domain it is conjectured that this activity is the result of an intermediary protein-protein interaction.

When all three domains are expressed together as full length Rx1 association with DNA is inhibited. The addition of the potato virus X viral coat protein CP106 will then

activate the full length Rx1 to bind DNA. This is not seen in the avirulent coat protein CP105. The absence of a DNA binding signal on the addition of Pto and AvrPto confirms that this is not an artefact resulting from a generic immune response.

A nucleocytoplasmic distribution of protein is required for DNA binding to occur. The use of nuclear localisation sequences and nuclear export sequences to sequester Rx1 in either the nucleus or cytoplasm exclusively prevents any binding occurring in the presence of CP106. This matches previous work showing that such a distribution is required for Rx1 to trigger immune signalling (Slootweg et al., 2010).

The immunologically autoactive Rx1 mutant D460V will constitutively bind DNA in the absence of CP106. This mutation was concluded to prevent inhibition of DNA binding by the LRR domain. The deactivation of the putative *p*-loop region of Rx1 in the mutant K176R does not affect the ability of the CC-NBARC domains to bind DNA, implying nucleotide hydrolysis may not be prerequisite for DNA binding. The S202F mutation results in the CC-NBARC domain being unable to bind DNA. However, coexpression with the LRR domain reverses this and restores normal protein activity. The D225E mutation inhibits the binding of the CC-NBARC to DNA. Coexpression with the LRR reverses this activity, resulting in a constitutively active set of domains. Whether these mutants behave this way due to changes in nucleotide hydrolysis activity or due to general changes in protein stability is unknown and requires further *In vitro* characterisation of these mutants (see Chapter 6).

The results show Rx1 DNA binding activity and it's link to the induction of immune signalling *in vivo* in response to virulent PVX coat protein CP106. This confirms the

initial hypothesis and validates the work done demonstrating Rx1 binding DNA *in vitro*. How this Rx1 DNA binding is regulated by other proteins and the impact of this on plant immunity was therefore of interest, and is explored in subsequent Chapters.

3.10 Discussion

The FRET-FLIM results suggest both the NBARC and CC domains of Rx1 associate with DNA. Homology modelling of the Rx1 NBARC domain predicts a possible DNA binding activity based on similarity to other DNA binding members of the STAND ATPase AAA+ superfamily (Fenyk et al,. 2015). No CC domains are known to have DNA binding activity and are more commonly associated with protein-protein interactions (Kohn et al., 1997). This suggests that the DNA binding domain of Rx1 is the NBARC domain, with the CC domain of the protein more likely to be involved with an interaction with another intermediate DNA binding protein. This association could position the domain physically close enough to the DNA binding LDS-751 to facilitate energy transfer.

The CC domain has been previously shown to associate with a high molecular weight complex in the nucleus (Slootweg et al., 2010). The energy transfer observed in the experiment suggests that this high molecular weight complex is genomic DNA. It was concluded that Rx1 binds genomic DNA in response to CP106.

Section 3.5 demonstrated that Nuclear localisation and accumulation of Rx1 was shown to be insufficient to trigger DNA binding; transport of Rx1 from the cytosol to the nucleus is required. Nucleocytoplasmic distribution of Rx1 is also known to be required to trigger immunity, and Rx1 had been shown to detect CP106 in the cytosol

(Slootweg et al., 2010). The results imply that Rx1 mediated immune signalling may be triggered by Rx1 DNA binding in the nucleus after the elicitor is sensed in the cytosol.

This DNA binding data is supported by work done showing that CCNBARC Rx1 binds DNA *in vitro* using recombinant refolded protein from *E. coli.* using EMSA and FRET-FLIM assays (Fenyk et al., 2015). EMSA also demonstrated that CCNBARC Rx1 protein purified from *N. benthamiana* leaves bound DNA (Fenyk et al., 2015). This demonstrates that the FRET-FLIM assay was measuring an active DNA binding activity of Rx1 CCNBARC and not an association with DNA mediated by another protein. The results show that the *in vitro* DNA binding observed in this paper also occurs within the plant cell. This paper also demonstrated that recombinant Rx1 CCNBARC had a bending and melting effect on DNA using FRET-FLIM, a common activity of transcription factors (Finzi et al., 2010). Section 3.4 showed Rx1 DNA binding in response to its cognate elicitor CP106. Together, these suggests that Rx1 DNA binding may stimulate gene expression in response to CP106 to trigger plant defence signalling. Rx1 DNA binding has been shown to be non-specific (Fenyk et al., 2015), suggesting that another protein would have to mediate this interaction to provide specificity (see Chapter 4) .

The FRET-FLIM experiments with mutant Rx1 constructs designed to investigate the impact of nucleotide hydrolysis/binding were inconclusive. I-2 nucleotide hydrolysis deficient mutants (S233F and D283E) result in I-2 auto-activity, whereas the nucleotide binding mutant K207R is inactive (Tameling et al., 2002). However S202F and D225E have not been described as causing immunological autoactivity in Rx1.

Nor is there any evidence of Rx1 nucleotide hydrolysis recorded in the literature for the K176R mutation to disrupt. Tough Rx1 DNA bending has been shown to be dependent on ADP and a functional *p*-loop (Fenyk at al., 2015). The NBARC domain of Rx1 may not hydrolyse or even bind ATP. The effects of these mutations may just be the structural destabilization of the NBARC domain resulting in partially misfolded, inactive protein.

The effects seen in the FRET-FLIM assay for these mutant constructs could be the result of either compromised nucleotide binding/hydrolysis activity, or compromised protein stability. The mutations could interrupt motifs required for protein folding and stability. Slight changes in protein folding with the NBARC domain could compromise inter-domain interactions in Rx1 that the D460V mutation indicates are immunologically relevant and functionally relevant to DNA binding. Changes in behaviour from co-expression with the LRR could be the result of the LRR stabilising a partially folded NBARC domain. Further work is required to elucidate this relationship (see Chapter 6).

4. The impact of the transcription factor *Nb*GLK1 on Rx1 triggered immunity

4.1 Introduction

NB-LRR protein activation is tightly regulated as their promiscuous activity can lead to cell death through the hypersensitive response (HR). Chapter 3 presented evidence that the NB-LRR protein Rx1 bound DNA in fixed plant leaf material. Previous work has demonstrated the ability of recombinant Rx1 protein to bind DNA *in vitro* (Fenyk et al., 2015). With the DNA binding activity of Rx1 established, it was hypothesised that this binding would be regulated so as to prevent an immune response in the absence of an immune elicitor.

To identify putative Rx1 interactors that may mediate its DNA binding activity, the CC domain of Rx1 (amino acids 1-144) was screened in a Yeast 2-hybrid assay against a mixed tissue *Nicotiana benthamiana* cDNA library. Positive matches from this screen were to be bioinformatically analysed to determine if they were likely to bind DNA. Putative DNA binding proteins were then hypothesised to be potential regulators of Rx1 DNA binding. This chapter describes the identification of one such protein, and further experiments with the aim of confirming its interaction with Rx1 and determining the mechanism through which any regulation of Rx1 DNA binding occurs.

The transcription factor *Nb*GLK1 (Golden-Like transcription factor 1) displayed affinity for the Rx1-CC domain in the Yeast 2-Hybrid assay. The GLK1 family of transcription factors have been shown to be involved in defence signalling (Han et al.,

2013, Murmu et al., 2014) and chloroplast development (Waters et al., 2009) in *Arabidopsis*. As a protein hypothesised to bind DNA and be involved in defence signalling, *Nb*GLK1 was identified as a potential regulator of Rx1 DNA binding.

The ability of *Nb*GLK1 to regulate Rx1 DNA binding activity was investigated. The impact of *Nb*GLK1 on Rx1 DNA binding, the Rx1 mediated defence response, and Rx1 mediated cell death was tested. The impact of Rx1 on *Nb*GLK1 DNA binding was also assayed, as was the ability of Rx1 and *Nb*GLK1 to interact *in planta*.

4.2 Yeast 2-hybrid screen results

CC domains are known to be involved in protein-protein interactions (Kohn et al., 1997). The Rx1 CC domain has been shown in previous work to be involved in protein-protein interactions, binding the protein RanGAP2 (Tameling el al., 2007). It was therefore hypothesised that proteins mediating Rx1 DNA binding would do so via this domain. The section describes a yeast 2-hybrid screen with the aim of identifying Rx1 CC interactors.

Amino acids 1-144 of Rx1 (residues corresponding to the CC domain) were cloned into a pB27 bait plasmid as a C-terminal LexA fusion. This was then subject to a Yeast 2 hybrid screen against a random-primed *Nicotiana benthamiana* mixed tissue cDNA library (https://www.hybrigenics-services.com/library/1) in a pP6 prey plasmid fused to a transcription-activating domain of the bacterial transcription factor Gal4. LexA is a bacterial DNA binding protein that when interacting with a Gal4 activating domain forms a functional Gal4 transcription factor. An interaction between a LexA fused CC domain with a protein from the library fused with the Gal4 activation domain results

in activation of the Gal4 promoted HIS3 histidine production gene on the pP6 plasmid. Clones expressing HIS3 were selected for through growth on media deficient in histidine leucine, tryptophan (Formstecher et al., 2005, see Materials and Methods section 2.4.4).

To confirm interactions, the colonies giving positive results from the initial screen were spotted onto plates containing media lacking leucine and tryptophan and medium lacking leucine, tryptophan and histidine supplemented with 10 or 50 mM 3-Amino-1,2,4-triazole (3-AT). 3-AT inhibits imidazoleglycerol-phosphate dehydratase, an enzyme involved in the production of histidine. Using low concentrations of this inhibitor in the media improves selection for the HIS3 histidine production gene used for selection in the Y2H screen. Positive prey colonies were sequenced, and putative protein domains determined through bioinformatics. Proteins with strong affinities for the CC domain that also contained DNA binding domains were identified as potential regulators of Rx1 DNA binding.

Among the hits generated by the initial screen were 7 positive results of overlapping sequence that were combined to a form Single Interacting Domain from a protein homologous to the one encoded by LOC102587163 (GenBank ID: 565364225) in the *Solanum tuberosum* genome library (see appendix 7.1-7.2 for full Yeast two-hybrid results). Homology to a protein from the same organism as Rx1 was necessary for the interaction to be considered biologically relevant. This was one of the highest confidence results in the screen with a PRBS (predicted biological score) of B, corresponding to ‘high confidence in the interaction’ (see methods and material 2.4.4 for a description of PRBS scores). A 1x1 Yeast 2 hybrid screen confirmed this result, showing yeast growth on the 10 mM 3-Amino-1,2,4-triazole (3-AT) supplemented

leucine, tryptophan and histidine deficient plate (Figure 21). No growth was seen on the corresponding plate for any of the negative controls.

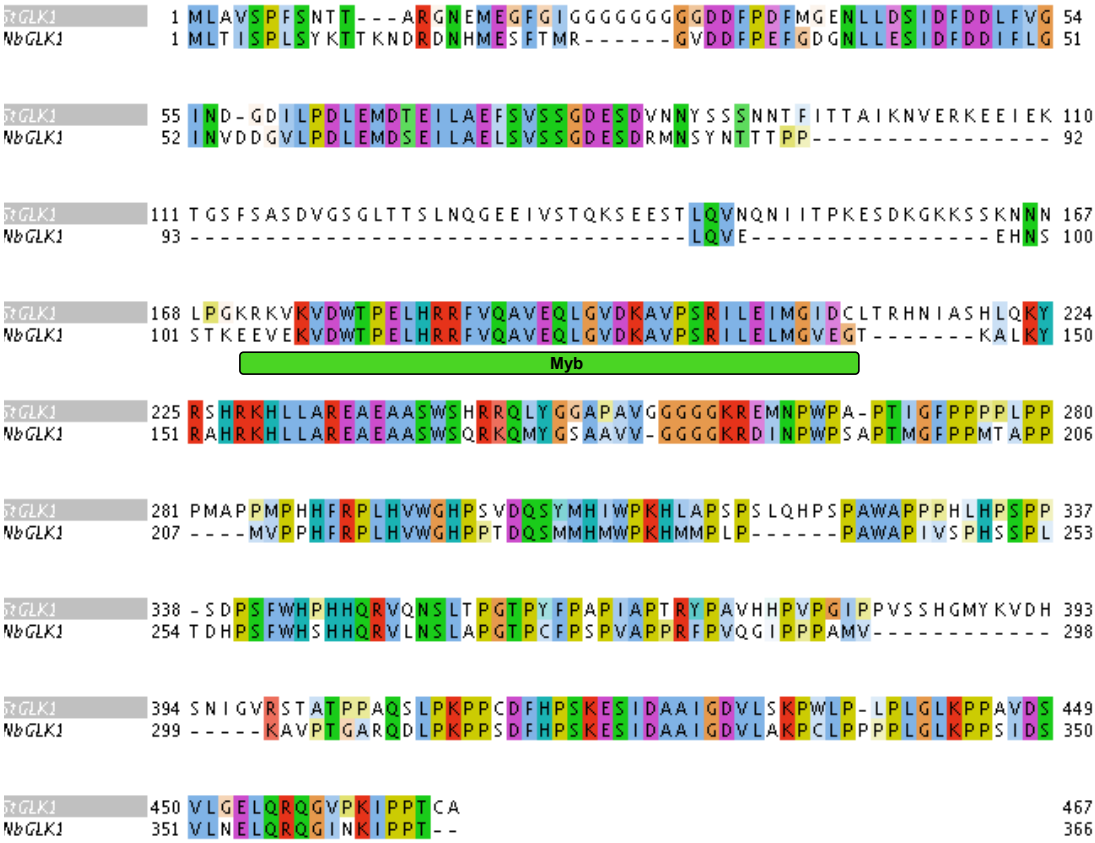

Figure 20. Sequence alignment of *Nicotiana benthamiana* GLK1 (*Nb*GLK1) amino acid sequence with *Solanumm tuberosum* GLK1 (*Sb*GLK1) using ClustalOmega. Conserved residues between the sequences are highlighted, and the putative *Nb*GLK1 Myb helix-turn helix DNA binding domain as annotated by Interpro (amino acids 104-144) is indicated.

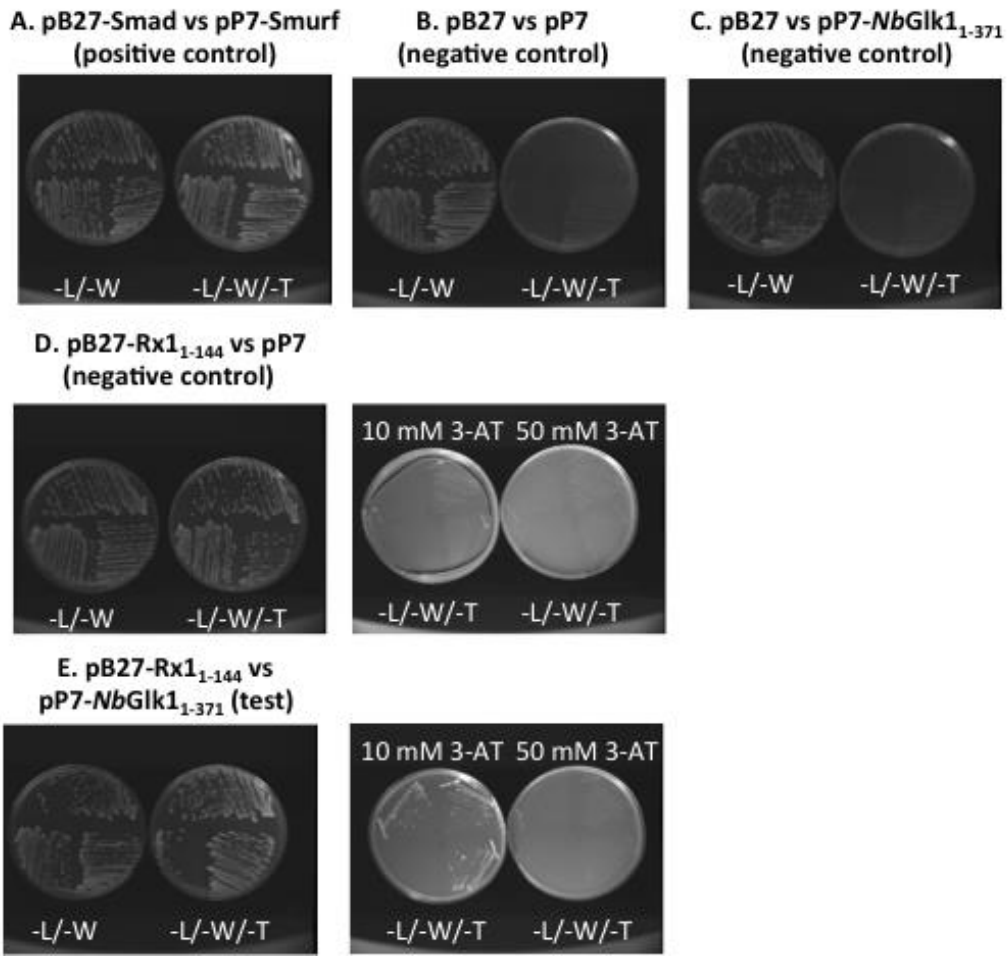

Figure 21. 1x1 Yeast 2 hybrid screen of Rx1-CC against *Nb*GLK1 performed by Hybrigenics. Rx1 was fused to the Gal4 DNA-binding domain and NbGLK1 was fused to the Gal4 activation domain. Plates were grown on medium lacking leucine and tryptophan (−L/−W) and medium lacking leucine, tryptophan, histidine (−L/−W/−T), supplemented with 10 or 50 mM 3-Amino-1,2,4-triazole (3-AT). A. Smad vs Smurf positive control B. Empty pB27 bait vs empty pP7 prey negative control. C empty pB27 bait vs *Nb*GLK1 in prey negative control. D. Rx1 containing bait vs empty pP7 prey negative control. E. CC Rx1 in pB27 bait plasmid with *Nb*GLK1 in pP7 prey plasmid.

Bioinformatic analysis using Clustal Omega for multiple sequence alignment (https://www.ebi.ac.uk/Tools/msa/clustalo/ (Sievers et al., 2011)) and Interpro for domain annotation (http://www.ebi.ac.uk/interpro/ (Mitchell et al., 2014)) suggested this protein was homologous to the protein GLK1 (Golden-Like transcription factor 1)(Figure 20). *Nb*GLK1 is hypothesised to bind DNA, containing a putative Myb helix-turn-helix DNA binding domain and belonging to a family of transcription factors (Han et al., 2013). GLK1 has been shown to be involved in defence signalling in *Arabidopsis*, providing resistance to cucumber mosaic virus (Han et al., 2013) and the fungal pathogens *Fusarium graminearum* and *Hyaloperonospora arabidopsidis* (Murmu et al., 2014). It was therefore identified a potential regulator of Rx1 DNA binding, and subject to further investigation.

4.3 *Nb*GLK1 promotes Rx1 DNA binding *in vivo*

Chapter 3 demonstrated that full length Rx1 bound genomic DNA in response to its viral elicitor, CP106, in fixed leaf material (Section 3.5). To investigate any impact *Nb*GLK1 had on Rx1 DNA binding, *Nb*GLK1-HA and GFP-Rx1 were co-expressed (Materials and Methods 2.3.1, Table 4) both with and without CP106 in *N. benthamiana* leaves via *Agrobacterium* mediated infiltration. *Nb*GLK1-HA and CP106 were infiltrated at OD_{600} = 0.4 to maximise expression and GFP-Rx1 was infiltrated at OD_{600} = 0.1 to prevent cell death via HR. The leaves were fixed in formaldehyde and stained with LDS-751. The same FRET-FLIM assay developed in Chapter 3 (section 3.2, Materials and Methods 2.3.2/3) was then performed on GFP-Rx1 to determine whether it bound genomic DNA.

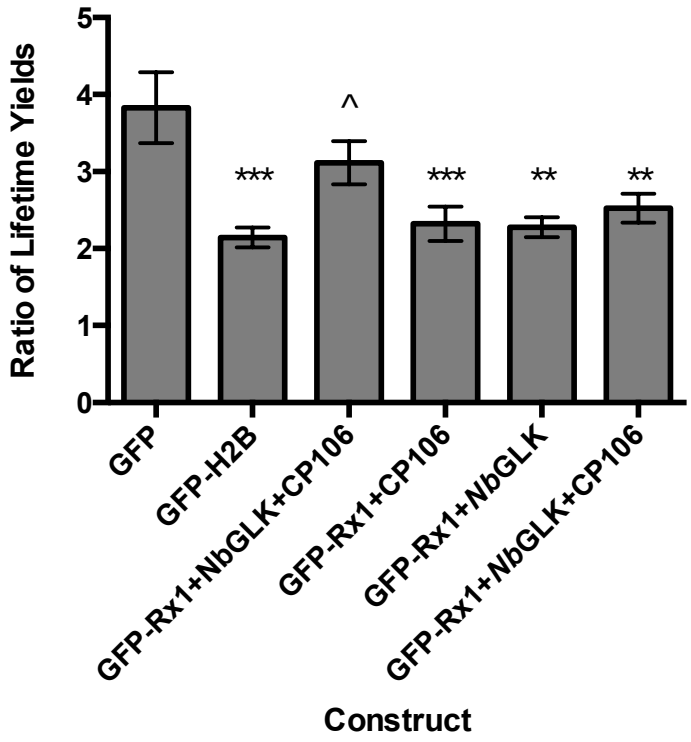

Figure 22. The average ratio of fluorescence lifetimes for *N. benthamiana* leaves expressing GFP-Rx1 in combination with *Nb*GLK1 and CP106 fixed in formaldehyde and stained with LDS-751. Free GFP and GFP-H2B expressing *N. benthamiana* are included as negative and positive controls. n = 6-10. ^ indicates adjusted p value > 0.05, * indicates adjusted p value < 0.05, ** indicates adjusted p value < 0.01. *** indicates adjusted p value < 0.001. Adjusted p values calculated using a Dunnett-Wilson multiple comparisons test.

Chapter 3 demonstrated that Rx1 bound DNA only when co-expressed with CP106 (section 3.4). This result was repeated in the experiment, with a similar statistically significant drop in Rx1 lifetime ratio seen upon co-expression with CP106. This indicates a shift to DNA binding and greater energy transfer to the LDS-751. However, the results also show that full length Rx1 displays a statistically significant decrease in lifetime ratio in the presence of *Nb*GLK1-HA in both the presence and absence of the CP106 viral coat protein (Figure 22). This suggests that Rx1 is binding DNA in both instances. It was concluded that *Nb*GLK1 was acting positive regulator of Rx1 DNA

binding, pulling the protein onto DNA when its cognate elicitor is absent. It should be noted that *Nb*GLK1 and Rx1 are both overexpressed in the experiment. Under standard physiological conditions *Nb*GLK1 may not trigger Rx1 DNA binding in the absence of it ellicitor.

4.4 The impact of Rx1 on *Nb*GLK1 binding *in vivo*

The previous section investigated the impact of *Nb*GLK1 on GFP-Rx1 DNA binding using FRET-FLIM. As a transcription factor, *Nb*GLK1 also binds DNA (Hao et al., 2013). The aim of this section is to determine the impact of Rx1 on GFP-*Nb*GLK1 DNA binding using the same FRET-FLIM analysis. Knowing this would in turn elucidate the mechanism through which *Nb*GLK1 regulates Rx1 DNA binding.

*Nb*GLK1 was cloned into the *Agrobacterium tumefaciens* vector pK7GF2 using a gateway reaction via a pDONR-207 intermediate vector (see Materials and Methods, 2.2.13), giving it an N-terminal GFP tag. This was then infiltrated into *N. benthamiana* leaves and expressed in the presence and absence of untagged Rx1 and CP106 (Materials and Methods 2.3.1, Table 4). GFP-*Nb*GLK1 and CP106 were infiltrated at OD_{600} = 0.4 to maximise expression and Rx1 was infiltrated at OD_{600} = 0.1 to prevent cell death via HR. The leaves were fixed in formaldehyde, stained with LDS-751, and assayed for *Nb*GLK1 DNA binding activity using FRET-FLIM.

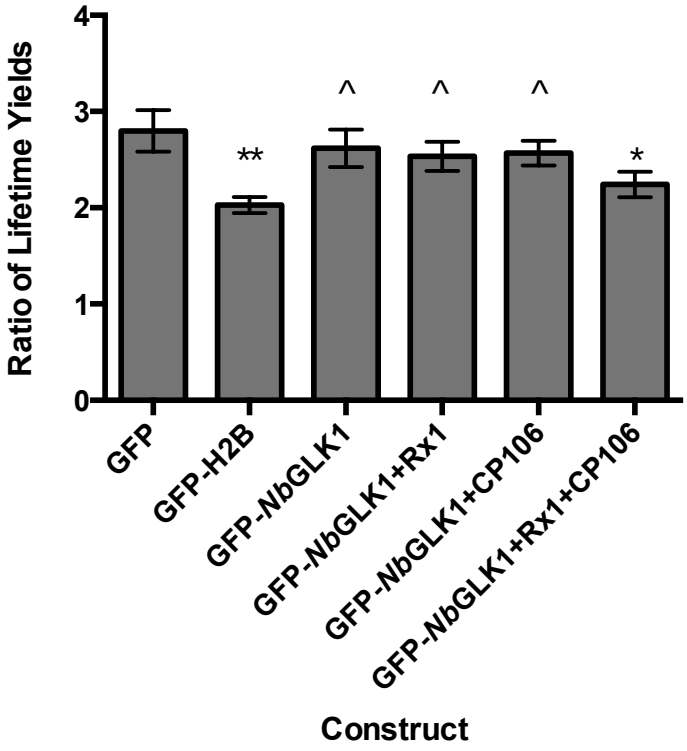

Figure 23. The average ratio of fluorescence lifetimes for *N. benthamiana* leaves expressing GFP-*Nb*GLK1 in combination with Rx1 and CP106 fixed in formaldehyde and stained with LDS-751. Free GFP and GFP-H2B expressing *N. benthamiana* are included as negative and positive controls. n = 11-14. ^ indicates adjusted p value > 0.05, * indicates adjusted p value < 0.05, ** indicates adjusted p value < 0.01. Adjusted p values calculated using a Dunnett-Wilson Multiple Comparison ANOVA test.

The results show no statistically significant decrease in GFP-*Nb*GLK1 ratio of lifetime yields from the free GFP negative control when expressed by itself, or when co-expressed with either Rx1 or CP106 individually. A drop in the ratio of lifetime yields was only seen when GFP-*Nb*GLK1 is expressed with both CP106 and Rx1 simultaneously (Figure 23). This implies that *Nb*GLK1 does not bind DNA in the plant cell until both of these proteins are present.

The previous section suggested that *Nb*GLK1 causes Rx1 to bind DNA in the absence of CP106. These results imply that Rx1 will not cause *Nb*GLK1 to bind DNA in the

absence of coat protein. If the two proteins were interacting it would be expected that they would bind both DNA together in the absence of CP106, but this was not seen.

This could be due to an excess of *Nb*GLK1 being expressed in the leaves relative to Rx1. *Agrobacterium* containing the Rx1 construct was infiltrated into leaves at a lower OD_{600} value than *Nb*GLK1 to avoid Rx1 triggered plant cell death, possibly resulting in lower expression. Any excess *Nb*GLK1 may not interact with Rx1, remaining inactive and not binding DNA, giving a negative result in the assay. Meanwhile all of the smaller amount of Rx1 may interact with the excess of *Nb*GLK1, promoting the Rx1 DNA binding activity. This would lead to the positive result seen in section 5.3.

4.5 *Nb*GLK1 promotes immunity to PVX independent of Rx1

Section 4.3 demonstrated that *Nb*GLK1 promoted Rx1 DNA binding. If Rx1 DNA binding initiates defence signalling, *Nb*GLK1 should act as a promoter of Rx1 triggered PVX resistance. This section investigates whether *Nb*GLK1 regulates Rx1 mediated immunity to Potato virus X (PVX).

Rx1 is known to prevent PVX virus accumulation in infected cells (Bendahmane et al., 1995). An *Agrobacterium* vector containing the PVX genome tagged with GFP, pGR208 (Peart el al., 2002), was infiltrated into an area of *N. benthamiana* leaves. This vector was also co-infiltrated with either Rx1, *Nb*GLK1-HA, or with both Rx1 and *Nb*GLK1 together in separate areas of the same leaf (see Materials and Methods 2.3.1, Table 4). The leaves were incubated for 4 days and the GFP fluorescence intensity of the infiltrated areas recorded. The increase and decrease of GFP

fluorescence across the different infiltrated areas of the leaf would indicate the different construct's impact on PVX immunity (see Materials and Methods 2.3.5).

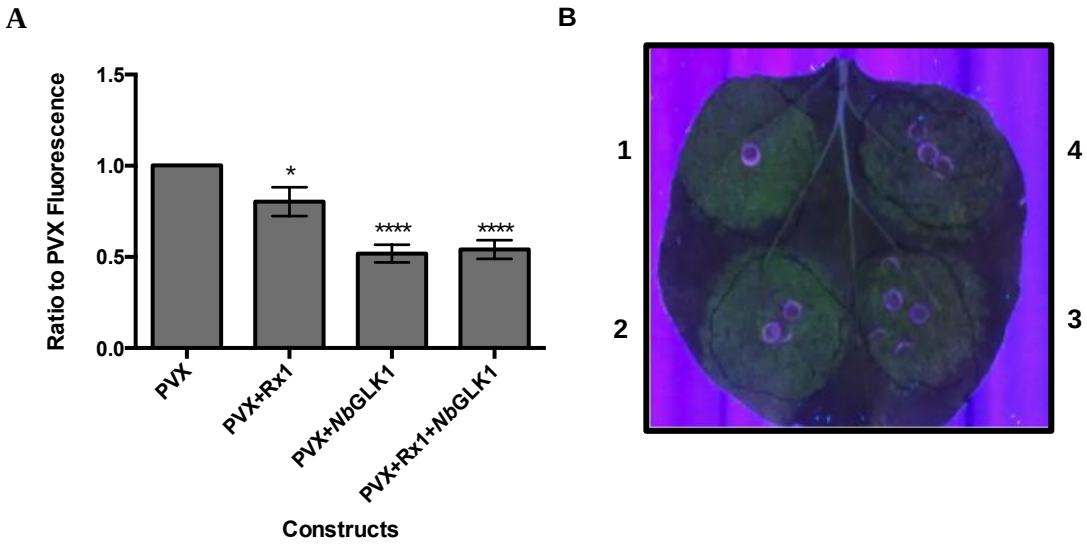

Figure 24. (A) The average ratio of fluorescence to a GFP-PVX control for *N. benthamiana* leaves expressing GFP-PVX in combinations with *Nb*GLK1 and Rx1. $n = 16$. ^ indicates adjusted p value > 0.05, * indicates adjusted p value < 0.05, **** indicates adjusted p value < 0.0001. Adjusted p values calculated using a Dunnett-Wilson Multiple Comparison ANOVA test. (B) A representative *N. benthamiana* leaf of the results under UV light showing the PVX fluorescence. 1 = PVX, 2 = PVX + Rx1, 3 = PVX + *Nb*GLK1, 4 = PVX + Rx1 + *N*bGLK1.

The results show a statistically significant drop in GFP-PVX fluorescence in the presence of Rx1 (Figure 24). This control demonstrates that Rx1 triggered an immune response to the viral genome, reducing viral accumulation, leading to a reduction in fluorescence intensity. However, *Nb*GLK1 also caused a statistically significant decrease in fluorescence both in the presence and absence of Rx1. The decrease in areas infiltrated with *Nb*GLK1 is greater than the decrease seen in areas infiltrated with only Rx1.

The decrease in fluorescence triggered by *Nb*GLK1 in the absence of Rx1 suggests *Nb*GLK1 can initiate immune signalling to PVX without Rx1. This would imply both that *Nb*GLK1 acts parallel to Rx1 in defence signalling transduction, and that this defence signalling can be independent of Rx1. *Nb*GLK1 acting parallel to Rx1 could allow it to promote resistance to a large range of pathogens by interacting with multiple NB-LRR proteins. This would fit with the multiple resistances *Nb*GLK1 is observed to promote in *Aribadopsis* (Han et al., 2013, Murmu et al., 2014).

4.6 The impact of *Nb*GLK1 on Rx1 mediated Cell Death

Rx1 has been shown to initiate two separate defence responses to PVX; the prevention of PVX viral accumulation in the infected cell (Bendahmane et al., 1995), and the triggering of plant cell death, the hypersensitive response (HR) (Bendahmane et al., 1999). The previous section assayed the impact of *Nb*GLK1 on viral accumulation. This section aims to determine the influence of *Nb*GLK1 on HR.

Sections of *N. benthamiana* leaves were infiltrated with *Nb*GLK1, *N*bGLK1 + Rx1, *Nb*GLK1 + CP106, *Nb*GLK1 + Rx1 + CP106 and Rx1 + CP106 (the positive control). *Nb*GLK1 and CP106 were infiltrated at OD_{600} = 0.4. Rx1 was infiltrated at OD_{600} = 0.1 (see Materials and Methods 2.3.1, Table 4). The leaves were then incubated and each infiltrated area scored for cell death from 1-5 (see Materials and Methods section 2.3.4).

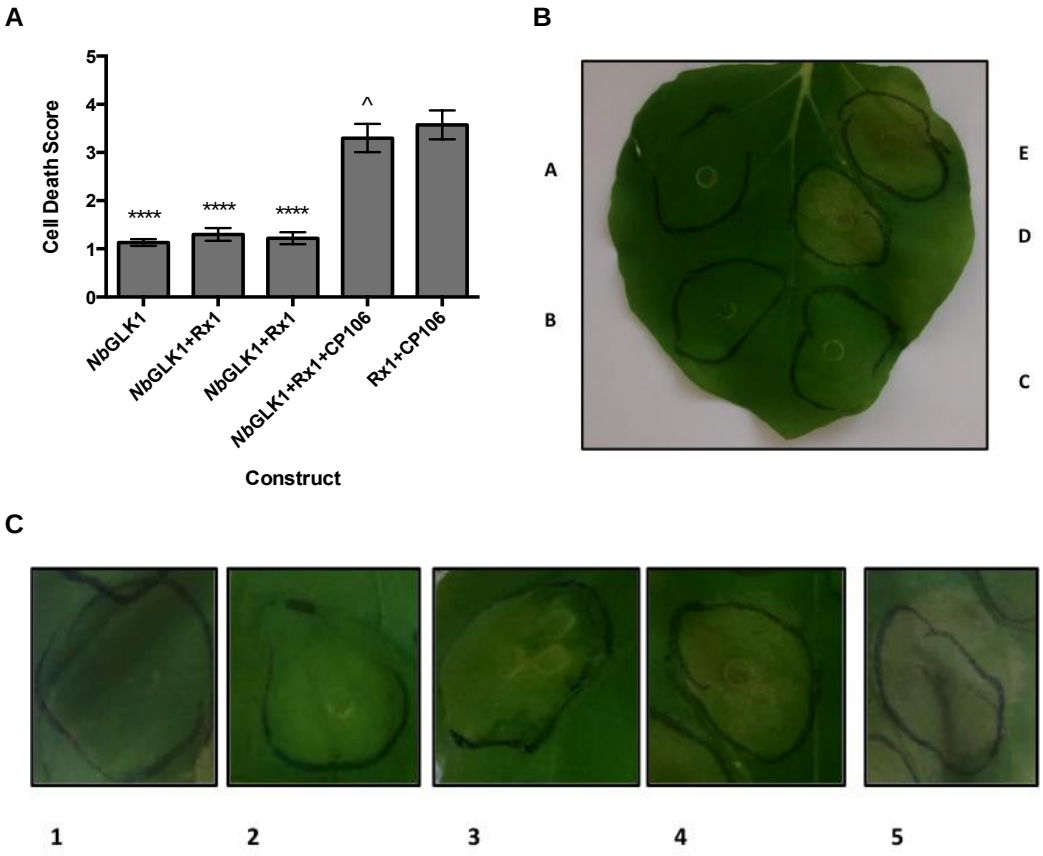

Figure 25. (A) The average cell death score for *N. benthamiana* leaves expressing NbGLK1 in combinations with CP106 and Rx1. $n = 24$. ^ indicates adjusted p value > 0.05, **** indicates adjusted p value < 0.0001. Adjusted p values calculated using a Dunnett-Wilson multiple comparisons test. (B) A representative *N. benthamiana* leaf of the results. A = *Nb*GLK1, B = *Nb*GLK1 + Rx1, C = *Nb*GLK1 + CP106, D = Rx1 + CP106, D = *Nb*GLK1 + Rx1 + CP106. (C) Representative images of *N. benthamiana* leaf areas for each cell death score.

Areas infiltrated with the Rx1 + CP106 positive control and *Nb*GLK1 + Rx1 + CP106 both gave a high cell death score, indicating HR (Figure 25). Areas infiltrated with *Nb*GLK1, *Nb*GLK1 + Rx1, and *Nb*GLK1 + CP106 all gave a statistically significant lower cell death score than the positive control, indicating no HR.

*Nb*GLK1 expression was only associated with cell death when co-expressed with both Rx1 and CP106, which together initiate HR in the absence of *Nb*GLK1. These results suggest that expression of *Nb*GLK1 has no impact on HR.

Section 4.3 showed *Nb*GLK1 promotes Rx1 DNA binding in the absence of coat protein. However, the results showed *Nb*GLK1 expression caused no increase in Rx1 mediated HR in the absence of coat protein. This implies that Rx1 DNA binding may have no impact on the HR.

Section 4.6 showed that *Nb*GLK1 promotes Rx1 mediated extreme resistance to PVX in *N benthamiana*, but this experiment shows that this immunity must be independent of HR. It was concluded that that *Nb*GLK1 promotes Rx1 DNA binding to trigger extreme resistance to PVX, but not HR. HR must therefore be triggered through a separate signal transduction pathway by Rx1 that may not involve DNA binding.

4.7 Co-immunoprecipitation of Rx1 and *Nb*GLK1

Yeast 2-hybrid screens (section 4.2) demonstrate a protein-protein interaction in a fungal protein expression system. It is possible this interaction was an artefact of the two proteins being expressed in a different environment. This section seeks to determine if the *Nb*GLK1-Rx1-CC interaction would occur in a plant expression system using co-immunoprecipitation. *Nb*GLK1 with an HA tag would be co-expressed with the Rx1-CC-myc domain in *N. benthamiana*. Protein would be extracted and the *Nb*GLK1-HA immunoprecipitated with an anti-HA antibody resin. Co-immunoprecipitation of the Rx1-CC-myc alongside the *Nb*GLK1-HA would demonstrate an interaction between the two.

4.7.1 Screen of *Nb*GLK1-HA Expression Conditions in *N. benthamiana*

Higher expression of *Nb*GLK1-HA increases the number of molecules for Rx1-CC protein molecules to interact with, increasing the sensitivity of the co-immunoprecipitation. A trial expression of *Nb*GLK1-HA in *N. benthamiana* via *Agrobacterium* mediated infiltration was performed to optimise protein expression conditions. The *Nb*GLK1 construct was infiltrated at an OD_{600} of 0.4 both with and without a P19 expressing vector at an OD_{600} 0.01 (see Materials and Methods 2.3.1, Table 4). The p19 protein is plant viral suppressor that increases transgene expression by repressing the plant gene silencing response against transgenes (Voinnet et al., 2003). Leaves were incubated for either 2 or 3 days after infiltration. Protein was then extracted from the leaves and visualised via Western blotting (see Materials and Methods 2.3.) using an HRP linked anti-HA antibody.

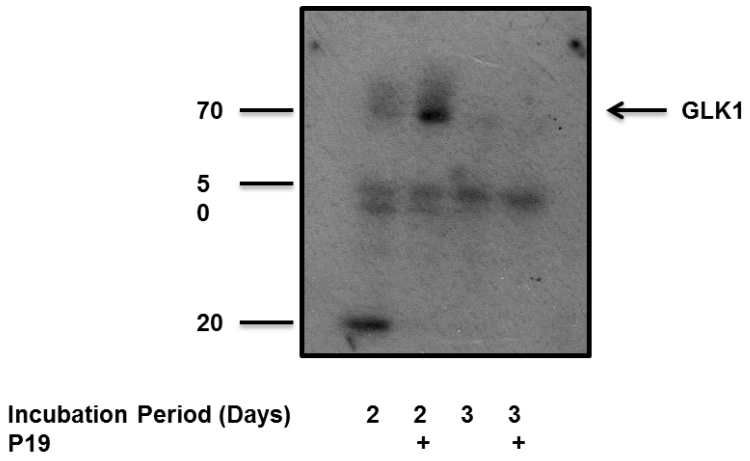

Figure 26: Western blot of trial *Nb*GLK1-HA expression extracted from *N benthamiana* leaves incubated for either 2 or three days in the either the presence or absence of P19 plant viral suppressor. Protein visualised using a HRP linked rat anti-HA antibody.

The strongest *Nb*GLK1 band was produced when the construct was co-infiltrated with P19 and then incubated for 2 days before protein expression (Figure 26). A 3-day incubation period resulted in a significant decrease in protein production. While a 2-day incubation in the absence of p19 decreased the strength of the *Nb*GLK1 band at 70 kDa and increased the strength of the 20 kDa band. This would suggest that that p19 prevented protein degradation. It was therefore decided to perform the co-immunoprecipitation on leaf material co-infiltrated with p19 after a 2-day incubation period.

4.7.2 Sephadex G-25 Column Screen

Previous co-immunoprecipitations to show interactions between the domains of Rx1 used a sephadex G-25 column to remove plant secondary metabolites that would interrupt interactions with antibodies from extracted plant material (Slootweg et al., 2013). A screen was performed to determine the optimal conditions for protein elution from the G25 column to maximise the yield of protein eluted, increasing the chance of a successful protein-protein interaction later on. Rx1-CC-myc was transiently expressed in *N benthamiana* leaves for 2 days and extracted (see Materials and Methods 2.3.1, Table 4). The plant protein extract was added to Sephadex G-25 columns of 3.5 ml volume. The columns were tested both under pressure via centrifugation and gravity. 5x1 ml fractions were collected from the gravity fed column to determine in which fractions the protein eluted.

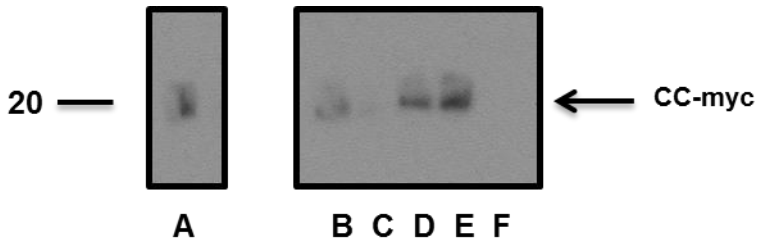

Figure 27: Western blot of Sephadex G-25 column screen on Rx1 CC-myc extracted from *N. benthamiana* leaves. Protein visualised using a goat anti-myc 1° antibody and an anti-goat HRP linked 2° antibody. A = initial plant protein extract. B = eluent from Sephadex G-25 column loaded with plant protein extract and centrifuged at 720 g for 1 min. C-F = sequential 1 ml fractions of eluent from a G-25 column eluted via gravity.

The results showed that the highest amount of protein present were in fractions D and E. These corresponded to the 2nd and 3rd ml eluted from the gravity fed column (Figure 27). A higher concentration of protein could be observed in these compared to the protein eluted from the centrifuged column (B). It was therefore decided to run the Sephadex column under room pressure, collect the 2nd and 3rd ml of eluent and pool them together. This mixture would then be used for the co-immunoprecipitation.

4.7.3 Co-immunoprecipitation of Rx1 and *Nb*GLK1 at 40 mM NaCL

The protocol for the co-immunoprecipitation was adapted from the method Slootweg et al. used to co-immunoprecipitate the LRR domain of Rx1 with the Rx1-CC domain (Slootweg et al., 2013, see Materials and Methods 2.4.3). Rx1 LRR-HA was used as a positive control and AVRRps4-HA was used as a negative control (see Materials and Methods 2.3.1, Table 4). All proteins were assayed both in the presence and absence of Rx1-CC-myc. Samples were taken from the experiment and protein visualised via Western blotting at the following points: After protein extraction from *N. benthamiana* to test for expression; after completion of the Sephadex G25 column to ensure elution; after the first centrifugation of the anti HA antibody resin to determine what protein failed to bind to the resin; and finally after elution from the resin to determine what protein was bound to the resin.

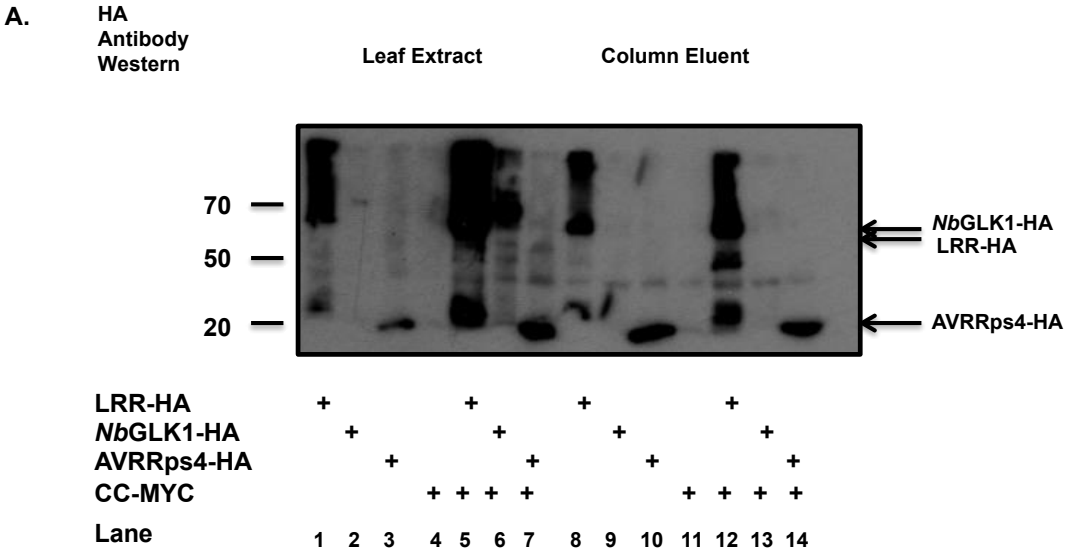
A.
HA
Antibody
Western
Leaf Extract
Column Eluent
70
50
20
NbGLK1-HA
LRR-HA
AVRRps4-HA
LRR-HA
NbGLK1-HA
AVRRps4-HA
CC-MYC
Lane
1 2 3 4 5 6 7 8 9 10 11 12 13 14

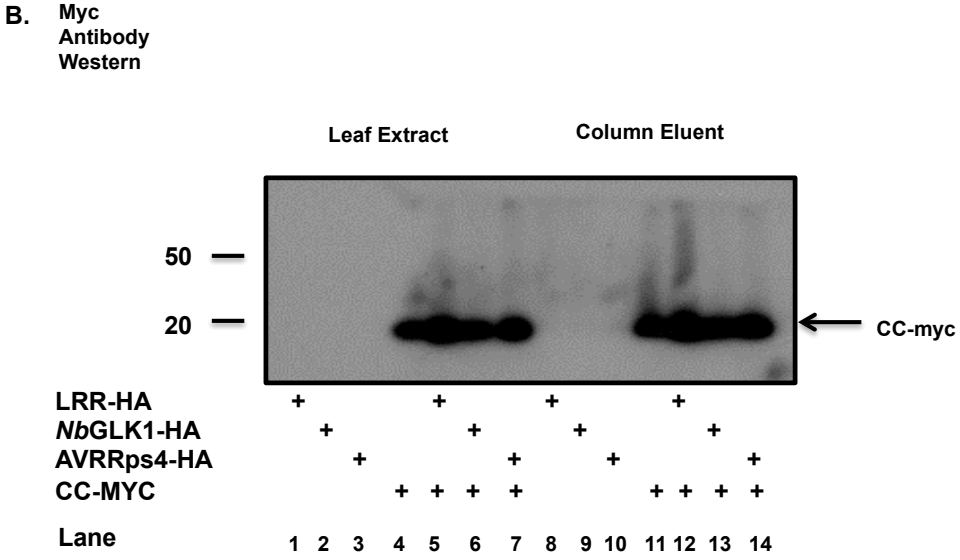
B.
Myc
Antibody
Western
Leaf Extract
Column Eluent
50
20
CC-myc
LRR-HA
NbGLK1-HA
AVRRps4-HA
CC-MYC
Lane
1 2 3 4 5 6 7 8 9 10 11 12 13 14

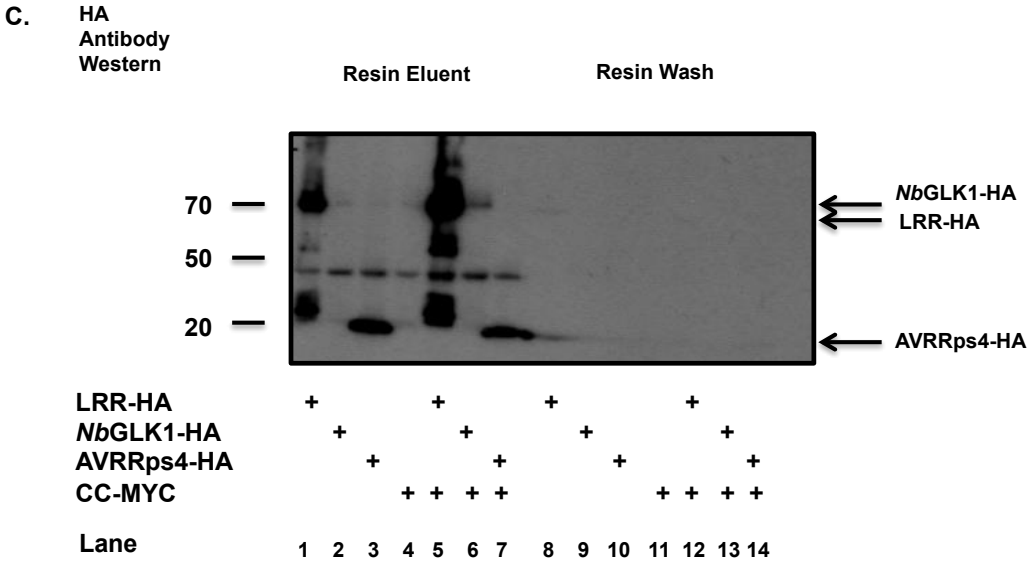
C.
HA
Antibody
Western
Resin Eluent
Resin Wash
70
50
20
NbGLK1-HA
LRR-HA
AVRRps4-HA
LRR-HA
NbGLK1-HA
AVRRps4-HA
CC-MYC
Lane
1 2 3 4 5 6 7 8 9 10 11 12 13 14

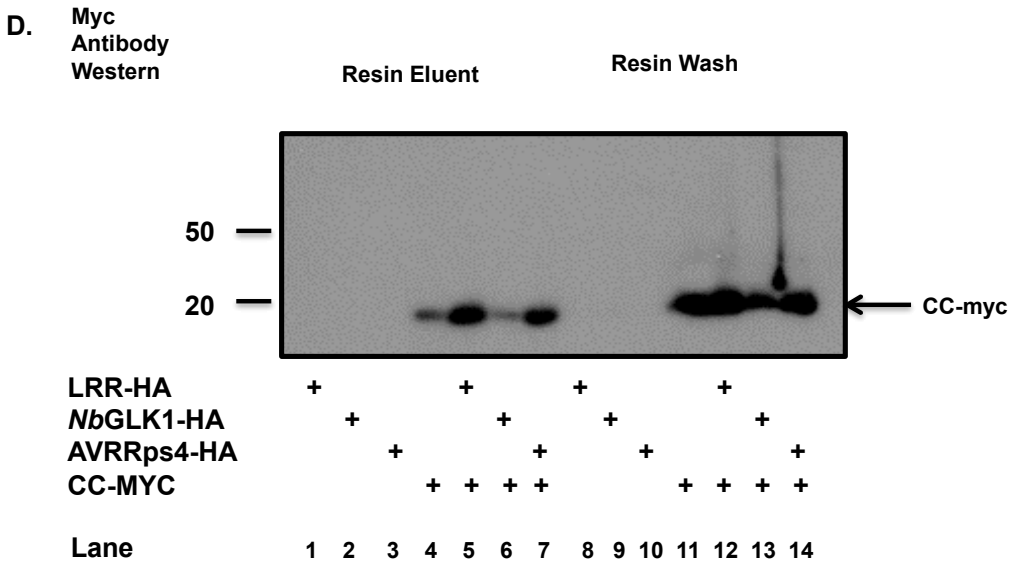

Figure 28: Western blot of co-immunoprecipitation of *N. benthamiana* leaf material expressing Rx1 CC-myc in combinations with and without a LRR-HA positive control, *Nb*GLK1-HA or an AVRRps4-HA negative control. Samples were taken after protein extraction, Sephadex G-25 column, washing the HA antibody resin, or eluting from the HA antibody resin. Protein was visualised using either a goat anti-myc 1° antibody and an anti-goat HRP linked 2° antibody or using a HRP linked rat anti-HA antibody.

The Western blotting of the protein extract from *N. benthamiana* showed all the proteins were expressing successfully (Figure 28 lanes A1-7, B4-7). However, the different proteins were expressing in very different amounts. Far more of the LRR-HA positive control and AVRRps4-HA negative control (lanes A1,3,5,7) was expressed than *Nb*GLK1-HA (A2,6).

The Western blotting of the samples taken from the Sephadex column eluent (lanes A8-14, B8-14) showed that almost all of the protein extract was successfully recovered from the column, with little to no noticeable drop in protein yield from the protein extract (lanes A1-7, B4-7).

Western blotting with an anti-HA antibody of the resin wash showed the complete absence of any HA tagged proteins (lanes C8-14). This show that all 3 HA tagged proteins successfully bound to the resin. All 3 were then successfully recovered in the elution stage as showed in the anti HA Western blot of the eluate (lanes C1-7).

Not all of the Rx1-CC present interacted with the resin and/or the HA tagged proteins, as protein could be observed in the resin wash for all samples in which it was present (lanes D11-14).

The CC domain was also eluted in all samples in which it was present (lanes D4-7). This includes both the negative control containing an AVRRps4-HA with Rx1-CC (D7) and the negative control containing only Rx1-CC with HA tagged protein at all (D4). Variations in the amount of Rx1-CC eluted between samples could be seen. But these correlated closely with variations amount of Rx1-CC being expressed in plants. The B7 and D7 negative control contain more than the B6 and D6 samples containing *Nb*GLK1 with Rx1-CC. i.e. more Rx1-CC was eluted in samples where more Rx1-CC was added to the resin, rather than as a result of a selective interaction with an HA tagged protein.

The elution of Rx1-CC from the sample lacking an HA tagged protein (D4) suggests that the CC domain was interacting directly with resin rather than with an intermediate protein. It was concluded that a stronger wash once the sample was loaded onto the resin was required to disrupt this interaction and provide selection solely on the basis of an interaction with the HA tagged protein.

4.7.4 Screen of Salt Concentration on co-immunoprecipitation of Rx1 and *Nb*GLK1

The previous section demonstrated that the resin wash buffer used in the co-immunoprecipitation was unable to wash non-specifically bound Rx1-CC off the resin. This section describes a screen of different wash conditions for the anti-HA antibody resin. The interaction between the different domains of Rx1 consists of an electrostatic attraction in current models (Slootweg et al., 2013). Structural characterisation of the interaction between the Rx1-CC domain and a known protein interactor RanGAP2, however, showed a hydrophobic interaction (Hao et al., 2013). It was hypothesised that wash conditions that promoted the electrostatic interaction between the LRR and the CC domain (used as a positive control in section 4.7.3) would not necessarily promote a possible hydrophobic interaction between *Nb*GLK1 and the CC domain. It was therefore decided to discard LRR as a positive control and instead focus on a comparison between the *Nb*GLK1-HA interaction with the Rx1-CC domain and the AVRRps4-HA negative control interaction with the Rx1-CC domain. Both of these were expressed in *N. benthamiana* and co-immunoprecipitated using a screened of various resin washes. Two wash buffers of increased NaCl concentration of 60mM and 80mM were trialled. As was another buffer of identical salt concentration to that used in section 4.7.3 (40mM), but with an increased concentration of Tween 20 from 0.1% (v/v) to 1% (v/v).

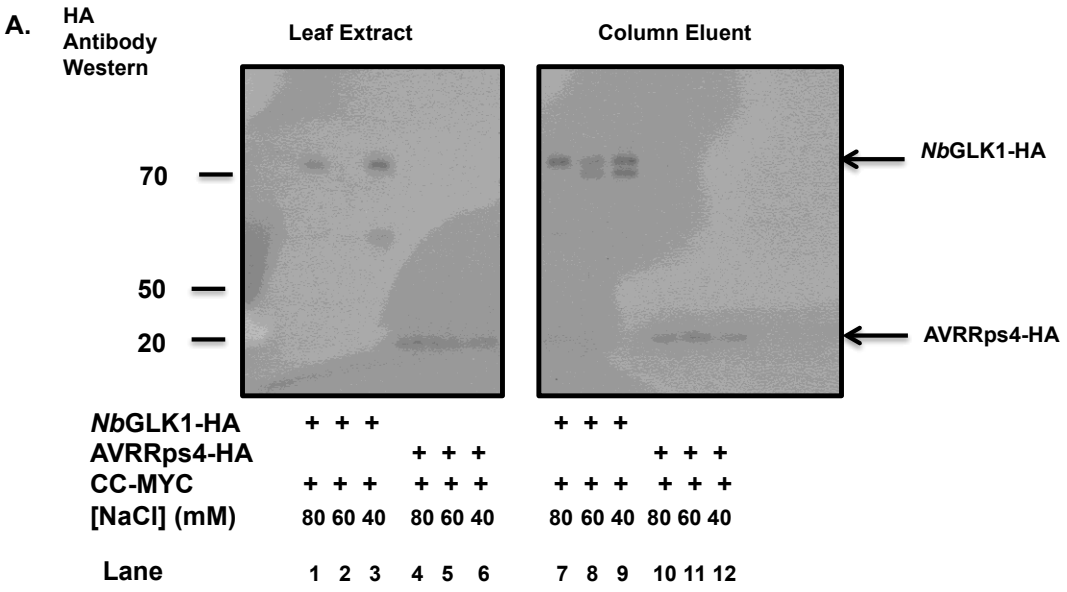
A.
HA Antibody Western
Leaf Extract
Column Eluent
70
50
20
NbGLK1-HA
AVRRps4-HA
NbGLK1-HA + + + + + +
AVRRps4-HA + + + + + +
CC-MYC + + + + + + + + + + + +
[NaCl] (mM) 80 60 40 80 60 40 80 60 40 80 60 40
Lane 1 2 3 4 5 6 7 8 9 10 11 12

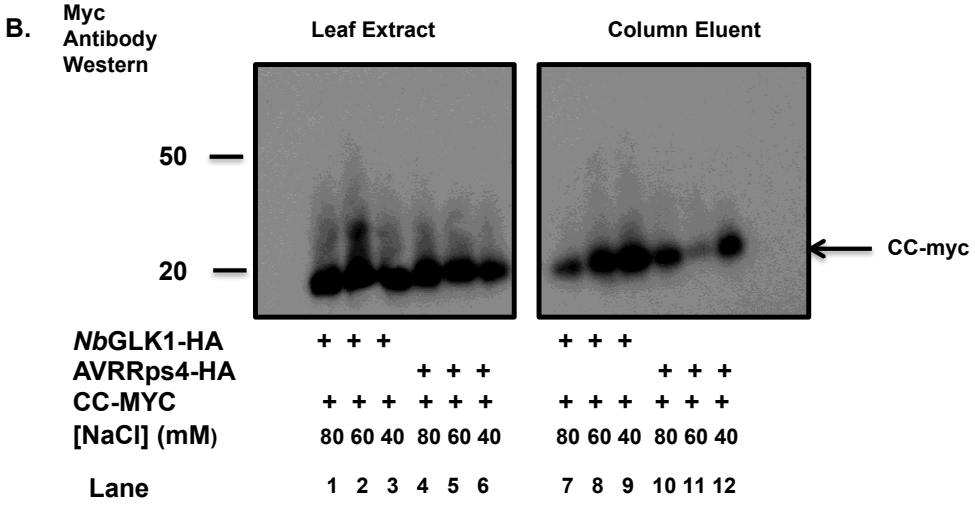
B.
Myc Antibody Western
Leaf Extract
Column Eluent
50
20
CC-myc
NbGLK1-HA + + + + + +
AVRRps4-HA + + + + + +
CC-MYC + + + + + + + + + + + +
[NaCl] (mM) 80 60 40 80 60 40 80 60 40 80 60 40
Lane 1 2 3 4 5 6 7 8 9 10 11 12

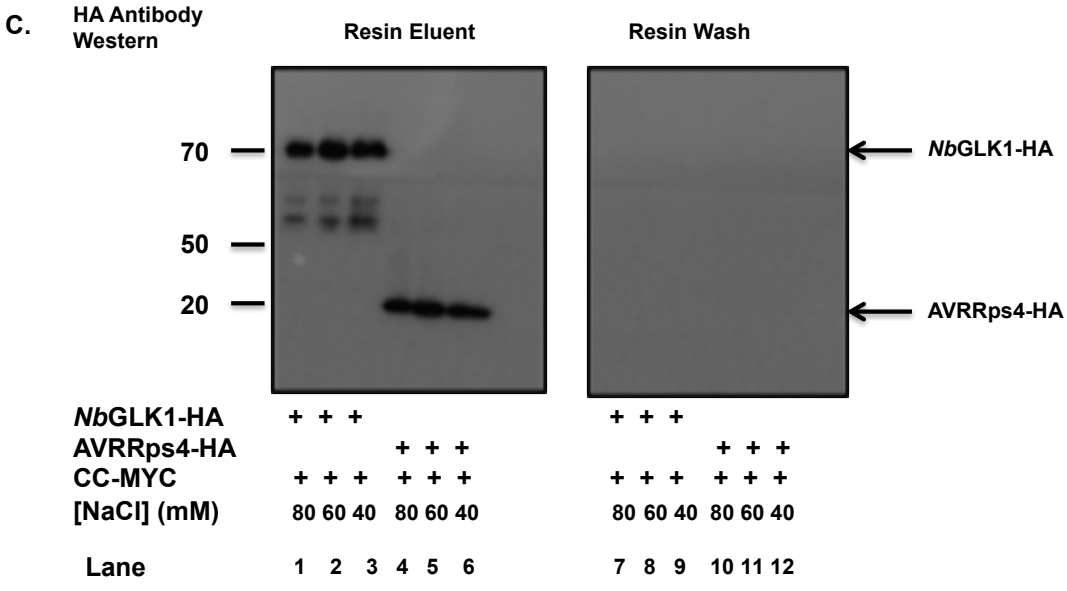
C.
HA Antibody Western
Resin Eluent
Resin Wash
70
50
20
NbGLK1-HA
AVRRps4-HA
NbGLK1-HA + + + + + +
AVRRps4-HA + + + + + +
CC-MYC + + + + + + + + + + + +
[NaCl] (mM) 80 60 40 80 60 40 80 60 40 80 60 40
Lane 1 2 3 4 5 6 7 8 9 10 11 12

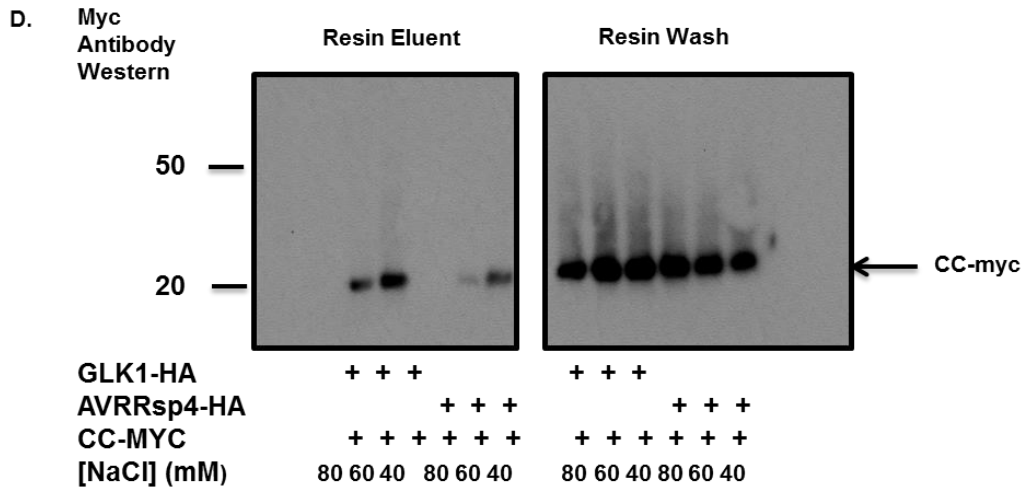

Figure 29: Western blot of a co-immunoprecipitation on *N. benthamiana* leaf material co-expressing Rx1-CC-myc with either *Nb*GLK1-HA or an AVRRps4-HA negative control. Samples taken after protein extraction, Sephadex G-25 column, washing the HA antibody resin, or eluting from the HA antibody resin. Anti HA antibody resin wash buffer contained 40, 60 or 80 mM NaCl as indicated. Protein was visualised using either a goat anti-myc 1° antibody and an anti-goat HRP linked 2° antibody or using a HRP linked rat anti-HA antibody.

The Western blot analysis of the post extraction and post column samples again showed all constructs expressing successfully (Figure 29. Lanes A1-6, B1-6) and passing through the Sephadex column (lanes A7-12, B7-12). The anti-HA Western blot of the resin wash and eluent showed both the desired HA tagged proteins successfully bound to the resin (lanes C1-6) and no detectable protein was washed off by any of the tested wash buffers (lanes C7-12).

The anti-myc Western blot showed changes in wash buffer did impact the affinity of the Rx1-CC domain for the resin. At the highest salt concentration (80mM NaCl) no Rx1-CC was eluted from the resin in the presence of both *Nb*GLK1 and AVRRps4 (lanesD1, D4). 80mM NaCl is therefore sufficient to disrupt non-specific interactions between Rx1-CC and the resin, but also disrupts any interaction there could potentially be with *Nb*GLK1. At the lowest NaCl concentration (40mM) with raised Tween 20 concentration (1% (v/v)) both *Nb*GLK1 and the negative control both eluted comparable amounts of Rx1-CC (lanes D3, D6). It was concluded that the elevated Tween 20 concentration had little effect on non-specific Rx1-CC interactions with the resin in the conditions tested.

The middle salt concentration (60mM NaCl) also displayed eluted Rx1-CC with both *Nb*GLK1 and AVRRps4 (D2, D5). However, the quantity of Rx1-CC visualised by the Western blot was far lower in the negative control (D5) than the *Nb*GLK1 (D2). Rx1-CC could therefore be interacting with *Nb*GLK1 over the negative control at these conditions. It should be noted however, that the leaves containing *Nb*GLK1 and Rx1-CC expressed more Rx1-CC (B2) than those containing AVRRps4 (B5). This means that any apparent selectivity may be an artefact caused by loading more Rx1-CC onto the resin.

4.7.5 Elution With Boiling SDS Sample Buffer

Section 4.7.4 showed a higher yield of eluted Rx1-CC for a *Nb*GLK1 sample over the negative control. To try and improve this selectivity observed in it was decided to use a harsher elution method on the anti-HA antibody resin to ensure all bound protein was removed. In previous sections the resin had been eluted using a 50 mM NaOH elution buffer at 4°C. A co-immunoprecipitation was carried out on *N. benthamiana* leaves expressing Rx1-CC-myc both with and without *Nb*GLK1, with protein eluted from the resin using SDS-PAGE loading buffer (see Materials and Methods 2.3.) at 95°C.

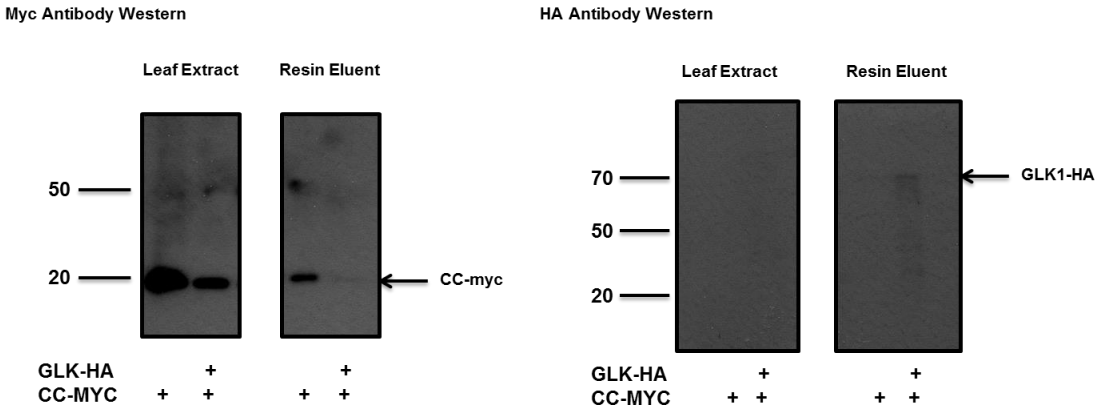

Figure 30: Western blot of co-immunoprecipitation on *N. benthamiana* leaf material expressing Rx1-CC-myc with and without *Nb*GLK1-HA. Samples taken after protein extraction and after eluting from the HA antibody resin. Protein was visualised using either a goat anti-myc 1° antibody and an anti-goat HRP linked 2° antibody or using a HRP linked rat anti-HA antibody.

The results show that *Nb*GLK1 was not visualised in the sample from the leaf extract (Figure 30, B2), but was in the resin eluent (B4), showing that the protein was expressed but required concentrating on the resin to visualise. More Rx1-CC was eluted in the absence of *Nb*GLK1 (lane A3) than with it present (lane A4). However lanes A1 and A2 on the myc antibody western show far more CC-myc expressed in the leaves without *Nb*GLK1 (A1) than with (A2). Rx1-CC elution was hence linked to variations in the amount expressed in leaves rather than the presence of *Nb*GLK1. It was therefore concluded that the new elution method was ineffective at improving selectivity for an interaction between Rx1-CC and *Nb*GLK1.

4.8 Conclusion

The Yeast 2-hybrid screen results identified *Nb*GLK1 as a potential regulator of Rx1 DNA binding, showing a strong binding affinity for the Rx1-CC domain and belonging to a known family of transcription factors. A FRET-FLIM assay on the effect of *Nb*GLK1 on Rx1 DNA binding in fixed leaf material showed that *Nb*GLK1 promotes Rx1 DNA binding in the absence of its cognate viral elicitor CP106. FRET-FLIM analysis of *Nb*GLK1 DNA binding showed that Rx1 did in turn promote *Nb*GLK1 DNA binding when co-expressed with CP106.

Analysis of the impact of *Nb*GLK1 on Rx1 mediated PVX immunity showed that *Nb*GLK1 inhibits viral replication of PVX in the absence of Rx1. However, *Nb*GLK1 did not promote HR in *N. benthamiana* when expressed in isolation or with Rx1 or CP106. *Nb*GLK1 linked immunity occurs independently of HR. *Nb*GLK1 was concluded to work parallel to Rx1 in a defence signal transduction pathway that did

not induce HR. However, NbGLK1 could not be shown to interact with the Rx1-CC domain *in planta* via co-immunoprecipitation.

This chapter concludes that *Nb*GLK1 acts as a positive regulator of Rx1 DNA binding and extreme resistance to PVX, but not Rx1 mediated HR. However, further work is required to establish whether or not an interaction occurs between the two proteins *in planta* (see Chapter 6).

4.9 Discussion

The FLIM-FRET work performed in fixed *N. benthamiana* is supported by *Nb*GLK1 DNA binding assays *in vitro* on recombinant protein using fluorescence anisotropy that show it possesses a DNA binding ability (Townsend et al., unpublished data). This *Nb*GLK1 DNA binding has also been shown to be sequence specific. Specificity in Rx1 DNA binding could therefore be mediated by an Rx-GLK1 interaction. The impact of Rx1 on *Nb*GLK1 DNA binding has also been demonstrated *in vitro* using fluorescence anisotropy with fluorescently tagged oligonucleotides. This showed that Rx1 CCNBARC and CC both inhibited *Nb*GLK1 DNA binding (Townsend et al., unpublished data). The *in planta* FRET-FLIM data showed full length Rx1 promoting *Nb*GLK1 DNA binding in the plant cell.

These results suggest that that *Nb*GLK1 enables site-specific DNA binding of Rx1 and this promotes Rx1 triggered extreme immunity to PVX, preventing the accumulation of PVX in infected cells. *Nb*GLK1 belongs to a known family of transcription factors (Chen et al., 2016). These have been previously demonstrated to have a role in immunity in *Arabidopsis* against cucumber mosaic virus and the fungal pathogens

Fusarium graminearum and *Hyaloperonospora arabidopsidis* (Han et al., 2013, Murmu et al., 2014). The fact that *Nb*GLK1 promoted immunity in the absence of Rx1 suggests it could also be acting in parallel, with multiple NBLRR proteins and this is supported by the fact that it also provides immunity to these other pathogens that are not sensed by Rx1. *Nb*GLK1 does not impact Rx1 mediated HR, implying that HR is caused by a separate signal transduction pathway, possibly not triggered by Rx1 DNA binding.

The results did not show an interaction between *Nb*GLK1 and Rx1 in the coimmunoprecipitation. However, *in vitro* analysis of recombinant *Nb*GLK1 and Rx1 CC using size exclusion gel chromatography shows co-elution of the two proteins (Townsend et al., unpublished data) which does support the yeast 2-hybrid data in suggesting a physical interaction is occurring between the two, suggesting further work is needed to clarify whether there is an interaction or not (see Discussion chapter, Section 6.3).

5. The impact of *Nb*MLHP on Rx1 triggered immunity

5.1 Introduction

Chapter 4 described a Yeast 2-hybrid experiment using the CC domain of Rx1 to identify potential regulators of Rx1 DNA binding from a *Nicotiana benthamiana* cDNA library. The protein *Nb*GLK1 was identified and characterised as a positive regulator of Rx1 DNA binding and PVX immunity.

However, the same Yeast 2-hybrid experiment generated other putative Rx1 CC interactors with DNA binding domains. This chapter describes experiments on a second potential regulator of Rx1 DNA binding, with the aim of confirming whether this protein affects Rx1 DNA binding, and what impact it has on Rx1 mediated immunity.

A protein with high homology to the predicted *Solanum tuberosum* protein MLHP (micronuclear linker histone polyprotein) displayed affinity for the CC domain in the Yeast 2-Hybrid assay. Bioinformatic analysis of this protein predicted a SANT domain at the N-terminus. SANT domains are DNA binding domains known to be involved in chromatin remodelling (Boyer et al., 2002). A bromodomain was also predicted in the central region. Bromodomains are domains with an acetyl lysine binding activity. Often proteins with this domain regulate gene expression via targeting of DNA binding protein such as histones, leading to changes in chromatin remodelling (Sanchez et al., 2009). It was therefore hypothesised that *Nb*MLHP was a regulator of Rx1 DNA binding.

This chapter describes experiments that investigate the impact of *Nb*MLHP on Rx1 activity. The impact of *Nb*MLHP on Rx1 DNA binding, the Rx1 mediated defence response, and Rx1 mediated cell death were all tested. The impact of Rx1 on *Nb*MLHP DNA binding was also assayed, as was the ability of Rx1 and *Nb*MLHP to interact *in planta.*

5.2 Yeast 2-hybrid results

The previous Chapter described a Yeast 2-hybrid screen using the Rx1 CC domain against a library of *N. benthamiana* cDNA with the aim of finding potential regulators of Rx1 DNA binding (see Section 4.2 and Materials and Methods section 2.3.4). Proteins with strong affinities for the CC domain that also contained putative DNA binding domains were identified as potential regulators of Rx1 DNA binding.

7 positive results from the initial screen were of an overlapping sequence that was combined to an SID of the bromodomain of a protein in the cDNA library. This protein displayed a high level of homology the predicted protein at LOC102600407 (GenBank ID: 565386739) in the potato genome (see appendices 7.1-2). Computational analysis determining the reliability of this positive result gave a PRBS score of A, corresponding to 'very high confidence in the interaction' (see Section 2.3.4 for an explanation of the PRBS score). The protein was subject to a 1x1 Yeast 2 hybrid screen as described in section 4.3, and this confirmed this result, showing yeast growth on the 10 mM 3-Amino-1,2,4-triazole (3-AT) supplemented leucine, tryptophan and histidine deficient plate (Figure 32). No growth was seen on the corresponding plate for any of the negative controls.

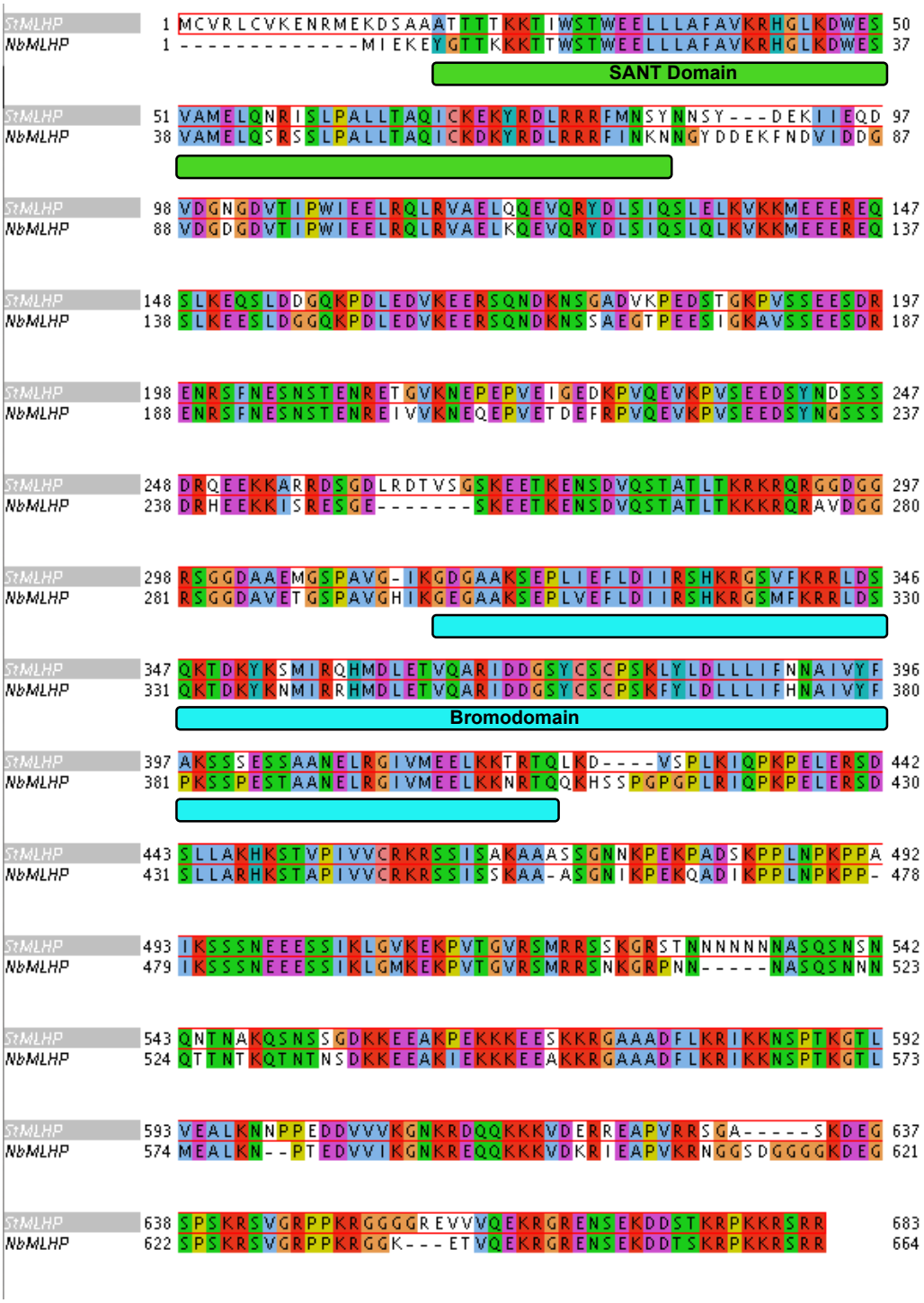

Figure 31. Sequence alignment of *Nicotiana benthamiana* MLHP (*Nb*MLHP) amino acid sequence with *Solanumm tuberosum* MLHP (*Sb*MLHP) using ClustalOmega. Conserved residues between the sequences are highlighted. A SANT domain is predicted between *Nb*MLHP residues 6-72 and a bromodomain predicted between residues 301-408 using InterPro domain annotation.

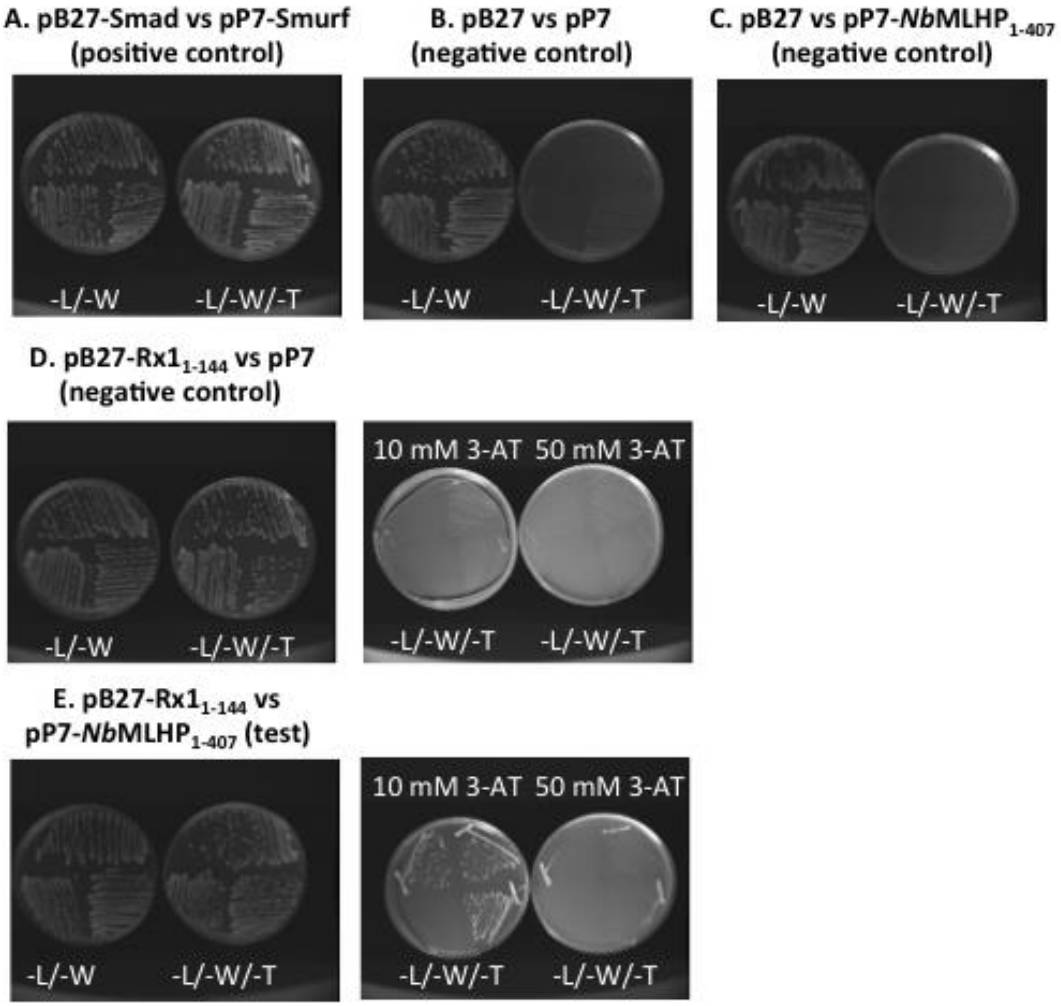

Figure 32. 1x1 Yeast 2 hybrid screen of CC Rx1 against *Nb*MLHP performed by Hybrigenics. Rx1 was fused to the Gal4 DNA-binding domain and *Nb*MLHP was fused to the Gal4 activation domain. Plates were grown on medium lacking leucine and tryptophan (−L/−W) and medium lacking leucine, tryptophan, histidine (−L/−W/−T), supplemented with 10 or 50 mM 3-Amino-1,2,4-triazole (3-AT). A. Smad vs Smurf positive control B. Empty pB27 bait vs empty pP7 prey negative control. C empty pB27 bait vs *Nb*MLHP in prey negative control. D. Rx1 containing bait vs empty pP7 prey negative control. E. CC Rx1 in pB27 bait plasmid with *Nb*MLHP in pP7 prey plasmid.

Bioinformatic analysis using ClustalOmega for multiple sequence alignment (https://www.ebi.ac.uk/Tools/msa/clustalo/ (Sievers et al., 2011)) and Interpro for domain annotation (http://www.ebi.ac.uk/interpro/ (Mitchell et al., 2014)) of this protein showed high homology to the *Solanum tuberosum* protein MLHP (micronuclear linker histone polyprotein) (Figure 30) and predicted 2 potential chromatin-associated domains. A SANT domain; a DNA binding domain known to be involved in chromatin remodelling (Boyer et al., 2002), and a bromodomain. Bromodomains are involved in acetyl lysine binding, and are not inherently chromatin associated (Boyer et al., 2002). A common target of their acetyl lysine binding activity is histones. Acetyl lysine binding of histones is associated with regulation of gene expression via chromatin remodelling (Sanchez et al., 2009). The presence of a DNA binding SANT domain that is associated with chromatin remodelling led to the hypothesis that the putative bromodomain in *Nb*MLHP also has a role in chromatin remodelling, and targets a DNA associated protein for acetyl lysine binding, possibly histones.

Bromodomain containing proteins have been shown to have a role in immunity in humans; BRD4 acetylates a lysine residue on NFκB to activate the inflammatory response (Huang el al,. 2009). BRD4 has also been shown to have a role in the transcription of viral genes, regulating HIV transcription (Zou et al., 2009), preventing papillovirus E2 protein (Gagnon et al., 2009), and interacting with Kaposi's sarcoma-associated herpesvirus-encoded LANA-1 (Ottinger et al., 2009). In plants the cucumber RNA binding bromodomain protein BRP1 has been shown to regulate cucumber mosaic virus (CMV) replication (Chaturvedi et al., 2016) and the bacterial

effector protein PopP2 deactivates a plant immunological WRKY transcription factor through an acetyl lysine binding activity (Sarris et al., 2015).

It was hypothesised that *Nb*MLHP regulated Rx1 DNA binding, and experiments with aim of characterising its activity and relationship with Rx1 were undertaken

5.3 *Nb*MLHP does not impact Rx1 DNA binding *in vivo*

Chapter 4 demonstrated that *Nb*GLK1 promoted Rx1 DNA binding in *N. benthamiana* using FRET-FLIM analysis. This section aims to determine if *Nb*MLHP also influences Rx1 DNA binding using the same method. *Nb*MLHP-HA and GFP-Rx1 were co-infiltrated (Materials and Methods 2.3.1, Table 4) both with and without CP106 into *Nicotiana benthamiana* leaves. *Nb*GLK1-HA and CP106 were infiltrated at OD_{600} = 0.4 to maximise expression and GFP-Rx1 was infiltrated at OD_{600} = 0.1 to prevent cell death via HR. The leaves were fixed in formaldehyde and stained with LDS-751. The same FRET-FLIM assay developed in Chapter 3 (section 3.2, Materials and Methods 2.3.2/3) was then performed on GFP-Rx1 to determine under which conditions it bound genomic DNA.

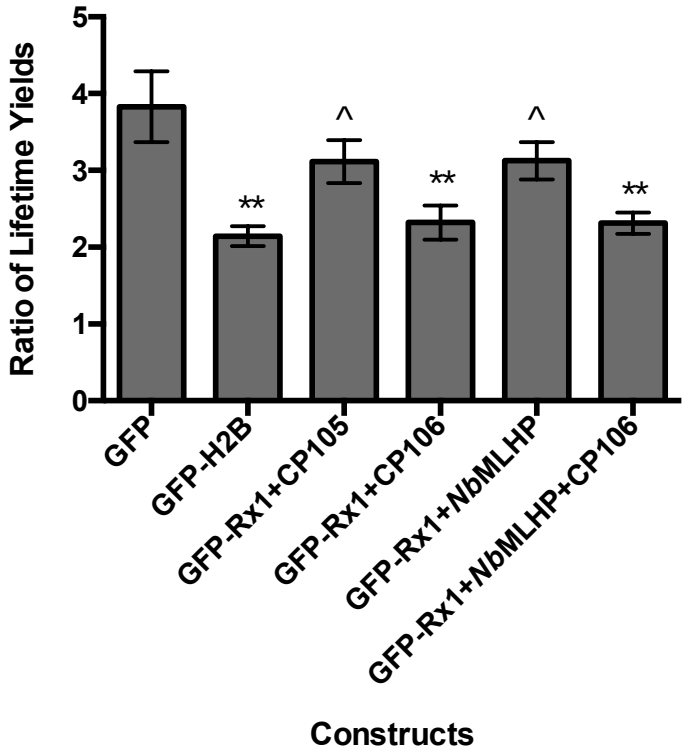

Figure 33. The average ratio of fluorescence lifetimes for *N. benthamiana* leaves expressing GFP-Rx1 in combination with *Nb*MLHP and CP106 fixed in formaldehyde and stained with LDS-751. Free GFP and GFP-H2B expressing *N. benthamiana* are included as negative and positive controls. n = 6-10. ^ indicates adjusted p value > 0.05, * indicates adjusted p value < 0.05, ** indicates adjusted p value < 0.01. Adjusted p values calculated using a Dunnett-Wilson Multiple Comparison ANOVA test.

The experiment showed GFP-Rx1 lifetime ratios did not differ from the GFP negative control in the absence of CP106 (Figure 33). Significant drops in lifetime ratio were then observed upon co-expression with CP106. This pattern occurred both with and without *Nb*MLHP coexpression. Sections 3.4 and 4.3 both concluded that Rx1 did not bind genomic DNA in the *N. benthamiana* leaves unless CP106 was co-expressed, as indicated by the drop in lifetime ratio. This experiment again repeated this result. That a similar drop in lifetime ratio occurs in the presence *Nb*MLHP-HA suggests the protein is not affecting Rx1 DNA binding.

5.4 The influence of Rx1 on *Nb*MLHP DNA binding *In Vivo*

Bioinformatic analysis predicted a DNA binding SANT domain in *Nb*MLHP (see section 5.2). The previous section concluded that *Nb*MLHP does not affect Rx1 DNA binding. It was hence thought that perhaps Rx1 acts upstream of *Nb*MLHP and the putative interaction between them involves Rx1 regulating *Nb*MLHP DNA binding. This section aims to determine if Rx1 affects any potential *Nb*MLHP DNA binding. To achieve this, *Nb*MLHP was cloned into the *Agrobacterium tumefaciens* vector pK7GF2 using a gateway reaction via a pDONR207 intermediate vector (see Section 2.2.13), providing an N-terminal GFP tag. The same FRET-FLIM experiment performed in section 5.3 was repeated, but with Rx1 expressed untagged and NbMLHP was expressed with an N-terminal GFP tag (Materials and Methods 2.3.1, Table 4). All incubation periods and OD_{600} infiltration values were unchanged from section 5.3. The fluorescence lifetimes of GFP-*Nb*MLHP were then analysed to determine under which, if any, conditions it bound genomic DNA.

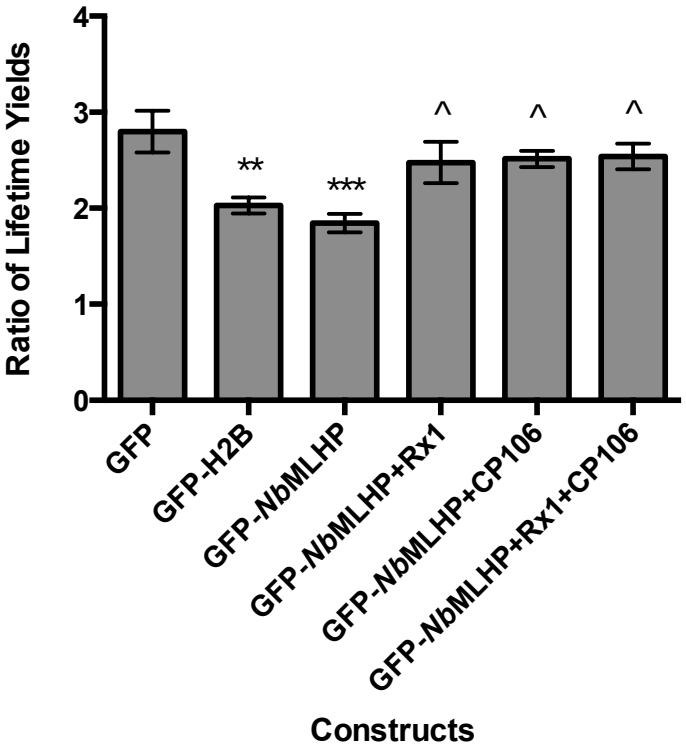

Figure 34. The average ratio of fluorescence lifetimes for *N. benthamiana* leaves expressing GFP-*Nb*MLHP in combination with Rx1 and CP106 fixed in formaldehyde and stained with LDS-751. Free GFP and GFP-H2B expressing *N. benthamiana* are included as negative and positive controls. n = 7-11. ^ indicates adjusted p value > 0.05, * indicates adjusted p value < 0.05, ** indicates adjusted p value < 0.01, *** indicates adjusted p value < 0.001. Adjusted p values calculated using a Dunnett-Wilson Multiple Comparison ANOVA test.

When expressed in isolation, GFP-*Nb*MLHP displayed a low lifetime ratio (Figure 33) comparable to the GFP-H2B positive control. This implies *Nb*MLHP binds genomic DNA. However, upon coexpression with either Rx1, CP106, or both Rx1 and CP106 together, a statistically significant rise in GFP-*Nb*MLHP lifetime ratio is seen. It was concluded that the expression of these proteins inhibits *Nb*MLHP DNA binding.

Expression of Rx1 and CP106 together reduced *Nb*MLHP DNA binding. This implies *Nb*MLHP may act as a negative regulator of plant immunity. In a resting state *Nb*MLHP might bind DNA via its SANT domain and supresses defence gene

activation through bromodomain mediated histone binding. CP106 activates Rx1 to trigger the Rx1 mediated defence response. Interaction between the active Rx1 CC domain and *Nb*MLHP might then reduce its ability to bind DNA.

Rx1 expression in the absence of CP106 also inhibited *Nb*MLHP DNA binding. Overexpression of Rx1 can lead to a plant immune response in the absence of C106 (Bendahmane et al., 2002). It may be that the result is an artefact of Rx1 overexpression initiating immunity and preventing *Nb*MLHP binding DNA.

CP106 in the absence of Rx1 inhibited *Nb*MLHP DNA binding. This could suggest that *Nb*MLHP acts parallel to Rx1 in defence signal transduction. Rx1 can deactivate *Nb*MLHP but so can other defence proteins present in the *N. benthamiana* leaf that are also activated by CP106 expression.

5.5 The impact of *Nb*MLHP on PVX Viral replication

Section 5.4 demonstrated Rx1 inhibited *Nb*MLHP DNA binding activity. It was hypothesised that *Nb*MLHP DNA binding supressed defence genes and that *Nb*MLHP expression would promote PVX infection. Chapter 4 showed *Nb*GLK1 promoted extreme resistance to PVX in *N. benthamiana* leaves using an *Agrobacterium* vector containing a GFP tagged PVX virus genome (section 4.5). This section investigates the impact of *Nb*MLHP expression on Rx1 mediated extreme resistance to PVX using the same GFP-PVX assay.

Different areas of the same *N. benthamiana* leaves were infiltrated with GFP-PVX, GFP-PVX and Rx1, GFP-PVX and *Nb*MLHP, and finally GFP-PVX with Rx1 and *Nb*MLHP (see Materials and Methods 2.3.1, Table 4). Areas of *N. benthamiana* leaves were infiltrated with *Agrobacterium* transformed with the pGR208 vector containing the GFP tagged PVX viral genome at OD_{600} = 0.4. HA-*Nb*MLHP was infiltrated at OD_{600} = 0.4. The leaves were incubated for 1 day before infiltration of the appropriate areas with Rx1 at OD_{600} = 0.05. GFP-PVX fluorescence intensity of the infiltrated leaf area was then recorded and the change in GFP-PVX expression across the differently infiltrated areas of the leaf analysed (see Materials and Methods 2.3.5).

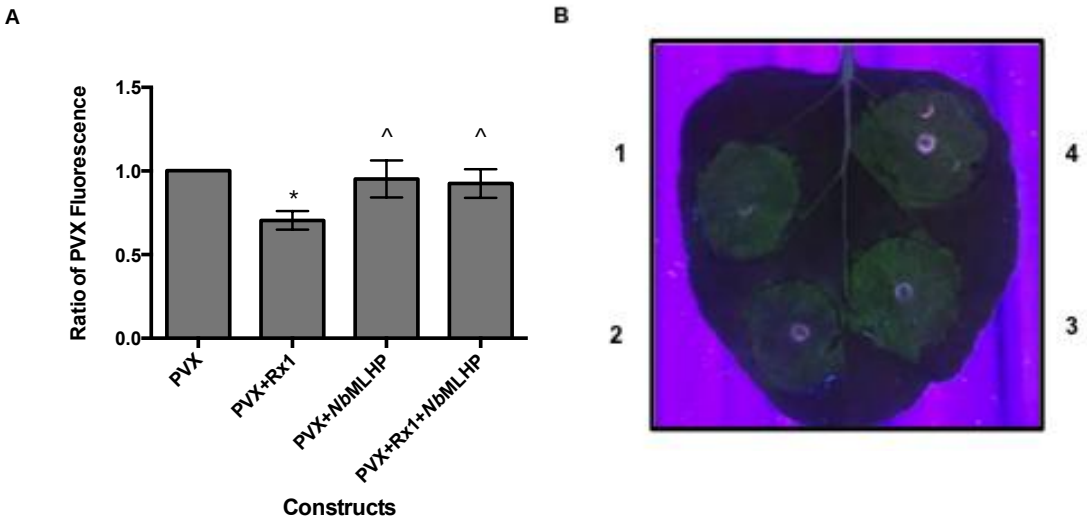

Figure 35. (A) The average ratio of fluorescence to a GFP-PVX control for *N. benthamiana* leaves expressing GFP-PVX in combinations with *Nb*MLHP and Rx1. n = 16. ^ indicates adjusted p value > 0.05, * indicates adjusted p value < 0.05,. Adjusted p values calculated using a Dunnett-Wilson Multiple Comparison ANOVA test. (B) A representative *N. benthamiana* leaf of the results under UV light showing the PVX fluorescence. 1 = PVX, 2 = PVX + Rx1, 3 = PVX + *Nb*MLHP, 4 = PVX + Rx1 + *Nb*MLHP

A drop in GFP-PVX fluorescence was observed upon co-infiltration with Rx1 (Figure 35). Co-expression with *Nb*MLHP or with both *Nb*MLHP and Rx1 together resulted in no significant change in GFP-PVX fluorescence from the GFP-PVX control. The drop in fluorescence with Rx1 was concluded to be the result of Rx1 triggered extreme immunity inhibiting viral replication. Co-expression with *Nb*MLHP inhibited this immune response. This result suggests that *Nb*MLHP suppresses Rx1 mediated viral resistance, and it was hypothesised that this suppression was mediated by the DNA binding activity of *Nb*MLHP demonstrated in section 3.4.

5.6 The effect of bromodomain mutation on PVX Viral replication

Bioinformatic analysis of *Nb*MLHP predicted the presence of a bromodomain and a DNA binding SANT domain (Figure 31). The presence of a SANT domain suggests that the protein with the acetyl lysine group *Nb*MLHP binds to may associate with DNA. It is common for bromodomain acetyl lysine binding on chromatin-associated proteins (usually histones) to promote gene expression through chromatin remodelling (Sanchez et al., 2009), and SANT domains are also associated with chromatin remodelling (Boyer et al., 2002). Previous sections showed *Nb*MLHP supressed an Rx1 triggered extreme resistance to PVX (section 5.5), and that Rx1 inhibited *Nb*MLHP DNA binding (section 5.4). It was hypothesised that *Nb*MLHP supressed Rx1 mediated extreme resistance to PVX through histone acetyl lysine binding subsequent to DNA binding, promoting transcription of genes that inhibit immunity.

To test this hypothesis, the bromodomain of *Nb*MLHP was mutated to inhibit binding to acetylated lysine. The residues responsible for bromodomain lysine binding have been previously elucidated for the human bromodomain containing protein Gcn5p, a histone acetyl lysine transferase (Owen et al., 2000). A protein BLAST search (https://blast.ncbi.nlm.nih.gov/Blast.cgi?PAGE=Proteins)(Altschul et al., 2007) was used to identify the corresponding residues in *Nb*MLHP and two highly conserved residues were picked for mutation, Y336 and E386. 2 HA tagged *Nb*MLHP bromodomain mutants were constructed by P. Townsend (Table 4) for transient expression in *N. benthamiana*; Y336F and E386L (Figure 36A).

These constructs were than used in a similar viral replication assay as described in section 5.5, with the wild type *Nb*MLHP previously used replaced with the bromodomain mutants Y336F and E386L (see Materials and Methods 2.3.1, Table 4). Mutants were infiltrated into and incubated in *N. benthamiana* leaves under the same conditions as wild type *Nb*MLHP was in section 5.5. The GFP-PVX viral fluorescence was recorded and analysed as described previously to determine the impact of these mutants on Rx1 mediated viral immunity (see section 5.5 and Materials and Methods section 2.2.).

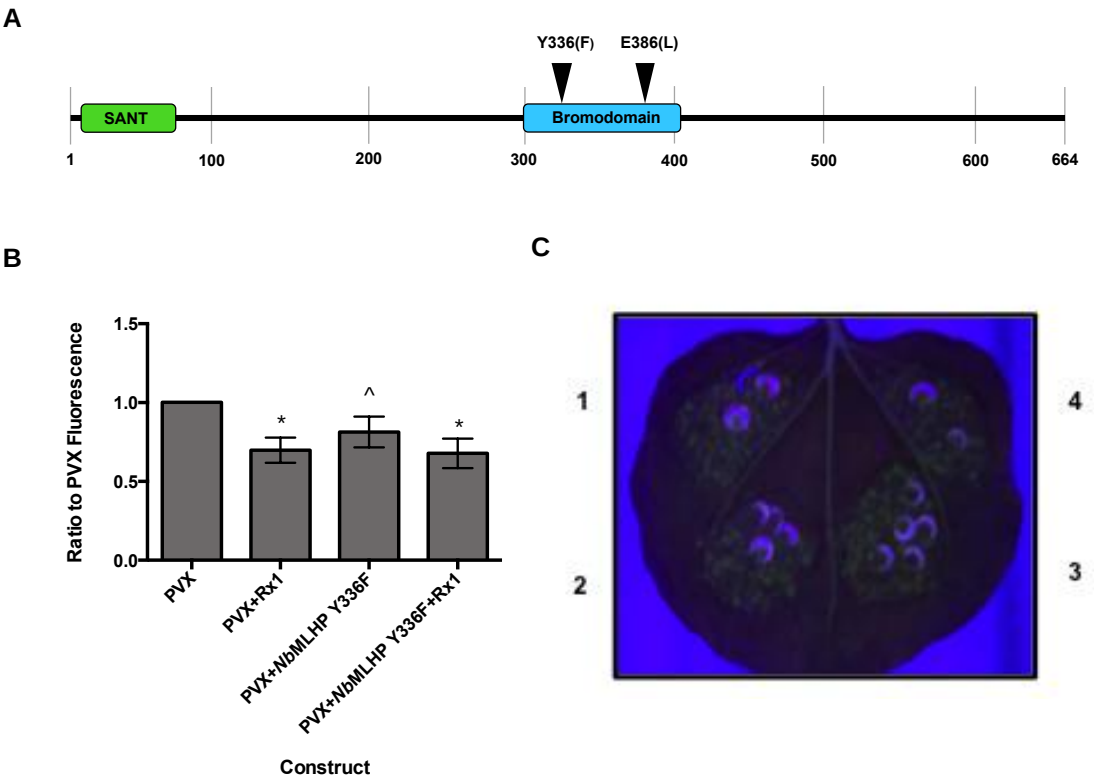

Figure 36. (A) A schematic of *Nb*MLHP protein sequence showing the location of the SANT domain (green), bromodomain (cyan) and two putative acetyl lysine binding sites selected for mutation at Y336 and E386. The letter in brackets at the mutation site indicates the substituted amino acid in the mutant constructs. Numbers indicate amino acid residues (B) The average ratio of fluorescence to a GFP-PVX control for *N. benthamiana* leaves expressing GFP-PVX in combinations with *Nb*MLHP and Rx1. $n = 20$. ^ indicates adjusted p value > 0.05, * indicates adjusted p value < 0.05. Adjusted p values calculated using a Dunnett-Wilson Multiple Comparison ANOVA test. (C) A representative *N. benthamiana* leaf of the results under UV light showing the PVX fluorescence. 1 = PVX, 2 = PVX + Rx1, 3 = PVX + *Nb*MLHP Y336F, 4 = PVX + Rx1 + *Nb*MLHP Y336F

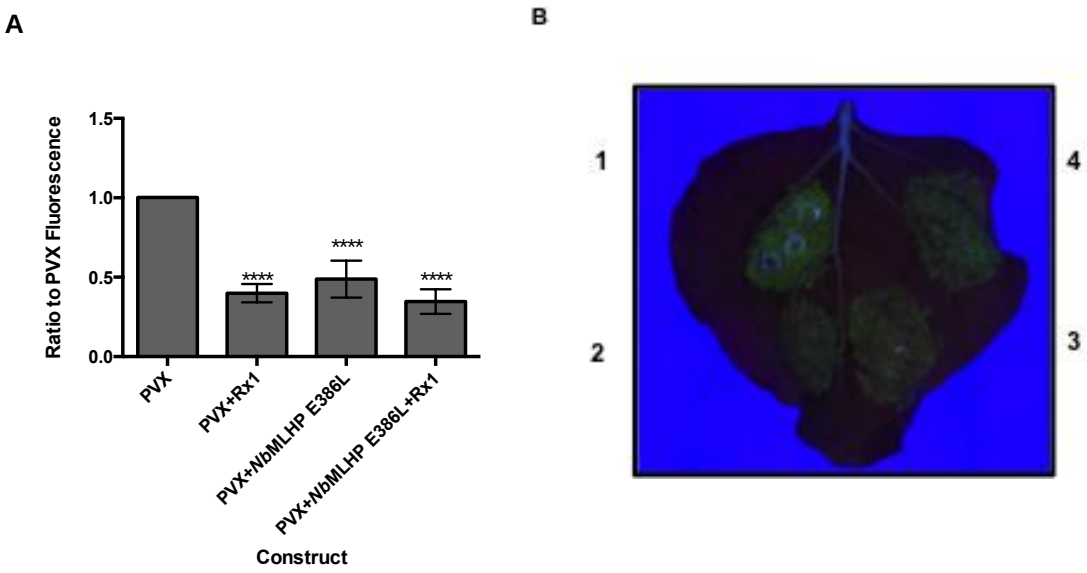

Figure 37 (A) The average ratio of fluorescence to a GFP-PVX control for *N. benthamiana* leaves expressing GFP-PVX in combinations with *Nb*MLHP E386L and Rx1. $n = 11$. ^ indicates adjusted p value > 0.05, **** indicates adjusted p value < 0.0001. Adjusted p values calculated using a Dunnett-Wilson's multiple comparisons test. (B) A representative *N. benthamiana* leaf of the results under UV light showing the PVX fluorescence. 1 = PVX, 2 = PVX + Rx1, 3 = PVX + *Nb*MLHP E386L, 4 = PVX + Rx1 + *Nb*MLHP E386L.

As seen previously, a drop viral fluorescence was observed upon co-expression of Rx1 in each of the mutant assays (Figures 36 and 37). This was concluded to be the result of Rx1 triggered immunity to PVX. Co-expression of GFP-PVX with *Nb*MLHP Y336F led to no statistically significant change in viral fluorescence, similar to the lack of change in fluorescence observed when wild type *Nb*MLHP was co-expressed with GFP-PVX (section 5.5). However, a drop in viral fluorescence was seen when both Rx1 and *Nb*MLHP Y336F were co-expressed with the viral genome. This drop was not observed upon co-expression of wild type *Nb*MLHP with Rx1. It was concluded that the suppression of Rx1 mediated viral resistance by *Nb*MLHP observed in section 5.5 was deactivated by the Y336F mutation.

The second mutant, E386L, caused a significant drop in viral fluorescence when expressed both with and without Rx1. It was concluded that this mutation reversed the effect of the wild type protein, promoting viral immunity rather than suppressing it. The results suggest the underlying hypothesis was correct and suppression of Rx1 mediated immunity by *Nb*MLHP likely occurs through acetyl lysine binding. Mutations in the protein preventing the theoretical binding to acetyl lysine either negate immune repression (Y335L), or result in active promotion of a plant immune response immune (E386L). However the acetyl lysine binding activity of *Nb*MLHP does require further experimental verification before this hypothesis can be confirmed (see section 6.4.2 for further details).

5.7 The impact of *Nb*MLHP with *Nb*GLK1 on Viral Replication

Section 5.5 showed *Nb*MLHP inhibited Rx1 triggered extreme immunity to PVX. Section 5.4 showed CP106 inhibited *Nb*MLHP DNA binding independently of Rx1. Chapter 4 showed *Nb*GLK1 inhibited PVX replication independently of Rx1 (see section 4.5). It was therefore hypothesised that *Nb*MLHP could inhibit *Nb*GLK1 triggered immunity to PVX independently of Rx1.

This section aims to test this hypothesis using the same GFP viral replication assay in the previous section, replacing Rx1 with the HA-*Nb*GLK1 construct used in section 4.5. All constructs were infiltrated under the same conditions used in section 5.4 and incubated for the same time period. HA-*Nb*GLK1 was infiltrated and incubated for the same time period as noted in section 4.5. GFP fluorescence intensity readings were recorded and analysed as described in Materials and Methods section 2.2.

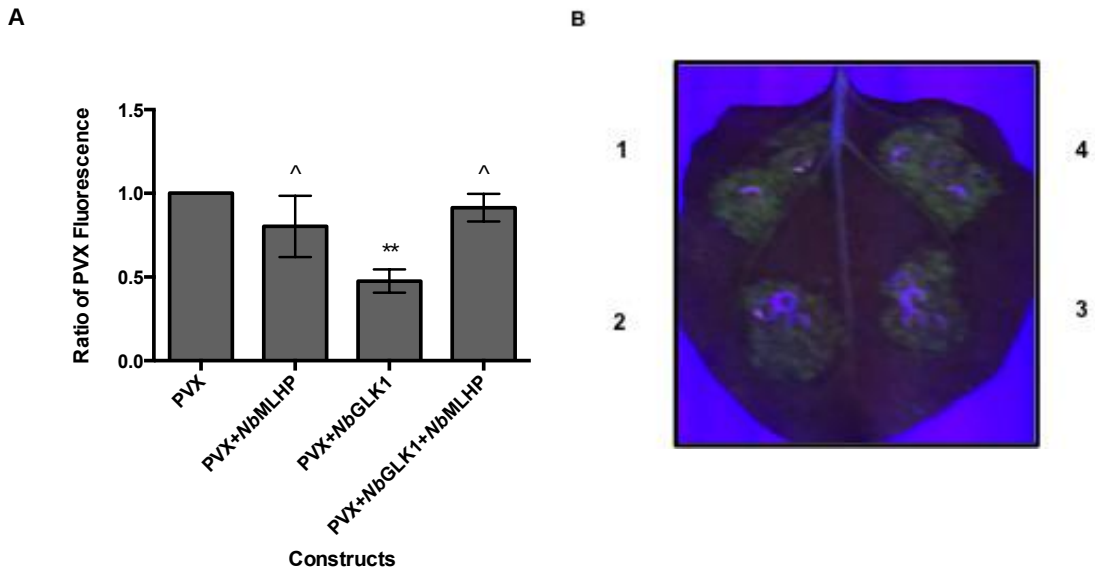

Figure 38. (A) The average ratio of fluorescence to a GFP-PVX control for *N. benthamiana* leaves expressing GFP-PVX in combinations with *Nb*MLHP and *Nb*GLK1. $n = 6$. ^ indicates adjusted p value > 0.05, **indicates adjusted p value < 0.01, Adjusted p values calculated using a Dunnett-Wilson multiple comparisons test. (B) A representative *N. benthamiana* leaf of the results under UV light showing the PVX fluorescence. 1 = PVX, 2 = PVX + *Nb*MLHP, 3 = PVX + *Nb*GLK1, 4 = PVX + *Nb*GLK1 + *Nb*MLHP

The results showed a significant drop GFP-PVX viral fluorescence upon the expression of *Nb*GLK1 (Figure 38). No significant change in viral fluorescence from the GFP-PVX control was observed upon co-expression with either *Nb*MLHP or *Nb*MLHP with *Nb*GLK1. The drop associated with NbGLK1 was also observed in the previous Chapter (see section 5.4) and was concluded to be the result of an immune response to PVX triggered by *Nb*GLK1. The lack of a drop in viral fluorescence observed when *Nb*GLK1 and *Nb*MLHP were expressed with the PVX vector was thought to be a result of *Nb*MLHP immune response suppression. It was concluded that *Nb*MLHP could repress a viral immune response independent of Rx1 and was hence acting in parallel to Rx1 in suppression of defence signalling.

5.8 The effect of *Nb*MLHP Bromodomain Mutation on *Nb*GLK1 mediated Viral Immunity

Section 5.6 showed *Nb*MLHP bromodomain mutants potentially unable to bind acetyl lysine no longer repressed Rx1 mediated viral resistance. This section aims to determine if the same mutants were also unable to repress the *Nb*GLK1 mediated viral immunity shown in section 5.7. To achieve this, both HA tagged mutant *Nb*MLHP constructs described in section 5.6 were used in the fluorescence *Nb*GLK1 viral replication assay used in section 5.7, replacing the wild type *Nb*MLHP. Mutants were infiltrated into and incubated in *N. benthamiana* leaves under the same conditions as wild type *Nb*MLHP.

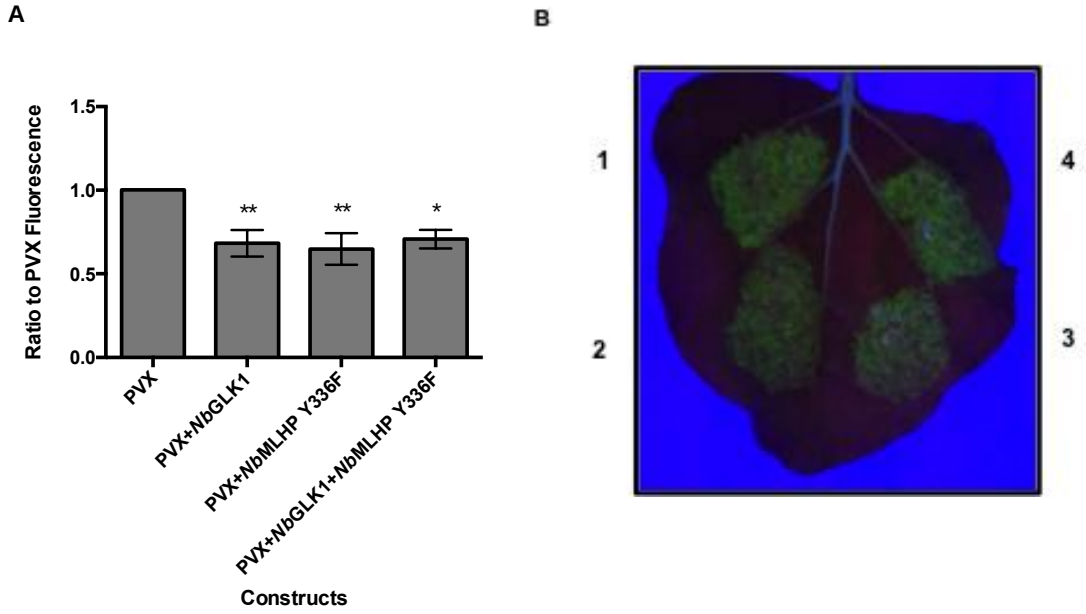

Figure 39. (A) The average ratio of fluorescence to a GFP-PVX control for *N. benthamiana* leaves expressing GFP-PVX in combinations with *Nb*MLHP and Rx1. $n = 13$. * indicates adjusted p value < 0.05, ** indicates adjusted p value < 0.01. Adjusted p values calculated using a Dunnett-Wilson multiple comparisons test. (B) A representative *N. benthamiana* leaf of the results under UV light showing the PVX fluorescence. 1 = PVX, 2 = PVX + *Nb*GLK1, 3 = PVX + *Nb*MLHP Y336F, 4 = PVX + *Nb*GLK11 + *Nb*MLHP Y336F

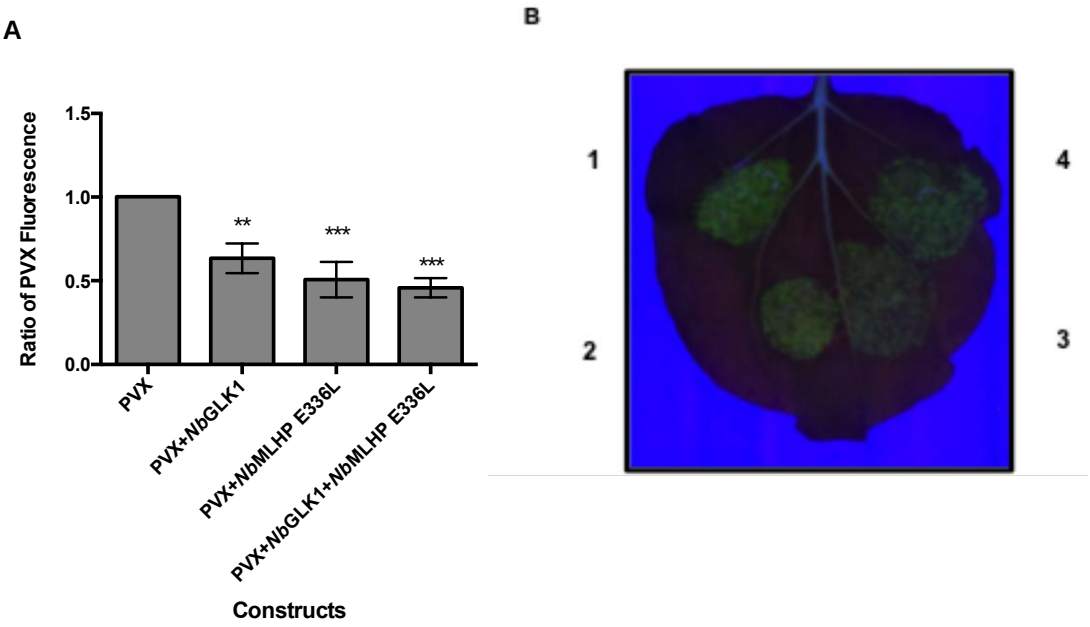

Figure 40. (A) The average ratio of fluorescence to a GFP-PVX control for *N. benthamiana* leaves expressing GFP-PVX in combinations with NbMLHP E386L and Rx1. $n = 6$. ** indicates adjusted p value < 0.01, *** indicates adjusted p value < 0.001, **** indicates adjusted p value < 0.0001. Adjusted p values calculated using a Dunnett-Wilson multiple comparisons test. (B) A representative *N. benthamiana* leaf of the results under UV light showing the PVX fluorescence. 1 = PVX, 2 = PVX + *Nb*GLK1, 3 = PVX + *Nb*MLHP E386L, 4 = PVX + *Nb*GLK1 + *Nb*MLHP E386L

All combinations of constructs for both mutants and *Nb*GLK1 resulted in a statistically significant drop in fluorescence from the control containing only PVX (Figures 39 and 40). These results showed that both mutations deactivated *Nb*MLHP repression of *Nb*GLK1 triggered immunity, in the same way they deactivated repression of Rx1 triggered immunity. Instead, both mutants caused active promotion of immunity, as demonstrated by the drop in fluorescence in the absence of *Nb*GLK1.

This independent promotion of immunity was seen for the E386L mutation in section 5.5. However, this section previously showed no promotion of an immune response by Y336F, merely an absence of repression. The previous Chapter showed *Nb*GLK1 caused a greater loss of viral replication than Rx1 under the assayed conditions (see section 5.4), indicating a stronger immune response. It is possible that this stronger response lead to systemic acquired resistance (SAR) across the assayed leaves, boosting the fluorescence loss. The results suggest that *Nb*MLHP suppression of the *Nb*GLK1 triggered defence response was also mediated by the putative *Nb*MLHP acetyl lysine binding activity. Hence, any acetyl lysine binding occurs parallel to Rx1 in defence signalling. Changes in resistance gene expression via transcription factor lysine acetyl binding is a known feature of plant immunity (Sarris et al., 2015) and the DNA binding activity of *Nb*MLHP make it highly possible that a DNA associated protein may be the target of any acetyl lysine binding activity.

5.9 Rx1 mediated Cell Death Assay

This section aims to determine what impact *Nb*MLHP expression has on Rx1 mediated HR. Chapter 4 demonstrated that regulation of Rx1 DNA binding by *Nb*GLK1 promoted extreme resistance to viral immunity, but did not impact HR. It was hence hypothesised that the DNA binding action of *Nb*MLHP that was previously demonstrated to supress Rx1 mediated extreme resistance to PVX (section 5.5) would also not be able to impact Rx1 mediated HR.

Sections of *N. benthamiana* leaves were infiltrated with *Nb*MLHP, *Nb*MLHP + Rx1, *Nb*MLHP + CP106, *Nb*MLHP + Rx1 + CP106 and Rx1 + CP106 (the positive control). *Nb*MLHP and CP106 were infiltrated at OD_{600} = 0.4. Rx1 was infiltrated at OD_{600} =

0.1 (see Materials and Methods 2.3.1, Table 4). The leaves were then incubated and each infiltrated area scored for cell death (see Materials and Methods section 2.3.4). A high cell death score would indicate HR was being triggered by the constructs, and a low cell death score would indicate the absence of HR.

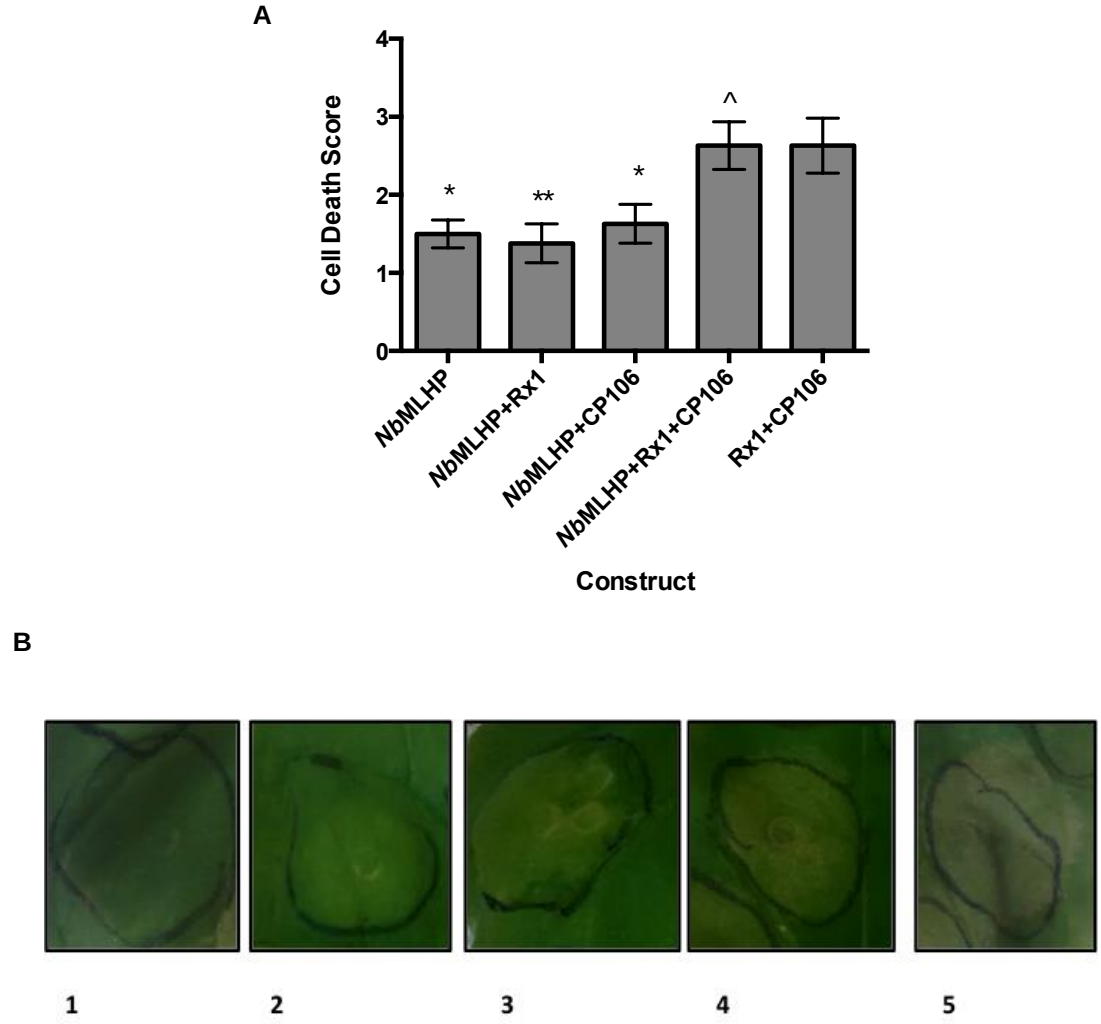

Figure 41. (A) The average cell death score for *N. benthamiana* leaves expressing *Nb*MLHP in combinations with CP106 and Rx1. $n = 24$. ^ indicates adjusted p value > 0.05, * indicates adjusted p value < 0.05 ** indicates adjusted p value < 0.01. Adjusted p values calculated using a Dunnett-Wilson multiple comparisons test. (B) Representative images of *N. benthamiana* leaf areas for each cell death score

Areas infiltrated with the Rx1 + CP106 positive control and *Nb*MLHP + Rx1 + CP106 both gave a high cell death score, indicating HR (Figure 41). Areas infiltrated with *Nb*MLHP, *Nb*MLHP + Rx1, and *Nb*MLHP + CP106 all gave a statistically significant lower cell death score than the positive control, displaying no HR.

*Nb*MLHP showed no ability to supress Rx1 and CP106 mediated HR. It was concluded that *Nb*MLHP DNA binding supresses extreme resistance to PVX without supressing HR, confirming the hypothesis.

5.10 Co-immunoprecipitation of Rx1 and *Nb*GLK1

Section 4.7 described a co-immunoprecipitation experiment designed to determine if the interaction between *Nb*GLK1 and Rx1 CC observed in the Yeast 2 hybrid screen was an artefact of the two proteins being expressed in a fungal expression system, or if the interaction would also occur in a plant expression system. This section describes a co-immunoprecipitation experiment with the aim of resolving the same issue for the *Nb*MLHP-Rx1 CC interaction.

The experimental set up was based around that of section 4.7, with *Nb*MLHP replacing *Nb*GLK1: NbMLHP with a HA tag would be co-expressed with the Rx1-CC-myc domain in *N. benthamiana* (see Materials and Methods 2.3.1, Table 4). Protein would be extracted and the *Nb*MLHP-HA immunoprecipitated with an anti-HA antibody resin. Co-immunoprecipitation of the CC-myc alongside the NbMLHP-HA would demonstrate an interaction between the two.

5.10.1 Screen of *Nb*GLK1-HA Expression Conditions in *Nicotiana benthamiana*

Higher expression of *Nb*MLHP-HA increases the number of molecules for Rx1-CC protein molecules to interact with, increasing the sensitivity of the co-immunoprecipitation. Section 4.7.1 described a trial expression of *Nb*GLK1-HA in *N. benthamiana* via *Agrobacterium* mediated infiltration to optimise protein expression conditions. The same expression screen was repeated replacing *Nb*GLK1-HA with *Nb*MLHP-HA. The cells were infiltrated at an OD_{600} of 0.4 both with and without a silencing P19 vector (the function of which is described in section 4.7.1) at OD_{600} = 0.01. Leaves were incubated for either 2 or 3 days after infiltration. Protein was then extracted from the leaves and visualised via Western blotting (see Materials and Methods 2.3) using an HRP linked anti-HA antibody.

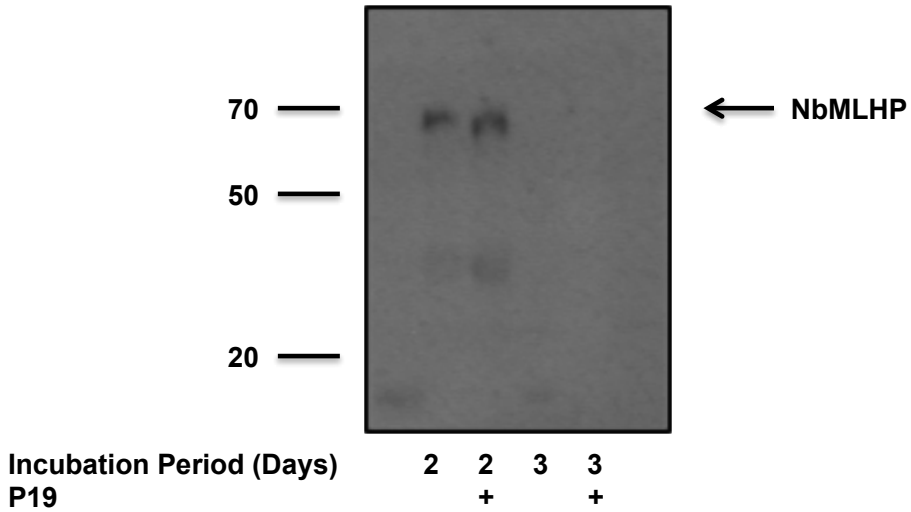

Figure 42: Western blot of a trial *Nb*MLHP-HA expression extracted from *N benthamiana* leaves incubated for either 2 or three days in the either the presence or absence of P19 plant viral suppressor. Protein visualised using a HRP linked rat anti-HA antibody.

The strongest *Nb*MLHP1 band was produced when the construct was co-infiltrated with P19 and then incubated for 2 days before protein expression (Figure 42). A 3-day incubation period resulted in a significant decrease in protein production. A 2-day incubation in the absence of p19 also decreased the strength of the *Nb*MLHP1 band at 70 kDa. It was therefore decided to perform the co-immunoprecipitation on leaf material co-infiltrated with p19 after a 2-day incubation period.

5.10.2 Screen of Salt Concentration on Co-immunoprecipitation of Rx1 and *Nb*MLHP

Section 4.7.4 describes a screen of resin wash buffer salt concentrations for a co-immunoprecipitation between *Nb*GLK1 and Rx1-CC. Resin wash buffers containing 80mM, 60mM and 40mM NaCl were all trialled. The experiment failed to establish conditions under which *Nb*GLK1 would immunoprecipitate with Rx1-CC that would not also immunoprecipitate Rx1-CC with the negative control AvrRPS4 (section 4.7.4.) This section describes an experiment aiming to determine if a resin wash buffer salt concentration condition could be found that would immunoprecpipitate *Nb*MLHP with Rx1-CC but not an AvrRPS4 negative control.

Three different combinations of constructs were transiently expressed in *N. benthamiana* leaves; *Nb*MLHP-HA with Rx1-CC-myc, AvrRPS4 with Rx12-CC-myc (negative control), and Rx1-CC-myc (negative control) (see Materials and Methods 2.3.1, Table 4). Protein was extracted, and a co-immunoprecipitation performed using the same methodology as previously described (see Materials and Methods 2.4.3). Anti-HA resin wash buffer containing either 60mM or 70mM NaCl was trialled on

each set of constructs. Samples were taken and visualised via Western blotting using both anti-HA and anti-myc antibodies after protein extraction, after the sephadex column, after washing the resin, and after eluting protein from the resin.

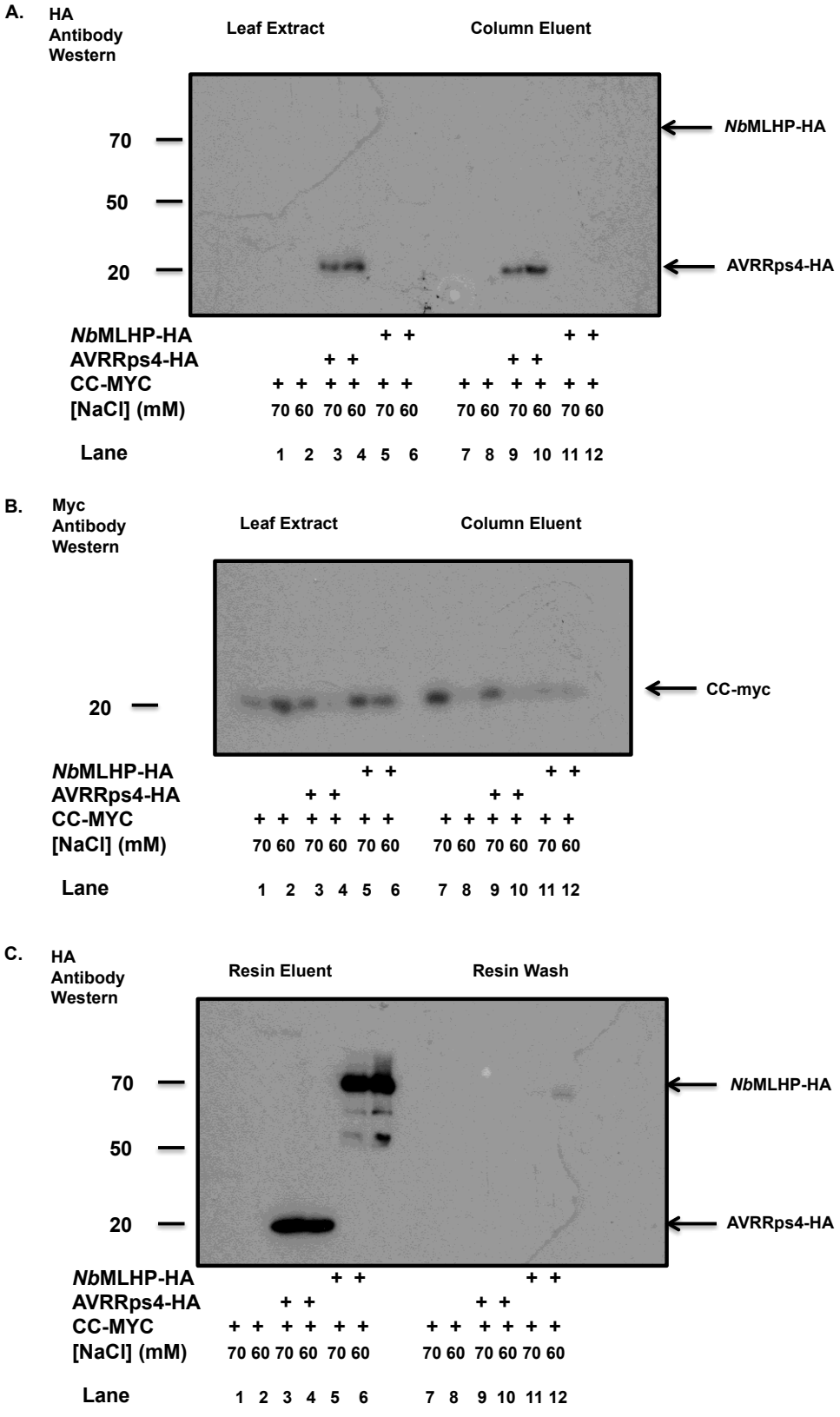

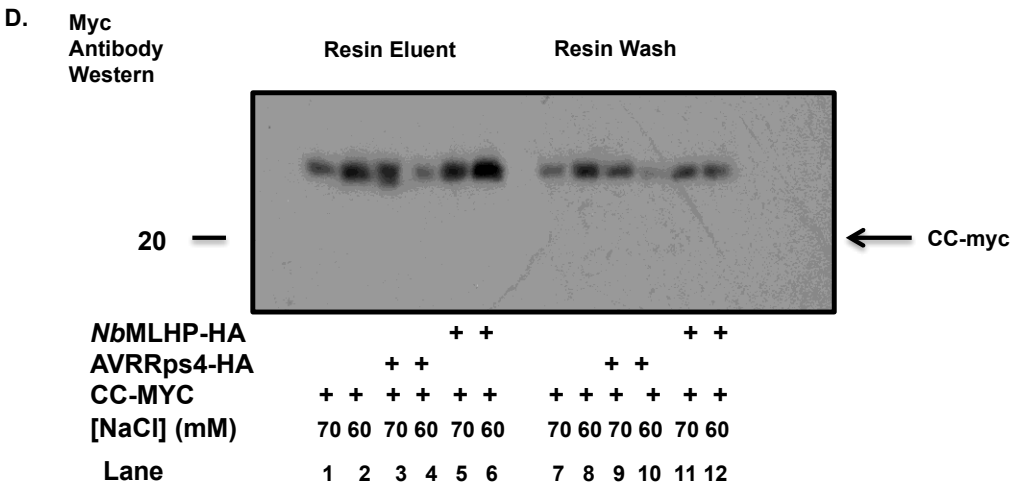

Figure 43: Western blot of a co-immunoprecipitation on *N. benthamiana* leaf material expressing solely Rx1-CC-myc, Rx1-CC-myc with *Nb*MLHP1-HA or Rx1 CC-myc with an AVRRps4-HA negative control. Samples taken after protein extraction, sephadex G-25 column, washing the HA antibody resin, or eluting from the HA antibody resin. Anti HA antibody resin wash buffer contained either 60 or 70 mM NaCl as indicated. Protein was visualised using either a goat anti-myc 1° antibody and an anti-goat HRP linked 2° antibody or using a HRP linked rat anti-HA antibody.

Lanes A 1-12 showed all the samples successfully expressed CC-myc and that this protein was eluted from the sephadex column (Figure 43). The anti-HA western blot of ground leaf material and column eluent showed AvrRPS4-HA expressing in lanes B3 and B4 and eluting from the column in lanes B9 and B10. No *Nb*MLHP-HA was visualised in this western (lanes B5, B6, B11, B12).

However, large amounts of *Nb*MLHP-HA were visualised eluting from the resin in lanes C5 and C6. Likewise, AvrRPS4-HA was visualised eluting in lanes C3 and C4. I was concluded that the *Nb*MLHP-HA was expressing in amounts to low to detect and then being concentrated on the resin. Hence it was not seen in B5, 6, 11 or 12, but visualised in C5 and 6 upon elution. Little to none of either protein was seen being washed of the resin in lanes C7-12.

All samples showed CC-myc both washing off the resin (lanes D7-12) and eluting from the resin (D1-6). No selectivity in binding was shown by samples containing NbMLHP-HA over the negative controls under either salt concentration. It was concluded CC-myc was interacting non-specifically with the resin itself and no protein-protein interaction was being demonstrated.

5.11 Conclusion

A Yeast 2-hybrid screen identified *Nb*MLHP as a potential mediator of Rx1 DNA binding interactions. FRET-FLIM analysis of the impact of *Nb*MLHP on Rx1 DNA binding *in planta* found that it had no effect. However, FRET-FLIM analysis of the effect of Rx1 on *Nb*MLHP DNA binding *in planta* suggested that Rx1 might inhibit *Nb*MLHP DNA binding. CP106 without Rx1 also inhibited *Nb*MLHP DNA binding, suggesting that any immune response inhibition of binding may not be specific to Rx1.

A fluorescent viral replication assay showed that *Nb*MLHP inhibited Rx1 mediated extreme resistance to PVX. Mutation of putative acetyl lysine binding sites in the *Nb*MLHP bromodomain either negated or reversed this inhibition. This would suggest that this inhibition is mediated by an *Nb*MLHP acetyl lysine binding activity. The presence of a putative SANT domain in the protein implies that this acetyl lysine binding activity alters gene transcription via chromatin remodelling to repress plant immunity.

Further fluorescent viral replication assays showed that *Nb*MLHP also inhibited *Nb*GLK1 mediated immunity to PVX, and that bromodomain mutation also reversed this effect. It was concluded that any *Nb*MLHP binding to acetyl lysine suppresses immunity parallel to Rx1.

Analysis of Rx1 mediated HR showed that *Nb*MLHP does not suppress HR. Rx1 mediated HR must therefore be activated by a separate signal transduction pathway to extreme resistance, unaffected by *Nb*MLHP. Co-immunoprecipitation failed to demonstrate a protein-protein interaction between *Nb*MLHP and Rx1-CC *in planta*.

This chapter concludes that *Nb*MLHP does not regulate Rx1 DNA binding, but does act as a suppressor of Rx1 mediated extreme resistance to PVX. It is hypothesised that this binding to acetyl lysine has a chromatin remodeling effect. However, further work is required to establish whether an interaction occurs between the two proteins *in planta (*see section. 6.4.3), whether *Nb*MLHP does bind acetyl lysine as predicted (see section 6.4.2), and both the target and effect of any acetyl lysine binding (see section 6.4.2).

5.12 Discussion

Transient expression of *Nb*MLHP in *N. benthamiana* leaves reversed suppression of GFP:PVX fluorescence by Rx1 and *Nb*GLK1. This suggests *Nb*MLHP inhibits both Rx1 and *Nb*GLK1 mediated extreme resistance to PVX. Virus induced silencing of *Nb*MLHP in *N. benthamiana* plants has also been shown to suppress viral replication of PVX using GFP:PVX (Townsend et al., unpublished data) supporting this observation and showing that it is not an artefact of overexpression.

*Nb*MLHP has no effect on Rx1 DNA binding. FRET-FLIM analysis on the impact of Rx1 on GFP-*Nb*MLHP binding in fixed leaf material showed a low lifetime ratio characteristic of DNA binding when *Nb*MLHP is expressed by itself. This then rises in the presence of Rx1, CP106, and Rx+CP106. This suggests that these constructs inhibit *Nb*MLHP DNA binding.

Bromodomain mutations designed to inactivate putative acetyl lysine binding result in the suppression of GFP:PVX viral fluorescence when expressed in *N. benthamiana,* independently of Rx1 and *Nb*GLK1, suggesting that overexpression of these mutants may trigger extreme resistance to PVX. Such a result would be expected if *Nb*MLHP inhibits *N. benthamiana* resistance to PVX through lysine acetylation. Transfer of lysine acetyl groups on histones is associated with chromatin remodelling linked changes in gene expression. Usually histone lysine acetylation results in the unfolding of chromatin, promoting gene expression (Shogren-Knaak et al., 2006). But the reverse, i.e. condensation of chromatin to suppress gene expression, is also known (Choi et al., 2012).

The co-immunoprecipitation between *Nb*MLHP and Rx1-CC performed showed no evidence of a physical interaction between the two proteins. However, co-immunoprecipitation using antibodies immobilised on magnetic beads and elution with pre-boiled SDS PAGE loading buffer has returned a positive result (Townsend et al., unpublished data). The same experimental design returned a negative result for full length Rx with *Nb*MLHP, suggesting Rx1 inter-domain interactions inhibit this in the full-length protein. Other work *in vitro* has shown co-elution of the *Nb*MLHP bromodomain with Rx1 CC via size exclusion chromatography (Townsend et al.,

unpublished data). This also provides evidence of a protein-protein interaction. This occurred with both wild type *Nb*MLHP and the Y335F acetyl lysine binding mutant, suggesting lysine acetyl binding is not required for the *Nb*MLHP- Rx1 CC interaction. These results refute the negative result of the coimmnocprecipitation and suggest that this was merely result of an unoptimized experimental setup.

Publications

Results from Chapter 3 of this thesis have been published in the following paper;

Fenyk, S., Townsend, P. D., Dixon, C. H., Spies, G. B., Campillo, A. D. S. E., Slootweg, E. J., Goverse, A. Takken, F.L. & Cann, M. J. (2015). The Potato Nucleotide-binding Leucine-rich Repeat (NLR) Immune Receptor Rx1 Is a Pathogen-dependent DNA-deforming Protein. *Journal of Biological Chemistry*, *290*(41), 24945-24960. (See Appendix 7.3)

The following Figures were published; Figures 9, 10, (as Figures 7a and b in the paper) and Figures 12, 14, 15 and 16 (as Figures 8 a, b, c and d).

6. Discussion

6.1 Introduction

This thesis demonstrates that Rx1 binds DNA in a coat protein dependent manner in fixed *N. benthamiana* leaf material using a FRET-FLIM assay. Two putative regulators of Rx1 DNA binding were identified through Yeast 2-hybrid assay; *Nb*GK1 and *Nb*MLHP. *Nb*GLK1 was shown to be a promoter of Rx1 DNA binding that also promotes Rx1 mediated resistance to PVX viral accumulation. *Nb*MLHP was not shown to affect Rx1 DNA binding. However, Rx1 suppressed *Nb*MLHP DNA binding, and *Nb*MLHP did inhibit Rx1 mediated resistance to PVX virus accumulation. This chapter summarises the results presented in chapters 3, 4 and 5, discuss the conclusions that can be drawn from them in the context of the current literature and other unpublished work, and propose ideas for further studies based on the findings.

6.2 Rx1 Binds DNA *in vivo* in response to CP106

6.2.1 Rx1 Binds DNA in Fixed *N. benthamiana* Leaf Material

To assess if Rx1 DNA binding could be measured in fixed *N. benthamiana* leaf material a FRET-FLIM assay was designed to measure energy transfer from transiently expressed GFP tagged protein to a DNA binding dye, LDS-751. The positive control construct GFP-H2B displayed a statistically significant drop in florescence lifetime ratio compared to a free GFP negative control, indicating successful measurement of energy transfer upon construct DNA binding.

Rx1 DNA binding was then assessed. It displayed a statistically significant drop in lifetime ratio upon co-expression with CP106 in fixed *N. benthamiana* leaf material stained with the DNA binding dye LDS-751. This was consistent with DNA binding as indicated by the positive control. A drop in lifetime ratio was not observed upon co-expression with CP105, a virulent form of PVX coat protein that does not trigger Rx1 mediated immunity. This shows that the drop in lifetime ratio was not an artefact of coat protein expression, and was triggered by Rx1 sensing CP106. Co-expression of GFP-Rx1 with Pto and AvrPto resulted in no drop in lifetime ratio and rules out this change in lifetime being the result of a generic plant immune response. It was concluded that Rx1 binds genomic DNA in response to CP106. No drop in lifetime ratio was seen with NES or NLS tagged Rx1 protein with or without CP106. This suggests that nucleocytoplasmic distribution of the Rx1 is required for DNA binding as it is for Rx1 immune signalling (Slootweg et al., 2010). The results imply that Rx1 mediated immune signalling may be triggered by DNA binding in the nucleus after the elicitor is sensed in the cytosol.

The individual domains of Rx1 were assessed for their DNA binding capabilities using the same assay. Any non-full length construct containing the CC or NBARC domains displayed a lifetime ratio significantly lower than the free GFP negative control, indicating energy transfer. Expression of the LRR domain by itself did not. The DNA binding domain of the protein was concluded to be NBARC domain based on homology modelling (Fenyk et al., 2015), with the CC domain of the protein more likely to be involved with an interaction with another DNA binding protein. This association could bring the domain physically close enough to the DNA binding LDS-751 to facilitate energy transfer.

This data is supported *in vitro* EMSA and FRET-FLIM assays (Fenyk et al., 2015). EMSA also demonstrated that CCNBARC Rx1 protein purified from *N. benthamiana* leaves bound DNA (Fenyk et al., 2015). This demonstrates that the FRET-FLIM assay was measuring an active DNA binding activity of Rx1 CCNBARC and not an association with DNA mediated by another protein. This work also demonstrated that Rx1 bends and melts DNA using FRET-FLIM. This suggests that Rx1 DNA binding may stimulate gene expression in response to CP106 to trigger plant defence signalling.

EMSA, fluorescence anisotropy and FRET-FLIM were also used to demonstrate a DNA binding and bending activity using recombinant refolded I-2, an NBLRR protein from tomato (Fenyk et al., 2016). This suggests DNA binding may be conserved between different NBLRR proteins and not unique to Rx1. That DNA bending is also conserved suggest that DNA binding to stimulate DNA melting and gene expression is also conserved.

There are, however, differences between I-2 and Rx1 DNA binding. I-2 has been found to bend DNA to a lesser degree, 22° as opposed to the 40° seen in Rx1, has a preference for binding dsDNA as opposed to the preference to ssDNA seen in Rx1. Its DNA binding was also found to be coupled to its ATP hydrolysis activity, with immunologically active ATP bound I-2 binding in preference over inactive ADP bound I-2. This has not been described for Rx1 (Fenyk et al., 2015, Fenyk et al., 2016). These differences suggest DNA binding may be adapted to different immunological roles in different proteins. While both appear to be stimulating DNA expression, the differing

mechanisms suggest they may be targeting differing genes to induce different immune response.

Further work is required to determine the physiological effects of Rx1 DNA binding. *In vitro* work done by Fenyk et al. only demonstrated non-specific DNA binding, raising the question of how specificity of Rx1 DNA binding is achieved *in vivo*. The genes targeted by Rx1 DNA binding are also unknown. Further evidence is also required to determine whether transcription of these genes is promoted or repressed by Rx1, and to ensure that the DNA bending an melting effect measured *in vitro* was not an artefact of using refolded protein from a prokaryotic protein production system. Which genes are targeted could be determined by CHIP analysis of Rx1 DNA binding, immunoprecipitating Rx1 from plant material with the DNA it binds to and sequencing this DNA. Proteomic and genomic analysis could then be used to show which proteins and genes are expressed or repressed by this DNA binding, using RNA sequencing to determine which gene transcripts are upregulated and mass spectrometry to determine which proteins are translated.

6.2.2 Effect of Rx1 mutation on DNA binding

The Rx1 D460V mutation results in protein autoactivity. Expression of this protein results in an immune response in the absence of CP106 (Bendahmane et al., 2002). This mutation targets the MHD motif in the NBARC domain, and is proposed to disrupt the interaction between the NBARC and LRR domains that maintains the wild type protein in an inactive state (Slootweg et al., 2012). FRET-FLIM analysis of GFP-Rx1 D460V in *N. benthamiana* leaves showed a significant reduction in lifetime ratio compared to wild type protein in the absence of CP106. This indicates that Rx1 D460V

was constitutively binding genomic DNA in the absence of CP106. It was concluded that the inter-domain interaction that held the protein in an immunologically inactive state also held the protein in a conformation that couldn't bind DNA. This implies that Rx1 DNA binding may initiate Rx1 mediated immunity.

Mutation of a putative nucleotide binding motif resulted in no change in DNA binding: CCNBARC Rx1 K176R displayed a low fluorescence lifetime ratio in FRET-FLIM analysis, indicating that nucleotide hydrolysis is not involved in DNA binding. CC-NBARC K176R Rx1 was also observed to possess DNA binding capabilities *in vitro* using EMSA and FRET-FLIM assays on recombinant refolded protein made in *E. coli* (Fenyk et al., 2015), but did not bend DNA in response to ATP *in vitro* as wild type recombinant protein was shown to do. This supports the DNA binding of CCNBARC K176R shown in the *in planta* FRET-FLIM experiment.

Mutations to the NBARC domain effecting putative nucleotide binding did result in changes to FRET-FLIM analysis of DNA binding; wild type GFP-CCNBARC Rx1 binds DNA; Rx1 S202F and D225E CCNBARC both showed significantly higher lifetime ratios indicating a lack of DNA binding. There has been no work performed using recombinant S202F and D225E CCNBARC Rx1 using EMSA or fluorescence anisotropy. Further *in vitro* work could be used to support the *in planta* data for these mutants.

Full-length constructs of K176R, S202F and D225E do not localize to the nucleus in *N. benthamiana* leaves (Slootweg et al., 2010). Co-expression with the LRR was intended to make truncated mutant constructs behave like a full-length protein while

still localizing to the nucleus. A proof of concept of this was performed on the wild type CCNBARC + LRR +/- CP106. The lifetime ratios were not statistically different from that of wild type full-length protein both with and without coat protein.

When co-expressed with LRR K176R CCNBARC did bind DNA, both with and without CP106. S202F did bind when with LRR, did bind with LRR+CP106. D225E did bind when with LRR, did bind when with LRR+CP106.

The immunological effects of S202F and D225E have not been studied and require further work to characterise. There is also currently no evidence of an Rx1 nucleotide hydrolysis activity for the K176R mutation to disrupt, and this too requires further study. The NBARC domain of Rx1 may not hydrolyse or even bind ATP. The effects of these mutations could just be structural destabilisation (see Section 3.10). Differences in DNA binding between Rx1 and I-2 in response to ATP/ADP have been previously observed (Fenyk et al., 2015, Fenyk et al., 2016) and this could be linked to different nucleotide binding activities between Rx1 and I-2. The NBLRR proteins R1 from rice and N from tobacco have already been show to have different nucleotide binding and hydrolysis activities to I-2, showing that no one conserved activity exists across all NBLRR proteins (Fenyk at al., 2012, Ueda et al., 2006, see Section 1.5.3)

Further work is required on the impact of these mutations before conclusions can be drawn on their effects. A DNA binding assay *in vivo* using FRET-FLIM performed on full length mutant K176R, S202F and D225E would elucidate the effect of the LRR on mutant NBARC domains. To avoid interference in signal from the localisation

effects of these mutations, lifetime reading would have to be spatially resolved within the cell to just the nucleus.

There is also a need for the development of a methodology for the recombinant production of LRR Rx1. *In vitro* analysis of recombinant K176R, S202F and D225E CCNBARC Rx1 with LRR DNA binding using EMSA can then be performed.

However, if protein stability is compromised by these NBARC domain mutations, expression of protein could problematic. A means of determining of recombinant protein folding could be used to assess the impact of mutation on protein stability. Circular dichroism (CD) spectroscopy provides a measure of protein secondary structure and could be used to determine differences between folding in different Rx1 mutants.

A true understanding of the impact of these mutations is only likely to be given by an in depth structural analysis of Rx1 and Rx1 DNA binding using x-ray crystallography or cryo-EM. If performed both for the wild type and for mutants, this would fully elucidate how DNA binding occurs, which residues and motifs are responsible for the interaction, and how interactions between Rx1 domains change protein conformation to affect this.

6.3 *Nb*GLK1 as a promoter of Rx1 mediated immunity

6.3.1 *Nb*GLK1 DNA binding

A Yeast 2-hybrid screen against the Rx1 CC domain identified *Nb*GLK1 as a potential interactor of Rx1 with a DNA binding domain. Hence making it a potential regulator of Rx1 DNA binding. A drop in GFP-Rx1 fluorescence lifetime is seen in fixed *N. benthamiana* leaf material when co-expressed with *Nb*GLK1 in the absence of coat protein. This suggests that *Nb*GLK1 promotes Rx1 DNA binding in the absence of CP106. GFP-*Nb*GLK1 displayed a significant decrease in fluorescence lifetime in fixed *N. benthamiana* leaf material when co-expressed with both Rx1 and coat protein, but not Rx1 alone. This implies that Rx1 promotes *Nb*GLK1 DNA binding as part of an immune response to CP106.

This work performed in fixed *N. benthamiana* is supported by *Nb*GLK1 DNA binding assays *in vitro* using fluorescence anisotropy (Townsend et al., unpublished data). This *Nb*GLK1 DNA binding has also been shown to be sequence specific. Specificity in Rx1 DNA binding could therefore be mediated by an Rx-GLK1 interaction. The impact of Rx1 on *Nb*GLK1 DNA binding has also be demonstrated *in vitro* using fluorescence anisotropy with fluorescently tagged oligonucleotides. This showed that Rx1 CCNBARC and CC both inhibited *Nb*GLK1 DNA binding (Townsend et al., unpublished data). The *in planta* FRET-FLIM data showed full length Rx1 promoting *Nb*GLK1 DNA binding in the plant cell. The discrepancy between these two may be the result of a third protein that forms part of the complex in the plant cell as seen with the NBLRR protein MLA10, which complexes with MYB6 and WRKY1 (Chang et al., 2013), or as a result of interactions with the LRR domain in the full length protein.

6.3.2 *Nb*GLK1 Viral Immunity

*Nb*GLK1 decreased GFP:PVX fluorescence upon transient co-expression in *N. benthamiana* leaves. This effect occurs independently of Rx1 expression, suggesting GLK1 may act in parallel to Rx1, interacting with multiple NBLRR proteins. This supports previous work that describes *Arabidopsis thaliana* GLK1 giving resistance to multiple pathogens (Murmu et al., 2014). Virus induced silencing of *Nb*GLK1 in *N. benthamiana* plants has also been shown to suppress viral replication of PVX using GFP:PVX (Townsend et al., unpublished data) supporting this observation, and showing that this was not an artefact of overexpression. No *Nb*GLK1 mediated effects were observed on Rx1 triggered HR in the cell death-scoring assay.

These results suggest that that *Nb*GLK1 enables site-specific DNA binding of Rx1 and this promotes Rx1 triggered extreme immunity to PVX, preventing the accumulation of PVX in infected cells. *Nb*GLK1 does not impact Rx1 mediated HR, implying that HR is caused by a separate signal transduction pathway, possibly not triggered by Rx1 DNA binding.

6.3.3 *Nb*GLK1-Rx1 Interaction characterisation

None of the co-immunoprecipitation conditions screened in this thesis successfully demonstrated an *Nb*GLK-Rx1 CC interaction in material extracted from *N. benthamiana* leaves. However the yeast 2-hybrid data and *in vitro* size exclusion gel chromatography (Townsend et al., unpublished data) did. Experiments performed on *Nb*MLHP suggest that changes from an agarose linked antibody resin to antibodies immobilised on magnetic beads can be used to improve selection for Rx1-CC interactions in co-immunoprecipitations (see section 6.4.3). This methodology

suggests the current co-immunoprecipitation data may be providing a false negative and should be trialled on *Nb*GLK1. A successful co-immunoprecipitation experiment is required to demonstrate that this is not an artefact of the refolded recombinant protein being partially folded and aggregating together.

If an interaction between *Nb*GLK1 and Rx1 CC is established, the effect of other Rx1 domains on this interaction should be examined. Whether the interaction occurs between full length Rx1 and *Nb*GLK1 should be examined via co-immunoprecipitation, both in the presence and absence of CP106. This would indicate whether the auto-inhibitory effect of Rx1 domain interactions prevents association with *Nb*GLK1. If inhibition does occur, the restoration of the Rx1-*Nb*Glk1 interaction in the presence of CP106 would link *Nb*GLK1-Rx1 association with an initiation of defence signalling. Testing the effect of the D460V autoactivity mutation on the interaction using co-immunoprecipitation could be used to further confirm this.

The effect of other Rx1 mutations on the interaction between *Nb*GLK1 and Rx1 could also be investigated. Chapter 3 showed putative nucleotide binding and hydrolysis mutations (K176R, S202F, D225E) affect Rx1 DNA binding. If they impact either nucleotide binding/hydrolysis or protein stability as concluded in section 6.2.2, they may also impact Rx1 CC – *Nb*GLK1 interactions in full length Rx1. Co-immunoprecipitation and *in vitro* studies on recombinant protein could be used to demonstrate this. Deletion of the areas flanking the EDVID motif in the CC domain are known to disrupt Rx1 CC binding of RanGAP2 (Rairdan et al., 2013). Analysis of CC domain construct with these areas deleted using co-immunoprecipitation could be used to determine if these areas are also required for *Nb*GLK1 binding.

6.3.4 *Nb*GLK1 Summary

The results suggest *Nb*GLK1 acts as a promoter of Rx1 mediated viral extreme resistance, but not HR, parallel to Rx1, potentially promoting this activity in other NBLRR receptors. FRET-FLIM analysis of DNA binding in fixed *N. benthamiana* leaves and unpublished *in vitro* DNA binding experiments suggest this activity may occur through providing specificity to Rx1 DNA binding, allowing it to target the activation of immune signalling genes. This fits with what is known of GLK1 transcription factors in other plants, with transcriptional activity promoting plant immunity. (Han et al., 2013, Murmu et al., 2014). Similarly, other proteins in Myb transcription factor superfamily are known to have a similar role: the immune promoter MYB6 interacts with the NBLRR protein MLA10 and this interaction promotes its immune signalling activity (Chang et al., 2013). There is a possibility that *St*GLK1 is a target of CP106 mediated immune repression. Rx1 could then guard GLK1 to initiate ETI. The related protein from the Myb superfamily MYB30 promotes HR (Raffaele et al., 2008), and is a known target of a bacterial effector protein XopD (Canonne et al., 2011). However the fact that a nucleur localisation of CP106 is required for HR (Slootweg et al., 2010) makes a transcription factor an unlikely target of action. Nor does this explain why *Nb*GLK1 activates an immune response in the presence of PVX but without any Rx1 present. A CP106 immune suppressant effect of also has not observed in any previous studies. It is most likely that *Nb*GLK1 is simply a transcription factor that interacts with Rx1 to provide specificity to Rx1 DNA binding to activate immune signalling gene transcription. However, further work is needed to elucidate the nature of the protein-protein interaction demonstrated the Yeast 2-hybrid assay and ensure that this was not a false positive.

6.4 *Nb*MLHP as an inhibitor of Rx1 mediated immunity

6.4.1 *Nb*MLHP DNA binding

The Yeast 2-hybrid data identified *Nb*MLHP1 as a potential mediator of Rx1 DNA binding interactionsFRET FLIM analysis indicated that *Nb*MLHP has no effect on Rx1 DNA binding, but both Rx1 and CP106 inhibit *Nb*MLHP DNA binding.

Further *in vitro* characterisation of this DNA binding interaction is required. Recombinant *Nb*MLHP DNA binding should be assayed using fluorescence anisotropy and EMSA. The impact of CC and full length Rx1 on *Nb*MLHP DNA binding can then be assessed to ensure that the results of FRET-FLIM DNA binding assay in *N. benthamiana* were not an artefact of overexpression.

6.4.2 *Nb*MLHP Viral Immunity

Transient expression of *Nb*MLHP in *N. benthamiana* leaves reversed suppression of GFP:PVX fluorescence by Rx1 and *Nb*GLK1. This suggests *Nb*MLHP inhibits both Rx1 and *Nb*GLK1 mediated extreme resistance to PVX. This is supported by virus induced silencing of *Nb*MLHP (Townsend et al., unpublished data). Bromodomain mutations designed to inactivate putative acetyl lysine binding result in the suppression of PVX accumulation independently of Rx1 and *Nb*GLK1, suggesting that overexpression of these mutants may trigger extreme resistance to PVX. Such a result would be expected if *Nb*MLHP inhibits *N. benthamiana* resistance to PVX through lysine acetylation (see Section 5.12)

It should be noted that at this stage the acetyl lysing binding activity of wild type *Nb*MLHP remains hypothetical. Further work is required to provide confirmation. This could be achieved using *in vitro* lysine acetyl binding assays on both wild type *Nb*MLHP and the bromodomain mutations with fluorescence anisotropy, ITC or gel filtration column. A loss of lysine acetyl binding on mutation would link PVX immune suppression to lysine acetyl binding activity.

The impact of the bromodomain on *Nb*MLHP DNA binding could also be investigated. The SANT domain is the only *Nb*MLHP domain predicted to bind DNA, but this currently remains hypothetical. A bromodomain histone acetyl lysine binding activity could be the interaction that keeps the protein associated with chromatin, enabling energy transfer to the DNA associated LDS-751 measured in chapter 5. The effect of both mutations on DNA binding should be assessed *in vitro* from recombinant protein made in *E. coli*. The impact of the mutations should also be assessed in *N. benthamiana* using the FRET-FLIM assay described in chapter 3.

The protein targeted by *Nb*MLHP lysine acetyl binding is also currently unknown. The presence of a SANT domain suggests the target may be histones (Shogren-Knaak et al., 2006). Knowing the target of *Nb*MLHP acetyl lysine binding would also elucidate its functions. Determining if *Nb*MLHP binds histone acetyl lysine residues through an *in vitro* binding assay or plant co-immunoprecipitation would provide evidence that it alters gene expression through chromatin remodelling. If the target is not a histone, what protein is targeted, and what impact does *Nb*MLHP binding have on its function should be investigated.

6.4.3 *Nb*MLHP-Rx1 interaction characterisation

The co-immunoprecipitation between *Nb*MLHP and Rx1-CC performed showed no evidence of a physical interaction between the two proteins. However this result is countered by other co-immunoprecipitation data (Townsend et al., unpublished data) and size exclusion chromatography (Townsend et al., unpublished data). These combined with the Yeast 2-hybrid data suggest the coimmunoprecipitation result in Chapter 5 is a false negative and the two proteins do in fact interact.

Further work can also be done to investigate the dynamics of this relationship. Co-immunoprecipitation can be used to show whether CP106 co-expression with full length Rx1 activates it to allow interaction with *Nb*MLHP. Co-immunoprecipitation can also be used to show the effect of the D460V autoactivity mutation on the Rx1 CC-*Nb*MLHP interaction.

As with *Nb*GLK1, the effect of other mutations in Rx1 should also be investigated (see section 6.3.3). The effect on *Nb*MLHP binding of putative nucleotide binding and hydrolysis mutations (K176R, S202F, D225E), and deletion of areas flanking the EDVID motif that domain disrupts Rx1 binding of RanGAP2 (Rairdan et al., 2013) should be investigated using co-immunoprecipitation. The Rx1 binding activity of different *Nb*MLHP constructs should also be investigated; mutation of acetyl lysine binding residues in the bromodomain and deletion of the SANT domain would reveal how *Nb*MLHP protein function affects Rx1 binding.

6.4.4 SANT domain characterisation

Chapter 4 describes experiments with the aim of investigating the impact of bromodomain mutation on *Nb*MLHP function. But the role of the *Nb*MLHP SANT domain in DNA binding and immunity was not investigated. SANT domains are known to be involved in DNA binding (Boyer et al., 2002), making it probable that this domain is responsible for *Nb*MLHP DNA binding activity. Point mutations in yeast SANT domains do not affect protein DNA binding. No one residue is responsible for DNA binding (Boyer et al., 2002). Instead, deletion of the SANT domain has been used to study its DNA binding activity.

The putative DNA binding activity of the *Nb*MLHP SANT domain should be demonstrated by investigating the effect of its deletion on *Nb*MLHP DNA binding. This can be assessed both *in planta* using FRET-FLIM, and *in vitro* using florescence anisotropy and EMSA. The effect of the SANT domain on *Nb*MLHP mediated immunity should then be investigated. Assuming the SANT domain does provide a DNA binding activity, *Nb*MLHP DNA binding could then be linked with an immunological impact. *Nb*MLHP constructs with the SANT domain deleted can be used in GFP:PVX viral replication assays and on HR cell death scoring assays as described in chapters 4 and 5 and compared to a wild type control.

6.4.5 *Nb*MLHP conclusion

*Nb*MLHP appears to be a protein that interacts with Rx1-CC but does not regulate Rx1 DNA binding. Rx1 does inhibit *Nb*MLHP DNA binding, but so does CP106 in the absence of Rx1. PVX viral replication assays suggest this DNA binding suppresses extreme resistance to PVX through a putative acetyl lysine binding activity.

It was theorised that *Nb*MLHP either activates or suppresses transcription of genes through chromatin remodelling to suppress Rx1 mediated extreme resistance to PVX but not HR. The SANT domain is hypothesised to enable the protein to associate with the DNA in chromatin, and the bromodomain then acetylates lysine residues on histones to either condense chromatin (to suppress gene expression), or to unravel it (promoting gene expression). However, more work is required to support this model; the acetyl lysine binding activity of *Nb*MLHP and the DNA binding activity of the SANT domain both require confirmation.

There are two possible modes of *Nb*MLHP action that fit with this model. Firstly, there is evidence that viroids utilise plant RNA binding bromodomain containing proteins for use in their own replication (Chaturvedi et al., 2016, Kalantidis et al., 2007, de Alba et al., 2003). *Nb*MLHP could be hijacked by PVX to help transcribe its genome. *Nb*MLHP overexpression in viral replication assays could then boost viral replication, making it appear as if immunity was being suppressed. *Nb*MLHP with mutated acetyl lysine sites would then associate with chromatin, but not aid viral transcription impeding virus accumulation. The suppression of *Nb*MLHP DNA binding by Rx1 could be the result Rx1 sensing *Nb*MLHP to trigger immunity. *Nb*MLHP could be the guardee protein Rx1 senses to initiate immunity.

The NBLRR protein RRS1 uses a similar system. The bacterial effector protein pop2 uses a lysine acetyl binding activity to deactivate plant WRKY transcription factors that trigger PAMP mediated immunity. (Sarris et al., 2015) RRS1 uses an integrated WRKY decoy to detect this effector and trigger HR. (Sarris et al., 2015) Similarly, if PVX uses *Nb*MLHP to aid bacterial transcription, Rx1 could utilise *Nb*MLHP as a guard to detect PVX.

There are several reasons this explanation is the less likely of the two: This model does also not explain why a nucleocytoplasmic distribution of Rx1 is required for DNA binding and defence signalling (Slootweg et al., 2010). *Nb*MLHP could easily be sensed in the nucleus and imitate Rx1 DNA binding there. Nor does this model explain why a cytoplasmic localisation of CP106 is required to initiate immunity if the guardee is a chromatin remodeller (Slootweg et al., 2010). Or why expression of CP106 in the absence of Rx1 inhibited *Nb*MLHP DNA binding.

The second and more probable explanation is that *Nb*MLHP is a native plant suppressor of defence signalling that is required to regulate the activity of NBLRR proteins and prevent their unwanted activation. It achieves this through chromatin remodelling as previously described (see Section 6.4.2). Overexpression hence represses Rx1 mediated immunity, and mutation promotes immunity. In this model Rx1 would behave similarly to the NBLRR protein MLA10. MLA10 associates with the suppressor of plant immunity WRKY1. This association with WRKY1 inhibits WRKY1 inhibition of MYB6 immune signalling. MYB6 promotes immunity in a manner similar to the way *Nb*GLK1 is hypothesised to in Section 6.3. Neither of these proteins has been characterised as a guard thus far (Chang et al., 2013).

6.5 *Nb*CHD1

The Yeast 2-hybrid assay described in chapter 4 (Section 4.2) also returned a third protein containing a predicted DNA binding domain, identifying it as a potential regulator of Rx1 DNA binding. The protein was determined through bioinformatic analysis to show high sequence similarity to the *Solanum tuberosum* Chromodomain helicase DNA binding domain protein 1 (CHD1, see Section 7.1/7.2).

CHD1 proteins have an ATP dependent helicase activity on chromatin (Kingston et al., 1999). This enables a transition of chromatin between condensed and loosened states. Usually CHD1 helicase activity loosens chromatin increase gene expression, often through a complex with a transcription factor, or histone lysine acetylase. However, the condensation of chromatin to decrease gene expression is also known (Choi et al., 2012).

*Nb*CHD1 requires characterisation to determine what impact, if any, it has on Rx1 defence signalling activity. The *Nb*CHD1 interaction with Rx1-CC indicated by the yeast 2-hybrid screen requires confirmation via co-immunoprecipitation. The impact of CHD1 on Rx1 DNA binding should be investigated and vice versa, both through *in planta* FRET-FLIM and *in vitro* EMSA. The impact of *Nb*CHD1 expression and silencing on PVX viral replication in *N. benthamiana* and HR should be determined.

1.

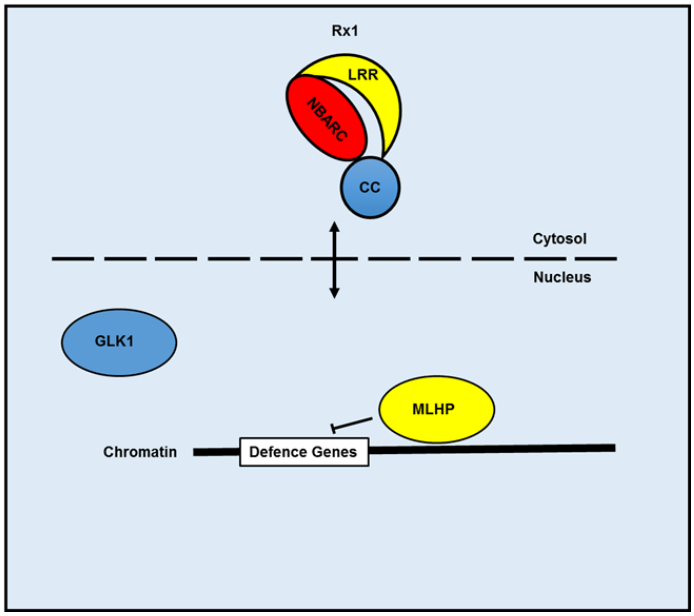
Rx1
LRR
NBARC
CC
Cytosol
Nucleus
GLK1
MLHP
Chromatin
Defence Genes

2.

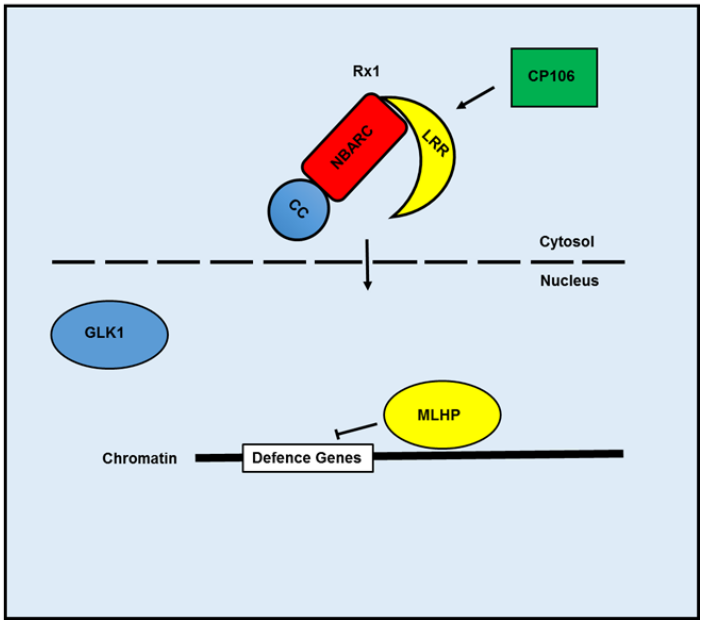
Rx1
CP106
NBARC
LRR
CC
Cytosol
Nucleus
GLK1
MLHP
Chromatin
Defence Genes

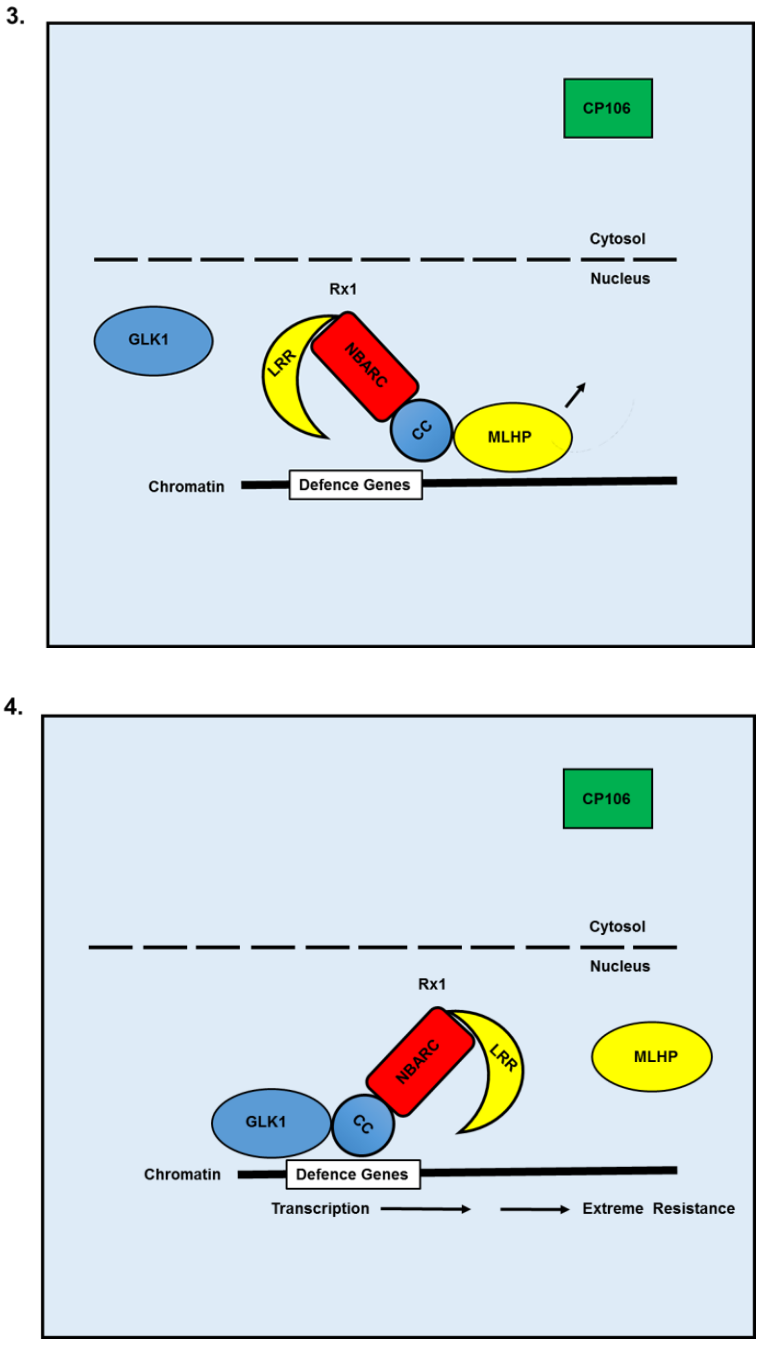

Figure 44. Schematic model of hypothesised Rx1 mode of action including regulation by GLK1 and MLHP. 1. In an uninfected cell Rx1 remains in an autoinhibited, 'off' conformation with a nucleocytoplasmic distribution. MLHP supresses defence gene transcription through a chromatin remodelling activity. 2. Upon infection by PVX, Rx1 Senses CP106 in the cytosol, shifting to an 'on' conformation and translocates to the nucleus to initiate defence signalling. 3. In the nucleus, Rx1 interacts with MLHP via the CC domain to inhibit its DNA binding and suppression of defence gene transcription. 3. The Rx1-GLK1 interaction provides DNA binding specificity, targeting defence genes. Rx1 bends DNA to promote defence gene transcription leading to extreme resistance.

6.6 Conclusion and Further Work

Plant NBLRR proteins are vital mediators of plant disease resistance. The potato NBLRR protein Rx1 mediates resistance to PVX by both preventing viral accumulation in infected plant cells and initiating the hypersensitive response (Bendahmane et al., 1999). This thesis provides evidence that Rx1 binds plant genomic DNA to initiate defence signalling to inhibit viral replication, and possibly HR. Further work is required to elucidate the role of any possible Rx1 nucleotide binding and/or hydrolysis activity in this via both *in vivo* and *in vitro* techniques.

Rx1 DNA binding appears to be positively regulated by the transcription factor *Nb*GLK1, which acts as promoter of this DNA binding and may help provide sequence specificity to stimulate gene expression. *Nb*MLHP appears to inhibit defence signalling through a chromatin remodelling activity. However, both of these proteins require further biophysical characterisation. *Nb*CHD1 was also identified as another potential regulator of Rx1 DNA binding, hypothetically through a chromatin remodelling activity, but remains unstudied.

There is some evidence that this DNA binding action may be conserved between NBLRR proteins: The tomato NBLRR protein I-2 has also been shown to possess a DNA activity (Fenyk et al., 2016) and other NBLRR proteins possess a DNA binding domains at their N-terminus (Milligan et al., 1998). This thesis concludes that Rx1 DNA binding and chromatin remodelling by associated proteins appears to mediate resistance to PVX and that this may be a conserved activity found in other NBLRR proteins.

7. Appendices

7.1 Summary of yeast 2-hybrid preliminary screen results

Table 8 Proteins determined to interact with the Rx1 CC domain with a PBS score of 'C' or above via the preliminary screen of the yeast 2-hybrid screen described in Section 4.2 and Section 2.4.4.

GenBank Protein Annotation	Reference Sequence	PRBS	Contig(s)	Hits
Homolog of Solanum lycopersicum Hop-interacting protein THI032 (LOC101055519), mRNA	NM_001279017.1 525314082 (NCBI)	C	70054343	3
PREDICTED: Homolog of Solanum tuberosum probable transcription factor GLK1-like (LOC102587163), mRNA	XM_006348765.1 (NCBI)	B	70054304 / 70053981	7
PREDICTED: Homolog of Solanum tuberosum serine--glyoxylate aminotransferase-like (LOC102592345), mRNA	XM_006349714.1 (NCBI)	C	70054322 / 70054343	17
PREDICTED: Homolog of Solanum tuberosum chromodomain-helicase-DNA-binding protein 1-like (LOC102593358), transcript variant X3, mRNA	XM_006349719.1 (NCBI)	A	70054171	15
PREDICTED: Homolog of Solanum tuberosum ATP synthase delta chain, chloroplastic-like (LOC102598933), mRNA	XM_006345483.1 (NCBI)	B	70054312	8
PREDICTED: Homolog of Solanum tuberosum micronuclear linker histone polyprotein-like (LOC102600407), mRNA	XM_006359105.1 (NCBI)	A	70054279	7
RAN GTPase-activating protein 2 (RanGAP2) mRNA, complete cds	EF396237.1 (GenBank)	A	70054294 / 70054289 / 70054003	9
S-adenosyl homocysteine hydrolase mRNA, complete cds	JQ890096.1 (GenBank)	A	70054202	20
Nicotiana benthamiana poly-A binding protein mRNA, partial cds	JQ347293.1 (GenBank)	C	70053954 / 70053951 / 70054159	2
Nicotiana benthamiana gfp gene for green fluorescent protein and pat gene for phosphinothricin acetyltransferase	HF675000.1 (GenBank)	A	70054077	10
Nicotiana benthamiana clone 12-130 unknown mRNA	AY310808.1 (GenBank)	A	70054378	37

7.2 Yeast 2-hybrid preliminary screen results

Table 9. Complete results of the preliminary screen of the yeast 2-hybrid screen between the Rx1 CC domain and the *N. benthamiana* mixed tissue cDNA library described in Section 4.2 and Section 2.4.4. IF = in frame, OOF = out of frame, + = sense, - = antisense

Clone Name	Contig(s) Name	Gene Name (Best Match)	GenBank ID	Global PRBS	Frame	Sense/ Antisense (+/-)	% Id 5p/3p
pB27_A-21	70054007 / 70054005	Nicotiana benthamiana - ARF1	296278601	D	IF	+	72.2 / 77.5
pB27_A-102	70053976	Nicotiana benthamiana - ATG9	468186891	N/A	??	-	92.1
pB27_A-263	70054030	Nicotiana benthamiana - Homolog of 24K germin like protein (Nicotiana tabacum)	31711506	D	IF	+	99.5 / 100.0
pB27_A-65	70054365	Nicotiana benthamiana - Homolog of CP12 (Nicotiana tabacum)	25990285	N/A	OOF2	+	100.0 / 100.0
pB27_A-154	70054129	Nicotiana benthamiana - Homolog of D6 (Nicotiana tabacum)	343424520	N/A	OOF1	+	100.0 / 99.8
pB27_A-159	70054122	Nicotiana benthamiana - Homolog of DIR2 (Nicotiana tabacum)	328685100	D	IF	+	100.0 / 100.0
pB27_A-148	70054142	Nicotiana benthamiana - Homolog of EIL5 (Nicotiana tabacum)	30016901	D	IF	+	99.5 / 100.0
pB27_A-107	70054142	Nicotiana benthamiana - Homolog of EIL5 (Nicotiana tabacum)	30016901	D	IF	+	99.2 / 99.2
pB27_A-85	70054266	Nicotiana benthamiana - Homolog of Fyn (Mus musculus)	171543840	D	IF	+	100.0 / 100.0
pB27_A-38	70053999 / 70053997	Nicotiana benthamiana - Homolog of GenMatch (Nicotiana sylvestris)	48249481	D	IF	+	100.0 / 57.7
pB27_A-161	70054117	Nicotiana benthamiana - Homolog of GenMatch (Nicotiana tabacum)	1617412	D	IF	+	99.7 / 99.3
pB27_A-259	70054355 / 70054353	Nicotiana benthamiana - Homolog of GenMatch (Nicotiana tabacum)	148498111	D	IF	+	100.0 / 57.2
pB27_A-147	70054145	Nicotiana benthamiana - Homolog of GenMatch (Nicotiana undulata)	347453879	D	IF	+	94.1 / 98.2
pB27_A-55	70054373	Nicotiana benthamiana - Homolog of GenMatch (Nicotiana undulata)	347453879	D	IF	+	100.0 / 98.2
pB27_A-160	70054119	Nicotiana benthamiana - Homolog of GenMatch (Torricellia tiliifolia)	37778905	D	IF	+	99.8 / 100.0
pB27_A-146	70053960	Nicotiana benthamiana - Homolog of Histone H4 (Medicago truncatula)	357454042	D	IF	+	100
pB27_A-225	70054061	Nicotiana benthamiana - Homolog of LHCI (Nicotiana tabacum)	493722	N/A	OOF1	+	98.4 / 98.8
pB27_A-44	70054343	Nicotiana benthamiana - Homolog of LOC101055519 (Solanum lycopersicum)	525314082	**C**	IF	+	97.3

Clone Name	Contig(s) Name	Gene Name (Best Match)	GenBank ID	Global PRBS	Frame	Sense/ Antisense (+/-)	% Id 5p/3p
pB27_A-77	70054343	Nicotiana benthamiana - Homolog of LOC101055519 (Solanum lycopersicum)	525314082	**C**	IF	+	98.2 / 98.2
pB27_A-13	70054343	Nicotiana benthamiana - Homolog of LOC101055519 (Solanum lycopersicum)	525314082	**C**	IF	+	90.9 / 87.6
pB27_A-93	70053980 / 70053978	Nicotiana benthamiana - Homolog of LOC101248270 (Solanum lycopersicum)	460412768	N/A	OOF2	+	100.0 / 74.4
pB27_A-229	70054057	Nicotiana benthamiana - Homolog of LOC101248280 (Solanum lycopersicum)	460415197	D	IF	+	96.9 / 96.3
pB27_A-119	70054425	Nicotiana benthamiana - Homolog of LOC101248941 (Solanum lycopersicum)	460375949	D	IF	+	97.4 / 96.2
pB27_A-34	70054425	Nicotiana benthamiana - Homolog of LOC101248941 (Solanum lycopersicum)	460375949	D	IF	+	98.7 / 98.8
pB27_A-247	70054047	Nicotiana benthamiana - Homolog of LOC101251606 (Solanum lycopersicum)	460399953	D	IF	+	100.0 / 100.0
pB27_A-152	70054134	Nicotiana benthamiana - Homolog of LOC101252253 (Solanum lycopersicum)	460411429	D	IF	+	99.2 / 100.0
pB27_A-187	70054100	Nicotiana benthamiana - Homolog of LOC101252775 (Solanum lycopersicum)	460384910	D	IF	+	97.7 / 98.1
pB27_A-133	70053970 / 70053968	Nicotiana benthamiana - Homolog of LOC101255271 (Solanum lycopersicum)	460412472	D	IF	+	100.0 / 58.1
pB27_A-108	70053974 / 70054378	Nicotiana benthamiana - Homolog of LOC101265689 (Solanum lycopersicum)	460407710	N/A	OOF2	+	100.0 / 81.5
pB27_A-185	70054024	Nicotiana benthamiana - Homolog of LOC101265915 (Solanum lycopersicum)	460383717	N/A	OOF2	+	96.9 / 97.4
pB27_A-265	70054024	Nicotiana benthamiana - Homolog of LOC101265915 (Solanum lycopersicum)	460383717	N/A	OOF2	+	98.0 / 98.4
pB27_A-114	70054230	Nicotiana benthamiana - Homolog of LOC101265925 (Solanum lycopersicum)	460387939	D	IF	+	99.7 / 100.0

Clone Name	Contig(s) Name	Gene Name (Best Match)	GenBank ID	Global PRBS	Frame	Sense/ Antisense (+/-)	% Id 5p/3p
pB27_A-223	70054064	Nicotiana benthamiana - Homolog of LOC102577588 (Solanum tuberosum)	568214299	N/A	OOF2	+	98.0 / 98.8
pB27_A-198	70054439 / 70054437	Nicotiana benthamiana - Homolog of LOC102578384 (Solanum tuberosum)	565393118	N/A	OOF2	+	100.0 / 64.2
pB27_A-158	70053959 / 70053957	Nicotiana benthamiana - Homolog of LOC102579571 (Solanum tuberosum)	565385252	D	IF	+	100.0 / 58.6
pB27_A-214	70054265 / 70054261	Nicotiana benthamiana - Homolog of LOC102579874 (Solanum tuberosum)	565371945	D	IF	+	94.6 / 87.4
pB27_A-94	70054265 / 70054261	Nicotiana benthamiana - Homolog of LOC102579874 (Solanum tuberosum)	565371945	D	IF	+	97.1 / 81.5
pB27_A-270	70054265 / 70054261	Nicotiana benthamiana - Homolog of LOC102579874 (Solanum tuberosum)	565371945	D	IF	+	99.1 / 85.1
pB27_A-123	70053973 / 70053971	Nicotiana benthamiana - Homolog of LOC102580230 (Solanum tuberosum)	568215560	D	IF	+	100.0 / 80.0
pB27_A-176	70054107	Nicotiana benthamiana - Homolog of LOC102580732 (Solanum tuberosum)	565361662	D	IF	+	98.8 / 98.1
pB27_A-100	70054241	Nicotiana benthamiana - Homolog of LOC102581057 (Solanum tuberosum)	565358447	N/A	OOF2	+	99.5 / 99.3
pB27_A-200	70054093	Nicotiana benthamiana - Homolog of LOC102581075 (Solanum tuberosum)	565403506	D	IF	+	99.3 / 100.0
pB27_A-264	70054028	Nicotiana benthamiana - Homolog of LOC102582052 (Solanum tuberosum)	565399087	N/A	OOF1	+	100.0 / 100.0
pB27_A-22	70054287	Nicotiana benthamiana - Homolog of LOC102582739 (Solanum tuberosum)	565362192	N/A	OOF1	+	96.9 / 97.3
pB27_A-210	70054435 / 70054432	Nicotiana benthamiana - Homolog of LOC102583251 (Solanum tuberosum)	565347061	N/A	OOF2	+	100.0 / 93.2
pB27_A-120	70054198	Nicotiana benthamiana - Homolog of LOC102583426 (Solanum tuberosum)	565374862	N/A	OOF2	+	97.6 / 96.0
pB27_A-2	70054011 / 70054009	Nicotiana benthamiana - Homolog of LOC102583814 (Solanum tuberosum)	565351888	N/A	OOF1	+	100.0 / 54.5
pB27_A-242	70054052	Nicotiana benthamiana - Homolog of LOC102584643 (Solanum tuberosum)	565373761	D	IF	+	94.2 / 95.6
pB27_A-51	70054419	Nicotiana benthamiana - Homolog of LOC102584719 (Solanum tuberosum)	565358649	D	IF	+	98.3 / 100.0

Clone Name	Contig(s) Name	Gene Name (Best Match)	GenBank ID	Global PRBS	Frame	Sense/ Antisense (+/-)	% Id 5p/3p
pB27_A-217	70054070	Nicotiana benthamiana - Homolog of LOC102585195 (Solanum tuberosum)	565387763	D	IF	+	100.0 / 100.0
pB27_A-95	70054259	Nicotiana benthamiana - Homolog of LOC102585410 (Solanum tuberosum)	565381410	D	IF	+	95.9 / 94.1
pB27_A-74	70054275	Nicotiana benthamiana - Homolog of LOC102585527 (Solanum tuberosum)	565385461	N/A	OOF1	+	97.4 / 84.0
pB27_A-39	70054421	Nicotiana benthamiana - Homolog of LOC102585620 (Solanum tuberosum)	565372959	N/A	OOF2	+	99.2 / 100.0
pB27_A-136	70053967 / 70053965	Nicotiana benthamiana - Homolog of LOC102586113 (Solanum tuberosum)	565391879	D	IF	+	100.0 / 83.3
pB27_A-33	70054001	Nicotiana benthamiana - Homolog of LOC102586241 (Solanum tuberosum)	565396859	N/A	??	+	100
pB27_A-83	70054270	Nicotiana benthamiana - Homolog of LOC102586241 (Solanum tuberosum)	565396859	N/A	OOF1	+	96.3 / 97.8
pB27_A-150	70054139	Nicotiana benthamiana - Homolog of LOC102586284 (Solanum tuberosum)	565366628	N/A	OOF2	+	96.5 / 98.4
pB27_A-82	70053989 / 70053986	Nicotiana benthamiana - Homolog of LOC102586594 (Solanum tuberosum)	565402967	D	IF	+	100.0 / 88.0
pB27_A-15	70054304	Nicotiana benthamiana - Homolog of LOC102587163 (Solanum tuberosum)	565364225	**B**	IF	+	97.6 / 98.5
pB27_A-23	70054304	Nicotiana benthamiana - Homolog of LOC102587163 (Solanum tuberosum)	565364225	**B**	IF	+	95.9 / 96.4
pB27_A-211	70054304	Nicotiana benthamiana - Homolog of LOC102587163 (Solanum tuberosum)	565364225	**B**	IF	+	97.3 / 98.3
pB27_A-220	70054304	Nicotiana benthamiana - Homolog of LOC102587163 (Solanum tuberosum)	565364225	**B**	IF	+	94.7 / 96.4
pB27_A-92	70054304 / 70053981	Nicotiana benthamiana - Homolog of LOC102587163 (Solanum tuberosum)	565364225	**B**	IF	+	93.6 / 77.2
pB27_A-32	70054304	Nicotiana benthamiana - Homolog of LOC102587163 (Solanum tuberosum)	565364225	**B**	IF	+	96.9 / 97.2
pB27_A-98	70054304	Nicotiana benthamiana - Homolog of LOC102587163 (Solanum tuberosum)	565364225	**B**	IF	+	95.3 / 95.3
pB27_A-132	70054162	Nicotiana benthamiana - Homolog of LOC102587186 (Solanum tuberosum)	565376434	D	IF	+	97.4 / 98.5

Clone Name	Contig(s) Name	Gene Name (Best Match)	GenBank ID	Global PRBS	Frame	Sense/ Antisense (+/-)	% Id 5p/3p
pB27_A-127	70054167	Nicotiana benthamiana - Homolog of LOC102587257 (Solanum tuberosum)	565357966	N/A	OOF2	+	100.0 / 100.0
pB27_A-139	70054151	Nicotiana benthamiana - Homolog of LOC102587717 (Solanum tuberosum)	565366808	D	IF	+	96.4 / 95.8
pB27_A-278	70054255	Nicotiana benthamiana - Homolog of LOC102587723 (Solanum tuberosum)	565370212	D	IF	+	100
pB27_A-75	70053993 / 70053990	Nicotiana benthamiana - Homolog of LOC102587822 (Solanum tuberosum)	565364229	N/A	OOF2	+	100.0 / 58.7
pB27_A-164	70054115	Nicotiana benthamiana - Homolog of LOC102588954 (Solanum tuberosum)	568214951	N/A	OOF2	+	97.1 / 97.4
pB27_A-62	70054369	Nicotiana benthamiana - Homolog of LOC102589744 (Solanum tuberosum)	565353745	D	IF	+	100.0 / 97.0
pB27_A-70	70053996 / 70053994	Nicotiana benthamiana - Homolog of LOC102589959 (Solanum tuberosum)	565351587	D	IF	+	100.0 / 63.1
pB27_A-27	70054277	Nicotiana benthamiana - Homolog of LOC102590376 (Solanum tuberosum)	565392709	N/A	OOF2	+	100.0 / 100.0
pB27_A-254	70054322	Nicotiana benthamiana - Homolog of LOC102592345 (Solanum tuberosum)	565366188	**C**	IF	+	99.7 / 99.7
pB27_A-236	70054322	Nicotiana benthamiana - Homolog of LOC102592345 (Solanum tuberosum)	565366188	**C**	IF	+	96.8 / 97.2
pB27_A-234	70054322	Nicotiana benthamiana - Homolog of LOC102592345 (Solanum tuberosum)	565366188	**C**	IF	+	98.9 / 98.9
pB27_A-56	70054322	Nicotiana benthamiana - Homolog of LOC102592345 (Solanum tuberosum)	565366188	**C**	IF	+	98.3 / 98.8
pB27_A-57	70054322 / 70054343	Nicotiana benthamiana - Homolog of LOC102592345 (Solanum tuberosum)	565366188	**C**	IF	+	99.3 / 99.3
pB27_A-84	70054322	Nicotiana benthamiana - Homolog of LOC102592345 (Solanum tuberosum)	565366188	**C**	IF	+	98.1 / 97.7
pB27_A-121	70054322 / 70054343	Nicotiana benthamiana - Homolog of LOC102592345 (Solanum tuberosum)	565366188	**C**	IF	+	99.3 / 99.3
pB27_A-138	70054322	Nicotiana benthamiana - Homolog of LOC102592345 (Solanum tuberosum)	565366188	**C**	IF	+	98.8 / 98.8
pB27_A-143	70054322	Nicotiana benthamiana - Homolog of LOC102592345 (Solanum tuberosum)	565366188	**C**	IF	+	98.8 / 98.8

Clone Name	Contig(s) Name	Gene Name (Best Match)	GenBank ID	Global PRBS	Frame	Sense/ Antisense (+/-)	% Id 5p/3p
pB27_A-155	70054322	Nicotiana benthamiana - Homolog of LOC102592345 (Solanum tuberosum)	565366188	**C**	IF	+	98.7 / 98.9
pB27_A-167	70054322	Nicotiana benthamiana - Homolog of LOC102592345 (Solanum tuberosum)	565366188	**C**	IF	+	98.3 / 98.3
pB27_A-7	70054322	Nicotiana benthamiana - Homolog of LOC102592345 (Solanum tuberosum)	565366188	**C**	IF	+	92.9
pB27_A-36	70054322 / 70054343	Nicotiana benthamiana - Homolog of LOC102592345 (Solanum tuberosum)	565366188	**C**	IF	+	99.3 / 99.3
pB27_A-43	70054322	Nicotiana benthamiana - Homolog of LOC102592345 (Solanum tuberosum)	565366188	**C**	IF	+	96.0 / 97.2
pB27_A-46	70054322	Nicotiana benthamiana - Homolog of LOC102592345 (Solanum tuberosum)	565366188	**C**	IF	+	98.5 / 99.1
pB27_A-54	70054322	Nicotiana benthamiana - Homolog of LOC102592345 (Solanum tuberosum)	565366188	**C**	IF	+	93.4 / 93.0
pB27_A-241	70054322	Nicotiana benthamiana - Homolog of LOC102592345 (Solanum tuberosum)	565366188	**C**	IF	+	98.5 / 98.5
pB27_A-151	70054137	Nicotiana benthamiana - Homolog of LOC102592995 (Solanum tuberosum)	565357243	N/A	OOF1	+	97.2 / 95.8
pB27_A-124	70054171	Nicotiana benthamiana - Homolog of LOC102593358 (Solanum tuberosum)	565366198	**A**	IF	+	93.8 / 94.6
pB27_A-267	70054171	Nicotiana benthamiana - Homolog of LOC102593358 (Solanum tuberosum)	565366198	**A**	IF	+	95.3 / 95.3
pB27_A-47	70054171	Nicotiana benthamiana - Homolog of LOC102593358 (Solanum tuberosum)	565366198	**A**	IF	+	94.8 / 96.1
pB27_A-3	70054171	Nicotiana benthamiana - Homolog of LOC102593358 (Solanum tuberosum)	565366198	**A**	IF	+	92.2 / 95.6
pB27_A-52	70054171	Nicotiana benthamiana - Homolog of LOC102593358 (Solanum tuberosum)	565366198	**A**	IF	+	95.4 / 95.9
pB27_A-149	70054171	Nicotiana benthamiana - Homolog of LOC102593358 (Solanum tuberosum)	565366198	**A**	IF	+	94.8 / 95.3
pB27_A-162	70054171	Nicotiana benthamiana - Homolog of LOC102593358 (Solanum tuberosum)	565366198	**A**	IF	+	95.2 / 96.8
pB27_A-183	70054171	Nicotiana benthamiana - Homolog of LOC102593358 (Solanum tuberosum)	565366198	**A**	IF	+	86.5

Clone Name	Contig(s) Name	Gene Name (Best Match)	GenBank ID	Global PRBS	Frame	Sense/ Antisense (+/-)	% Id 5p/3p
pB27_A-239	70054171	Nicotiana benthamiana - Homolog of LOC102593358 (Solanum tuberosum)	565366198	**A**	IF	+	93.4 / 94.3
pB27_A-31	70054171	Nicotiana benthamiana - Homolog of LOC102593358 (Solanum tuberosum)	565366198	**A**	IF	+	94.2 / 95.4
pB27_A-202	70054171	Nicotiana benthamiana - Homolog of LOC102593358 (Solanum tuberosum)	565366198	**A**	IF	+	89.8 / 91.4
pB27_A-189	70054171	Nicotiana benthamiana - Homolog of LOC102593358 (Solanum tuberosum)	565366198	**A**	IF	+	97.1 / 90.9
pB27_A-141	70054171	Nicotiana benthamiana - Homolog of LOC102593358 (Solanum tuberosum)	565366198	**A**	IF	+	96.1 / 98.2
pB27_A-174	70054171	Nicotiana benthamiana - Homolog of LOC102593358 (Solanum tuberosum)	565366198	**A**	IF	+	96.4 / 96.4
pB27_A-235	70054171	Nicotiana benthamiana - Homolog of LOC102593358 (Solanum tuberosum)	565366198	**A**	IF	+	94.3 / 93.5
pB27_A-87	70053985 / 70053983	Nicotiana benthamiana - Homolog of LOC102595490 (Solanum tuberosum)	565388955	N/A	OOF2	+	100.0 / 68.9
pB27_A-101	70054239	Nicotiana benthamiana - Homolog of LOC102596217 (Solanum tuberosum)	565362766	D	IF	+	97.5 / 99.8
pB27_A-256	70054038	Nicotiana benthamiana - Homolog of LOC102596435 (Solanum tuberosum)	565365600	D	IF	+	95.9 / 95.2
pB27_A-170	70054038	Nicotiana benthamiana - Homolog of LOC102596435 (Solanum tuberosum)	565365600	D	IF	+	93.7
pB27_A-168	70054038	Nicotiana benthamiana - Homolog of LOC102596435 (Solanum tuberosum)	565365600	N/A	??	-	94.2 / 94.5
pB27_A-275	70054321 / 70054301	Nicotiana benthamiana - Homolog of LOC102596966 (Solanum tuberosum)	568214797	N/A	OOF2	+	100.0 / 78.0
pB27_A-129	70054164	Nicotiana benthamiana - Homolog of LOC102598876 (Solanum tuberosum)	565342363	N/A	OOF1	+	99.0 / 99.2
pB27_A-169	70054312	Nicotiana benthamiana - Homolog of LOC102598933 (Solanum tuberosum)	565357427	**B**	IF	+	89.6 / 92.3
pB27_A-268	70054312	Nicotiana benthamiana - Homolog of LOC102598933 (Solanum tuberosum)	565357427	**B**	IF	+	95.3 / 97.0
pB27_A-68	70054312	Nicotiana benthamiana - Homolog of LOC102598933 (Solanum tuberosum)	565357427	**B**	IF	+	99.0 / 99.2

Clone Name	Contig(s) Name	Gene Name (Best Match)	GenBank ID	Global PRBS	Frame	Sense/ Antisense (+/-)	% Id 5p/3p
pB27_A-125	70054312	Nicotiana benthamiana - Homolog of LOC102598933 (Solanum tuberosum)	565357427	**B**	IF	+	94.9 / 95.0
pB27_A-97	70054312	Nicotiana benthamiana - Homolog of LOC102598933 (Solanum tuberosum)	565357427	**B**	IF	+	91.3 / 95.4
pB27_A-237	70054312	Nicotiana benthamiana - Homolog of LOC102598933 (Solanum tuberosum)	565357427	**B**	IF	+	97.3 / 96.0
pB27_A-255	70054312	Nicotiana benthamiana - Homolog of LOC102598933 (Solanum tuberosum)	565357427	**B**	IF	+	96.7 / 97.3
pB27_A-240	70054312	Nicotiana benthamiana - Homolog of LOC102598933 (Solanum tuberosum)	565357427	**B**	IF	+	97.1 / 96.7
pB27_A-283	70054013	Nicotiana benthamiana - Homolog of LOC102599206 (Solanum tuberosum)	565386733	D	IF	+	93.1 / 98.1
pB27_A-30	70054268	Nicotiana benthamiana - Homolog of LOC102599526 (Solanum tuberosum)	565342734	N/A	OOF2	+	98.8 / 99.2
pB27_A-28	70054272	Nicotiana benthamiana - Homolog of LOC102599631 (Solanum tuberosum)	565382323	D	IF	+	93.6 / 97.4
pB27_A-24	70054272	Nicotiana benthamiana - Homolog of LOC102599631 (Solanum tuberosum)	565382323	D	IF	+	99.8 / 99.6
pB27_A-72	70054279	Nicotiana benthamiana - Homolog of LOC102600407 (Solanum tuberosum)	565386739	**A**	IF	+	96.9 / 97.1
pB27_A-209	70054279	Nicotiana benthamiana - Homolog of LOC102600407 (Solanum tuberosum)	565386739	**A**	IF	+	94.4 / 97.2
pB27_A-16	70054279	Nicotiana benthamiana - Homolog of LOC102600407 (Solanum tuberosum)	565386739	**A**	IF	+	96.0 / 94.3
pB27_A-179	70054279	Nicotiana benthamiana - Homolog of LOC102600407 (Solanum tuberosum)	565386739	**A**	IF	+	96.2 / 92.8
pB27_A-88	70054279	Nicotiana benthamiana - Homolog of LOC102600407 (Solanum tuberosum)	565386739	**A**	IF	+	97.9 / 100.0
pB27_A-226	70054279	Nicotiana benthamiana - Homolog of LOC102600407 (Solanum tuberosum)	565386739	**A**	IF	+	98.6 / 98.2
pB27_A-40	70054279	Nicotiana benthamiana - Homolog of LOC102600407 (Solanum tuberosum)	565386739	**A**	IF	+	94.8 / 96.6
pB27_A-165	70054113	Nicotiana benthamiana - Homolog of LOC102601433 (Solanum tuberosum)	565387535	N/A	OOF2	+	99.7 / 100.0

Clone Name	Contig(s) Name	Gene Name (Best Match)	GenBank ID	Global PRBS	Frame	Sense/ Antisense (+/-)	% Id 5p/3p
pB27_A-277	70054020	Nicotiana benthamiana - Homolog of LOC102601925 (Solanum tuberosum)	565400596	N/A	OOF1	+	100.0 / 100.0
pB27_A-252	70054042	Nicotiana benthamiana - Homolog of LOC102602229 (Solanum tuberosum)	565350375	N/A	OOF2	+	99.7 / 100.0
pB27_A-196	70054095	Nicotiana benthamiana - Homolog of LOC102602408 (Solanum tuberosum)	565376678	N/A	OOF1	+	97.7 / 97.3
pB27_A-231	70054055	Nicotiana benthamiana - Homolog of LOC102604573 (Solanum tuberosum)	565389935	D	IF	+	99.7 / 100.0
pB27_A-213	70054431 / 70054429	Nicotiana benthamiana - Homolog of LOC102604617 (Solanum tuberosum)	565363138	N/A	OOF1	+	100.0 / 68.6
pB27_A-61	70054371	Nicotiana benthamiana - Homolog of LOC102604680 (Solanum tuberosum)	565391346	N/A	OOF2	+	99.4 / 99.8
pB27_A-245	70054049	Nicotiana benthamiana - Homolog of LOC102604815 (Solanum tuberosum)	565351842	N/A	OOF1	+	94.3 / 97.7
pB27_A-145	70054148	Nicotiana benthamiana - Homolog of LOC102604882 (Solanum tuberosum)	565341786	N/A	OOF2	+	100.0 / 100.0
pB27_A-244	70054362 / 70054360	Nicotiana benthamiana - Homolog of LOC102604919 (Solanum tuberosum)	565351684	D	IF	+	100.0 / 58.4
pB27_A-111	70054232	Nicotiana benthamiana - Homolog of LOC102605062 (Solanum tuberosum)	568214452	D	IF	+	94.7 / 93.7
pB27_A-199	70054124 / 70054436	Nicotiana benthamiana - Homolog of LOC102606384 (Solanum tuberosum)	565352653	D	IF	+	97.9 / 72.2
pB27_A-156	70054124	Nicotiana benthamiana - Homolog of LOC102606384 (Solanum tuberosum)	565352653	D	IF	+	96.1
pB27_A-67	70054363	Nicotiana benthamiana - Homolog of LOC543976 (Solanum lycopersicum)	460412300	N/A	OOF1	+	95.1 / 96.3
pB27_A-115	70054227	Nicotiana benthamiana - Homolog of MIP2 (Nicotiana glauca)	12006840	D	IF	+	99.8 / 100.0
pB27_A-203	70054091	Nicotiana benthamiana - Homolog of NtGT2 (Nicotiana tabacum)	20146092	D	IF	+	100.0 / 100.0
pB27_A-171	70054109	Nicotiana benthamiana - Homolog of NtROS3 (Nicotiana tabacum)	138996993	D	IF	+	94.8
pB27_A-216	70054109 / 70054428	Nicotiana benthamiana - Homolog of NtROS3 (Nicotiana tabacum)	138996993	D	IF	+	100.0 / 85.9
pB27_A-99	70054243	Nicotiana benthamiana - Homolog of PHA2 (Solanum tuberosum)	568214506	D	IF	+	95.3 / 96.1
pB27_A-253	70054356	Nicotiana benthamiana - Homolog of PSY2 (Solanum lycopersicum)	350534779	N/A	??	+	100

Clone Name	Contig(s) Name	Gene Name (Best Match)	GenBank ID	Global PRBS	Frame	Sense/ Antisense (+/-)	% Id 5p/3p
pB27_A-184	70053955	Nicotiana benthamiana - Homolog of chlorophyll a/b bindingprotein (Nicotiana tabacum)	29123377	N/A	OOF1	+	100
pB27_A-218	70054423	Nicotiana benthamiana - Homolog of glyceraldehyde-3-phosphate dehydrogenaseA-subunit (Nicotiana tabacum)	170236	D	IF	+	100
pB27_A-261	70054033	Nicotiana benthamiana - Homolog of hypothetical protein (Populus trichocarpa)	566183522	D	IF	+	99.0 / 98.5
pB27_A-280	70054016	Nicotiana benthamiana - Homolog of jasmonate ZIM domain protein b (Nicotiana attenuata)	389986096	D	IF	+	98.5 / 98.9
pB27_A-243	70054016	Nicotiana benthamiana - Homolog of jasmonate ZIM domain protein b (Nicotiana attenuata)	389986096	D	IF	+	100.0 / 100.0
pB27_A-257	70054035	Nicotiana benthamiana - Homolog of ked (Nicotiana tabacum)	8096268	N/A	OOF2	+	98.5 / 98.6
pB27_A-106	70054234	Nicotiana benthamiana - Homolog of plastid transketolase (Nicotiana tabacum)	194396260	N/A	OOF2	+	100.0 / 100.0
pB27_A-191	70054098	Nicotiana benthamiana - Homolog of putative 60S ribosomal protein L9 (Leishmania mexicana MHOM/GT/2001/U1103)	401425990	N/A	OOF2	+	95.6 / 96.6
pB27_A-208	70054073	Nicotiana benthamiana - Homolog of putative phosphate-induced protein (Capsicum chinense)	171854680	N/A	OOF1	+	100.0 / 99.8
pB27_A-222	70054066	Nicotiana benthamiana - Homolog of unnamed protein (Petunia x hybrida)	169213	D	IF	+	99.8 / 100.0
pB27_A-63	70054367	Nicotiana benthamiana - Impa1	119866034	D	IF	+	99.6 / 99.6
pB27_A-142	70054349	Nicotiana benthamiana - NbROS1	478620804	D	IF	+	67.0 / 74.5
pB27_A-45	70054349	Nicotiana benthamiana - NbROS1	478620804	D	IF	+	68.0 / 74.4
pB27_A-5	70054349	Nicotiana benthamiana - NbROS1	478620804	D	IF	+	68.0 / 74.5
pB27_A-116	70054224	Nicotiana benthamiana - NbWIPK	27374987	N/A	??	-	94.9 / 98.1
pB27_A-269	70054294 / 70054289	Nicotiana benthamiana - RanGAP2	147882992	**A**	IF	+	97.1 / 92.8
pB27_A-71	70054294 / 70054289	Nicotiana benthamiana - RanGAP2	147882992	**A**	IF	+	93.7 / 95.1
pB27_A-59	70054294	Nicotiana benthamiana - RanGAP2	147882992	**A**	IF	+	96.0 / 99.6
pB27_A-17	70054294	Nicotiana benthamiana - RanGAP2	147882992	**A**	OOF1	+	100.0 / 100.0
pB27_A-193	70054294	Nicotiana benthamiana - RanGAP2	147882992	**A**	IF	+	100.0 / 100.0
pB27_A-25	70054294 / 70054003	Nicotiana benthamiana - RanGAP2	147882992	**A**	OOF1	+	98.2 / 97.9

Clone Name	Contig(s) Name	Gene Name (Best Match)	GenBank ID	Global PRBS	Frame	Sense/ Antisense (+/-)	% Id 5p/3p
pB27_A-113	70054294	Nicotiana benthamiana - RanGAP2	147882992	**A**	OOF1	+	98.2 / 98.2
pB27_A-37	70054294	Nicotiana benthamiana - RanGAP2	147882992	**A**	OOF1	+	98.2 / 98.2
pB27_A-221	70054294	Nicotiana benthamiana - RanGAP2	147882992	**A**	OOF1	+	98.2 / 98.2
pB27_A-118	70054202	Nicotiana benthamiana - S-adenosyl homocysteine hydrolase	387861273	**A**	IF	+	91.7 / 92.8
pB27_A-178	70054202	Nicotiana benthamiana - S-adenosyl homocysteine hydrolase	387861273	**A**	IF	+	90.8 / 95.5
pB27_A-204	70054202	Nicotiana benthamiana - S-adenosyl homocysteine hydrolase	387861273	**A**	IF	+	98.2 / 98.3
pB27_A-1	70054202	Nicotiana benthamiana - S-adenosyl homocysteine hydrolase	387861273	**A**	OOF2	+	90.4 / 92.7
pB27_A-10	70054202	Nicotiana benthamiana - S-adenosyl homocysteine hydrolase	387861273	**A**	OOF2	+	94.8 / 93.0
pB27_A-182	70054202	Nicotiana benthamiana - S-adenosyl homocysteine hydrolase	387861273	**A**	IF	+	93.4
pB27_A-144	70054202	Nicotiana benthamiana - S-adenosyl homocysteine hydrolase	387861273	**A**	IF	+	94.7 / 94.6
pB27_A-78	70054202	Nicotiana benthamiana - S-adenosyl homocysteine hydrolase	387861273	**A**	IF	+	94.3 / 97.0
pB27_A-103	70054202	Nicotiana benthamiana - S-adenosyl homocysteine hydrolase	387861273	**A**	IF	+	90.3 / 96.6
pB27_A-29	70054202	Nicotiana benthamiana - S-adenosyl homocysteine hydrolase	387861273	**A**	IF	+	91.5 / 95.5
pB27_A-42	70054202	Nicotiana benthamiana - S-adenosyl homocysteine hydrolase	387861273	**A**	IF	+	94.9 / 95.2
pB27_A-249	70054202	Nicotiana benthamiana - S-adenosyl homocysteine hydrolase	387861273	**A**	IF	+	90.1 / 94.5
pB27_A-232	70054202	Nicotiana benthamiana - S-adenosyl homocysteine hydrolase	387861273	**A**	IF	+	94.7 / 95.2
pB27_A-233	70054202	Nicotiana benthamiana - S-adenosyl homocysteine hydrolase	387861273	**A**	IF	+	95.0 / 95.7
pB27_A-212	70054202	Nicotiana benthamiana - S-adenosyl homocysteine hydrolase	387861273	**A**	IF	+	93.7 / 96.1
pB27_A-227	70054202	Nicotiana benthamiana - S-adenosyl homocysteine hydrolase	387861273	**A**	IF	+	92.3 / 93.5

Clone Name	Contig(s) Name	Gene Name (Best Match)	GenBank ID	Global PRBS	Frame	Sense/ Antisense (+/-)	% Id 5p/3p
pB27_A-207	70054202	Nicotiana benthamiana - S-adenosyl homocysteine hydrolase	387861273	**A**	IF	+	94.4 / 95.2
pB27_A-8	70054202	Nicotiana benthamiana - S-adenosyl homocysteine hydrolase	387861273	**A**	IF	+	95.0 / 94.6
pB27_A-6	70054202	Nicotiana benthamiana - S-adenosyl homocysteine hydrolase	387861273	**A**	IF	+	94.2
pB27_A-26	70054202	Nicotiana benthamiana - S-adenosyl homocysteine hydrolase	387861273	**A**	IF	+	90.8 / 93.7
pB27_A-131	70054202	Nicotiana benthamiana - S-adenosyl homocysteine hydrolase	387861273	**A**	??	+	90.7
pB27_A-135	70054156	Nicotiana benthamiana - TRXh	257222627	N/A	??	-	100.0 / 100.0
pB27_A-140	70053962	Nicotiana benthamiana - No Match	(no match found in GenBank)	D	IF	+	100
pB27_A-228	70054059	Nicotiana benthamiana - No Match	(no match found in GenBank)	D	IF	+	100.0 / 100.0
pB27_A-137	70054154	Nicotiana benthamiana - No Match	(no match found in GenBank)	D	IF	+	98.2 / 99.5
pB27_A-285	70054247 / 70054245	Nicotiana benthamiana - No Match	(no match found in GenBank)	D	IF	+	100.0 / 75.5
pB27_A-284	70054250 / 70054248	Nicotiana benthamiana - No Match	(no match found in GenBank)	D	IF	+	100.0 / 76.0
pB27_A-281	70054251	Nicotiana benthamiana - No Match	(no match found in GenBank)	D	IF	+	100
pB27_A-279	70054253	Nicotiana benthamiana - No Match	(no match found in GenBank)	D	IF	+	100
pB27_A-276	70054257	Nicotiana benthamiana - No Match	(no match found in GenBank)	D	IF	+	100
pB27_A-272	70054347 / 70054341	Nicotiana benthamiana - No Match	(no match found in GenBank)	D	IF	+	100.0 / 57.7
pB27_A-188	70053954 / 70053951	Nicotiana benthamiana - poly-A binding protein	400234897	**C**	OOF2	+	70.0 / 66.8
pB27_A-134	70054159	Nicotiana benthamiana - poly-A binding protein	400234897	**C**	OOF2	+	93.5 / 92.6
pB27_A-248	70054045	Nicotiana benthamiana - psbQ1	384038828	D	IF	+	96.6 / 97.6
pB27_A-180	70054103	Nicotiana benthamiana - s/s2	18920395	N/A	OOF1	+	79.9 / 85.6
pB27_A-130	70054103	Nicotiana benthamiana - s/s2	18920395	N/A	??	-	77.2 / 73.0
pB27_A-219	70054068	Nicotiana benthamiana - translation elongation factor 1 alpha	37783254	N/A	OOF2	+	91.2 / 78.9
pB27_A-274	70054022	Nicotiana benthamiana - GenMatch	576528492	D	IF	+	99.7 / 100.0
pB27_A-206	70054077	Nicotiana benthamiana - GenMatch	576528492	**A**	IF	+	96.8 / 99.3
pB27_A-64	70054077	Nicotiana benthamiana - GenMatch	576528492	**A**	OOF1	+	97.3 / 100.0

Clone Name	Contig(s) Name	Gene Name (Best Match)	GenBank ID	Global PRBS	Frame	Sense/ Antisense (+/-)	% Id 5p/3p
pB27_A-128	70054077	Nicotiana benthamiana - GenMatch	576528492	**A**	OOF1	+	99.8 / 100.0
pB27_A-41	70054077	Nicotiana benthamiana - GenMatch	576528492	**A**	OOF1	+	100.0 / 99.3
pB27_A-195	70054077	Nicotiana benthamiana - GenMatch	576528492	**A**	OOF1	+	99.5
pB27_A-60	70054077	Nicotiana benthamiana - GenMatch	576528492	**A**	OOF1	+	98.7
pB27_A-282	70054077	Nicotiana benthamiana - GenMatch	576528492	**A**	OOF1	+	98
pB27_A-18	70054077	Nicotiana benthamiana - GenMatch	576528492	**A**	OOF1	+	98.7 / 100.0
pB27_A-112	70054077	Nicotiana benthamiana - GenMatch	576528492	**A**	OOF1	+	100.0 / 100.0
pB27_A-186	70054077	Nicotiana benthamiana - GenMatch	576528492	**A**	OOF1	+	100.0 / 99.4
pB27_A-153	70054131	Nicotiana benthamiana - GenMatch	32478710	D	IF	+	98.0 / 100.0
pB27_A-122	70054195	Nicotiana benthamiana - GenMatch	576528492	D	IF	+	99.0 / 100.0
pB27_A-104	70054237	Nicotiana benthamiana - GenMatch	32478725	D	IF	+	98.8 / 100.0
pB27_A-19	70054292	Nicotiana benthamiana - GenMatch	32478716	D	IF	+	100.0 / 100.0
pB27_A-250	70054378 / 70054358	Nicotiana benthamiana - GenMatch	32478741	**A**	IF	+	100.0 / 92.2
pB27_A-266	70054378	Nicotiana benthamiana - GenMatch	32478741	**A**	IF	+	99.8 / 100.0
pB27_A-238	70054378	Nicotiana benthamiana - GenMatch	32478741	**A**	IF	+	100.0 / 100.0
pB27_A-126	70054378	Nicotiana benthamiana - GenMatch	32478741	**A**	IF	+	100.0 / 100.0
pB27_A-173	70054378	Nicotiana benthamiana - GenMatch	32478741	**A**	IF	+	100.0 / 100.0
pB27_A-224	70054378	Nicotiana benthamiana - GenMatch	32478741	**A**	IF	+	100.0 / 100.0
pB27_A-230	70054378	Nicotiana benthamiana - GenMatch	32478741	**A**	IF	+	100.0 / 100.0
pB27_A-20	70054378	Nicotiana benthamiana - GenMatch	32478741	**A**	IF	+	99.6 / 99.8
pB27_A-197	70054378	Nicotiana benthamiana - GenMatch	32478741	**A**	IF	+	100.0 / 100.0
pB27_A-105	70054378	Nicotiana benthamiana - GenMatch	32478741	**A**	IF	+	91.3
pB27_A-192	70054378	Nicotiana benthamiana - GenMatch	32478741	**A**	IF	+	99.6 / 99.1
pB27_A-181	70054378	Nicotiana benthamiana - GenMatch	32478741	**A**	IF	+	94.6 / 96.0
pB27_A-12	70054378	Nicotiana benthamiana - GenMatch	32478741	**A**	IF	+	99.4
pB27_A-273	70054378	Nicotiana benthamiana - GenMatch	32478741	**A**	IF	+	99.8 / 100.0
pB27_A-90	70054378	Nicotiana benthamiana - GenMatch	32478741	**A**	IF	+	100.0 / 97.7
pB27_A-80	70054378	Nicotiana benthamiana - GenMatch	32478741	**A**	IF	+	100.0 / 100.0
pB27_A-49	70054378	Nicotiana benthamiana - GenMatch	32478741	**A**	IF	+	100.0 / 100.0
pB27_A-48	70054378	Nicotiana benthamiana - GenMatch	32478741	**A**	IF	+	100.0 / 100.0
pB27_A-35	70054378	Nicotiana benthamiana - GenMatch	32478741	**A**	IF	+	100.0 / 100.0
pB27_A-53	70054378	Nicotiana benthamiana - GenMatch	32478741	**A**	IF	+	100.0 / 100.0
pB27_A-177	70054378	Nicotiana benthamiana - GenMatch	32478741	**A**	IF	+	100.0 / 100.0
pB27_A-81	70054378	Nicotiana benthamiana - GenMatch	32478741	**A**	IF	+	100.0 / 100.0
pB27_A-194	70054378	Nicotiana benthamiana - GenMatch	32478741	**A**	IF	+	100.0 / 100.0

Clone Name	Contig(s) Name	Gene Name (Best Match)	GenBank ID	Global PRBS	Frame	Sense/ Antisense (+/-)	% Id 5p/3p
pB27_A-201	70054378	Nicotiana benthamiana - GenMatch	32478741	**A**	IF	+	97.8 / 97.3
pB27_A-117	70054378	Nicotiana benthamiana - GenMatch	32478741	**A**	IF	+	99.8 / 100.0
pB27_A-58	70054378	Nicotiana benthamiana - GenMatch	32478741	**A**	IF	+	99.7 / 99.7
pB27_A-69	70054378	Nicotiana benthamiana - GenMatch	32478741	**A**	IF	+	90.7 / 96.2
pB27_A-50	70054378	Nicotiana benthamiana - GenMatch	32478741	**A**	IF	+	100.0 / 100.0
pB27_A-11	70054378	Nicotiana benthamiana - GenMatch	32478741	**A**	IF	+	99.6 / 100.0
pB27_A-163	70054378	Nicotiana benthamiana - GenMatch	32478741	**A**	IF	+	91.6 / 95.9
pB27_A-110	70054378	Nicotiana benthamiana - GenMatch	32478741	**A**	IF	+	96.5
pB27_A-258	70054378	Nicotiana benthamiana - GenMatch	32478741	**A**	IF	+	100.0 / 100.0
pB27_A-260	70054378	Nicotiana benthamiana - GenMatch	32478741	**A**	IF	+	100.0 / 100.0
pB27_A-271	70054378	Nicotiana benthamiana - GenMatch	32478741	**A**	IF	+	94.1 / 97.4
pB27_A-91	70054378	Nicotiana benthamiana - GenMatch	32478741	**A**	IF	+	100.0 / 100.0
pB27_A-246	70054378	Nicotiana benthamiana - GenMatch	32478741	**A**	IF	+	100.0 / 100.0
pB27_A-96	70054378	Nicotiana benthamiana - GenMatch	32478741	**A**	IF	+	97.4 / 94.8
pB27_A-9	70054378	Nicotiana benthamiana - GenMatch	32478741	**A**	IF	+	99.6 / 98.5

7.3 Publication

✖ *Author's Choice*

THE JOURNAL OF BIOLOGICAL CHEMISTRY VOL. 290, NO. 41, pp. 24945–24960, October 9, 2015

The Potato Nucleotide-binding Leucine-rich Repeat (NLR) Immune Receptor Rx1 Is a Pathogen-dependent DNA-deforming Protein*

Received for publication, June 15, 2015, and in revised form, August 14, 2015 Published, JBC Papers in Press, August 25, 2015, DOI 10.1074/jbc.M115.672121

Stepan Fenyk[‡§], Philip D. Townsend[‡§], Christopher H. Dixon[‡§], Gerhard B. Spies[‡§], Alba de San Eustaquio Campillo[‡§], Erik J. Slootweg[¶], Lotte B. Westerhof[¶], Fleur K. K. Gawehns[‖], Marc R. Knight[‡§], Gary J. Sharples[‡§], Aska Goverse[¶], Lars-Olof Pålsson[**], Frank L. W. Takken[‖1], and Martin J. Cann[‡§1,2]

From the [‡]School of Biological and Biomedical Sciences, [§]Biophysical Sciences Institute, [**]Department of Chemistry, Durham University, South Road, Durham DH1 3LE, United Kingdom, the [¶]Laboratory of Nematology, Department of Plant Sciences, Wageningen University, 6708 PB, Wageningen, The Netherlands, and [‖]Molecular Plant Pathology, Swammerdam Institute for Life Sciences, University of Amsterdam, Science Park 904, 1098 XH, Amsterdam, The Netherlands

Background: Direct targets for plant NLR proteins in immune signaling are largely unknown.
Results: The Rx1 NLR protein of potato binds and distorts DNA following pathogen perception, resulting in immune activation.
Conclusion: DNA is a direct signaling target for a plant NLR immune receptor.
Significance: Plant NLR receptors might regulate immune transcriptional responses by directly interacting with plant chromatin.

Plant nucleotide-binding leucine-rich repeat (NLR) proteins enable cells to respond to pathogen attack. Several NLRs act in the nucleus; however, conserved nuclear targets that support their role in immunity are unknown. Previously, we noted a structural homology between the nucleotide-binding domain of NLRs and DNA replication origin-binding Cdc6/Orc1 proteins. Here we show that the NB-ARC (nucleotide-binding, Apaf-1, R-proteins, and CED-4) domain of the Rx1 NLR of potato binds nucleic acids. Rx1 induces ATP-dependent bending and melting of DNA *in vitro*, dependent upon a functional P-loop. *In situ* full-length Rx1 binds nuclear DNA following activation by its cognate pathogen-derived effector protein, the coat protein of potato virus X. In line with its obligatory nucleocytoplasmic distribution, DNA binding was only observed when Rx1 was allowed to freely translocate between both compartments *and* was activated in the cytoplasm. Immune activation induced by an unrelated NLR-effector pair did not trigger an Rx1-DNA interaction. DNA binding is therefore not merely a consequence of immune activation. These data establish a role for DNA distortion in Rx1 immune signaling and define DNA as a molecular target of an activated NLR.

Plants and animals possess innate immune systems enabling individual cells to mount a defense response upon pathogen perception (1–4). The NLR[3] family immune receptors perceive non-self and modified self molecules inside host cells and mediate immune responses to invading microorganisms. Plant NLRs typically detect strain-specific pathogen effectors, whereas the animal NLRs commonly recognize microbe- or damage-associated molecular patterns (3, 5, 6). The NLR families in both kingdoms belong to the STAND P-loop ATPases of the AAA+ superfamily, whose multidomain structure allows them to function simultaneously as sensor, switch, and response factor (7, 8).

Plant NLRs are named after their central NB and C-terminal LRR domains. The N terminus is highly divergent; in plants, this region typically encompasses CC or TIR domains (3). The NB domain of plant NLRs is commonly referred to as the NB-ARC domain and has been proposed to function as a molecular switch (8–10). The LRR confers pathogen recognition specificity and maintains the NLR protein in a signaling-competent yet autoinhibited state. Biochemical analysis of tomato I-2 and Mi-1, flax M and L6, and barley MLA27 revealed that the NB-ARC domain is ADP-bound in the autoinhibited state (11–13). LRR-mediated pathogen recognition is proposed to permit the exchange of ADP for ATP, allowing the NB-ARC domain to adopt an activated or "on" state. ATP hydrolysis to ADP enables the "off" state to be re-established. Support for this model comes from studies where I-2 mutants defective in ATP hydrolysis *in vitro* are autoactivated *in vivo* and from an autoactive flax M mutant that preferentially co-purifies with ATP (12, 13).

* This work was supported by Biotechnology and Biological Sciences Research Council Grant BB/I0119994/1 and BB/M007405/1 (to M. J. C., G. J. S., and M. R. K.), European Union-funded Integrated Project BIOEXPLOIT (to A. G., E. J. S., F. L. W. T., and F. K. K. G.), and Top Technology Institute Green Genetics and the Dutch Science Foundation for Earth and Life Sciences (to A. G. and L. B. W.). The authors declare that they have no conflicts of interest with the contents of this article.

[1] Both authors contributed equally to this work.
[2] To whom correspondence should be addressed: School of Biological and Biomedical Sciences, Durham University, South Road, Durham DH1 3LE, United Kingdom. Tel.: 44-191-3343985; Fax: 44-191-3341201; E-mail: m.j.cann@durham.ac.uk.

[3] The abbreviations used are: NLR, nucleotide-binding leucine-rich repeat; AAA+, ATPases associated with diverse cellular activities; CC, coiled-coil; FLIM, fluorescence lifetime imaging microscopy; NB, nucleotide-binding; NB-ARC, nucleotide-binding, Apaf-1, R-proteins, and CED-4; LRR, leucine-rich repeat; NES, nuclear export sequence; NLS, nuclear localization sequence; PSIP, pollen-signaling protein; PVX, protein virus X; STAND, signal transduction ATPases with numerous domains; TIR, Toll-interleukin 1 receptor; Bistris propane, 1,3-bis[tris(hydroxymethyl)methylamino] propane; ANOVA, analysis of variance; PDB, Protein Data Bank.

Recently, the NB subdomain of rice Os2g_25900 and NB-ARC domains of maize pollen-signaling protein (PSiP) and *Arabidopsis* Rpm1 were demonstrated to possess a nucleotide phosphatase activity compatible with the switch model (14).

Activation of animal NLRs typically triggers NB domain-mediated self-association, resulting in the formation of a cytoplasmic signaling scaffold on which partners are activated due to their induced proximity (15). For plant NLRs, such partners have not been identified, and a pivotal yet unanswered question concerns the nature of the downstream signaling component(s) and how these are activated by NLR proteins in their "on" state. The identity of the specific NLR subdomain that transduces a signal to such a downstream component is also unresolved. Whereas for Rx1, the NB subdomain of Rx1 induces cell death, the N-terminal TIR domains of L6 and RPS4 or the coiled-coil domain of MLA10 suffices to trigger cell death, suggesting that the signaling domain might vary for different NLRs or that they act as heterodimers (11, 16–18). The location of the NLR signaling event is also the subject of increased scrutiny. Several NLR proteins, including N, Mla10, and Rx1 have a dynamic nuclear-cytoplasmic distribution, whereas RRS1-R is restricted to the nucleus, dependent upon the presence of the PopP2 immune elicitor (19–23). Genetic screens for compromised NLR-mediated resistance identified genes encoding components of the nuclear pore complex (24), indicating involvement of nuclear transport in immune signaling. More direct proof for nuclear activity is the observed nuclear localization for barley MLA1 and MLA10, *Arabidopsis* RPS4 and SNC1, and the tobacco N protein (22, 25–27). Redirection of nucleus resident MLA10, N, RPS4, and SNC1 to the cytoplasm compromises their ability to activate immune signaling, suggesting a nuclear signaling target (19, 22, 26, 28). The potato Rx1 protein, which confers PVX resistance, localizes to both cytoplasm and nucleus (23). The Rx1 N terminus interacts with a member of the RanGAP2 family that controls nuclear-cytoplasmic trafficking through the nuclear pore (29). Together, these studies indicate that nuclear-cytoplasmic trafficking and compartmentalization are essential for NLR protein function and suggest distinct activities in different cellular compartments. Recent studies on *Arabidopsis* RPS4 and barley Mla10 (25, 30) have shown that induction of cell death is associated with cytoplasmic localization, whereas nuclear localization of RPS4 is associated with local resistance responses. The presence of a WRKY DNA-binding domain in RRS1-R (21) and the association of Mla10 with both Myb and WRKY transcription factors (31) have led to the hypothesis that plant NLRs regulate transcription in the immune response (32). This notion is further supported by interactions between an SPL transcription factor and the tobacco N NLR protein, the interaction between the SNC1 NLR protein of *Arabidopsis* and the TPR1 transcriptional corepressor, and the presence of BED DNA-binding domains in many plant NLRs (27, 33–35).

Based on these observations, signaling from plant NLRs can be viewed from two perspectives that are not necessarily mutually exclusive. In the first perspective, activated NLRs may act as platforms from which signaling proteins promoting immune responses are permitted to function. Alternatively, NLRs may themselves have an additional biochemical activity, independent of their ATPase activity, required for direct activation of plant immunity. In support of the latter model, we here demonstrate that the Rx1 NLR protein of potato is able to bind DNA *in vitro* and *in situ* and that its *in vitro* activity consists of bending and melting DNA. We further demonstrate that the interaction of Rx1 with DNA as observed *in situ* only occurs after its genuine activation by the coat protein of PVX virus.

Experimental Procedures

Structural Modeling—Protein fold searches using the Phyre^2 protein homology/analogy recognition engine version 2.0 (36) were undertaken using amino acids 143–488 of Rx1, using both normal and intensive modeling modes. Similar structural homology was also detected using the SAM-T08, Hidden Markov Model-based protein structure prediction server (37). All superpositions were performed using the SSM algorithm in Coot (38). Models of Rx1 based on Cdc6/Orc1 (PDB accession number 2V1U) were made using Chainsaw within the CCP4 package (39), and sequence alignments were generated by the Phyre^2 server. Side chain packing and energy minimization was performed using GalaxyRefine (40). Figures were generated using the PyMOL molecular graphics system (41).

Plasmids—A PCR product spanning residues 1–489 of Rx1 (GenBank^{TM} accession number AJ011801.1) was cloned into the NcoI and BamHI sites of pET32c (pET32c-Rx1(1–489)) and fitted with a hexahistidine tag for affinity purification of recombinant protein. The oligonucleotides used to construct pET32c-Rx1(1–489) were 5′-GCC CCA TGG CTT ATG CTG CTG TTA C-3′ (sense) and 5′-GGC GGA TCC TTA TGC ACA TGA ATT TTG ATC ACT C-3′ (antisense). Mutant constructs were generated by site-directed mutagenesis. A PCR product corresponding to amino acids 177–339 of PSiP (Gene ID 542027) was cloned into the XhoI and NcoI sites of pRSET-B (pRSET-PSiP(177–339)) and fitted with a hexahistidine tag for affinity purification of recombinant protein. The primers used to construct pRSET-PSiP(177–339) were 5′-GGC CTC GAG AAA GGC TGT GGG TGG CCT TG-3′ (sense) and 5′-GGC CCA TGG TCA CTT GAT TGC ACA ATA ATG CCC A-3′ (antisense). A PCR product corresponding to amino acids 1–126 of histone H2B of *Arabidopsis thaliana* (locus AT3G-09480) was subcloned into the Gateway entry vector pDONR-207 via BP recombinant reaction and transferred via LR reaction into the plant binary vector pK7WGF2 (pK7WGF2-H2B) to fuse the open reading frame (ORF) to an N-terminal green fluorescent protein (GFP) ORF. The primers used to construct pK7WGF2-H2B were 5′-GGG GAC AAG TTT GTA CAA AAA AGC AGG CTA CAA CAA TGG CCATG GCA CCG AAG GCA GAG-3′ (sense) and 5′-GGG GAC CAC TTT GTA CAA GAA AGC TGG GTC AGA ACT GGT GAA TTT GGT G-3′ (antisense). pBIN-35S-based plasmids corresponding to NBARC-GFP, CC-NBARC-GFP, NBARC-LRR-GFP, GFP-LRR, CC-GFP, Rx1-GFP, GFP-NLS-Rx1, GFP-NES-Rx1, CP105, and CP106 are as described (23). Mutant constructs were generated by site-directed mutagenesis. Pto and AvrPto were expressed using a construct that contains 35S promoter-driven *Pto* and *avrPto* as described (42). For the construction of Rx1-4Strep, a double STREPII tag (43) (-asWSHPQFEKggWS-HPQFEKts-) was created by annealing the oligonucleotides

m-Str1 (5′-GGC CGC TAG CTG GAG TCA CCC TCA GTT CGA GAA GGG TGG ATG GTC ACA TCC ACA ATT TGA AAA GAC TAG TTA AT-3′) and m-Str2 (5′-CTA GAT TAA CTA GTC TTT TCA AAT TGT GGA TGT GAC CAT CCA CCC TTC TCG AAC TGA GGG TGA CTC CAG CTA GC-3′) and ligating the annealed oligonucleotides between the NotI and XbaI of pRAP 35S:YFP-myc (23), replacing the sequence encoding the Myc tag. From the resulting pRAP::YFP-STR2, a 4-fold STREPII tag was generated by fusing the AscI-SpeI 35S::YFP-STR2 with the NheI-PacI STR2-Tnos segment in pRAP digested with AscI-PacI. In the resulting pRAP::YFP-STR4 vector, GFP was replaced by Rx1 cDNA using the NcoI and NotI sites as described for pRAP:Rx-GFP (23). The expression cassette was excised using the AscI and PacI restriction sites and introduced into the expression vector pHYG (44). The expression vector pHYG-Rx1-4Strep was transformed to *Agrobacterium tumefaciens* strain MOG101 for plant expression.

Protein Expression and Purification—Protein corresponding to the NB-ARC domain of PSiP (amino acids 178–505; PSiP-NBARC) was generated as described previously (14).

A 10-ml culture of pET32c-Rx1(1–489) (Rx1(1–489) wild type and mutant proteins) in *Escherichia coli* C41(DE3) was grown overnight in Luria broth supplemented with 100 μg ml^{-1} ampicillin at 37 °C. This culture was diluted into 1 liter of Luria broth supplemented with 100 μg ml^{-1} ampicillin and grown at 37 °C to $A_{600\ nm}$ = 0.7. The growth temperature was reduced to 22 °C, and growth continued to $A_{600\ nm}$ = 1.0. Protein production was induced at 22 °C for 16 h with 100 μM isopropyl-β-D-thiogalactoside. Pelleted cells were washed with 50 mM Tris-HCl, pH 8.5, 1 mM EDTA, and the pellet was resuspended in twice its volume of 50 mM Tris-HCl, pH 7.5, 100 mM NaCl, 5 mM EDTA. Cells were centrifuged (2700 × *g*, 30 min, 10 °C), and the pellet was resuspended in twice its volume of 50 mM Tris-HCl, pH 7.5, 100 mM NaCl, 5 mM EDTA, 1% (v/v) Triton X-100. Cells were lysed by sonication (150 s) and centrifuged (75,500 × *g*, 60 min, 10 °C), and inclusion bodies were washed twice in 5 ml of 50 mM Tris-HCl, pH 8.0, 100 mM NaCl, 5 mM EDTA, 1% (v/v) Triton X-100. The final pellet was resuspended in 2 ml of 50 mM Tris-HCl, pH 9.0, 100 mM NaCl, 1 mM EDTA, 1 mM dithiothreitol, 8 M urea). Material was incubated at 50 °C for 20 min prior to centrifugation (20,000 × *g*, 30 min, 15 °C) and the pellet was discarded. The supernatant was dialyzed into 50 mM Tris-HCl, pH 8.5, 100 mM NaCl, 7 M urea and incubated with Ni^{2+}-nitrilotriacetic acid resin (Qiagen) for 60 min at 4 °C. Resin was washed with 10 bed volumes of buffer A (50 mM Tris-HCl, pH 7.5, 400 mM NaCl, 20 mM $MgCl_2$, 0.25 mM imidazole, 7 M urea), 10 bed volumes of buffer B (buffer A with 1.5 M NaCl, 20 mM imidazole), and 20 bed volumes of buffer C (buffer B with 10 mM NaCl). Protein was eluted with 5 bed volumes of elution buffer (buffer C with 200 mM imidazole). Protein was resuspended at 1 mg ml^{-1} in 50 mM Tris-HCl, pH 8.5, 9.6 mM NaCl, 0.4 mM KCl, 2 mM $MgCl_2$, 2 mM $CaCl_2$, 0.5 M arginine, 0.4 M sucrose, 0.75 M guanidine HCl, 1 mM glutathione, 0.1 mM reduced glutathione and incubated at 4 °C for 1 h. Refolded protein was dialyzed into 20 mM Tris-HCl, pH 7.5, 50 mM NaCl, 2 mM $MgCl_2$, loaded onto a monoQ anion exchange column (GE Healthcare), and eluted using a 50 mM to 1 M NaCl gradient. Peak fractions containing Rx1(1–489) protein were concentrated; dialyzed into 20 mM Tris-HCl, pH 7.5, 150 mM NaCl, 2 mM $MgCl_2$; and loaded onto a Superdex 200 gel filtration column, and peak fractions were eluted in the same buffer.

pRSET-PSiP(177–339) (PSiP-NB) was expressed in *E. coli* BL21(DE3) *cya::kan* at 22 °C for 16 h with 100 μM isopropyl-β-D-thiogalactoside. Pelleted cells were washed with 50 mM Tris-HCl, pH 7.5, 1 mM EDTA resuspended in 50 mM Tris-HCl, pH 7.5, 250 mM NaCl, 100 μM EDTA and lysed by sonication (150 s), and the supernatant was incubated with Ni^{2+}-nitrilotriacetic acid resin for 60 min at 4 °C. Resin was washed with 10 bed volumes of buffer D (50 mM Tris-HCl, pH 7.5, 400 mM NaCl, 5 mM imidazole, 100 μM EDTA), buffer E (buffer D with 1.5 M NaCl and 20 mM imidazole), and buffer F (buffer E with 40 mM NaCl). Protein was eluted with 5 bed volumes of buffer F containing 200 mM imidazole. PSiP-NB was subsequently purified by anion exchange chromatography as described previously (14). Orc1-1 and Orc1-3 of *Sulfolobus solfataricus* were expressed and purified as described previously (45).

For Rx1-4Strep, *A. tumefaciens* strain MOG101 was transformed with construct pHYG-Rx1-4Strep and grown to $A_{600\ nm}$ of 1.0 in 20 g liter^{-1} sucrose, 5 g liter^{-1} Murashige and Skoog basal salt mixture, 1.95 g liter^{-1} MES, pH 5.6, 200 μM acetosyringone. The two youngest fully expanded leaves of 5–6-week-old *Nicotiana benthamiana* plants were infiltrated completely. Infiltration was performed by injecting the *Agrobacterium* suspension into a *N. benthamiana* leaf at the abaxial side using a 1-ml syringe. Leaf material was harvested after 48 h and ground in liquid nitrogen with a mortar and pestle. Ground material was resuspended 1:10 (w/v) in 10% (v/v) glycerol, 50 mM Tris-HCl, pH 8.5, 150 mM NaCl, 2 mM $MgCl_2$, 0.1% (v/v) Tween 20, 5 mM DTT, 0.02 g ml^{-1} polyvinylpolypyrrolidone, 0.2 mg ml^{-1} Pefabloc SC protease inhibitor (Roche Applied Science). Cell debris and polyvinylpolypyrrolidone were removed by centrifugation (20,000 × *g*, 20 min, 4 °C). The extract was passed through a Sephadex G25 column, and the flow-through was supplemented with 5 mM DTT, 0.2 mg ml^{-1} Pefabloc SC protease inhibitor, and 20 μg ml^{-1} avidin. The extract was incubated with Streptactin superflow resin (IBA) at 4 °C overnight. Resin was washed with 10 bed volumes wash buffer (10% (v/v) glycerol, 50 mM Tris-HCl, pH 8.5, 150 mM NaCl, 2 mM $MgCl_2$, 0.1% (v/v) Tween 20, 5 mM DTT). Protein was eluted with 2 bed volumes of wash buffer supplemented with 15 mM desthiobiotin. Purified protein was dialyzed into 20 mM Tris-HCl, pH 7.5, 150 mM NaCl, 2 mM $MgCl_2$ before use.

Circular Dichroism—80 μM protein was dialyzed into double-distilled H_2O at 4 °C. The baseline CD spectra of blank sample (double-distilled H_2O) and 1.7 μM protein were measured using a J-810 spectropolarimeter (Jasco) at 180–300 nm (20 nm min^{-1}). The averaged data of replicate blank spectra were subtracted from the protein spectra, and the data were normalized to zero at 250 nm. The corrected CD spectra from 190–240 nm were analyzed using CDPro (46). The protein database generating the lowest root mean square deviation was used as the best approximation for secondary structure content.

Electrophoretic Mobility Shift Assays—The oligonucleotides used for quantitative EMSA are derived from a series of oligonucleotides that enables a comparison of relative DNA binding

affinity to varying DNA topologies independent of DNA sequence (47). The oligonucleotides sequences were 5′-TGG GTC AAC GTG GGC AAA GAT GTC CTA GCA ATG TAA TCG TCT ATG ACG TT-3′ (SS1; DNA sense strand), 5′-AAC GTC ATA GAC GAT TAC ATT GCT AGG ACA TCT TTG CCC ACG TTG ACC CA-3′ (SS2; DNA antisense strand), and 5′-UGG GUC AAC GUG GGC AAA GAU GUC CUA GCA AUG UAA UCG UCU AUG ACG UU-3′ (RNA sense strand) (47). Oligonucleotides were end-labeled with 10 μCi of [γ-^{32}P]ATP using T4 polynucleotide kinase, and unincorporated nucleotides were removed using Micro Bio-Spin columns (Bio-Rad). Protein and 0.15 nM nucleic acids (oligonucleotide 1 ssDNA, annealed oligonucleotide 1 and oligonucleotide 2 dsDNA, and ssRNA) were incubated in 20 mM Tris-HCl, pH 8.0, 60 mM NaCl (unless otherwise stated), 2 mM EDTA, 1 mM DTT, 10% (v/v) glycerol, 0.1 mg/ml BSA for 20 min on ice. Quantitative EMSAs were separated on a native 7% (w/v) polyacrylamide gel. Experiments to assess the role of nucleotides in DNA binding used binding reactions and gels supplemented with 10 mM $ZnCl_2$ and nucleotide. Polyacrylamide gels were dried and analyzed by autoradiography. EMSAs using unlabeled virion DNA were separated using 0.8% (w/v) Tris acetate-EDTA-agarose gels and stained with ethidium bromide. All reported values for K_d represent apparent K_d due to the potential for dissociation of protein-DNA complexes during electrophoresis. Curves were fitted by non-linear regression in GraphPad Prism version 6.0.

Construction of DNA Structures—DNA substrates corresponding to double-stranded branched structures (F12-ds/ds), branch structures with two single-stranded arms (F12-ss/ss), and branch structures with one double-stranded and one single-stranded arm (F12-ds/ss) were made by annealing synthetic oligonucleotides from a series that enables the comparison of relative DNA binding affinity to varying DNA topologies independent of DNA sequence (47). Oligonucleotide sequences were 5′-GAC GCT GCC GAA TTC TGG CTT GCT AGG ACA TCT TTG CCC ACG TTG ACC C-3′ (SS3), 5′-GCC AGA ATT CGG CAG CGT C-3′ (LAG), and 5′-AAC GTC ATA GAC GAT TAC A-3′ (LEAD). SS3 was end-labeled with 10 μCi of [γ-^{32}P]ATP using T4 polynucleotide kinase, and unincorporated nucleotides were removed using Micro Bio-Spin columns (Bio-Rad). SS3, SS1, LAG, and LEAD were annealed to make F12-ds/ds. SS3, SS1, and LEAD were annealed to make F12-ds/ss. SS3 and SS1 were annealed to make F12-ss/ss. SS3 and the corresponding antisense oligonucleotide (5′-GGG TCA ACG TGG GCA AAG ATG TCC TAG CAA GCC AGA ATT CGG CAG CGT C-3′) were annealed to make a linear dsDNA control (dsF12) and SS3 used as linear ssDNA control (ssF12). Annealing synthetic oligonucleotides with a defined sequence mismatch made DNA substrates corresponding to linear DNA containing bubbles of defined length. Oligonucleotide sequences were 5′-TTT GGT CTA ACT TTA CCG CTA CTA AAT GCC GCG GAT TGG TTT CGC TGA ATC AGG TTA TTA-3′ (P1), 5′-TAA TAA CCT GAT TCA GCG AAA CCA ATC CGC GGC ATT TAG TAG CGG TAA AGT TAG ACC AAA-3′ (P2), 5′-TAA TAA CCT GAT TCA GCG AAC CAA TCG CAA CCA TTT AGT AGC GGT AAA GTT AGA CCA AA-3′ (P5), 5′-TAA TAA CCT GAT TCA GCG AAA CAT TGT AGG TAA GCT TAG TAG CGG TAA AGT TAG ACC AAA-3′ (P6), and 5′-TAA TAA CCT GAT TCA GCG AAT GAC CGA TAA CGT CCA CTT GAG CGG TAA AGT TAG ACC AAA-3′ (P7). P1 was end-labeled with 10 μCi of [γ-^{32}P]ATP using T4 polynucleotide kinase, and unincorporated nucleotides were removed using Micro Bio-Spin columns. P1 and P2 were annealed to make linear dsDNA (dsP1). P1 and P5 were annealed to make linear dsDNA with a 5-nucleotide bubble (dsP1-5). P1 and P6 were annealed to make linear dsDNA with a 13-nucleotide bubble (dsP1-13). P1 and P7 were annealed to make linear dsDNA with a 20-nucleotide bubble (dsP1-20). P1 was used on its own as a ssDNA control (ssP1). All substrates were gel-purified on a native 10% (w/v) polyacrylamide gel. EMSA was performed as described above.

ATPase Assays—ATPase assays were typically performed at 37 °C for 30 min with 2.3 μM protein in 50 mM Bistris propane, pH 7.5, 10 mM $MgCl_2$, and 5 μM ATP. Reactions were spiked with 0.5 μCi of 2,8-^{3}H-labeled ATP for quantitation. Reactions were spotted onto a silica thin layer chromatography plate with 1 mM ADP to act as marker and carrier. The plates were developed in isobutyl alcohol/3-methyl-1-butanol/2-ethoxyethanol/ammonia/H_2O (9:6:18:9:15). Spots were visualized at 256 nm and quantified using an AR-2000 TLC scanner.

Time-resolved FRET in Vitro—Synthetic oligonucleotides, unlabeled or end-labeled with fluorescein or tetramethylrhodamine, were purchased from Eurofins MWG. The oligonucleotides used were 5′-TGG GTC AAC GTG GGC AAA GA-3′ (sense strand) and 5′-TCT TTG CCC ACG TTG ACC CA-3′ (antisense strand). Strands were annealed by heating to 90 °C for 3 min in 10 mM Tris, pH 8.0, 1 mM EDTA before cooling to room temperature. Measurements used 1.5 μM protein with 50 nM DNA in the presence of 60 mM NaCl and were incubated for 10 min at room temperature before analysis. Time-resolved FRET was assessed using the time-correlated, single photon counting technique. The excitation source was a Picoquant pulsed diode laser LDH-P-C-485 (excitation wavelength 485 nm, 70-ps pulse full width at half-maximum at 20 MHz). Fluorescence was detected using an avalanche photodiode (Id Quantique 100-50) linked to a Becker and Hickl SPC 130 time-correlated, single photon counting module. An instrument response function of ~200 ps was measured from Rayleigh scattered light. Fluorescence decays were collected for both donor- and donor-acceptor-labeled double-stranded DNA with or without protein using band pass filter detection of the donor emission and at magic angle polarization. Data were analyzed by the Grinvald-Steinberg method (48) to obtain the fluorescence lifetime for the donor and acceptor (τ_{DA})- and donor only (τ_D)-labeled oligonucleotides. The data were fitted to a sum of exponentials using an iterative least squares reconvolution procedure with the optical/electrical excitation profile to produce a biexponential decay containing two lifetimes. This profile was obtained from a slide covered with silica LUDOX® particles, which provides an instant scatter of the excitation pulse. This data-fitting method provided more accuracy in the determination of shorter lifetimes than calculating a single average lifetime. Donor-acceptor distances (R) were calculated using the equation, $E = R_0^6/(R_0^6 + R^6)$, and a calculated Förster distance (R_0) of 49.99 Å. The total length of the oligonucleotide

with linkers and fluorescent dyes, at maximum extension, was calculated as 81.1 Å.

P_1 Nuclease Sensitivity—Oligonucleotides for P_1 nuclease sensitivity were 5′-CTC AAT ACA ATT GTC TCT GTG TAA ATT TCC TAC GTT TCA TCT GAA AAT CTA GCT ATT AGA GCT TGG TTT A-3′ (sense strand) and 5′-TAA ACC AAG CTC TAA TAG CTA GAT TTT CAG ATG AAA CGT AGG AAA TTT ACA CAG AGA CAA TTG TAT TGA G-3′ (antisense strand) and represent the C3/mORB dual site sequence at *oriC2* of *S. solfataricus* (49). The sense strand oligonucleotide was end-labeled with 10 μCi of [γ-^{32}P]ATP as described above, and sense and antisense oligonucleotides were annealed as required. Reactions were performed in 20-μl volumes containing 20 mM Tris acetate, pH 7.5, 10 mM magnesium acetate, 100 mM NaCl, 0.15 nM oligonucleotide, and 1.5 μM protein. Protein was allowed to bind for 10 min at 37 °C. P_1 nuclease was added to a final concentration of 0.01–0.1 units μl^{-1} and incubated for a further 20–60 min at 37 °C. Reactions were stopped with 5 μl of 100 mM Tris-HCl, pH 8.0, 2.5% (w/v) SDS, 100 mM EDTA, 10 units μl^{-1} proteinase K. 5 μl of loading buffer (97.5% (v/v) formamide, 10 mM EDTA, 0.3% (w/v), 0.3% bromphenol blue) was added, and reactions were electrophoresed on a 15% (w/v) polyacrylamide gel with 8 M urea. Polyacrylamide gels were dried and analyzed by autoradiography.

Time-resolved FRET in Situ—*A. tumefaciens* strain GV3101 (pMP90) was transformed with constructs pK7WGF2 (GFP negative control), pK7WGF2-H2B (GFP-H2B positive control), pBIN35S-NBARC-GFP, pBIN35S-CC-NBARC-GFP, pBIN35S-NBARC-LRR-GFP, pBIN35S-GFP-LRR, pBIN35S-CC-GFP, pBIN35S-Rx1-GFP, pBIN35S-CP105, or pBIN35S-CP106 and grown to $A_{600\ nm}$ 0.8 in YEB medium supplemented with 20 μM acetosyringone and 10 mM MES, pH 5.6. Cells were washed three times in infiltration medium (10 mM MES, pH 5.6, 2% (w/v) sucrose, 20 μM acetosyringone) and infiltrated at $A_{600\ nm}$ 0.4 into 4–5-week-old *N. benthamiana* leaves. Leaves were harvested after 72 h and prior to any observed cell death in a compatible immune interaction, and the agroinfiltrated region was infiltrated with 10 μg/ml LDS 751 (Molecular Probes, Inc.). For experiments with CP105 and CP106, the elicitor-encoding *A. tumefaciens* culture was infiltrated into preinfiltrated sectors after 48 h (24 h before harvest). Leaves were fixed for 4 h at room temperature in 4% (w/v) paraformaldehyde in phosphate-buffered saline (PBS). Fixative was quenched for 30 min at room temperature in 125 mM glycine, and leaves were washed in PBS at 4 °C before mounting. A modified Zeiss Axiovert inverted epifluorescence microscope was used for time-resolved fluorescence microscopy. The overall excitation/detection of the fluorescence was performed using the time-correlated single photon counting technique. The excitation source was a Picoquant pulsed diode laser LDH-P-C-440 (excitation wavelength 440 nm, 70-ps pulse full width at half-maximum at 20 MHz). The objective lens (Zeiss ×100 oil immersion Ph3) focused the excitation light on the sample material. The emission was detected using suitable band pass/long pass filters for GFP and LDS 751 fluorescence, respectively. Fluorescence was detected with a photon counting module (Id Quantique 100-50) in a single photon counting mode. Data fitting was performed as for time-resolved FRET *in vitro*. The relative orientation of the GFP tag does not affect Rx1 function (23); nor does it affect the ability to observe energy transfer. All data are reported for the analysis of GFP lifetimes because LDS 751 emission is influenced by photobleaching and variability in concentration.

Statistical Analysis—*Error bars* represent the S.E. with the number of replicates as indicated in the figure legends. Statistical comparisons (p values) for data that pass a test for normality (D'Agostino and Pearson omnibus normality test and Shapiro-Wilk normality test) were obtained from one-way ANOVA with the indicated post hoc test. Statistical comparisons (p values) for data that do not pass a test for normality were obtained from a Kruskal-Wallis test with a post hoc multiple comparisons test. p values in statistical comparisons are indicated in the figures through *letters* and indicate compared data sets as described in the figure legends.

Results

Plant NLRs Are Structurally Related to Cdc6/Orc1 Family Proteins—The *Rx1* gene, introgressed in potato from the wild species *Solanum andigena*, confers resistance to PVX upon recognition of its coat protein (50, 51). The Rx1 protein is a member of the CC-NB-LRR class of plant NLR proteins that consists of an N-terminal CC domain, a central NB-ARC domain, and a C-terminal LRR domain. The NB domain, containing a central β-sheet flanked by α-helices, is flanked by two ARC subdomains. ARC1 forms a four-helix bundle, and ARC2 adopts a winged helix fold characteristic of DNA-binding transcription factors (52). We hypothesized that an investigation of proteins structurally related to the Rx1 NB-ARC domain could provide insight into NLR biochemistry. Amino acids 143–488, encompassing the NB-ARC domain, were analyzed using the Phyre^2 protein fold recognition engine and expected matches with the pro-apoptotic proteins CED-4 (PDB code 2A5Y) and Apaf-1 (PDB code 1Z6T) were recovered to 100% confidence (10, 52). In agreement with earlier structural studies (12), high scoring matches (>99.4% confidence) were obtained with the Cdc6/Orc1 proteins of *Pyrobaculum aerophilum* (PDB 1FNN) and of *Aeropyrum pernix* in complex with DNA (PDB 2V1U). These proteins are members of a family of proteins involved in origin recognition and DNA replication in archaea and eukaryotes (45, 49, 53, 54). NB subdomain and tandem ARC domain residues (ARC1 and ARC2) of Rx1 are conserved between Cdc6/Orc1 of *A. pernix* and Rx1 (35.0% similarity and 12.7% identity between amino acids 134–479 of Rx1 and amino acids 13–382 of PDB entry 2V1U) (Fig. 1*A*).

Both the N-terminal NB and C-terminal ARC domain-like regions of Cdc6/Orc1 contact DNA, inducing deformation of the double helix (45, 49). The modeled tertiary structure of Rx1 (Fig. 1*B*, *left*) was related to Cdc6/Orc1 bound to DNA (PDB code 2V1U) (Fig. 1*B*, *center*) but differed from Cdc6/Orc1 in the DNA-unbound state (PDB code 1FNN) (Fig. 1*B*, *right*). An overlay demonstrated that the difference between the modeled tertiary structure of Rx1 and Cdc6/Orc1 in the DNA unbound state (PDB code 1FNN) was due to rotation of amino acids 279–388 of the C-terminal Cdc6/Orc1 ARC-like domain (Fig. 1*C*, *left* and *center*). Amino acids 279–388 of the Cdc6/Orc1 C-terminal ARC-like domain can be excised from PDB entry

1FNN and directly superimposed onto the Rx1 ARC2 domain to demonstrate how this rotation has occurred in the absence of any global structural change (Fig. 1*C*, *right*). Cdc6/Orc1 forms part of a larger family of structural homologues that includes the AAA+ ATPase SSO1545 from *Sulfolobus*, RuvB from *Thermus*, Orc2 from *Aeropyrum*, mammalian Apaf-1, CED-4 from *Caenorhabditis elegans*, and NLRC4 from mouse (9, 35, 55–61). These proteins all show a similar domain arrangement

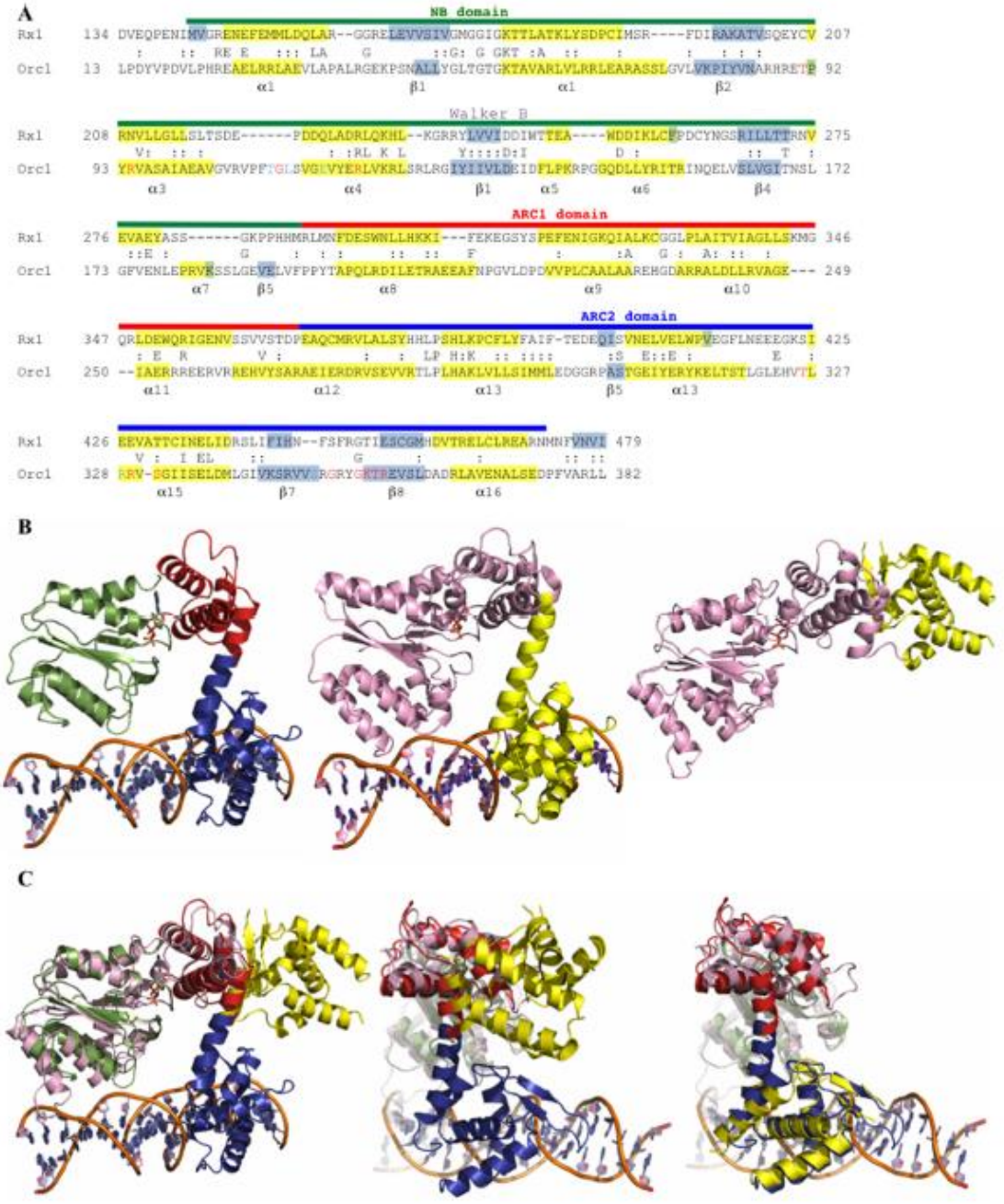

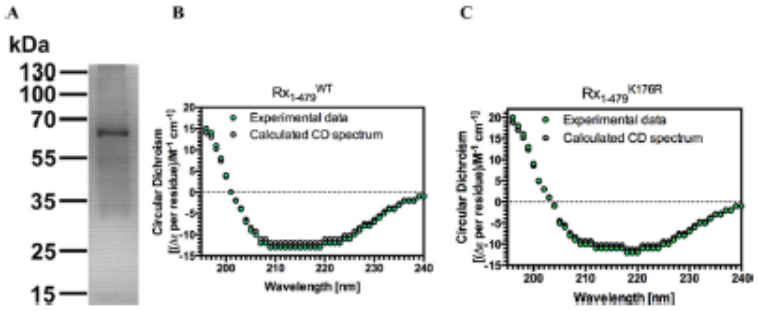

FIGURE 2. **Production and characterization of a recombinant Rx1 protein.** *A*, purified Rx1 protein (1.5 μg) was separated by 12.5% SDS-polyacrylamide gel electrophoresis and stained with Coomassie Blue. Molecular mass standards (in kDa) are indicated. Protein identity was confirmed by trypsin digest and MALDI-TOF analysis. Shown are a circular dichroism spectrum for Rx1(1–489)^{WT} (*B*) and Rx1(1–489)^{K176R} (*C*) depicting experimental data (*green dots*) and the spectrum calculated using CDSSTR (*gray dots*).

of an NB domain that is coupled via its neighboring ARC1 domain to a C-terminal ARC2 domain with varying orientations. For example, the individual domains of the closed form of mouse NLRC4 (PDB code 4KXF) can be extracted and superimposed onto Cdc6/Orc1 in the DNA-bound state (PDB 2V1U), although their actual orientation does not support a DNA binding activity. The modeled structural relationship with Cdc6/Orc1 suggests the intriguing possibility that Rx1 might also interact directly with DNA. We therefore investigated whether Rx1 is a DNA-binding protein.

Rx1 Binds Nucleic Acids in Vitro—A possible direct Rx1-DNA interaction was investigated through *in vitro* experiments. EMSA using nucleic acid fragments of >5 kb derived from circular bacteriophage ϕX174 (62) represents a straightforward methodology to qualitatively assess interactions between a protein and either ssDNA or dsDNA with identical sequences. EMSAs were therefore performed using recombinant wild-type Rx1 protein (Rx1(1–489)^{WT}), consisting of the CC-NB-ARC region but lacking the LRR domain (Fig. 2*A*). EMSA experiments performed with the Rx1(1–489)^{WT} protein showed an association with both ssDNA and dsDNA, producing a small upward shift in the migration of the nucleic acid that is fully consistent with similar EMSA experiments using unrelated DNA-binding proteins (Fig. 3*A*) (63). No mobility shift was observed with a control protein (BSA) that has a similar mass and isoelectric point as Rx1(1–489)^{WT}.

The K176R mutation in the P-loop of Rx1 abolishes its ability to mount an immune response in the presence of the viral coat protein (23). The Rx1(1–489)^{K176R} loss-of-function mutant exhibited a barely detectable binding to DNA as compared with wild type Rx1 protein under these conditions (Fig. 3*A*). This difference is unlikely to be due to misfolding of the mutant because comparison of Rx1(1–489)^{WT} and Rx1(1–489)^{K176R} by circular dichroism (CD) reveals a generally similar secondary structure composition (Fig. 2, *B* and *C*). The CDSSTR method for secondary structure fraction prediction gave similar estimates for secondary structure content for both Rx1(1–489)^{WT} (61.6% helix, 14.8% sheet, 7.9% turn, 15.1% unresolved; normalized root mean square deviation = 0.066) and Rx1(1–489)^{K176R} (68.6% helix, 14.1% sheet, 7.9% turn, 8.7% unresolved; normalized root mean square deviation = 0.043) (64). Hence, subtle structural changes rather than an improperly folded protein probably explain differences in DNA binding between Rx1(1–489)^{WT} and Rx1(1–489)^{K176R}.

The Rx1-DNA interaction was relatively stable because it could be visualized after gel electrophoresis (Fig. 3*A*). Nevertheless, although EMSA using circular bacteriophage ϕX174 DNA is a well established method to qualitatively assess protein-DNA interactions, it does not enable robust quantification of the affinity of a protein for nucleic acids. EMSA with small synthetic oligonucleotides is a standard method to quantify protein-nucleic acid interactions (65). Furthermore, the high molecular weight of ϕX174 DNA and consequent small band shifts were not suited to further analysis. We therefore quantified the affinity of Rx1(1–489) for various nucleic acids by EMSA using ^{32}P-labeled synthetic oligonucleotides whose sequences were unrelated to that of bacteriophage ϕX174 DNA and which should provide more robust band shifts on EMSA due to their lower molecular weights (Fig. 3*A*). Rx1(1–489)^{WT} showed broadly similar apparent affinities (K_d^{app}) for dsDNA

FIGURE 1. **Structural modeling of the Rx1 NB-ARC domains.** *A*, alignment of Rx1 (residues 134–479) with Orc1 of *A. pernix* (PDB code 2V1U; residues 13–382). *Numbers* denote amino acid residue position. Sequences are in standard single-letter amino acid code, and functionally related residues between the two proteins are indicated by a *colon*. The Rx1 domain structure is denoted by a *colored line above* the Rx1 sequence and corresponds to the NB (*green*), ARC1 (*red*), and ARC2 (*blue*) domains. Residues in *light blue* contact DNA bases in the Orc1-DNA structure, whereas those in *red* contact DNA bases and/or the DNA backbone (45, 49). Known (Orc1) and predicted (Rx1) secondary structures (α-helix (*yellow*) or β-sheet (*gray*)) are indicated. *B*, structural homology model for Rx1 based on the crystal structure of DNA-bound Cdc6/Orc1 from *A. pernix*. *Left*, structural homology model of the NB-ARC domain of Rx1 (amino acids 143–478), with associated ADP (NB domain (*green*), ARC1 domain (*red*), or ARC2 (*blue*)). *Center*, crystal structure of *A. pernix* Cdc6/Orc1 in complex with DNA (PDB 2V1U) (*pink*, amino acids 13–279; *yellow*, amino acids 280–399). *Right*, crystal structure for Cdc6/Orc1 of *P. aerophilum* not bound to DNA (PDB code 1FNN) (*pink*, amino acids 1–278; *yellow*, amino acids 279–388). *C*, comparison of the PDB 2V1U-based Rx1 homology model with the crystal structure of Cdc6/Orc1 of *P. aerophilum* (PDB code 1FNN). *Left*, complete overlay of both structures. Note that only the NB (*green*) and ARC1 (*red*) superimposes and that the ARC2 domain (*blue*) of Rx1 is rotated compared with the C-terminal region of Cdc6/Orc1 of *P. aerophilum* (*yellow*). *Center*, overlay highlighting the C-terminal ARC1 (*red*) and ARC2 (*blue*) domains of Rx1. *Right*, superposition of the C-terminal domain of Cdc6/Orc1 of *P. aerophilum* onto the Rx1 model. Domain designations are as in *B*.

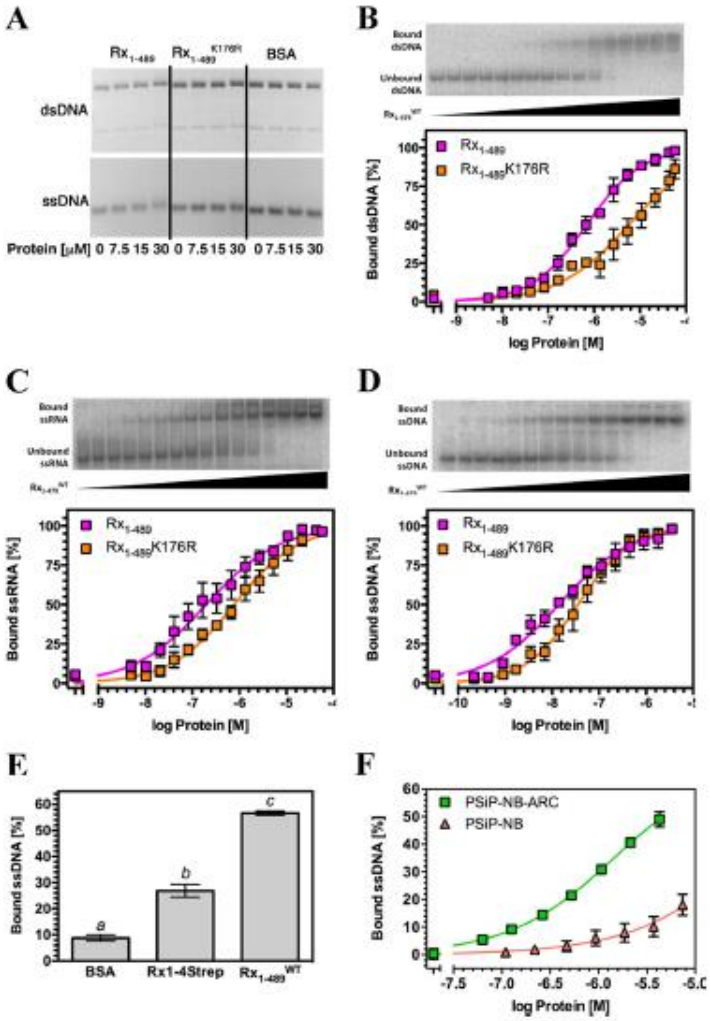

FIGURE 3. **The Rx1 CC-NBARC domains bind nucleic acids *in vitro*.** *A*, EMSA for Rx1(1–489)^{WT}, Rx1(1–489)^{K176R}, and BSA using 100 ng of ϕX174 virion DNA (ssDNA) or ϕX174 virion RF I DNA (dsDNA). For dsDNA, the *top band* represents relaxed circular DNA, whereas the *bottom band* represents supercoiled circular DNA. *B–D*, *top panels*, representative EMSA for Rx1(1–479)^{WT} showing raw data for binding to nucleic acids. *Bottom panels*, quantitative EMSA analysis giving apparent affinities of Rx1(1–489)^{WT} and Rx1(1–489)^{K176R} for dsDNA (*B*), ssRNA (*C*), and ssDNA (*D*) (means ± S.E. (*error bars*); $n = 3–6$). *E*, quantitative EMSA showing binding of 1 μM full-length plant-expressed Strep-tagged Rx1 (Rx1-4Strep), *E. coli* produced Rx1(1–489)^{WT}, or BSA to ssDNA (means ± S.E.; $n = 8$; *bars* with *different letters* are significantly different ($p < 0.05$); one-way ANOVA with post hoc Tukey's multiple comparison). *F*, quantitative EMSA analysis giving comparative affinities of PSIP-NB-ARC and PSIP-NB for ssDNA (means ± S.E.; $n = 3$).

and ssRNA but exhibited a significantly higher apparent affinity for ssDNA (Fig. 3, *B–D*, and Table 1). The affinity of Rx1(1–489)^{WT} for dsDNA is within the submicromolar range and is of a similar magnitude as both eukaryotic and prokaryotic Cdc6/Orc1 proteins (66, 67). The apparent affinity of the Rx1(1–489)^{K176R} mutant for ssDNA, dsDNA, and ssRNA was lower than the apparent affinity of wild type Rx1 in each case, which corresponds to the observed lower affinity established using the ϕX174 DNA (Akaike information criterion, $p > 0.99$). To

TABLE 1

Apparent dissociation constants for recombinant NLR domain interactions with nucleic acids

Values shown are the mean ± S.D. ND, not determined.

Protein	K_d^{app} ssDNA	K_d^{app} dsDNA	K_d^{app} ssRNA
	μM	μM	μM
Rx(1–489)^{WT}	0.014 ± 0.002	0.70 ± 0.05	0.20 ± 0.03
Rx(1–489)^{K176R}	0.036 ± 0.004	5.69 ± 0.85	0.77 ± 0.09
PSiP-NB	>50	ND	ND
PSiP-NB-ARC	4.08 ± 0.26	ND	ND

exclude the possibility that the observed nucleic acid binding was an artifact of the recombinant protein, we purified full-length Rx1 protein from plants. The protein was purified using a C-terminal 4-fold Strep-tag (Rx1-4Strep) from agroinfiltrated *N. benthamiana* leaves. The amount of purified Rx1 protein obtained was limited but sufficient to demonstrate that plant-derived Rx1-4Strep is also able to bind to ssDNA *in vitro* (Fig. 3*E*). Plant-derived Rx1-4Strep DNA binding was weaker than that of bacterially derived protein, which could be due to the fact that the majority of the full-length Rx1 is presumably in the autoinhibited off-state. Only a small fraction is proposed to be spontaneously active and thought to be responsible for the weak HR phenotype observed when Rx1 is overexpressed in the absence of the CP elicitor (68). In addition, the possibility cannot be excluded that the tag has impacted folding of a portion of the plant-expressed Rx1 protein.

The NLR NB-ARC Domain Binds Nucleic Acids in Vitro—Despite the structural relationship between the Rx1 NB-ARC domains and Cdc6/Orc1 proteins, it is formally possible that the data of Fig. 3 can be explained by an interaction between nucleic acids and the N-terminal CC domain of Rx1(1–489) rather than its NB-ARC domain. We were unable to produce truncated Rx1 fragments encompassing solely the NB or NB-ARC domains. We therefore examined another plant NLR protein to assess whether the NB-ARC domain alone is able to bind nucleic acids and whether DNA binding is unique to Rx1 or represents a common property of at least a subset of plant NLRs. The NLR subdomains of the orphan NLR of the monocot *Zea mays* were chosen because both the NB and NB-ARC domains can be produced as soluble recombinant protein (14). We compared ssDNA binding of the NB subdomain of PSiP alone (PSiP-NB) with that of the complete NB-ARC domain of PSiP (PSiP-NB-ARC) (Fig. 3*F*). Although both fragments bound, the PSiP-NB-ARC domains bound ssDNA with a considerably higher affinity than the PSiP-NB domain alone (Table 1). Together, these data demonstrate that the NB-ARC domain is sufficient for nucleic acid binding in Rx1 and PSiP, that DNA binding is a property of at least a subset of plant NLR proteins, and that both the NB and the ARC subdomains contribute to the DNA interaction.

Rx1 Deforms DNA—In the "switch" model for plant NLR activation, binding of ATP to the NB-ARC domain establishes the "on" state, whereas hydrolysis of ATP to ADP restores the "off" state (9). An intact P-loop is essential for nucleotide binding, and mutations in this motif typically result in loss-of-function alleles (9). We therefore investigated the relationship between P-loop-dependent ATPase activity and DNA binding. We detected no ATPase activity in Rx1(1–489)^{WT}, possibly indicating the absence of a catalytic water molecule, as observed previously for the STAND ATPase Ced-4 (69). Neither ATP nor ADP had any discriminatory influence on Rx1(1–489) binding to dsDNA (Fig. 4*A*). We therefore investigated whether Rx1 has activities at DNA other than binding that are affected by the type of nucleotide (ATP/ADP) bound. The Cdc6/Orc1 family proteins ORC1 of *A. pernix* and the Orc1-1/Orc1-3 heterodimer of *S. solfataricus* substantially deform origin DNA by bending it with angles of 35 and 20°, respectively, thereby inducing localized melting of the double helix (45, 49, 70). We

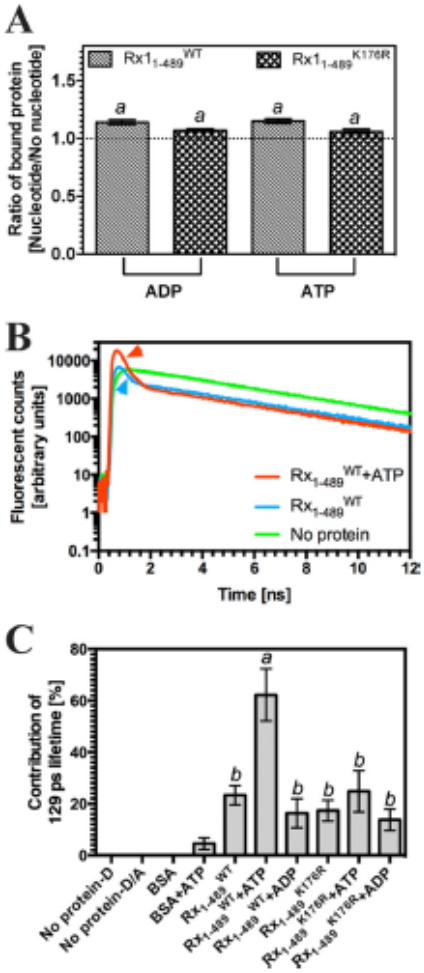

FIGURE 4. **Rx1(1–489) bends dsDNA.** *A*, double-stranded DNA-binding by Rx1(1–489)^{WT} and Rx1(1–489)^{K176R} assessed by EMSA plotted as a ratio of binding in the presence of 1 μM nucleotide compared with no nucleotide (means ± S.E. (*error bars*); $n = 3$; *a*, $p > 0.05$). The DNA used is identical to that used for Fig. 3*B*. *B*, sample time-resolved data for a control (*No protein*) and Rx(1–489)^{WT} with and without ATP. The data show fluorescent counts from the fluorescent donor plotted against time. The appropriately *colored arrowhead* indicates the 129-ps lifetime associated with energy transfer. *C*, the percentage contribution of the 129-ps lifetime for fluorescent donor in the presence of BSA or Rx1(1–489) and nucleotides (*D*, donor-labeled oligonucleotide only, no protein; *D/A*, donor- and acceptor-labeled oligonucleotide, no protein) (means ± S.E.; $n = 3$–11; *bars* with *different letters* are significantly different ($p < 0.05$); one-way ANOVA with post hoc Tukey's multiple comparison).

therefore examined whether Rx1(1–489) can deform DNA in a similar fashion and whether this process is nucleotide type-dependent. To measure DNA bending, time-resolved FRET was used because it allows measurements of distances between fluorophores. This method offers considerable advantages over steady-state FRET because the fluorescence lifetime represents an intrinsic property of the fluorophore and is independent of concentration, photobleaching, or light scattering (71). We monitored DNA deformation using time-resolved FRET with

dual end-labeled dsDNA (72). Upon FRET, the fluorescence lifetime of the donor fluorophore decreases; therefore, we deconvoluted the fluorescence donor emission for its constituent lifetime components. We hypothesized that following DNA bending, we would observe a shortened donor lifetime due to energy transfer to the acceptor. DNA bending was assessed under conditions to saturate binding of Rx1(1–489)^{WT} or Rx1(1–489)^{K176R} to dsDNA. Bending was evident as a decrease in the contribution of a 4.1-ns component (indicative of unperturbed donor emission; fluorescein fluorescence) to and the appearance of a 129-ps component during the total fluorescence decay of FRET donor emission (Fig. 4*B*, the 129-ps component is marked with an *arrow*). The 129-ps lifetime component, attributed to energy transfer, was only observed for the Rx1(1–489)^{WT} protein and Rx1(1–489)^{K176R} protein and not in controls without protein or with BSA except for a minor contribution with the latter in the presence of ATP (Fig. 4*C*). The 129-ps lifetime corresponds to a calculated donor-acceptor distance of 29 Å (assuming isotropic orientations) and therefore an overall bend angle of 42° around a presumed oligonucleotide midpoint.

Next, it was investigated whether nucleotides had an influence on the observed DNA bending. Notably ATP, but not ADP, strongly increased the contribution of the 129-ps lifetime to the overall time-resolved data. This increase was only observed for the Rx1(1–489)^{WT} protein and not for the Rx1(1–489)^{K176R} mutant, indicating that DNA bending requires an intact P-loop capable of binding nucleotides. The distinct response of the Rx1(1–489)^{WT} protein following incubation with either ADP or ATP provides additional support for a correct native fold of the nucleotide-binding pocket in the recombinant protein. The absence of any change in the value of the shortened lifetime (129 ps) shows that the calculated donor-acceptor distance is constant. Because the relative proportion of the 129 ps lifetime to the total fluorescence signal increases in the presence of ATP and Rx1(1–489)^{WT}, we can conclude that ATP binding enhances the pool of protein-DNA complexes in the bent state but not the bending angle.

Time-resolved FRET is a well validated method to examine intramolecular distances and therefore DNA topology, but it does not provide further information on other DNA distortions associated with changes in topology. To examine whether Rx1(1–489) can induce local DNA melting, as has been observed for Orc1, we explored a non-fluorescence-based methodology. P_1 nuclease has been used previously as a tool to examine local DNA distortion using the Orc1 protein of *A. pernix* (70). We therefore examined the sensitivity of dsDNA oligonucleotides to the ssDNA-specific P_1 nuclease in the presence of Rx1(1–489) (73). As expected, ssDNA was significantly degraded by P_1 nuclease (positive control), whereas dsDNA, in the presence of BSA (negative control), was largely resistant to P_1 nuclease activity (Fig. 5). Although dsDNA was more sensitive to P_1 nuclease in the presence of Rx1(1–489), the mutant Rx1(1–489)^{K176R} did not induce local DNA melting because no increased DNA degradation was observed. Thus, although in the *absence* of nucleotides, Rx1(1–489)^{K176R} bends dsDNA to a similar magnitude as Rx1(1–489)^{WT}, its failure to melt DNA might be a manifestation of subtle changes to DNA binding

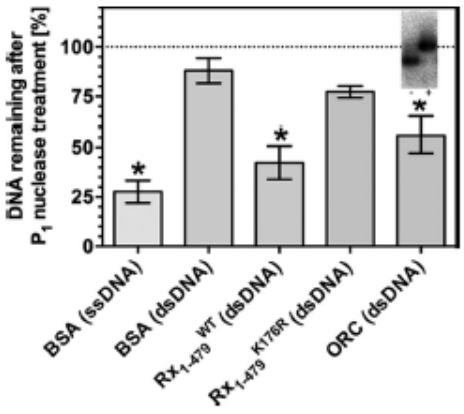

FIGURE 5. **Rx1(1–489) induces localized DNA melting.** DNA remaining undigested after treatment with P_1 nuclease in the presence of BSA, Rx1(1–489)^{WT}, Rx1(1–489)^{K176R}, or ORC as a percentage of total DNA (means ± S.E. (*error bars*); $n = 6–19$; *, $p < 0.05$ compared with dsDNA in the presence of BSA by one-way ANOVA with post hoc Dunnett test). The *inset* shows a control EMSA using the C3/mORB dual site DNA sequence at *orlC2* of *S. solfataricus* in the presence or absence of 1.5 μM ORC.

evidenced through the decrease in binding affinity (Fig. 3, *B–D*). These experiments were insufficiently sensitive to examine the further influence of nucleotides on NLR-mediated DNA melting. The P_1 sensitivity of dsDNA in the presence of Orc1-1/Orc1-3 was indistinguishable from that of dsDNA in the presence of Rx1(1–489)^{WT}, supporting the interpretation that plant NLRs can cause local dsDNA melting. In conclusion, Rx1 is able to both bend DNA and provoke local DNA melting, and this bending activity requires an intact P-loop and is stimulated by the presence of ATP.

Rx1 Preferentially Binds Specific DNA Topologies in Vitro—We sought independent experimental support for Rx1-mediated distortion of DNA. We hypothesized that if Rx1 distorts linear DNA, then the free energy of Rx1 binding to DNA structures that resemble the distorted state would be favored (with a corresponding increase in affinity). Indeed, Rx1 bound branched double-stranded DNA with a significantly higher affinity than control linear double-stranded DNA of similar sequence (Fig. 6*A*; compare *dsF12* with *F12-ds/ds*). The branched double-stranded DNA represents a non-natural DNA and is a control to demonstrate a preference for Rx1(1–489) binding to a branched topology. When comparing binding affinities for naturally occurring branched topologies, we noted a higher affinity for branched structures with one dsDNA and two ssDNA arms (*e.g.* similar to a transcription bubble) compared with structures with one or two duplex arms (*e.g.* resembling a DNA replication fork) (Fig. 6*A*, compare *F12-ds/ss* with *F12-ss/ss*). Consistent with our model of local DNA melting, Rx1(1–489) showed a higher affinity for small DNA bubbles compared with linear dsDNA (Fig. 6*B*). This increased affinity was not due to the increased affinity for ssDNA because affinity did not correlate with increasing DNA bubble size. Although these data cannot reveal the exact nature of the distorted DNA state on DNA bending (Fig. 4) and melting (Fig. 5), analysis of the relative affinities does demonstrate that Rx1 shows an

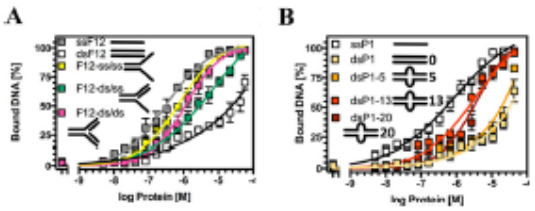

FIGURE 6. **Rx1 preferentially binds distorted DNA topologies.** *A*, quantitative EMSA analysis giving comparative affinities of Rx1(1–489)^{WT} for ssDNA (*ssF12*), dsDNA (*dsF12*), branched dsDNA with two dsDNA arms (*F12-ds/ds*), branched dsDNA with two ssDNA arms (*F12-ss/ss*), and branched dsDNA with one ssDNA and one dsDNA arm (*F12-ds/ss*) (means ± S.E. (*error bars*); n = 3–4). *B*, quantitative EMSA analysis giving comparative affinities of Rx1(1–489)^{WT} for ssDNA (*ssP1*), dsDNA (*dsP1*), and dsDNA with bubbles of varying sizes (means ± S.E.; n = 3–4).

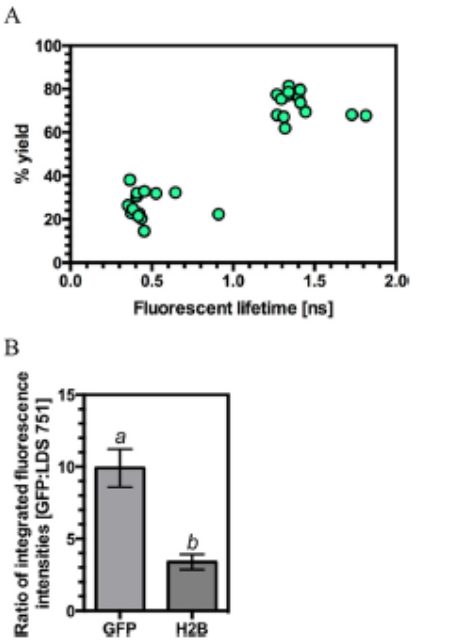

FIGURE 7. **Individual fluorescent lifetime signals for GFP can be resolved from agroinfiltrated plants.** *A*, plot of the identified fluorescent lifetimes for GFP from agroinfiltrated *N. benthamiana* epithelial cell nuclei against the percentage yield for that lifetime. The graph represents 14 measurements from seven independently infiltrated leaves with each measurement providing two fluorescent lifetime values. *B*, ratios for the integrated emission intensities for GFP and LDS 751 in GFP (negative control) and H2B-GFP (positive control) agroinfiltrated *N. benthamiana* (n = 6–7; *bars* with *different letters* are significantly different ($p < 0.05$); Student's t test). *Error bars*, S.E.

increased affinity for specific DNA structures, and the DNA distortion we observed in the presence of Rx1 is probably a genuine response following its activation.

Rx1 DNA Binding Is Specifically Activated by Its Cognate Elicitor in Vivo—DNA binding, bending, and melting is a new aspect of plant NLR biochemistry. To validate DNA as a downstream target for NLR signaling and link this biochemical activity to its function in plant cells, we tested whether Rx1 is able to interact with DNA *in vivo*. To investigate the possibility of a direct interaction with genomic DNA inside the cell, we studied Rx1-DNA interactions in the nucleus using Forster resonance energy transfer-fluorescence lifetime imaging microscopy (FRET-FLIM). FRET-FLIM has been used previously to demonstrate transcription factor binding to DNA in response to environmental signals (74).

N. benthamiana was infiltrated with *A. tumefaciens* carrying constructs encoding either GFP (negative control), a protein consisting of *A. thaliana* histone H2B fused to GFP (GFP-H2B; positive control), or discrete domains of Rx1 fused to GFP. Previous work has similarly utilized H2B-GFP and naked GFP as controls for DNA binding in paraformaldehyde-fixed preparations (74). The constituent fluorescence lifetimes for the GFP tag were examined in leaves counterstained with LDS 751. LDS 751 is a cell-permeable nucleic acid stain with an excitation maximum, when bound to DNA, that overlaps with the GFP emission spectrum. GFP showed two distinct lifetimes at ~0.5 and 1.5 ns (Fig. 7*A*). Because energy transfer from donor (GFP) to acceptor (LDS 751) decreases the fluorescent lifetime, we hypothesized that the shorter lifetime for GFP is representative of energy transfer consistent with an interaction between the fluorophores. Notably, such a decrease in the GFP fluorescence lifetime by time-correlated single-photon counting is independent of protein expression levels, quenching, photobleaching, or fluctuations in the excitation source. A decrease in lifetime can therefore specifically be attributed to quenching of the excited state of the GFP and represents strong evidence for energy transfer from GFP to LDS 751 and thus a direct protein-DNA interaction. Consistent with this interpretation, a significant decrease in the ratio of the yields of the GFP fluorescence lifetimes was observed for the DNA-binding protein GFP-H2B (Fig. 8*A*). To demonstrate that energy transfer to LDS 751, and not to surrounding proteins, explains the data, we confirmed that the decrease in the fluorescence GFP lifetime ratio indicative of DNA binding was correlated with an increase in LDS 751 emission that does not arise from the excitation source (Fig. 7*B*). Although the exact stoichiometry of GFP and LDS 751 levels is not known in each experiment, the finding that the ratio of fluorescence emission for GFP/LDS 751 is significantly decreased for H2B compared with the negative control is strong evidence that the reduction in GFP lifetimes is due to energy transfer to LDS 751 and not to an alternative molecule. As predicted, Rx1-GFP fusions containing the NB-ARC domain (NB-ARC-GFP, CC-NB-ARC-GFP, and NB-ARC-LRR-GFP) showed a significant decrease in the ratio of GFP lifetime yields, consistent with its observed DNA binding activity *in vitro*, whereas the LRR (GFP-LRR) domain did not. Surprisingly, the CC domain alone (CC-GFP) also showed a decrease in the ratio of GFP lifetime yields. The Rx1 CC domain has been shown previously to associate with a high molecular weight complex in the nucleus (23), and our findings indicate that this complex probably contains genomic DNA. Taken together, these data demonstrate that the CC and CC-NB-ARC Rx1 domains can form a stable interaction with DNA *in situ*. The FRET-FLIM methodology used is independent of expression levels of the various constructs. However, the methodology can be sensitive to cleavage of the GFP tag of even a small percentage of

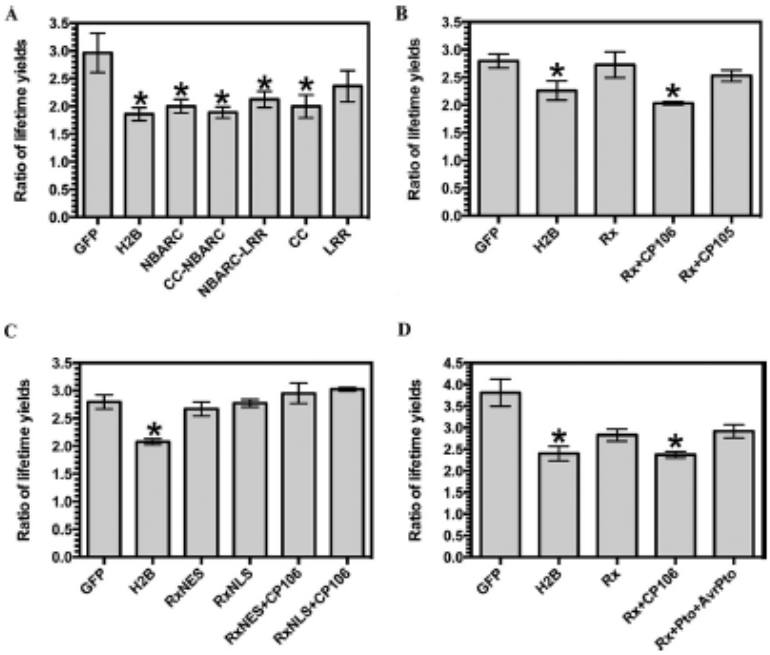

FIGURE 8. **Binding of Rx1 protein domains to DNA *in situ*.** *A*, the ratio of the long (>1.0 ns) to short (<0.5 ns) GFP lifetimes for GFP fusion constructs representing varying Rx1 subdomains produced in *N. benthamiana* leaves using agroinfiltration ($n > 6$; *, $p < 0.05$ compared with GFP by one-way ANOVA with post hoc Dunnett test). *B*, ratio of the long (>1.0 ns) to short (<0.5 ns) GFP lifetimes for Rx1-GFP full-length constructs alone and upon co-expression with virulent (CP105) and avirulent alleles (CP106) of the PVX CP ($n > 6$; *, $p < 0.05$ compared with GFP by one-way ANOVA with post hoc Dunnett test). *C*, ratio of the long (>1.0 ns) to short (<0.5 ns) GFP lifetimes for GFP-NLS-Rx1 and GFP-NES-Rx1 full-length constructs alone and upon co-expression with the avirulent allele of PVX, CP106 ($n = 4$; *, $p < 0.05$ compared with GFP by one-way ANOVA with post hoc Dunnett test). *D*, ratio of the long (>1.0 ns) to short (<0.5 ns) GFP lifetimes for Rx1-GFP full-length construct alone and upon co-expression with either the avirulent allele of PVX, CP106, or the Pto kinase and AvrPto ($n = 12–20$; *, $p < 0.05$ compared with GFP by one-way ANOVA with post hoc Dunnett test). *Error bars*, S.E.

expressed protein. Fortunately, cleavage of the GFP tag can be resolved because it yields a *high* rather than the observed *low* ratio of fluorescence lifetimes, allowing us to conclude that the positive results for DNA binding *in situ* are not attributable to tag cleavage.

Next, we investigated whether the full-length Rx1 molecule (Rx1-GFP) also binds to DNA in the plant cell. Notably, a full-length Rx1-GFP fusion showed no binding to DNA as compared with the negative control (Fig. 8*B*). This implies that the inactive full-length Rx1 protein adopts a structure refractory to interacting with DNA. To test whether there is a relationship between DNA-binding and Rx1 activation and subsequent immune signaling, we next co-expressed Rx1 with the PVX coat protein elicitor, which is known to trigger immunity (23). Full-length Rx1-GFP was found to bind to DNA only in the presence of the wild type (avirulent) coat protein (CP106) and not in the presence of a mutant (virulent) elicitor (CP105) that is unable to activate Rx1 (Fig. 8*B*). These data show that DNA binding *in vivo* by Rx1 only occurs upon perception of its cognate elicitor.

To test whether DNA binding *in situ* requires elicitor recognition in the cytoplasm, we investigated DNA binding of Rx1-GFP fused to either an NLS or an NES. These chimeric tags have been demonstrated previously to constrain Rx1 to the nucleus or cytoplasm, respectively (23). This experiment addresses two questions. 1) Is enforced nuclear accumulation of a GFP fusion protein sufficient to confer DNA binding? 2) At what subcellular localization can Rx1 be activated by the coat protein to permit DNA binding? GFP-NLS-Rx1 did not bind DNA in the presence or absence of CP106, demonstrating that enforced Rx1 accumulation in the nucleus is insufficient to drive DNA binding *and* that DNA binding requires CP106 recognition in the cytoplasm, consistent with previous findings (23) (Fig. 8*C*). GFP-NES-Rx1 also did not bind DNA in the presence or absence of CP106, demonstrating that the DNA binding signal is dependent on the ability of the cytosolic Rx1 protein to gain access to genomic DNA regardless of exposure to CP106. GFP-NES-Rx1 and GFP-NLS-Rx1 are not sensitive to cleavage of GFP, thus excluding the possibility that the observed absence of DNA binding is due to sensitivity to proteolysis (23). Taken together, the data support a model where Rx1 binding to DNA is a specific nuclear event in immune activation subsequent to coat protein detection in the cytosol.

We further investigated binding of Rx1-GFP to DNA upon activation of another immune receptor to exclude the possibility that Rx1 binds DNA as a nonspecific consequence of defense activation. We co-infiltrated *N. benthamiana* with *A. tumefaciens* carrying constructs encoding Rx1-GFP, the Pto kinase of tomato, and the AvrPto effector. The Pto kinase activates an immune response in *N. benthamiana* upon binding the AvrPto effector of *Pseudomonas syringae* pv. tomato (75–77). Rx1-GFP

did not bind DNA when Pto was activated by AvrPto, indicating that Rx1-GFP DNA binding is not a generic response following defense activation (Fig. 8*D*). Because the role of Rx1 in immunity is dependent upon both its activation by the viral coat protein in the cytoplasm and its DNA binding activity in the nucleus, our findings therefore provide the first evidence for a direct molecular target between activation of a plant NLR and subsequent cellular immune responses.

Discussion

The molecular mechanism underlying the function of activated NLR proteins in plant immunity is a crucial, but still unanswered, question. Existing *in vitro*, *in vivo*, and bioinformatics data pinpoint the NB-ARC domain as a central switch in regulating NLR activity. We here propose that the NB-ARC domain also possesses an intrinsic DNA binding activity, and we demonstrate that its DNA binding activity is associated with the cellular immune response. The Rx1 protein is observed to bind and deform dsDNA *in vitro* and to bind cellular DNA in response to activation following elicitor perception. Importantly, although the described biochemistry for Rx1 is novel for a NLR protein, DNA distortion is a well characterized feature of other proteins that interact with DNA through non-sequence-specific interactions, including TATA box-binding protein (78, 79), integration host factor (80), and the HMG box (81). Rx1 biochemistry is therefore consistent with the activity of known DNA-binding proteins.

Our observation that Rx1 can interact with DNA in response to immune activation might provide a rationale for its nuclear localization. For example, a P-loop mutant in Rx1 can potentially establish a correlation between DNA binding and immunity. The K176R P-loop mutant of Rx1 is defective in triggering immunity (23) to PVX. We show that this mutant is also defective in nucleotide-dependent DNA bending and DNA melting *in vitro*. This finding represents a potential link between the ability of Rx1 to distort DNA *in vitro* and the ability to trigger immunity *in planta*. Equivalent mutations in the NB domain of Cdc6 have been used to investigate the activity of Cdc6 at dsDNA (82, 83).

In vivo activation of Rx1 by the PVX coat protein induces the plant immune response (84) (Fig. 8*B*). We found that Rx1 only bound nuclear DNA following recognition of the CP106 coat protein and not the CP105 variant, which is unable to trigger Rx1 signaling. These data show that only properly activated Rx1 has the ability to interact with DNA *in situ*. In addition, only cytosolic recognition of CP106, followed by translocation of activated Rx1 to the nucleus, results in full activation of immunity (23). We demonstrate that, even in the presence of the CP106 coat protein, no DNA binding occurs when Rx1 is artificially retained in either cytosol or nucleus (Fig. 8*C*). This finding presents a potential link between the known spatial requirements for Rx1-mediated immune activation and the DNA binding observed *in situ*. Such a translocation mechanism might be analogous to that of WHIRLY1, an immune activated transcriptional regulator that translocates to the nucleus and is involved in defense gene expression (85). *In vitro*, full-length (hence mostly inactive) Rx1 purified from *N. benthamiana* did interact with DNA, albeit less strongly than the CC-NBARC form produced in *E. coli* ($Rx1(1-489)^{WT}$) (Fig. 3*E*), which is free of the autoinhibitory constraint posed by the LRR domain (86). DNA binding *in vitro* with full-length Rx1 occurred under conditions where relatively high protein concentrations can be assayed. Presumably, Rx1 levels *in vivo* are too low to observe DNA binding in its non-activated state (Fig. 8*B*). The observed DNA binding by full-length Rx1 *in situ* is not a generic consequence of plant immunity because activation of immunity through another immune receptor (Pto/AvrPto) did not induce Rx1 DNA binding. We therefore propose that DNA binding by Rx1 upon PVX coat protein perception is an essential, specific, and early step in the cellular immune response.

The Rx1 NBARC domains share remarkable biochemical properties with the Cdc6/Orc1 family DNA-binding proteins. Rx1 was observed to bind both ssDNA and dsDNA similar to ORC of *Saccharomyces cerevisiae* (87). The Cdc6/Orc1 homology with NLR proteins and the DNA binding characteristics of the separate PSiP NB and NB-ARC domains accord with multiple contacts with DNA across both NB and ARC domains. Hence, single point mutations are unlikely to abolish DNA binding, and, consistent with previous observations (67), we have not identified point mutations that ablate DNA binding. Eukaryotic ORCs lack DNA sequence specificity *in vitro* but show higher affinity for specific DNA topologies (88, 89). Consistent with this, Rx1 shows higher affinity for branched and melted DNA topologies than for dsDNA. The bend angle introduced into DNA by Rx1(1–489) is also of a magnitude similar to that observed in crystal structures of ORC1 from *A. pernix* (45). Analysis of *A. pernix* ORC2 revealed a considerable conformational flexibility stabilized by ATP (54). In this context, it is interesting to note that although the bend angle is identical for both wild type and mutant Rx1 proteins in the absence of nucleotide or presence of ADP, the *population* of DNA in the bent state was more prevalent in $Rx1(1-489)^{WT}$ supplemented with ATP. The Rx1 activated state is therefore specifically linked to DNA distortion.

The activity of Rx1 on DNA provides biochemical evidence that Rx1 might act as a transcriptional regulator through its NB-ARC domain. DNA binding by a NLR is a signaling event because the NB-ARC domain is not involved in recognition specificity. Pathogen recognition by NLRs is typically determined by the LRR, often in conjunction with integrated effector targets (90, 91). A key process in transcriptional activation is the distortion of DNA to enable the formation of the transcription preinitiation complex (92–95). In the cell, Rx1 protein might have sequence-specific DNA binding conferred by interacting protein partners, whereas the NB-ARC domain distorts DNA to a state that activates or represses transcription, depending upon the locus (96). The region encompassing the CC domain, which might interact with DNA via an accessory protein (*e.g.* a transcription factor), could confer this sequence specificity. The identification of such a binding partner that can confer sequence specificity to the Rx1-DNA interaction represents a significant challenge for the future.

In summary, we have identified a conserved DNA binding and distorting activity in the NB-ARC domain of the Rx1 protein *in vitro* and link Rx1 activation following elicitor recognition to nuclear DNA binding *in situ*. Rx1 induces cellular

immune responses after viral coat protein recognition. We hypothesize that a function for Rx1 is to manipulate DNA into an "immune competent" state. The precise nature and role of this Rx1 protein-DNA immune competent state can now be addressed in future studies.

Author Contributions—S. F., P. D. T., C. H. D., G. B. S., A. S. E. C., E. J. S., L. B. W., and F. K. K. G. performed the experiments. S. F., P. D. T., C. H. D., G. B. S., E. J. S., G. J. S., A. G., L.-O. P., F. L. W. T., and M. J. C. analyzed the data. M. R. K., G. J. S., A. G., L.-O. P., F. L. W. T., and M. J. C. conceived the experiments. M. J. C. and F. L. W. T. conceived the overall project and wrote the manuscript. All authors reviewed the results and approved the final version of the manuscript.

Acknowledgments—We thank Sarah Peyton for help with method development, Rikus Pomp for technical support and helpful advice, and Martijn Rep for critical feedback on the manuscript.

References

1. Dangl, J. L., and Jones, J. D. (2001) Plant pathogens and integrated defence responses to infection. *Nature* **411**, 826–833
2. Jones, J. D., and Dangl, J. L. (2006) The plant immune system. *Nature* **444**, 323–329
3. Maekawa, T., Kufer, T. A., and Schulze-Lefert, P. (2011) NLR functions in plant and animal immune systems: so far and yet so close. *Nat. Immunol.* **12**, 817–826
4. Medzhitov, R. (2007) Recognition of microorganisms and activation of the immune response. *Nature* **449**, 819–826
5. Eitas, T. K., and Dangl, J. L. (2010) NB-LRR proteins: pairs, pieces, perception, partners, and pathways. *Curr. Opin. Plant Biol.* **13**, 472–477
6. Staskawicz, B. J., Mudgett, M. B., Dangl, J. L., and Galan, J. E. (2001) Common and contrasting themes of plant and animal diseases. *Science* **292**, 2285–2289
7. Leipe, D. D., Koonin, E. V., and Aravind, L. (2004) STAND, a class of P-loop NTPases including animal and plant regulators of programmed cell death: multiple, complex domain architectures, unusual phyletic patterns, and evolution by horizontal gene transfer. *J. Mol. Biol.* **343**, 1–28
8. Takken, F. L., and Tameling, W. I. (2009) To nibble at plant resistance proteins. *Science* **324**, 744–746
9. Takken, F. L., Albrecht, M., and Tameling, W. I. (2006) Resistance proteins: molecular switches of plant defence. *Curr. Opin. Plant Biol.* **9**, 383–390
10. van der Biezen, E. A., and Jones, J. D. (1998) The NB-ARC domain: a novel signalling motif shared by plant resistance gene products and regulators of cell death in animals. *Curr. Biol.* **8**, R226–R227
11. Maekawa, T., Cheng, W., Spiridon, L. N., Töller, A., Lukasik, E., Saijo, Y., Liu, P., Shen, Q. H., Micluta, M. A., Somssich, I. E., Takken, F. L., Petrescu, A. J., Chai, J., and Schulze-Lefert, P. (2011) Coiled-coil domain-dependent homodimerization of intracellular barley immune receptors defines a minimal functional module for triggering cell death. *Cell Host. Microbe* **9**, 187–199
12. Tameling, W. I., Vossen, J. H., Albrecht, M., Lengauer, T., Berden, J. A., Haring, M. A., Cornelissen, B. J., and Takken, F. L. (2006) Mutations in the NB-ARC domain of I-2 that impair ATP hydrolysis cause autoactivation. *Plant Physiol.* **140**, 1233–1245
13. Williams, S. J., Sornaraj, P., deCourcy-Ireland, E., Menz, R. I., Kobe, B., Ellis, J. G., Dodds, P. N., and Anderson, P. A. (2011) An autoactive mutant of the M flax rust resistance protein has a preference for binding ATP, while wild-type M protein has a preference for binding ADP. *Mol. Plant Microbe Interact.* **24**, 897–906
14. Fenyk, S., Campillo Ade, S., Pohl, E., Hussey, P. J., and Cann, M. J. (2012) A nucleotide phosphatase activity in the nucleotide binding domain of an orphan resistance protein from rice. *J. Biol. Chem.* **287**, 4023–4032
15. von Moltke, J., Ayres, J. S., Kofoed, E. M., Chavarría-Smith, J., and Vance, R. E. (2013) Recognition of bacteria by inflammasomes. *Annu. Rev. Immunol.* **31**, 73–106
16. Bernoux, M., Ve, T., Williams, S., Warren, C., Hatters, D., Valkov, E., Zhang, X., Ellis, J. G., Kobe, B., and Dodds, P. N. (2011) Structural and functional analysis of a plant resistance protein TIR domain reveals interfaces for self-association, signaling, and autoregulation. *Cell Host Microbe* **9**, 200–211
17. Rairdan, G. J., Collier, S. M., Sacco, M. A., Baldwin, T. T., Boettrich, T., and Moffett, P. (2008) The coiled-coil and nucleotide binding domains of the Potato Rx disease resistance protein function in pathogen recognition and signaling. *Plant Cell* **20**, 739–751
18. Swiderski, M. R., Birker, D., and Jones, J. D. (2009) The TIR domain of TIR-NB-LRR resistance proteins is a signaling domain involved in cell death induction. *Mol. Plant Microbe Interact.* **22**, 157–165
19. Burch-Smith, T. M., Schiff, M., Caplan, J. L., Tsao, J., Czymmek, K., and Dinesh-Kumar, S. P. (2007) A novel role for the TIR domain in association with pathogen-derived elicitors. *PLoS Biol.* **5**, e68
20. Caplan, J. L., Mamillapalli, P., Burch-Smith, T. M., Czymmek, K., and Dinesh-Kumar, S. P. (2008) Chloroplastic protein NRIP1 mediates innate immune receptor recognition of a viral effector. *Cell* **132**, 449–462
21. Deslandes, L., Olivier, J., Peeters, N., Feng, D. X., Khounlotham, M., Boucher, C., Somssich, I., Genin, S., and Marco, Y. (2003) Physical interaction between RRS1-R, a protein conferring resistance to bacterial wilt, and PopP2, a type III effector targeted to the plant nucleus. *Proc. Natl. Acad. Sci. U.S.A.* **100**, 8024–8029
22. Shen, Q. H., Saijo, Y., Mauch, S., Biskup, C., Bieri, S., Keller, B., Seki, H., Ulker, B., Somssich, I. E., and Schulze-Lefert, P. (2007) Nuclear activity of MLA immune receptors links isolate-specific and basal disease-resistance responses. *Science* **315**, 1098–1103
23. Slootweg, E., Roosien, J., Spiridon, L. N., Petrescu, A. J., Tameling, W., Joosten, M., Pomp, R., van Schaik, C., Dees, R., Borst, J. W., Smant, G., Schots, A., Bakker, J., and Goverse, A. (2010) Nucleocytoplasmic distribution is required for activation of resistance by the potato NB-LRR receptor Rx1 and is balanced by its functional domains. *Plant Cell* **22**, 4195–4215
24. Wiermer, M., Germain, H., Cheng, Y. T., García, A. V., Parker, J. E., and Li, X. (2010) Nucleoporin MOS7/Nup88 contributes to plant immunity and nuclear accumulation of defense regulators. *Nucleus* **1**, 332–336
25. Bai, S., Liu, J., Chang, C., Zhang, L., Maekawa, T., Wang, Q., Xiao, W., Liu, Y., Chai, J., Takken, F. L., Schulze-Lefert, P., and Shen, Q. H. (2012) Structure-function analysis of barley NLR immune receptor MLA10 reveals its cell compartment specific activity in cell death and disease resistance. *PLoS Pathog.* **8**, e1002752
26. Wirthmueller, L., Zhang, Y., Jones, J. D., and Parker, J. E. (2007) Nuclear accumulation of the *Arabidopsis* immune receptor RPS4 is necessary for triggering EDS1-dependent defense. *Curr. Biol.* **17**, 2023–2029
27. Zhu, Z., Xu, F., Zhang, Y., Cheng, Y. T., Wiermer, M., Li, X., and Zhang, Y. (2010) *Arabidopsis* resistance protein SNC1 activates immune responses through association with a transcriptional corepressor. *Proc. Natl. Acad. Sci. U.S.A.* **107**, 13960–13965
28. Cheng, Y. T., Germain, H., Wiermer, M., Bi, D., Xu, F., García, A. V., Wirthmueller, L., Després, C., Parker, J. E., Zhang, Y., and Li, X. (2009) Nuclear pore complex component MOS7/Nup88 is required for innate immunity and nuclear accumulation of defense regulators in *Arabidopsis*. *Plant Cell* **21**, 2503–2516
29. Tameling, W. I., Nooijen, C., Ludwig, N., Boter, M., Slootweg, E., Goverse, A., Shirasu, K., and Joosten, M. H. (2010) RanGAP2 mediates nucleocytoplasmic partitioning of the NB-LRR immune receptor Rx in the Solanaceae, thereby dictating Rx function. *Plant Cell* **22**, 4176–4194
30. Heidrich, K., Wirthmueller, L., Tasset, C., Pouzet, C., Deslandes, L., and Parker, J. E. (2011) *Arabidopsis* EDS1 connects pathogen effector recognition to cell compartment-specific immune responses. *Science* **334**, 1401–1404
31. Chang, C., Yu, D., Jiao, J., Jing, S., Schulze-Lefert, P., and Shen, Q. H. (2013) Barley MLA immune receptors directly interfere with antagonistically acting transcription factors to initiate disease resistance signaling. *Plant Cell* **25**, 1158–1173
32. Roberts, M., Tang, S., Stallmann, A., Dangl, J. L., and Bonardi, V. (2013) Genetic requirements for signaling from an autoactive plant NB-LRR in-

tracellular innate immune receptor. *PLoS Genet.* **9**, e1003465
33. Caplan, J., Padmanabhan, M., and Dinesh-Kumar, S. P. (2008) Plant NB-LRR immune receptors: from recognition to transcriptional reprogramming. *Cell Host Microbe* **3**, 126–135
34. Germain, H., and Séguin, A. (2011) Innate immunity: has poplar made its BED? *New Phytol.* **189**, 678–687
35. Yan, N., Chai, J., Lee, E. S., Gu, L., Liu, Q., He, J., Wu, J. W., Kokel, D., Li, H., Hao, Q., Xue, D., and Shi, Y. (2005) Structure of the CED-4-CED-9 complex provides insights into programmed cell death in *Caenorhabditis elegans*. *Nature* **437**, 831–837
36. Kelley, L. A., and Sternberg, M. J. (2009) Protein structure prediction on the Web: a case study using the Phyre server. *Nat. Protoc.* **4**, 363–371
37. Karplus, K. (2009) SAM-T08, HMM-based protein structure prediction. *Nucleic Acids Res.* **37**, W492–W497
38. Emsley, P., Lohkamp, B., Scott, W. G., and Cowtan, K. (2010) Features and development of Coot. *Acta Crystallogr. D Biol. Crystallogr.* **66**, 486–501
39. Winn, M. D., Ballard, C. C., Cowtan, K. D., Dodson, E. J., Emsley, P., Evans, P. R., Keegan, R. M., Krissinel, E. B., Leslie, A. G., McCoy, A., McNicholas, S. J., Murshudov, G. N., Pannu, N. S., Potterton, E. A., Powell, H. R., Read, R. J., Vagin, A., and Wilson, K. S. (2011) Overview of the CCP4 suite and current developments. *Acta Crystallogr D Biol. Crystallogr.* **67**, 235–242
40. Heo, L., Park, H., and Seok, C. (2013) GalaxyRefine: protein structure refinement driven by side-chain repacking. *Nucleic Acids Res.* **41**, W384–W388
41. DeLano, W. L. (2010) The PyMOL Molecular Graphics System, version 1.3r1, Schroedinger, LLC, New York
42. Peart, J. R., Lu, R., Sadanandom, A., Malcuit, I., Moffett, P., Brice, D. C., Schauser, L., Jaggard, D. A., Xiao, S., Coleman, M. J., Dow, M., Jones, J. D., Shirasu, K., and Baulcombe, D. C. (2002) Ubiquitin ligase-associated protein SGT1 is required for host and nonhost disease resistance in plants. *Proc. Natl. Acad. Sci. U.S.A.* **99**, 10865–10869
43. Schmidt, T. G., Koepke, J., Frank, R., and Skerra, A. (1996) Molecular interaction between the Strep-tag affinity peptide and its cognate target, streptavidin. *J. Mol. Biol.* **255**, 753–766
44. Westerhof, L. B., Wilbers, R. H., Roosien, J., van de Velde, J., Goverse, A., Bakker, J., and Schots, A. (2012) 3D domain swapping causes extensive multimerisation of human interleukin-10 when expressed in planta. *PLoS One* **7**, e46460
45. Gaudier, M., Schuwirth, B. S., Westcott, S. L., and Wigley, D. B. (2007) Structural basis of DNA replication origin recognition by an ORC protein. *Science* **317**, 1213–1216
46. Sreerama, N., and Woody, R. W. (2000) Estimation of protein secondary structure from circular dichroism spectra: comparison of CONTIN, SELCON, and CDSSTR methods with an expanded reference set. *Anal. Biochem.* **287**, 252–260
47. Green, V., Curtis, F. A., Sedelnikova, S., Rafferty, J. B., and Sharples, G. J. (2013) Mutants of phage bIL67 RuvC with enhanced Holliday junction binding selectivity and resolution symmetry. *Mol. Microbiol.* **89**, 1240–1258
48. Grinvald, A., and Steinberg, I. Z. (1974) On the analysis of fluorescence decay kinetics by the method of least-squares. *Anal. Biochem.* **59**, 583–598
49. Dueber, E. L., Corn, J. E., Bell, S. D., and Berger, J. M. (2007) Replication origin recognition and deformation by a heterodimeric archaeal Orc1 complex. *Science* **317**, 1210–1213
50. Bendahmane, A., Kanyuka, K., and Baulcombe, D. C. (1999) The Rx gene from potato controls separate virus resistance and cell death responses. *Plant Cell* **11**, 781–792
51. Bendahmane, A., Köhn, B. A., Dedi, C., and Baulcombe, D. C. (1995) The coat protein of potato virus X is a strain-specific elicitor of Rx1-mediated virus resistance in potato. *Plant J.* **8**, 933–941
52. Albrecht, M., and Takken, F. L. (2006) Update on the domain architectures of NLRs and R proteins. *Biochem. Biophys. Res. Commun.* **339**, 459–462
53. Liu, J., Smith, C. L., DeRyckere, D., DeAngelis, K., Martin, G. S., and Berger, J. M. (2000) Structure and function of Cdc6/Cdc18: implications for origin recognition and checkpoint control. *Mol. Cell* **6**, 637–648
54. Singleton, M. R., Morales, R., Grainge, I., Cook, N., Isupov, M. N., and Wigley, D. B. (2004) Conformational changes induced by nucleotide binding in Cdc6/ORC from *Aeropyrum pernix*. *J. Mol. Biol.* **343**, 547–557
55. Chattopadhyaya, R., and Pal, A. (2008) Three-dimensional models of NB-ARC domains of disease resistance proteins in tomato, *Arabidopsis*, and flax. *J. Biomol. Struct. Dyn.* **25**, 357–371
56. Riedl, S. J., Li, W., Chao, Y., Schwarzenbacher, R., and Shi, Y. (2005) Structure of the apoptotic protease-activating factor 1 bound to ADP. *Nature* **434**, 926–933
57. Shrivastava, D., Nain, V., Sahi, S., Verma, A., Sharma, P., Sharma, P. C., and Kumar, P. A. (2011) Insights from molecular modeling and dynamics simulation of pathogen resistance (R) protein from brinjal. *Bioinformation* **5**, 326–330
58. Takken, F. L., and Goverse, A. (2012) How to build a pathogen detector: structural basis of NB-LRR function. *Curr. Opin. Plant Biol.* **15**, 375–384
59. van Ooijen, G., Mayr, G., Kasiem, M. M., Albrecht, M., Cornelissen, B. J., and Takken, F. L. (2008) Structure-function analysis of the NB-ARC domain of plant disease resistance proteins. *J. Exp. Bot.* **59**, 1383–1397
60. Hu, Z., Yan, C., Liu, P., Huang, Z., Ma, R., Zhang, C., Wang, R., Zhang, Y., Martinon, F., Miao, D., Deng, H., Wang, J., Chang, J., and Chai, J. (2013) Crystal structure of NLRC4 reveals its autoinhibition mechanism. *Science* **341**, 172–175
61. Xu, Q., Rife, C. L., Carlton, D., Miller, M. D., Krishna, S. S., Elsliger, M. A., Abdubek, P., Astakhova, T., Chiu, H. J., Clayton, T., Duan, L., Feuerhelm, J., Grzechnik, S. K., Hale, J., Han, G. W., Jaroszewski, L., Jin, K. K., Klock, H. E., Knuth, M. W., Kumar, A., McMullan, D., Morse, A. T., Nigoghossian, E., Okach, L., Oommachen, S., Paulsen, J., Reyes, R., van den Bedem, H., Hodgson, K. O., Wooley, J., Deacon, A. M., Godzik, A., Lesley, S. A., and Wilson, I. A. (2009) Crystal structure of a novel archaeal AAA+ ATPase SSO1545 from *Sulfolobus solfataricus*. *Proteins* **74**, 1041–1049
62. Sanger, F., Coulson, A. R., Friedmann, T., Air, G. M., Barrell, B. G., Brown, N. L., Fiddes, J. C., Hutchison, C. A., 3rd, Slocombe, P. M., and Smith, M. (1978) The nucleotide sequence of bacteriophage phiX174. *J. Mol. Biol.* **125**, 225–246
63. Yokoyama, H., Kurumizaka, H., Ikawa, S., Yokoyama, S., and Shibata, T. (2003) Holliday junction binding activity of the human Rad51B protein. *J. Biol. Chem.* **278**, 2767–2772
64. Johnson, W. C. (1999) Analyzing protein circular dichroism spectra for accurate secondary structures. *Proteins* **35**, 307–312
65. Gaudreault, M., Gingras, M.-E., Lessard, M., Leclerc, S., and Guerin, S. L. (2009) Electrophoretic mobility shift assays for the analysis of DNA-protein interactions. in *DNA-Protein Interactions: Principles and Protocols* (Moss, T., and Leblanc, B., eds) pp. 15–35, 3rd Ed., Humana Press, New York
66. Capaldi, S. A., and Berger, J. M. (2004) Biochemical characterization of Cdc6/Orc1 binding to the replication origin of the euryarchaeon *Methanothermobacter thermoautotrophicus*. *Nucleic Acids Res.* **32**, 4821–4832
67. Feng, L., Wang, B., Driscoll, B., and Jong, A. (2000) Identification and characterization of *Saccharomyces cerevisiae* Cdc6 DNA-binding properties. *Mol. Biol. Cell* **11**, 1673–1685
68. Harris, C. J., Slootweg, E. J., Goverse, A., and Baulcombe, D. C. (2013) Stepwise artificial evolution of a plant disease resistance gene. *Proc. Natl. Acad. Sci. U.S.A.* **110**, 21189–21194
69. Qi, S., Pang, Y., Hu, Q., Liu, Q., Li, H., Zhou, Y., He, T., Liang, Q., Liu, Y., Yuan, X., Luo, G., Li, H., Wang, J., Yan, N., and Shi, Y. (2010) Crystal structure of the *Caenorhabditis elegans* apoptosome reveals an octameric assembly of CED-4. *Cell* **141**, 446–457
70. Grainge, I., Gaudier, M., Schuwirth, B. S., Westcott, S. L., Sandall, J., Atanassova, N., and Wigley, D. B. (2006) Biochemical analysis of a DNA replication origin in the archaeon *Aeropyrum pernix*. *J. Mol. Biol.* **363**, 355–369
71. Parkhurst, L. J., Parkhurst, K. M., Powell, R., Wu, J., and Williams, S. (2001) Time-resolved fluorescence resonance energy transfer studies of DNA bending in double-stranded oligonucleotides and in DNA-protein complexes. *Biopolymers* **61**, 180–200
72. Gohlke, C., Murchie, A. I., Lilley, D. M., and Clegg, R. M. (1994) Kinking of DNA and RNA helices by bulged nucleotides observed by fluorescence resonance energy transfer. *Proc. Natl. Acad. Sci. U.S.A.* **91**, 11660–11664
73. Fujimoto, M., Kuninaka, A., and Yoshino, H. (1974) Studies on a nuclease from *Penicillium citrinum*: 1. Purification of a nuclease from *Penicillium*

citrinum. *Agric. Biol. Chem.* **38**, 777–783
74. Cremazy, F. G., Manders, E. M., Bastiaens, P. I., Kramer, G., Hager, G. L., van Munster, E. B., Verschure, P. J., Gadella, T. J., Jr., and van Driel, R. (2005) Imaging *in situ* protein-DNA interactions in the cell nucleus using FRET-FLIM. *Exp. Cell Res.* **309**, 390–396
75. Scofield, S. R., Tobias, C. M., Rathjen, J. P., Chang, J. H., Lavelle, D. T., Michelmore, R. W., and Staskawicz, B. J. (1996) Molecular basis of gene-for-gene specificity in bacterial speck disease of tomato. *Science* **274**, 2063–2065
76. Spehr, M., Schwane, K., Riffell, J. A., Barbour, J., Zimmer, R. K., Neuhaus, E. M., and Hatt, H. (2004) Particulate adenylate cyclase plays a key role in human sperm olfactory receptor-mediated chemotaxis. *J. Biol. Chem.* **279**, 40194–40203
77. Tang, X., Frederick, R. D., Zhou, J., Halterman, D. A., Jia, Y., and Martin, G. B. (1996) Initiation of plant disease resistance by physical interaction of AvrPto and Pto kinase. *Science* **274**, 2060–2063
78. Kim, J. L., Nikolov, D. B., and Burley, S. K. (1993) Co-crystal structure of TBP recognizing the minor groove of a TATA element. *Nature* **365**, 520–527
79. Kim, Y., Geiger, J. H., Hahn, S., and Sigler, P. B. (1993) Crystal structure of a yeast TBP/TATA-box complex. *Nature* **365**, 512–520
80. Rice, P. A., Yang, S., Mizuuchi, K., and Nash, H. A. (1996) Crystal structure of an IHF-DNA complex: a protein-induced DNA U-turn. *Cell* **87**, 1295–1306
81. Werner, M. H., Huth, J. R., Gronenborn, A. M., and Clore, G. M. (1995) Molecular basis of human 46X, Y sex reversal revealed from the three-dimensional solution structure of the human SRY-DNA complex. *Cell* **81**, 705–714
82. Fernández-Cid, A., Riera, A., Tognetti, S., Herrera, M. C., Samel, S., Evrin, C., Winkler, C., Gardenal, E., Uhle, S., and Speck, C. (2013) An ORC/Cdc6/MCM2–7 complex is formed in a multistep reaction to serve as a platform for MCM double-hexamer assembly. *Mol. Cell* **50**, 577–588
83. Randell, J. C., Bowers, J. L., Rodríguez, H. K., and Bell, S. P. (2006) Sequential ATP hydrolysis by Cdc6 and ORC directs loading of the Mcm2–7 helicase. *Mol. Cell* **21**, 29–39
84. Goulden, M. G., Köhm, B. A., Santa Cruz, S., Kavanagh, T. A., and Baulcombe, D. C. (1993) A feature of the coat protein of potato virus X affects both induced virus resistance in potato and viral fitness. *Virology* **197**, 293–302
85. Foyer, C. H., Karpinska, B., and Krupinska, K. (2014) The functions of WHIRLY1 and REDOX-RESPONSIVE TRANSCRIPTION FACTOR 1 in cross tolerance responses in plants: a hypothesis. *Phil. Trans. R. Soc. B* **369**, 20130226
86. Slootweg, E. J., Spiridon, L. N., Roosien, J., Butterbach, P., Pomp, R., Westerhof, L., Wilbers, R., Bakker, E., Bakker, J., Petrescu, A. J., Smant, G., and Goverse, A. (2013) Structural determinants at the interface of the ARC2 and leucine-rich repeat domains control the activation of the plant immune receptors Rx1 and Gpa2. *Plant Physiol.* **162**, 1510–1528
87. Lee, D. G., Makhov, A. M., Klemm, R. D., Griffith, J. D., and Bell, S. P. (2000) Regulation of origin recognition complex conformation and ATPase activity: differential effects of single-stranded and double-stranded DNA binding. *EMBO J.* **19**, 4774–4782
88. MacAlpine, H. K., Gordân, R., Powell, S. K., Hartemink, A. J., and MacAlpine, D. M. (2010) *Drosophila* ORC localizes to open chromatin and marks sites of cohesin complex loading. *Genome Res.* **20**, 201–211
89. Remus, D., Beall, E. L., and Botchan, M. R. (2004) DNA topology, not DNA sequence, is a critical determinant for *Drosophila* ORC-DNA binding. *EMBO J.* **23**, 897–907
90. Cesari, S., Bernoux, M., Moncuquet, P., Kroj, T., and Dodds, P. N. (2014) A novel conserved mechanism for plant NLR protein pairs: the "integrated decoy" hypothesis. *Front. Plant Sci.* **5**, 606
91. Wu, C. H., Krasileva, K. V., Banfield, M. J., Terauchi, R., and Kamoun, S. (2015) The "sensor domains" of plant NLR proteins: more than decoys? *Front. Plant Sci.* **6**, 134
92. Finzi, L., and Dunlap, D. D. (2010) Single-molecule approaches to probe the structure, kinetics, and thermodynamics of nucleoprotein complexes that regulate transcription. *J. Biol. Chem.* **285**, 18973–18978
93. Kim, H., Tang, G. Q., Patel, S. S., and Ha, T. (2012) Opening-closing dynamics of the mitochondrial transcription pre-initiation complex. *Nucleic Acids Res.* **40**, 371–380
94. Liu, X., Bushnell, D. A., Wang, D., Calero, G., and Kornberg, R. D. (2010) Structure of an RNA polymerase II-TFIIB complex and the transcription initiation mechanism. *Science* **327**, 206–209
95. Tang, G. Q., Deshpande, A. P., and Patel, S. S. (2011) Transcription factor-dependent DNA bending governs promoter recognition by the mitochondrial RNA polymerase. *J. Biol. Chem.* **286**, 38805–38813
96. Fogg, J. M., Randall, G. L., Pettitt, B. M., Sumners de, W. L., Harris, S. A., and Zechiedrich, L. (2012) Bullied no more: when and how DNA shoves proteins around. *Q. Rev. Biophys.* **45**, 257–299

References

Ade, J., DeYoung, B. J., Golstein, C., & Innes, R. W. (2007). Indirect activation of a plant nucleotide binding site–leucine-rich repeat protein by a bacterial protease. *Proceedings of the National Academy of Sciences*, *104*(7), 2531-2536.

Altschul, S. F., Madden, T. L., Schäffer, A. A., Zhang, J., Zhang, Z., Miller, W., & Lipman, D. J. (1997). Gapped BLAST and PSI-BLAST: a new generation of protein database search programs. *Nucleic acids research*, *25*(17), 3389-3402.

Atkinson, K.E. (2008). *An introduction to numerical analysis* (2nd Ed.). John Wiley & Sons.

Bernoux, M., Ve, T., Williams, S., Warren, C., Hatters, D., Valkov, E., Zhang, X., Ellis, J.G., Kobe, B. & Dodds, P.N., (2011). Structural and functional analysis of a plant resistance protein TIR domain reveals interfaces for self-association, signaling, and autoregulation. *Cell host & microbe*, *9*(3), 200-211.

Bendahmane, A., Farnham, G., Moffett, P. and Baulcombe, D.C., (2002). Constitutive gain-of-function mutants in a nucleotide binding site–leucine rich repeat protein encoded at the Rx locus of potato. *The Plant Journal*, *32*(2), 195-204.

Bendahmane, A., Kanyuka, K., & Baulcombe, D. C. (1999). The Rx gene from potato controls separate virus resistance and cell death responses. *The Plant Cell*, *11*(5), 781-791.

Bendahmane A., Köhn B. A., Dedi C., Baulcombe D. C. (1995) The coat protein of potato virus X is a strain-specific elicitor of Rx1-mediated virus resistance in potato. *Plant J*. 8, 933–941

Bieri, S., Mauch, S., Shen, Q.H., Peart, J., Devoto, A., Casais, C., Ceron, F., Schulze, S., Steinbiß, H.H., Shirasu, K. & Schulze-Lefert, P. (2004). RAR1 positively controls steady state levels of barley MLA resistance proteins and enables sufficient MLA6 accumulation for effective resistance. *The Plant Cell*, *16*(12), 3480-3495.

Bi, D., Johnson, K., Huang, Y., Zhu, Z., Li, X., & Zhang, Y. (2011). Mutations in an atypical TIR-NB-LRR-LIM resistance protein confer autoimmunity. *Frontiers in plant science*, *2*, 71.

Boyer, L. A., Langer, M. R., Crowley, K. A., Tan, S., Denu, J. M., & Peterson, C. L. (2002). Essential role for the SANT domain in the functioning of multiple chromatin remodeling enzymes. *Molecular cell*, *10*(4), 935-942.

Brueggeman, R., Druka, A., Nirmala, J., Cavileer, T., Drader, T., Rostoks, N., Mirlohi, A., Bennypaul, H., Gill, U., Kudrna, D. & Whitelaw, C. (2008). The stem rust

resistance gene Rpg5 encodes a protein with nucleotide-binding-site, leucine-rich, and protein kinase domains. *Proceedings of the National Academy of Sciences*, *105*(39), 14970-14975.

Canonne, J., Marino, D., Jauneau, A., Pouzet, C., Brière, C., Roby, D., & Rivas, S. (2011). The Xanthomonas type III effector XopD targets the Arabidopsis transcription factor MYB30 to suppress plant defense. *The Plant Cell*, *23*(9), 3498-3511.

Capaldi, S. A., & Berger, J. M. (2004). Biochemical characterization of Cdc6/Orc1 binding to the replication origin of the euryarchaeon Methanothermobacter thermoautotrophicus. *Nucleic acids research*, *32*(16), 4821-4832.

Caplan, J. L., Mamillapalli, P., Burch-Smith, T. M., Czymmek, K., & Dinesh-Kumar, S. P. (2008). Chloroplastic protein NRIP1 mediates innate immune receptor recognition of a viral effector. *Cell*, *132*(3), 449-462.

Casey, L.W., Lavrencic, P., Bentham, A.R., Cesari, S., Ericsson, D.J., Croll, T., Turk, D., Anderson, P.A., Mark, A.E., Dodds, P.N. & Mobli, M. (2016). The CC domain structure from the wheat stem rust resistance protein Sr33 challenges paradigms for dimerization in plant NLR proteins. *Proceedings of the National Academy of Sciences*, 201609922.

Césari, S., Kanzaki, H., Fujiwara, T., Bernoux, M., Chalvon, V., Kawano, Y., Shimamoto, K., Dodds, P., Terauchi, R.& Kroj, T. (2014). The NB-LRR proteins RGA4 and RGA5 interact functionally and physically to confer disease resistance. *The EMBO journal*, *33*(17), 1941-1959.

Cesari, S., Thilliez, G., Ribot, C., Chalvon, V., Michel, C., Jauneau, A., Rivas, S., Alaux, L., Kanzaki, H., Okuyama, Y. & Morel, J. B. (2013). The rice resistance protein pair RGA4/RGA5 recognizes the Magnaporthe oryzae effectors AVR-Pia and AVR1-CO39 by direct binding. *The Plant Cell*, *25*(4), 1463-1481.

Chang, C., Yu, D., Jiao, J., Jing, S., Schulze-Lefert, P., & Shen, Q. H. (2013). Barley MLA immune receptors directly interfere with antagonistically acting transcription factors to initiate disease resistance signaling. *The Plant Cell*, *25*(3), 1158-1173.

Chaturvedi, Sonali, and A. L. N. Rao. "A shift in plant proteome profile for a Bromodomain containing RNA binding Protein (BRP1) in plants infected with Cucumber mosaic virus and its satellite RNA." *Journal of proteomics* 131 (2016): 1-7.

Cheng, Y. T., Li, Y., Huang, S., Huang, Y., Dong, X., Zhang, Y., & Li, X. (2011). Stability of plant immune-receptor resistance proteins is controlled by SKP1-

CULLIN1-F-box (SCF)-mediated protein degradation. *Proceedings of the National Academy of Sciences*, *108*(35), 14694-14699.

Cockerham, G. Genetical studies on resistance to potato viruses X and Y. *Heredity* 25 (1970): 309-48.

Collier, S. M., Hamel, L. P., & Moffett, P. (2011). Cell death mediated by the N-terminal domains of a unique and highly conserved class of NB-LRR protein. *Molecular plant-microbe interactions*, *24*(8), 918-931.

Cremazy, F.G., Manders, E.M., Bastiaens, P.I., Kramer, G., Hager, G.L., Van Munster, E.B., Verschure, P.J., Gadella, T.J. & van Driel, R. (2005). Imaging in situ protein–DNA interactions in the cell nucleus using FRET–FLIM. *Experimental cell research*, *309*(2), 390-396.

Crick, F. H. (1953). The Fourier transform of a coiled-coil. *Acta crystallographica*, *6*(8-9), 685-689.

Danot, O., Marquenet, E., Vidal-Ingigliardi, D., & Richet, E. (2009). Wheel of life, wheel of death: a mechanistic insight into signaling by STAND proteins. *Structure*, *17*(2), 172-182.

de Alba, A. E. M., Sägesser, R., Tabler, M., & Tsagris, M. (2003). A bromodomain-containing protein from tomato specifically binds potato spindle tuber viroid RNA in vitro and in vivo. *Journal of virology*, *77*(17), 9685-9694.

Deslandes, L., Olivier, J., Peeters, N., Feng, D.X., Khounlotham, M., Boucher, C., Somssich, I., Genin, S.& Marco, Y. (2003). Physical interaction between RRS1-R, a protein conferring resistance to bacterial wilt, and PopP2, a type III effector targeted to the plant nucleus. *Proceedings of the National Academy of Sciences*, *100*(13), 8024-8029.

Dodds, P.N., Lawrence, G.J., Catanzariti, A.M., Teh, T., Wang, C.I., Ayliffe, M.A., Kobe, B. & Ellis, J. G. (2006). Direct protein interaction underlies gene-for-gene specificity and coevolution of the flax resistance genes and flax rust avirulence genes. *Proceedings of the National Academy of Sciences*, *103*(23), 8888-8893.

Feng, L., Wang, B., Driscoll, B., & Jong, A. (2000). Identification and characterization of Saccharomyces cerevisiae Cdc6 DNA-binding properties. *Molecular biology of the cell*, *11*(5), 1673-1685.

Fenyk, S., Campillo, A. D. S. E., Pohl, E., Hussey, P. J., & Cann, M. J. (2012). A nucleotide phosphatase activity in the nucleotide binding domain of an orphan resistance protein from rice. *Journal of Biological Chemistry*, *287*(6), 4023-4032.

Fenyk, S., Dixon, C.H., Gittens, W.H., Townsend, P.D., Sharples, G.J., Pålsson, L.O., Takken, F.L. & Cann, M. J. (2016). The Tomato Nucleotide-binding Leucine-rich Repeat Immune Receptor I-2 Couples DNA-binding to Nucleotide-binding Domain Nucleotide Exchange. *Journal of Biological Chemistry*, *291*(3), 1137-1147.

Fenyk, S., Townsend, P.D., Dixon, C.H., Spies, G.B., Campillo, A.D.S.E., Slootweg, E.J., Westerhof, L.B., Gawehns, F.K., Knight, M.R., Sharples, G.J., Goverse, A. Takken, F.L. & Cann, M. J. (2015). The Potato Nucleotide-binding Leucine-rich Repeat (NLR) Immune Receptor Rx1 Is a Pathogen-dependent DNA-deforming Protein. *Journal of Biological Chemistry*, *290*(41), 24945-24960.

Finzi, L., & Dunlap, D. D. (2010). Single-molecule approaches to probe the structure, kinetics, and thermodynamics of nucleoprotein complexes that regulate transcription. *Journal of Biological Chemistry*, *285*(25), 18973-18978.

Formstecher, E., Aresta, S., Collura, V., Hamburger, A., Meil, A., Trehin, A., Reverdy, C., Betin, V., Maire, S., Brun, C. & Jacq, B. (2005). Protein interaction mapping: a Drosophila case study. *Genome research*, *15*(3), 376-384.

Gagnon, D., Joubert, S., Sénéchal, H., Fradet-Turcotte, A., Torre, S., & Archambault, J. (2009). Proteasomal degradation of the papillomavirus E2 protein is inhibited by overexpression of bromodomain-containing protein 4. *Journal of virology*, *83*(9), 4127-4139.

Han, X. Y., Li, P. X., Zou, L. J., Tan, W. R., Zheng, T., Zhang, D. W., & Lin, H. H. (2016). GOLDEN2-LIKE transcription factors coordinate the tolerance to Cucumber mosaic virus in Arabidopsis. *Biochemical and Biophysical Research Communications*, *477*(4), 626-632.

Hao, W., Collier, S. M., Moffett, P., & Chai, J. (2013). Structural basis for the interaction between the potato virus X resistance protein (Rx) and its cofactor Ran GTPase-activating protein 2 (RanGAP2). *Journal of Biological Chemistry*, *288*(50), 35868-35876.

Harris, C. J., Slootweg, E. J., Goverse, A., & Baulcombe, D. C. (2013). Stepwise artificial evolution of a plant disease resistance gene. *Proceedings of the National Academy of Sciences*, *110*(52), 21189-21194.

Heidrich, K., Wirthmueller, L., Tasset, C., Pouzet, C., Deslandes, L., & Parker, J. E. (2011). Arabidopsis EDS1 connects pathogen effector recognition to cell compartment–specific immune responses. *Science*, *334*(6061), 1401-1404.

Huang B, Yang XD, Zhou MM, Ozato K, Chen LF (2009). BRD4 coactivates transcriptional activation of NF-κB via specific binding to acetylated RelA. *Mol Cell Biol. 29*(5), 1375–1387.

Hyun, K. G., Lee, Y., Yoon, J., Yi, H., & Song, J. J. (2016). Crystal structure of Arabidopsis thaliana SNC1 TIR domain. *Biochemical and Biophysical Research Communications*.

Jia, Y., McAdams, S. A., Bryan, G. T., Hershey, H. P., & Valent, B. (2000). Direct interaction of resistance gene and avirulence gene products confers rice blast resistance. *The EMBO journal*, *19*(15), 4004-4014.

Jones, J. D., & Dangl, J. L. (2006). The plant immune system. *Nature*, *444*(7117), 323-329.

Kadota, Y., Amigues, B., Ducassou, L., Madaoui, H., Ochsenbein, F., Guerois, R., & Shirasu, K. (2008). Structural and functional analysis of SGT1–HSP90 core complex required for innate immunity in plants. *EMBO reports*, *9*(12), 1209-1215.

Kingston, R. E., & Narlikar, G. J. (1999). ATP-dependent remodeling and acetylation as regulators of chromatin fluidity. *Genes & development*, *13*(18), 2339-2352.

Kobe, B., & Kajava, A. V. (2001). The leucine-rich repeat as a protein recognition motif. *Current opinion in structural biology*, *11*(6), 725-732.

Kohler, A., Rinaldi, C., Duplessis, S., Baucher, M., Geelen, D., Duchaussoy, F., Meyers, B.C., Boerjan, W. & Martin, F. (2008). Genome-wide identification of NBS resistance genes in Populus trichocarpa. *Plant molecular biology*, *66*(6), 619-636.

Kohm, Barbel A., Matthew G. Goulden, Julie E. Gilbert, Tony A. Kavanagh, & David C. Baulcombe. (1993) A Potato virus X resistance gene mediates an induced, nonspecific resistance in protoplasts. *The Plant Cell, 5*(8), 913-920.

Kohn, W. D., Mant, C. T., & Hodges, R. S. (1997). α-Helical protein assembly motifs. *Journal of Biological Chemistry*, *272*(5), 2583-2586.

Larquet, E., Schreiber, V., Boisset, N., & Richet, E. (2004). Oligomeric assemblies of the Escherichia coli MalT transcriptional activator revealed by cryo-electron microscopy and image processing. *Journal of molecular biology*, *343*(5), 1159-1169.

Lewis, J.D., Lee, A.H.Y., Hassan, J.A., Wan, J., Hurley, B., Jhingree, J.R., Wang, P.W., Lo, T., Youn, J.Y., Guttman, D.S. & Desveaux, D. (2013). The Arabidopsis ZED1 pseudokinase is required for ZAR1-mediated immunity induced by the Pseudomonas syringae type III effector HopZ1a. *Proceedings of the National Academy of Sciences*, *110*(46), 18722-18727.

Liu, Y., Schiff, M., Serino, G., Deng, X. W., & Dinesh-Kumar, S. P. (2002). Role of SCF ubiquitin-ligase and the COP9 signalosome in the N gene–mediated resistance response to Tobacco mosaic virus. *The Plant Cell*, *14*(7), 1483-1496.

Liu, Y., Burch-Smith, T., Schiff, M., Feng, S., & Dinesh-Kumar, S. P. (2004). Molecular chaperone Hsp90 associates with resistance protein N and its signaling proteins SGT1 and Rar1 to modulate an innate immune response in plants. *Journal of Biological Chemistry*, *279*(3), 2101-2108.

Lukasik-Shreepaathy, E., Slootweg, E., Richter, H., Goverse, A., Cornelissen, B. J., & Takken, F. L. (2012). Dual regulatory roles of the extended N terminus for activation of the tomato Mi-1.2 resistance protein. *Molecular Plant-Microbe Interactions*, *25*(8), 1045-1057.

Lukasik, E., & Takken, F. L. (2009). STANDing strong, resistance proteins instigators of plant defence. *Current opinion in plant biology*, *12*(4), 427-436.

Maekawa, T., Cheng, W., Spiridon, L.N., Töller, A., Lukasik, E., Saijo, Y., Liu, P., Shen, Q.H., Micluta, M.A., Somssich, I.E. & Takken, F. L. (2011). Coiled-coil domain-dependent homodimerization of intracellular barley immune receptors defines a minimal functional module for triggering cell death. *Cell host & microbe*, *9*(3), 187-199.

Maqbool, A., Saitoh, H., Franceschetti, M., Stevenson, C.E.M., Uemura, A., Kanzaki, H., Kamoun, S., Terauchi, R. & Banfield, M. J. (2015). Structural basis of pathogen recognition by an integrated HMA domain in a plant NLR immune receptor. *Elife*, *4*, e08709.

Mazourek, M., Cirulli, E.T., Collier, S.M., Landry, L.G., Kang, B.C., Quirin, E.A., Bradeen, J.M., Moffett, P. & Jahn, M. M. (2009). The fractionated orthology of Bs2 and Rx/Gpa2 supports shared synteny of disease resistance in the Solanaceae. *Genetics*, *182*(4), 1351-1364.

Mestre, P., & Baulcombe, D. C. (2006). Elicitor-mediated oligomerization of the tobacco N disease resistance protein. *The Plant Cell*, *18*(2), 491-501.

Meyers, B. C., Dickerman, A. W., Michelmore, R. W., Sivaramakrishnan, S., Sobral, B. W., & Young, N. D. (1999). Plant disease resistance genes encode members of an ancient and diverse protein family within the nucleotide-binding superfamily. *The Plant Journal*, *20*(3), 317-332.

Meyers, B. C., Kozik, A., Griego, A., Kuang, H., & Michelmore, R. W. (2003). Genome-wide analysis of NBS-LRR–encoding genes in Arabidopsis. *The Plant Cell*, *15*(4), 809-834.

Mitchell, A., Chang, H.Y., Daugherty, L., Fraser, M., Hunter, S., Lopez, R., McAnulla, C., McMenamin, C., Nuka, G., Pesseat, S. & Sangrador-Vegas, A. (2014). The InterPro protein families database: the classification resource after 15 years. *Nucleic acids research*, gku1243.

Milligan, S. B., Bodeau, J., Yaghoobi, J., Kaloshian, I., Zabel, P., & Williamson, V. M. (1998). The root knot nematode resistance gene Mi from tomato is a member of the leucine zipper, nucleotide binding, leucine-rich repeat family of plant genes. *The Plant Cell*, *10*(8), 1307-1319.

Moffett, P., Farnham, G., Peart, J. and Baulcombe, D.C. (2002.) Interaction between domains of a plant NBS–LRR protein in disease resistance-related cell death. *The EMBO journal*, *21*(17), pp.4511-4519.

Morel, J. B., & Dangl, J. L. (1997). The hypersensitive response and the induction of cell death in plants. *Cell death and differentiation*, *4*(8), 671-683.

Murmu, J., Wilton, M., Allard, G., Pandeya, R., Desveaux, D., Singh, J., & Subramaniam, R. (2014). Arabidopsis GOLDEN2-LIKE (GLK) transcription factors activate jasmonic acid (JA)-dependent disease susceptibility to the biotrophic pathogen *Hyaloperonospora arabidopsidis*, as well as JA-independent plant immunity against the necrotrophic pathogen Botrytis cinerea. *Molecular plant pathology*, *15*(2), 174-184.

Muskett, P. R., Kahn, K., Austin, M. J., Moisan, L. J., Sadanandom, A., Shirasu, K., ... & Parker, J. E. (2002). Arabidopsis RAR1 exerts rate-limiting control of R gene–mediated defenses against multiple pathogens. *The Plant Cell*, *14*(5), 979-992.

Nandety, R. S., Caplan, J. L., Cavanaugh, K., Perroud, B., Wroblewski, T., Michelmore, R. W., & Meyers, B. C. (2013). The role of TIR-NBS and TIR-X proteins in plant basal defense responses. *Plant physiology*, *162*(3), 1459-1472.

Ntoukakis, V., Balmuth, A. L., Mucyn, T. S., Gutierrez, J. R., Jones, A. M., & Rathjen, J. P. (2013). The tomato Prf complex is a molecular trap for bacterial effectors based on Pto transphosphorylation. *PLoS Pathog*, *9*(1), e1003123.

Ottinger, M., Christalla, T., Nathan, K., Brinkmann, M. M., Viejo-Borbolla, A., & Schulz, T. F. (2006). Kaposi's sarcoma-associated herpesvirus LANA-1 interacts with the short variant of BRD4 and releases cells from a BRD4-and BRD2/RING3-induced G1 cell cycle arrest. *Journal of virology*, *80*(21), 10772-10786.

Owen, D.J., Ornaghi, P., Yang, J.C., Lowe, N., Evans, P.R., Ballario, P., Neuhaus, D., Filetici, P. & Travers, A. A. (2000). The structural basis for the recognition of acetylated histone H4 by the bromodomain of histone acetyltransferase gcn5p. *The EMBO journal*, *19*(22), 6141-6149.

Padmanabhan, M., Cournoyer, P., & Dinesh-Kumar, S. P. (2009). The leucine-rich repeat domain in plant innate immunity: a wealth of possibilities. *Cellular microbiology*, *11*(2), 191-198.

Peart, J. R., Cook, G., Feys, B. J., Parker, J. E., & Baulcombe, D. C. (2002). An EDS1 orthologue is required for N-mediated resistance against tobacco mosaic virus. *The Plant Journal*, *29*(5), 569-579.

Qi, D., DeYoung, B. J., & Innes, R. W. (2012). Structure-function analysis of the coiled-coil and leucine-rich repeat domains of the RPS5 disease resistance protein. *Plant physiology*, *158*(4), 1819-1832.

Raffaele, S., Vailleau, F., Léger, A., Joubès, J., Miersch, O., Huard, C., Blée, E., Mongrand, S., Domergue, F. & Roby, D. (2008). A MYB transcription factor regulates very-long-chain fatty acid biosynthesis for activation of the hypersensitive cell death response in Arabidopsis. *The Plant Cell*, *20*(3), 752-767.

Rairdan, G. J., Collier, S. M., Sacco, M. A., Baldwin, T. T., Boettrich, T., & Moffett, P. (2008). The coiled-coil and nucleotide binding domains of the potato Rx disease resistance protein function in pathogen recognition and signaling. *The Plant Cell*, *20*(3), 739-751.

Rairdan, G. J., & Moffett, P. (2006). Distinct domains in the ARC region of the potato resistance protein Rx mediate LRR binding and inhibition of activation. *The Plant Cell*, *18*(8), 2082-2093.

Sacco, M. A., Mansoor, S., & Moffett, P. (2007). A RanGAP protein physically interacts with the NB-LRR protein Rx, and is required for Rx-mediated viral resistance. *The Plant Journal*, *52*(1), 82-93.

Sambrook, J., Fritsch, E. F., & Maniatis, T. (1989). *Molecular cloning: a laboratory manual* (2nd Ed.). Cold Spring Harbor Laboratory Press.

Sanchez, R., & Zhou, M. M. (2009). The role of human bromodomains in chromatin biology and gene transcription. *Current opinion in drug discovery & development*, *12*(5), 659.

Sarris, P.F., Duxbury, Z., Huh, S.U., Ma, Y., Segonzac, C., Sklenar, J., Derbyshire, P., Cevik, V., Rallapalli, G., Saucet, S.B. & Wirthmueller, L. (2015). A plant immune

receptor detects pathogen effectors that target WRKY transcription factors. *Cell*, *161*(5), 1089-1100.

Sela, H., Spiridon, L.N., Petrescu, A.J., Akerman, M., Mandel-Gutfreund, Y.A.E.L., Nevo, E., Loutre, C., Keller, B., Schulman, A.H. & Fahima, T. (2012). Ancient diversity of splicing motifs and protein surfaces in the wild emmer wheat (Triticum dicoccoides) LR10 coiled coil (CC) and leucine-rich repeat (LRR) domains. *Molecular plant pathology*, *13*(3), 276-287.

Shan, L., He, P., Li, J., Heese, A., Peck, S.C., Nürnberger, T., Martin, G.B. & Sheen, J. (2008). Bacterial effectors target the common signaling partner BAK1 to disrupt multiple MAMP receptor-signaling complexes and impede plant immunity. *Cell host & microbe*, *4*(1), 17-27.

Shen, Q.H., Saijo, Y., Mauch, S., Biskup, C., Bieri, S., Keller, B., Seki, H., Ülker, B., Somssich, I.E. & Schulze-Lefert, P. (2007). Nuclear activity of MLA immune receptors links isolate-specific and basal disease-resistance responses. *science*, *315*(5815), 1098-1103.

Sievers, F., Wilm, A., Dineen, D., Gibson, T.J., Karplus, K., Li, W., Lopez, R., McWilliam, H., Remmert, M., Söding, J. & Thompson, J. D. (2011). Fast, scalable generation of high-quality protein multiple sequence alignments using Clustal Omega. *Molecular systems biology*, *7*(1), 539.

Slootweg, E., Roosien, J., Spiridon, L.N., Petrescu, A.J., Tameling, W., Joosten, M., Pomp, R., van Schaik, C., Dees, R., Borst, J.W. & Smant, G. (2010). Nucleocytoplasmic distribution is required for activation of resistance by the potato NB-LRR receptor Rx1 and is balanced by its functional domains. *The Plant Cell*, *22*(12), 4195-4215.

Slootweg, E.J., Spiridon, L.N., Roosien, J., Butterbach, P., Pomp, R., Westerhof, L., Wilbers, R., Bakker, E., Bakker, J., Petrescu, A.J. & Smant, G. (2013). Structural determinants at the interface of the ARC2 and leucine-rich repeat domains control the activation of the plant immune receptors Rx1 and Gpa2. *Plant physiology*, *162*(3), 1510-1528.

Staal, J., Kaliff, M., Dewaele, E., Persson, M., & Dixelius, C. (2008). RLM3, a TIR domain encoding gene involved in broad-range immunity of Arabidopsis to necrotrophic fungal pathogens. *The Plant Journal*, *55*(2), 188-200.

Sukarta, O. C., Slootweg, E. J., & Goverse, A. (2016, May). Structure-informed insights for NLR functioning in plant immunity. In *Seminars in cell & developmental biology*. Academic Press.

Takken, F. L., Albrecht, M., & Tameling, W. I. (2006). Resistance proteins: molecular switches of plant defence. *Current opinion in plant biology*, *9*(4), 383-390.

Takken, F. L., & Goverse, A. (2012). How to build a pathogen detector: structural basis of NB-LRR function. *Current opinion in plant biology*, *15*(4), 375-384.

Tameling, W. I., & Baulcombe, D. C. (2007). Physical association of the NB-LRR resistance protein Rx with a Ran GTPase–activating protein is required for extreme resistance to Potato virus X. *The Plant Cell*, *19*(5), 1682-1694.

Tameling, W. I., Elzinga, S. D., Darmin, P. S., Vossen, J. H., Takken, F. L., Haring, M. A., & Cornelissen, B. J. (2002). The tomato R gene products I-2 and MI-1 are functional ATP binding proteins with ATPase activity. *The Plant Cell*, *14*(11), 2929-2939.

Tameling, W.I., Vossen, J.H., Albrecht, M., Lengauer, T., Berden, J.A., Haring, M.A., Cornelissen, B.J. & Takken, F.L., (2006). Mutations in the NB-ARC domain of I-2 that impair ATP hydrolysis cause autoactivation. *Plant physiology*, *140*(4), pp.1233-1245.

Tang, X., Frederick, R. D., Zhou, J., & Halterman, D. A. (1996). Initiation of plant disease resistance by physical interaction of AvrPto and Pto kinase. *Science*, *274*(5295), 2060.

Ueda, H., Yamaguchi, Y., & Sano, H. (2006). Direct interaction between the tobacco mosaic virus helicase domain and the ATP-bound resistance protein, N factor during the hypersensitive response in tobacco plants. *Plant molecular biology*, *61*(1-2), 31-45.

Van der Hoorn, R. A., & Kamoun, S. (2008). From guard to decoy: a new model for perception of plant pathogen effectors. *The Plant Cell*, *20*(8), 2009-2017.

Van Ooijen, G., Lukasik, E., Van Den Burg, H. A., Vossen, J. H., Cornelissen, B. J., & Takken, F. L. (2010). The small heat shock protein 20 RSI2 interacts with and is required for stability and function of tomato resistance protein I-2. *The Plant Journal*, *63*(4), 563-572.

Van Ooijen, G., Mayr, G., Kasiem, M. M., Albrecht, M., Cornelissen, B. J., & Takken, F. L. (2008). Structure–function analysis of the NB-ARC domain of plant disease resistance proteins. *Journal of experimental botany*, *59*(6), 1383-1397.

Ve, T., Williams, S. J., & Kobe, B. (2015). Structure and function of Toll/interleukin-1 receptor/resistance protein (TIR) domains. *Apoptosis*, *20*(2), 250-261.

Voinnet, O., Rivas, S., Mestre, P., & Baulcombe, D. (2003). An enhanced transient expression system in plants based on suppression of gene silencing by the p19 protein of tomato bushy stunt virus. *The Plant Journal*, *33*(5), 949-956.

Waters, M. T., Wang, P., Korkaric, M., Capper, R. G., Saunders, N. J., & Langdale, J. A. (2009). GLK transcription factors coordinate expression of the photosynthetic apparatus in Arabidopsis. *The Plant Cell*, *21*(4), 1109-1128.

Wang, G. F., Ji, J., Farid, E. K., Dangl, J. L., Johal, G., & Balint-Kurti, P. J. (2015). Molecular and functional analyses of a maize autoactive NB-LRR protein identify precise structural requirements for activity. *PLoS Pathog*, *11*(2), e1004674.

Weiberg, A., Wang, M., Lin, F.M., Zhao, H., Zhang, Z., Kaloshian, I., Huang, H.D. & Jin, H. (2013). Fungal small RNAs suppress plant immunity by hijacking host RNA interference pathways. *Science*, *342*(6154), 118-123.

Williams, S.J., Sohn, K.H., Wan, L., Bernoux, M., Sarris, P.F., Segonzac, C., Ve, T., Ma, Y., Saucet, S.B., Ericsson, D.J. & Casey, L. W. (2014). Structural basis for assembly and function of a heterodimeric plant immune receptor. *Science*, *344*(6181), 299-303.

Williams, S.J., Sornaraj, P., deCourcy-Ireland, E., Menz, R.I., Kobe, B., Ellis, J.G., Dodds, P.N. & Anderson, P. A. (2011). An autoactive mutant of the M flax rust resistance protein has a preference for binding ATP, whereas wild-type M protein binds ADP. *Molecular plant-microbe interactions*, *24*(8), 897-906.

Wirthmueller, L., Zhang, Y., Jones, J. D., & Parker, J. E. (2007). Nuclear accumulation of the Arabidopsis immune receptor RPS4 is necessary for triggering EDS1-dependent defense. *Current Biology*, *17*(23), 2023-2029.

Xiang, T., Zong, N., Zou, Y., Wu, Y., Zhang, J., Xing, W., Li, Y., Tang, X., Zhu, L., Chai, J. & Zhou, J. M. (2008). Pseudomonas syringae effector AvrPto blocks innate immunity by targeting receptor kinases. *Current Biology*, *18*(1), 74-80.

Xiao, S., Ellwood, S., Calis, O., Patrick, E., Li, T., Coleman, M., & Turner, J. G. (2001). Broad-spectrum mildew resistance in Arabidopsis thaliana mediated by RPW8. *Science*, *291*(5501), 118-120.

Xue, J.Y., Wang, Y., Wu, P., Wang, Q., Yang, L.T., Pan, X.H., Wang, B. & Chen, J. Q. (2012). A primary survey on bryophyte species reveals two novel classes of nucleotide-binding site (NBS) genes. *PLoS One*, *7*(5), e36700.

Yan, N., Chai, J., Lee, E.S., Gu, L., Liu, Q., He, J., Wu, J.W., Kokel, D., Li, H., Hao, Q. & Xue, D. (2005). Structure of the CED-4–CED-9 complex provides insights into programmed cell death in Caenorhabditis elegans. *Nature*, *437*(7060), 831-837.

Yang, H., Shi, Y., Liu, J., Guo, L., Zhang, X., & Yang, S. (2010). A mutant CHS3 protein with TIR-NB-LRR-LIM domains modulates growth, cell death and freezing tolerance in a temperature-dependent manner in Arabidopsis. *The Plant Journal*, *63*(2), 283-296.

Yang, Y., Shah, J., & Klessig, D. F. (1997). Signal perception and transduction in plant defense responses. *Genes & Development*, *11*(13), 1621-1639.

Yue, J. X., Meyers, B. C., Chen, J. Q., Tian, D., & Yang, S. (2012). Tracing the origin and evolutionary history of plant nucleotide-binding site–leucine-rich repeat (NBS-LRR) genes. *New Phytologist*, *193*(4), 1049-1063.

Zhang, L., Chen, S., Ruan, J., Wu, J., Tong, A.B., Yin, Q., Li, Y., David, L., Lu, A., Wang, W.L & Marks, C. (2015). Cryo-EM structure of the activated NAIP2-NLRC4 inflammasome reveals nucleated polymerization. *Science*, *350*(6259), 404-409.

Zhao, T., Rui, L., Li, J., Nishimura, M.T., Vogel, J.P., Liu, N., Liu, S., Zhao, Y., Dangl, J.L. & Tang, D. (2015). A truncated NLR protein, TIR-NBS2, is required for activated defense responses in the exo70B1 mutant. *PLoS Genet*, *11*(1), e1004945.

Zhou, M., Huang, K., Jung, K.J., Cho, W.K., Klase, Z., Kashanchi, F., Pise-Masison, C.A. & Brady, J. N. (2009). Bromodomain protein Brd4 regulates human immunodeficiency virus transcription through phosphorylation of CDK9 at threonine 29. *Journal of virology*, *83*(2), 1036-1044.

Zhou, M., Li, Y., Hu, Q., Bai, X.C., Huang, W., Yan, C., Scheres, S.H. & Shi, Y. (2015). Atomic structure of the apoptosome: mechanism of cytochrome c-and dATP-mediated activation of Apaf-1. *Genes & development*, *29*(22), 2349-2361.